Advancing silver nanostructures towards antibacterial applications

Vivian L. Li
B.Sc. (Applied Chemistry) (Honours)
B. Sc. (Applied Chemistry)

A thesis submitted in fulfilment of the requirements for the degree of

Doctor of Philosophy

School of Applied Sciences

RMIT University

July 2014

Declaration

I certify that except where due acknowledgment has been made, the work is that of the author alone; the work has not been submitted previously, in whole or in part, to qualify for any other academic award; the content of the thesis is the result of work which has been carried out since the official commencement date of the approved research program; and, any editorial work, paid or unpaid, carried out by a third party is acknowledged.

Vivian Li

This dissertation is dedicated to my family, especially to Gon Gon.

I hope I have made you proud.

Acknowledgements

This thesis would not have been possible without the help and support from some of the wonderful people that have contributed in one way or another during this PhD candidature.

First and foremost, I would like to take this opportunity to express my gratitude to my senior supervisor, Associate Professor Vipul Bansal for the guidance and support throughout this journey. Thank you for introducing me to the world of nanobiotechnology, ever since completing Honours with you, I knew I wanted to further my studies in this exciting and growing field. Your vast knowledge and guidance in the directions of this thesis is greatly appreciated. Thank you for being a great mentor and not giving up on me throughout these years. To Professor Suresh K. Bhargava, I still remember that afternoon of undergrad graduation and you opened the opportunity to work with you and your group. That opportunity turned into Honours and now a PhD degree. I thank you for all the support, encouragement and motivation to achieve for the greatest heights in life. I am forever grateful to the both of you for the opportunities provided and support throughout my candidature.

Many thanks to NanoBiotechnology Research Laboratory (NBRL) and Centre of Advanced Materials and Industrial Chemistry (CAMIC), I am grateful for the opportunity to be part of such great multidisciplinary teams. I thank members past and present for the contribution of their knowledge, providing me with positive criticism and encouragement to ensure I excel as a young researcher.

I would also like to thank some senior researchers who have contributed to my thesis, namely Dr. Selvakannan, for your research assistance, continual support and words of encouragement. Thank you for sharing your knowledge and scientific advice, I

will always cherish it. Secondly, to the new Endeavour postdoctoral research fellow Dr. Tarun Sharma, I am grateful that you have joined NBRL during this last stage of my PhD candidature. Not only have you contributed in this thesis, but also provided guidance and knowledge in the field of nanobiotechnology. Thank you for your friendship and support during these final stages of my PhD journey. Also, thanks are due to Prof. Shimshom Belkin from Hebrew University of Jerusalem for providing the plasmid for the genotoxicity and cellular toxicity studies. To Dr. Anthony O`Mullane, I thank you for the electrochemistry expertise, your kind words and your valued collaboration and contribution to this thesis. Also a sincere thanks to Dr. Hemant Daima, for all the assistance, guidance and immense motivation and encouragement you provided me just before you left RMIT University. I will cherish our memories and your friendship.

To the lovely Dr. Lisa Dias, you have helped in so many ways from keeping me on track to the continuous motivation and words of encouragement to help me finish my thesis. Thank you so much for your endless support every time I visit.

I would like to acknowledge the technical staff of Building 3, Mr. Frank Antolasic, Mrs. Nadia Zakhartchouk, Mrs. Ruth Cepriano-Hall, Mr. Howard Anderson, Mrs. Diane Mileo, Mr. Karl Lang and Mr. Paul Morrison for their hard work ensuring the laboratories are running efficiently and always lending a helpful hand. Moreover, for the invaluable expertise in the instruments I worked on during my candidature. Special thanks go to Ms. Zahra Davoudi, my mother at RMIT, without you, I would not have been able to finish this thesis. I am forever grateful for our conversations, your knowledge that you have passed down to me, the ongoing support and encouragement throughout this journey. For this I cannot thank you enough.

To the staff at RMIT Microscopy and Microanalysis Facility, especially Mr. Peter Rummel and Dr. Matthew Field who have spent countless hours to teach the finer points and techniques of imaging on the electron microscopes from the old days of developing films to the current advanced digital imaging.

I have made some great friendships during this PhD journey; I thank Rahul Ram, Fiona Charalambous, Elizabeth Kulikov, Kat Fortig, Emma Goethals, Jos Cambell, Jarrod Newnham, Andrew Pearson, Hailey Daly, Nathan Thompson, Dave Tonkin, Rajesh Ramanathan, Blake Plowman, Ilija Najdovski, Ahmad Esmaielzadeh, Nafisa Zohora, Vishal Mistry, Katie Tur, Manika Mahajan, Bebeto Lay, Daniel Oppedisano, Aaron Raynor and Qing Hong Loh. You are all great individuals and I thank you all for your friendship and providing such a pleasant environment in the office and the laboratory. A special mention also goes to Nicola Nola for your endless support and encouragement throughout this candidature. Thank you for your help in the analysis of data and presentation of schematics. To Amanda Abraham, thank you for your help in assisting with laboratory techniques during my candidature. You have been a great help and saved me a vast amount of time.

I thank the Australian government for the APA scholarship. I am also thankful for receiving a travel bursary from RACI to attend the CHEMECA conference. I would also like to thank Jigsaw and the girls who I have worked with past and present whilst writing my thesis. Thank you for all the support and motivation throughout the years and giving me the balance I need from work and university.

To all my friends in my life, you have all been very supportive and keeping me sane. Thank you for believing in me and keeping our friendship alive. Now that I have finished, we'll have time to make more happy memories.

My love and gratitude to my entire family here and overseas, thank you for all the support and motivation throughout my PhD candidature. Thank you for always believing in me and encouraging me to try my best at all times. In particular, a special mention to my mother, father and sister for their endless love and support.

Last but not least, a big thank you to Dr. Andrew Basile. Thank you for always being there, for the sacrifices, patience and continual love and support throughout this occasionally stressful journey. I am glad we were able to experience this chapter together as one, and share an understanding on how it is. Finally, thank you for believing in me and encouraging me to achieve the best I can always.

Vivian Li

Table of Contents

List of Figures

List of Tables

Nomenclature

AAS	Atomic absorption spectroscopy
Ag	Silver
AgNP	Silver nanoparticle
AMP	Ampicillin
ArOH	Phenolic antioxidant
ATP	Adenosine triphosphate
ATR	Attenuated total reflection infrared
BDE	Bond dissociation energy
BE	Binding energy
CD	Cell death
CFU	Colony forming unit
Curc-AgNPs	Curcumin Ag nanoparticles
CV	Cyclic voltammetry
DLS	Dynamic light scattering
DNA	Deoxyribonucleic acid
E. coli	*Escherichia coli*
ECMP	*E. coli* membrane protein
EG	Ethylene gylcol
EGCG	Epigallocatechin gallate
EGCG-AgNPs	Epigallocatechin gallate Ag nanoparticles
fcc	Face-centered cubic
FTIR	Fourier transform infrared
GADDS	General area detector diffraction system

GFP	Green fluorescence protein
HAT	Hydrogen atom transfer
hcp	Hexagonally closed pack
IP	Ionisation energy
IR	Infrared
Kd	Dissociation constant
LB	Lauria Bertani
NAG	*N*-acetylglucosamine
NAL	Nalidixic acid
NAM	*N*-acetylmuramic acid
NP	Nanoparticle
OD	Optical density
PECS	Precision etching coating system
PCG	Penicillin G
PIA	Polysaccharide intercellular adhesion
PMB	Polymyxin B
PVP	Polyvinylpyrrolidone
PSSS	Poly sodium styrenesulphonate
R•	Free radical
REDOX	Reduction-oxidation
RFP	Red fluorescence protein
ROS	Reactive oxygen species
S. albus	*Staphylococcus albus*
SAMP	*S. albus* membrane protein

SEM	Scanning electron microscope
SET	Single electron transfer
SERS	Surface-enhanced Raman scattering
SPR	Surface plasmon resonance
STEC	Shiga toxin-producing *Escherichia coli*
TEM	Transmission electron microscope
trp	Tryptophan
Tyr-AgNPs	Tyrosine Ag nanoparticles
UV-Vis	Ultraviolet- visible
XPS	X-ray photoelectron spectroscopy
XRD	X-ray diffraction

Abstract

There is a growing concern on the emergence and re-emergence of drug-resistant pathogens such as multi-resistant bacterial strains. Hence, the development of new antimicrobial compounds or the modification of those that already exist in order to improve antimicrobial activity is a high priority area of research. In this endeavour, nanobiotechnology provides the means to modify distinct features of diverse materials, including metal nanoparticles. Silver has a strong antimicrobial potential, which has been exploited since ancient times. Therefore, the explorations of Ag nanomaterials for antimicrobial applications were pursued. Various Ag nanomaterials were synthesised, characterised and tested for their antibacterial activity. Tailoring nanomaterials for biological applications has become an emerging area of research. However, this warrants the need to understand the interaction between the materials with various biological applications. This thesis focuses on the influence of shape and surface functionalisation of Ag nanoparticles towards their antibacterial applications, while also exploring the synergism between existing antibiotics and Ag nanoparticles towards enhanced antibacterial activity.

Different shapes of Ag nanoparticles were synthesised via various chemical methods. Ag nanospheres were synthesised with the use of tyrosine as a reducing and capping agent. Ag nanocubes were obtained by mediating a polyol process with ethylene glycol and Ag nanoprisms were achieved by a seed-based thermal procedure. The comparison of these different shapes of Ag nanoparticles was tested for their antibacterial activity against model strains of Gram negative bacteria *Escherichia coli* and Gram positive bacteria *Staphylococcus albus*. All shape-dependent Ag nanoparticles

exhibited antibacterial activity against both Gram negative and Gram positive strains. However, Ag nanocubes exhibited the highest antibacterial activity overall.

Tyrosine reduced Ag nanoparticles were found to be the most stable and facile to synthesise. Therefore, these particles were selected as the model Ag nanoparticles for further studies. These nanoparticles were employed as antibiotic carriers for antibacterial activity. Traditional broad and narrow spectrums of antibiotics including ampicillin, penicillin G and polymyxin B were utilised as functional conjugates to influence antibacterial capabilities on the surface of Ag nanoparticles. The combination of Ag nanoparticles and antibiotics demonstrated synergistic effects at the lower concentrations of silver employed in the studies and revealed physical mode of action against bacteria causing cell wall cleavage and cell lysis.

The control of surface functionalisation and composition of nanoparticles via a green and eco-friendly approach was also achieved. Three particular phenolic compounds including tyrosine, curcumin and epigallocatechin gallate (EGCG) were utilised as a reducing as well as a capping agent to synthesise functional Ag nanoparticles. These phenolic compounds incorporate one or multiple phenolic groups which were instigated as organic surface coronas surrounding Ag nanoparticles. Ag nanoparticles containing equimolar and various mole ratios of these phenolic compounds were synthesised according to the number of phenolic groups present within each molecule. These functionalised Ag nanoparticles were tested for their antibacterial activity and their correlation between surface coronas and composition of nanoparticles was studied. The functionalised Ag nanoparticles of various mole ratios all exhibited significant antibacterial activity with physical damage to bacterial cells. Efforts were made to understand the role of surface functionalisation in conjugation with Ag nanoparticles in

dictating their ability to differentially interact with bacterial membranes. This led to the mechanistic insight into the antibacterial performance of Ag nanomaterials. Electrochemical and biological techniques were elucidated to assist in the proposed mechanism of Ag nanomaterials' and interaction with both Gram negative and Gram positive bacterial cells. Cyclic voltammetry studies complimented antibacterial studies through which it was noted that the lower the potential required to oxidise Ag nanoparticles into Ag^+ ions, the higher the antibacterial effect. Therefore, in the case of functionalised Ag nanoparticles, curcumin reduced Ag nanoparticles at 1:2 mole ratios exhibited the highest antibacterial activity.

The interaction of nanoparticles to bacterial membrane protein was also studied. Additionally, the investigation of the effect at gene and protein level, genotoxicity and cellular toxicity was explored. Membrane protein studies demonstrated that EGCG Ag nanoparticles exhibited more affinity for *E. coli* membrane proteins compared to curcumin Ag nanoparticles. However, for *S. albus* membrane proteins, curcumin Ag nanoparticles demonstrated a 30 fold increase in affinity compared to EGCG Ag nanoparticles. The cellular toxicity induction of the functionalised Ag nanoparticles revealed that curcumin Ag nanoparticles (synthesised at 1:2 mole ratio with respect to curcumin:silver) demonstrated the highest stress response. Irrespective of capping agents, all functionalised Ag nanoparticles induced DNA damage and SOS response. Therefore, it was proposed that Ag nanomaterials may display various mode of action for antibacterial activity which may not be solely restricted to interaction with membranes, genotoxicity and cytotoxicity.

These studies have demonstrated that the antibacterial activity of silver can be enhanced through the use of several methodologies outlined within this thesis. Several

factors can influence the microbial effectiveness of silver nanomaterials, including their shape and surface functionality, as well as their conjugation with well-proven traditional antibacterial compounds.

Chapter I

Introduction

1.1 Antimicrobial resistance

There has been an incoming tide of apprehension on the overuse of antibiotics and the effectual rise of antimicrobial resistance. Resistance can threaten the effective prevention and treatment of an ever-increasing range of infections caused by bacteria, parasites, viruses and fungi. When microorganisms develop resistance to antimicrobial agents such as antibiotics, they are usually referred to as "superbugs".[1] This is a main concern as a resistant pathogen may spread or impose substantial costs to individuals and society. Antimicrobial resistance is the broader term coined to describe resistance in a variety of microbes which are resistant to one or more than one antimicrobial drug.[1-7]

The majority of antibiotic use is found in two areas: humans in the community and in animals for growth promotion and prophylaxis.[8] The antibiotics used in human medicine belong to the same conventional class as those used in animals. In many cases even if they do not possess similar compounds, their mode of action is essentially the same.[9] Antibiotics are employed in diverse settings for food production. Animals are treated with antibiotics for both curing diseases and promoting growth,[10, 11] fruit trees are often treated prophylactically with antibiotics to control bacterial infections and

aquaculture relies on antibiotics to manage infectious disease. In each of these situations, the effects of the antibiotics extend beyond the site of use.[12]

In the past 70 years, people have accepted antibiotics as their right to obtain a prescription at the first signs of common infection or treat themselves with a handful of economical antibiotics. Although one cannot conceive a restoration of pre-antibiotic times, yet the overuse of these agents in man and animals is relentlessly driving us in that direction.

Over the last 30 years, limited new types of antibiotics have been developed.[13, 14] As the use of conventional antibiotics rises, antimicrobial resistance patterns are developing which necessitates the continuous need for novel and more effective alternatives. One of the recent efforts in addressing this challenge lies within the study of nanotechnology.

1.2 Introduction to nanotechnology and nanobiotechnology

Nanotechnology is the field of research and fabrication that is on a scale between 1 to 100 nm. The initial concept was introduced by Nobel laureate Richard P. Feynman during his renowned lecture "*There's plenty of room at the bottom*" at the annual meeting of the American Physical Society, the Californian Institute of Technology.[15] Since then, there have been numerous revolutionary developments in physics, chemistry and biology that have validated Feynman's ideas of manipulating matter at an immensely small scale, the level of molecules and atoms, i.e. the nanoscale. The prefix *nano* is derived from the Greek word *nanos* meaning "dwarf". Today, it is used as a prefix describing 10^{-9} of a measuring unit. Nanotechnology is the understanding, control and restructuring of

matter on the order of nanometres to create materials with fundamentally novel properties and functions.[16-18]

Currently, there are two approaches to synthesising nanomaterials, the "top -down" or "bottom-up" approach.[19] The top-down approach seeks the means in which larger structures are reduced in size to nanoscale while preserving their original properties without atomic-level control or deconstructed from larger structures into their smaller composite parts.[20] The bottom-up approach, also referred to as molecular nanotechnology is when materials are assembled from atoms or molecular components through a process of assembly or self-assembly.[20] Although most present technologies rely on the "top-down" approach, "bottom-up" approach holds great promise for advancements in materials and manufacturing,[21-23] electronics,[24] energy,[25-27] biotechnology,[28-30] medicine and healthcare.[31-34]

Unlike non-biological systems that are typically formulated top-down, biological systems are built up from the molecular level in a bottom-up manner. This is achieved via a collection of molecular tool kits of atomic resolution that are used to fabricate micro and macrostructure compositions. Biological nanotechnology or "nanobiotechnology" can be perceived in many ways, one in particular is to incorporate nanoscale applications into biological organisms for the key purpose of improving the organism's quality of life.[35, 36]

Presently, there are numerous methods for synthesising nanodevices that have the potential to be utilised for biological applications to construct nano to microstructures.[37, 38] However, the broad overview is perhaps the one that will include both and can be defined as, the engineering, construction and manipulation of entities in the 1 to 100 nm range using biologically based methodologies or for the benefit of biological systems. The biological approaches can be an inspired way of mimicking

biological structures or the actual use of biological building blocks and platforms to assemble nanostructures.[39, 40]

As already mentioned, there are two elemental assemblies to creating nanostructures: top-down and bottom-up. The bottom-up approach exploits biological structures and processes to create novel functional materials, biosensors and bioelectronics for various applications.[26, 41] In terms of top-down approach in nanobiotechnology, tools and processes of nano or micro fabrication to synthesise nanostructures with defined surface features are applied.[39] One of the key differences between nanotechnology and nanobiotechnology is that in the former, the dominant approach is top-down whereas in the latter, it is bottom-up. This multidisciplinary field covers a vast and diverse array of technologies encompassing engineering, physics, chemistry and biology. It is the combination of these fields that has led to the birth of a new generation of materials and methods of preparation.

1.3 Nanomaterials: synthesis and applications

The fundamental challenge in the growth of nanotechnology is to synthesise nanostructures of desired material with tailored properties suitable for these particular applications. Contrarily, functionalising these nanostructures by altering their optical, electrical and optoelectronic properties through suitable control of size, shape, doping, assembly or incorporating in host matrix opens up more possibilities for their applications. Hence, while the novel and unconventional fabrication methodologies are emerging to prepare nanostructures of several morphologies, their physical properties are being studied in detail to explore their applicability.[42]

Traditionally, nanoparticles were synthesised only via physical and chemical methods. Some of the commonly used physical and chemical routes are ion sputtering, solvothermal synthesis, reduction and sol gel technique. Some of the commonly used physical and chemically techniques include:

a) Sol-gel technique: wet chemical method used for the fabrication of metal oxides from a chemical solution which acts as a precursor for integrated network (gel) of several particles or polymers. The precursor sol can either be deposited on the substrate to form a film, cast into a suitable container with desired shape or utilised in the synthesis of powders.[43]
b) Solvothermal synthesis: versatile low temperature route in which polar solvents under pressure and temperatures above their boiling points are employed. The solubility of reactants increase notably which enables a reaction to take place at lower temperature when under solvothermal conditions.[44]
c) Chemical reduction: synthesis involving the reduction of an ionic salt in a suitable medium in the presence or absence of a surfactant using reducing agents. Some commonly used reducing agents are sodium borohydride, hydrazine hydrate and sodium citrate.[45]
d) Laser ablation: a process which involves removing material from a solid surface by irradiating with a laser beam. At low laser flux, the material is heated by absorbed laser energy and evaporates or sublimates. Higher flux causes the material to convert to plasma. The depth over which laser energy is absorbed and the amount of material removed by single laser pulse is determined by the material's wavelength and optical properties. One well established route for carbon nanotubes synthesis is via laser ablation.[46]

e) Inert gas condensation: metals are evaporated in separate crucibles inside a high vacuum chamber filled with helium or argon gas. The evaporated metal atoms lose their kinetic energy and condense in the form of small crystals which accumulate on liquid nitrogen filled cold finger as a result of inert atomic collision with gas atoms in the chamber.[47]

Chemical reduction is the most common route in metal nanoparticle synthesis due to their facile protocols, fine shape and size control achieved. The control of size, shape and stability of nanoparticles can be achieved by integrating different capping agents, solvents and templates. Capping agents utilised include simple ions to polymeric molecules and biomolecules.[48]

While physical and chemical approaches have dominated the synthesis of nanostructures, recently considerable attention is placed upon the application of biological systems. Biological systems are known to construct intricate structures at the nano and micro scale with precise control in normal environmental conditions. This property has attracted researchers to understand and discover the underlying mechanisms used by the biological systems and thus explore the biomimetic methodology towards nanomaterial synthesis. Biomimetic refers to the application of biological principles for materials formation. One of the primary processes in biomimetics involves bioreduction- the use of organisms such as bacteria, actinomycetes, fungi and plants to synthesise nanomaterials.[49-53]

1.3.1 Metal nanoparticles

Metal particles are particularly interesting nanoscale systems due to the ease with which they can be synthesised and modified chemically. From the perspective of

understanding their optical and electronic effects, metal nanostructures also offer an advantage over other systems as their optical constants resemble those of the bulk metal to exceedingly small dimensions (i.e. <5 nm).[54]

Synthesis of metal nanostructures has been widely researched due to their interesting size and shape-dependent properties. These novel properties can be tailored by controlling their size, shape, composition, structure and crystallinity. Emphasis is placed on shape control as this allows optical, electronic, magnetic, catalytic and other properties of the nanostructures to be altered for versatile applications. Thus it has been established that the optical and electro-magnetic properties of a metal nanostructure is greatly dependent not only on the size of the structure, but also on the shape.[55-59]

The synthesis and properties of a number of different types of metal nanoparticles have been investigated. These include gold,[60-62] silver,[63-65] palladium,[66, 67] platinum,[68-70] titanium,[71-73] etc. Among these, gold and silver nanoparticles have been most commonly studied for diverse range of applications. This thesis focuses on exploring the potential of silver (Ag) nanoparticles for antimicrobial applications.

1.3.2 Silver nanoparticles

Elemental silver, both in bulk and dispersed state has been known for its unique chemical and physical properties, i.e. chemical stability, electrical and thermal conductivities, catalytic and antibacterial activity and malleability.[74] Silver has been studied as a material utilised within nanostructures for its superior performance in applications including plasmonics and surface-enhanced Raman scattering (SERS). Silver nanostructures have also been synthesised with a range of different shapes including spheres,[75] rods,[76] wires,[76] prisms[77] and cubes.[78] However, it was its simple use in

decorative ornaments and as a biocide that first captivated the interest of early civilizations.

The applications of silver have advanced since the time of ancient Greece and Rome; this is primarily due to its distinctive electrical properties which promoted its first use in electrical devices. Since silver is identified to be among the best electrical and thermal conductors of all noble metals, it is widely used in conductors, switches, contacts and fuses.[79, 80] The most significant use of metallic silver in electronics has been in the preparation of thick-film pastes, typically in pure silver-palladium formulations for use in silk screened circuit paths, multi-layer ceramics capacitors and conductive adhesives.[81]

1.4 Antimicrobial applications of Ag nanoparticles

Ag nanoparticles have been used to treat burns, wounds and infections.[82, 83] In addition, various salts of silver and their derivatives have been used as antimicrobial agents.[84] Numerous studies have reported that Ag nanoparticles exhibit antimicrobial properties. Ag nanoparticles have been studied as a medium for antibiotic delivery, synthesis of composites for the use as disinfecting filters and coating materials.[85-88]

Owing to their small sizes and higher surface-to-volume ratio, Ag nanoparticles possess a wider contact area with microorganisms. This property can enhance biological and chemical activity, hence provides Ag nanoparticles with high antibacterial activity. Ag nanoparticles have the ability to disturb functions of cell membranes such as permeability and respiration. Furthermore, upon penetration of the bacteria cell, Ag nanoparticles can disturb and react with the functions of sulphur containing proteins and phosphorus containing compounds such as deoxyribonucleic acid (DNA).[89-92]

Although Ag nanoparticles exhibit significant antibacterial properties, they also possess some disadvantages. Studies have found that nanoparticles have demonstrated toxic action on particular mammalian cells.[93-96] However, recent studies have demonstrated that combining Ag nanoparticles with antibiotics may reduce the toxicity of both agents towards mammalian cells and synergistically enhance their antimicrobial activity.[86, 97-100] Moreover, combination of nanoparticles and antibiotics lower the amount of both agents in the dosage which also increases antimicrobial properties. Due to this conjugation, the concentrations of antibiotics were increased at the site of antibiotic to microbe contact and thus accelerated the binding between microbes and antibiotics.[101]

Another alternative to overcome the toxicity towards mammalian cells is the use of peptide linkages to Ag nanoparticles. The interaction of metal ions with biomolecular targets i.e. amino acids, peptides or proteins is known to play a fundamental role in several biological routes including electron transfer reactions, metal transport and storage. Additionally, the inhibitions of enzymes by metal complexes with ligands are well known. It functions by ligand exchange reactions where the ligand present in the administered drug is substituted by the targeted enzyme which is a primary application in many metal-based drugs. Therefore, it is one of the most significant processes in bioinorganic chemistry.[102-105]

Surface modification of Ag nanoparticles can also help in tuning their properties to suit various applications and determine the interaction of the components as such chemical functionalisation of the surface of Ag nanoparticles has attracted much attention.[106-108] Functionalised nanoparticles can be applied in various areas including engineering, medical and biological applications. The main aspect of functionalisation is

to optimise the active sites on the nanoparticle surface i.e. hydrophilic, hydrophobic, conductive etc.[109] It can be broadly classified into two categories, non-covalent binding physisorption or covalent binding chemisorption. In terms of physisorption, the binding is fairly weak where the ligand and the nanomaterial are bound through weak electrostatic interactions, hydrogen bonding and or hydrophobic interactions. This nature of surface functionalisation is beneficial for forming the surface coatings for stabilising individual nanoparticles in solution. In contrast, chemisorption is greater than the non-covalent bonds formed by physisorption. The majority of the surface functionalisation methods are based on covalent bond formation. This technique provides a stronger bond which allows the ligand to be more stable on the surface which makes the linkage robust. Functional groups present on the ligand react with the substrate material and chemisorb onto the nanomaterial surface to yield self-assembled structures.[110-112]

Surface modification of nanoparticles may generate novel and interesting opportunities to develop efficient antimicrobial agent. To this end, nature has developed unique protein-based effective antibacterial platforms including lysozyme and antimicrobial peptides to control bacterial growth.[113-115] These natural antibacterial applications normally cause bacterial cell lysis and hence microorganisms find it challenging to gain resistance against these biologically nature produced antibiotics.

1.5 Distinctive features of the bacterial cell

Bacteria are prokaryotes with a simple internal structure and no membrane bound organelles. Bacteria display a wide diversity of morphology comprising of various sizes and shapes. These bacterial cells are approximately one tenth the sizes of eukaryotic cells

and are normally 0.5 to 5.0 μm in length.[116] Bacterial outer envelope that protects it from the external environment can have the following structural characteristics:

- Polysaccharide membrane (capsule)
- Lipid bilayer (outer membrane)
- Peptidoglycan (cell wall)
- Periplasmic space
- Periplasmic membrane (cytoplasmic plasma membrane)

Bacteria can possess different cell wall structures on the basis of their Gram stain. This staining technique was founded by Hans Christian Gram to distinguish bacteria into two major categories based on their response to the Gram stain procedure. In a Gram stain test, Gram positive bacteria would retain the crystal violet dye purple while a counterstain added to the crystal violet produces Gram negative bacteria a red or pink stain.[117, 118] The structural difference between Gram negative and Gram positive bacteria is also in the organisation of peptidoglycan layer which is the key component of the cell wall.[119]

1.5.1 Structure of Gram negative and Gram positive bacterial cell

The cell walls of bacteria consist of covalently linked polysaccharide and polypeptide chains which form a round macromolecule that entirely encases the cell. This framework is known as peptidoglycan, a polymer composed of two sugar derivatives: *N*-acetylglucosamine (NAG) and *N*-acetylmuramic acid (NAM). The main component of this polymer is composed with the repeating units of NAM and NAG which forms a carbohydrate backbone (glycan portion). A tetrapeptide chain comprising of four alternating D- and L- amino acids is attached to the carboxyl group of NAM. Chains of

linked peptidoglycan are connected by cross linkers between peptides while the carboxylic group of the terminal D-alanine is attached directly to the amino group of diaminopimelic acid. In addition, a peptide inter-bridge may be an alternative option, however most Gram negative cell wall peptidoglycan lacks the peptide inter-bridge.[120, 121]

Illustrated in Figure 1.1 is the schematic representation of Gram positive and Gram negative bacteria. In the case of Gram positive bacteria, it consists of a thick multilayered cell wall composed of peptidoglycan surrounding the cytoplasmic membrane. In addition, a peptide inter-bridge and greater amount of teichoic acids (polymer of glycerol or ribitol joined by phosphate groups) exists. Amino acids such as D-alanine are attached to the glycerol and ribitol groups. Teichoic acid is covalently linked to muramic acid and connects various layers of the peptidoglycan mesh together. Teichoic acid may prevent extensive wall breakdown and cell lysis during cell growth and is the provider of the cell wall's antigenicity.[120]

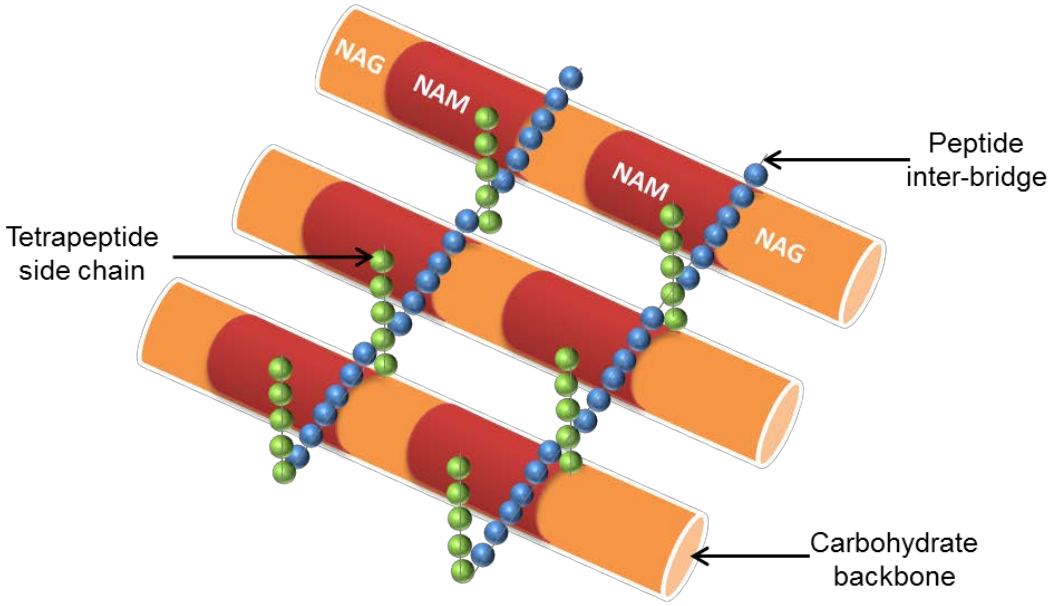

Figure 1.1 - Schematic representing peptidoglycan structure.

Gram negative bacterial cell walls have a more complicated structure than Gram positive bacteria both structurally and chemically. Structurally, in a Gram negative cell wall two layers external to the cytoplasmic membrane are apparent. Immediately external to the cytoplasmic membrane is a thin peptidoglycan layer which accounts for merely 5 to 10% of the Gram negative cell wall by weight. There are no teichoic or lipoteichoic acids present in the cell wall. Peripheral to the peptidoglycan layer is the outer membrane, which is unique to Gram negative bacteria. The area found between the external surface of the cytoplasmic membrane and the internal surface of the outer membrane is referred to as the periplasmic space. The periplasm compartment contains a battery of hydrolytic enzymes which are imperative to the cell for the breakdown of large macromolecules for metabolism. These enzymes normally include proteases, phosphatases, lipases, nucleases and carbohydrate degrading enzymes. Furthermore, there are fewer proteins in the outer membrane than in the cytoplasmic membrane. Porins are particularly important components due to their role in the permeability of the outer membrane to small molecules. Porins are proteins that form pores in the outer membrane large enough to allow passage of most small hydrophilic molecules.[120]

Overall, the difference between the cell walls of Gram positive and Gram negative bacteria greatly influence the success of the microbes in their environments. The thick cell wall of Gram positive cells allows them to perform better in dry conditions as it reduces water loss. The outer membrane and its lipopolysaccharides aid Gram negative cells to excel in the intestines and other host environments.

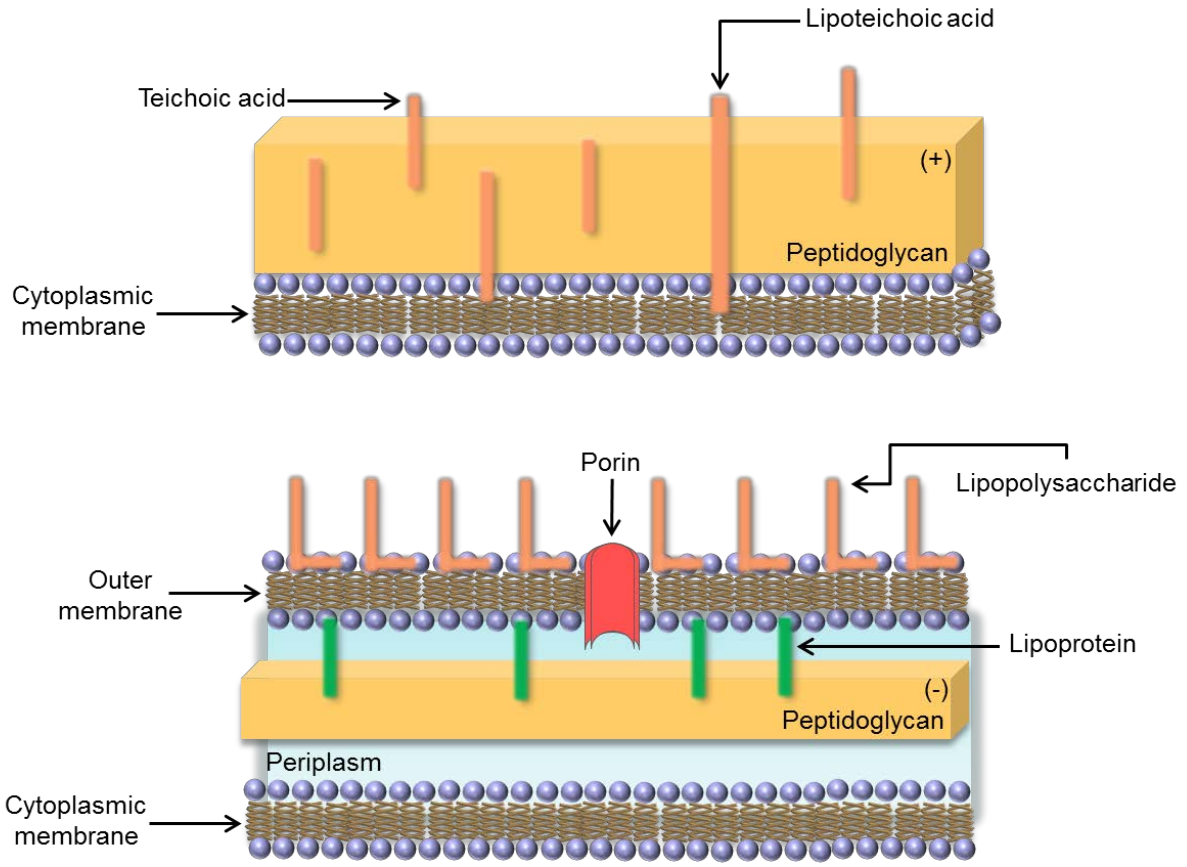

Figure 1.2 – Schematic representation of Gram positive and Gram negative bacteria.

One of the main objectives of the work presented in this thesis is to investigate the interactions between different silver nanostructures and various bacterial strains. Therefore, well established model microorganisms *Staphylococcus albus* (*S. albus*) and *Escherichia coli* (*E. coli*) were utilised in this study. *S. albus*, is a Gram positive bacterium belonging to the genus *Staphylococcus* that is spherical and grow in a grapelike cluster. It forms white, raised, cohesive colonies approximately 1-2 mm in diameter. It is of low pathogenicity, while occasional strains may be coagulase positive and produce hemolysis. They are generally part of the normal human commensal on the skin and nasal passages.[122] *S. albus* have the ability to form a hydrophobic biofilm on plastic devices which is a major hindrance to society. *S. albus* creates an extracellular polysaccharide material known as polysaccharide intercellular adhesion (PIA), which is made up of

sulphated polysaccharide. The gene *icaADBC* is responsible for both the polysaccharide capsule and the polysaccharide intracellular adhesion used in biofilm formation. This allows other bacteria to bind to the already existing biofilm, which in turn produces a multilayer biofilm. The metabolic activity of bacteria within is therefore decreased. This film is adhesive to hydrophobic biopolymers of prosthetics, creating diseases such as endocarditis.[123, 124]

E. coli is a Gram negative, rod shaped bacterium of the genus *Escherichia* which is typically found in the lower intestine of warm blooded organisms. Most *E. coli* strains are harmless however some strains may cause severe food poisoning in their hosts and are seldom liable for food contamination.[125] Some *E. coli* cause disease by producing a toxin called Shiga toxin. Thus the bacteria that create these toxins are known as "Shiga toxin-producing" *E. coli* or STEC. The most common type of STEC is *E. coli* O157:H7 which causes severe, acute haemorrhagic diarrhoea and abdominal cramps.[126, 127]

These bacteria were chosen as they are well understood and these are an important model organism in a number of fields of research, particularly genetics, molecular biology and biochemistry. The bacteria are easy to grow under laboratory conditions and strains are relatively safe to work with.

1.6 Rationale of thesis

The importance of metal nanostructures is apparent from the various platforms that are being pursued towards their potential applications. It is apparent that there are numerous pursuits to synthesise and characterise nanomaterials in biological and medicinal applications.[30, 38, 58, 128-132] In particular, Ag nanoparticles have been exploited

as an excellent antimicrobial agent and one that can cause cell lysis or inhibit cell transduction.[33, 74, 85, 87, 90, 133-136]

Moreover, the use of nanomaterials for a variety of biological applications has become an emerging interdisciplinary area of science. Yet, an understanding of how nanomaterials interact with different biological components is still a poorly understood area.[30, 137-139] Comprehension of biologically mimicked and naturally occurring materials can progress to the development of novel nanomaterials, nanodevices and processes with tailored functionalities. Nature itself has derived desired biological and chemical applications using commonly found materials.[140-142] Directions in construction and design of nanomaterials with novel applications can only be achieved by the fundamental understandings of biology at the molecular level. The four main essential bio-macromolecules include nucleic acid, proteins, lipids, and polysaccharides which are made up of nucleotide, amino and fatty acids and sugars.[128, 143]

Though Ag nanoparticles have found use in antibacterial applications, their mode of action on microbes is not fully understood. As the field of bionanotechnology continues to advance, studies on the mechanism of Ag nanoparticles (with respect to their size, shape and composition) interaction with microorganisms are required in order to facilitate nanotechnology for biomedical applications.

The work presented in this thesis emphasises on the synthesis, characterisation and antibacterial activity of Ag nanostructures.

a) Shape-dependent properties of Ag nanoparticles and their potential antibacterial activity (Chapter III).
b) Coupling Ag nanoparticles with conventional antibiotics to increase the antibacterial activity and determine their synergistic effects (Chapter IV).

c) A non-toxic green synthesis of functionalised Ag nanoparticles using phenolic compounds (e.g. phytochemicals or amino acids) to enhance antibacterial activity due to antioxidant corona layers (Chapter V).

d) Investigation of new interdisciplinary techniques to understand the role of surface corona and Ag nanoparticle shape on antibacterial activity (Chapter VI).

1.7 Outline of thesis

In this thesis, the major interest is the antibacterial capabilities of Ag nanoparticles. The synthesis of several Ag nanostructures incorporates the chemical reduction techniques with an end goal of synthesising a material which exhibits antibacterial activity with respect to already available nanomaterials. More importantly, it has been demonstrated that using these chemical routes, a collection of Ag nanomaterials with functional properties can be synthesised in a repeatable process to enhance antibacterial activity.

Chapter II deals with a range of characterisation techniques that were employed in this thesis. As discussed in Chapter III, Ag nanospheres, cubes and prisms were synthesised via different chemical methodologies. Ag nanospheres were synthesised with amino acid tyrosine as a reducing as well as a capping agent, Ag nanocubes were achieved by mediating a polyol process and Ag nanoprisms were synthesised by a seed-based thermal method. The comparison of various shapes of Ag nanoparticles was tested against representative Gram negative and Gram positive bacteria for their antibacterial activity. Tyrosine reduced Ag nanospheres were the most stable as well as isotropic. Additionally these particles were synthesised via a 1:1 ratio of silver stock to the monophenolic tyrosine amino acid which was least complicated. Therefore, these

tyrosine reduced Ag nanoparticles were chosen as model Ag nanoparticles for further studies throughout the thesis.

In Chapter IV, Tyrosine reduced Ag nanoparticles were used as antibiotic carriers for antibacterial activity. Broad and narrow spectrums of antibiotics (ampicillin, penicillin G and polymyxin B) were employed as functional fragments to influence antibacterial potential on the surfaces of Ag nanoparticles. This combination can therefore provide synergistic observations towards antibacterial effects. The measure of synergism was studied and the method of binding was revealed.

Chapter V dealt with the control of surface functionality and composition of nanoparticles using green and eco-friendly synthetic routes. Three different biochemicals including tyrosine, curcumin and epigallocatechin gallate (EGCG) were employed as a reducing and capping agent to synthesise Ag nanoparticles. These biochemicals possess one or multiple phenolic groups and were implemented as organic surface coronas surrounding Ag nanoparticles. Equimolar and various mole ratios of these biochemicals were used according to the number of phenolic groups present in their structure. These nanoparticles were synthesised and tested for their antibacterial activity. The interface of nanoparticles and the correlation between the surface coronas and composition of nanoparticles were studied.

Finally in Chapter VI, to establish the surface coating corona and shape relation to antibacterial activity, interaction of nanoparticles to bacterial membrane protein were studied. Further to understand the effect of different Ag nanoparticles at gene and protein level, genotoxicity and cellular toxicity study was also performed. Mechanistic insight into the antibacterial performance of Ag nanomaterials was also obtained using electrochemistry experiments. The mode of action and toxicity was understood by

electrochemical and biological techniques helped in proposing potential mechanisms of Ag nanostructures and their ability to interact with Gram negative and Gram positive bacterial cells.

Last but not the least, Chapter VII summarises the overall outcome of the thesis and proposes some of the future work that may be built upon the outcomes obtained from this study.

1.8 References

[1] Davies, J.; Davies, D., Origins and evolution of antibiotic resistance. *Microbiology and Molecular Biology Reviews* **2010,** *74* (3), 417-433.

[2] Bax, R.; Griffin, D., Introduction to antibiotic resistance. In *Antibiotic Resistance*, Springer: 2012; pp 1-12.

[3] Eliopoulos, G. M.; Cosgrove, S. E.; Carmeli, Y., The impact of antimicrobial resistance on health and economic outcomes. *Clinical Infectious Diseases* **2003,** *36* (11), 1433-1437.

[4] Walsh, C., *Antibiotics: actions, origins, resistance*. American Society for Microbiology (ASM): 2003.

[5] Allen, H. K.; Donato, J.; Wang, H. H.; Cloud-Hansen, K. A.; Davies, J.; Handelsman, J., Call of the wild: antibiotic resistance genes in natural environments. *Nat. Rev. Microbiol.* **2010,** *8* (4), 251-259.

[6] Neu, H. C., The crisis in antibiotic resistance. *Science* **1992,** *257* (5073), 1064-1073.

[7] Levy, S. B., The challenge of antibiotic resistance. *Scientific American* **1998,** *278* (3), 32-9.

[8] Singer, R. S.; Finch, R.; Wegener, H. C.; Bywater, R.; Walters, J.; Lipsitch, M., Antibiotic resistance—the interplay between antibiotic use in animals and human beings. *The Lancet infectious diseases* **2003,** *3* (1), 47-51.

[9] Phillips, I.; Casewell, M.; Cox, T.; De Groot, B.; Friis, C.; Jones, R.; Nightingale, C.; Preston, R.; Waddell, J., Does the use of antibiotics in food animals pose a risk to human health? A critical review of published data. *Journal of antimicrobial Chemotherapy* **2004,** *53* (1), 28-52.

[10] Turnidge, J., Antibiotic use in animals—prejudices, perceptions and realities. *Journal of Antimicrobial Chemotherapy* **2004,** *53* (1), 26-27.

[11] Gustafson, R.; Bowen, R., Antibiotic use in animal agriculture. *Journal of Applied Microbiology* **1997,** *83* (5), 531-541.

[12] McManus, P. S.; Stockwell, V. O.; Sundin, G. W.; Jones, A. L., Antibiotic use in plant agriculture. *Annual Review of Phytopathology* **2002,** *40* (1), 443-465.

[13] WHO *Antimicrobial resistance: global report on surveillance*; World Health Organization: 2014; p 257.

[14] Butler, M. S.; Blaskovich, M. A.; Cooper, M. A., Antibiotics in the clinical pipeline in 2013. *The Journal of antibiotics* **2013,** *66* (10), 571-591.

[15] Feynman, R. P., There's plenty of room at the bottom. *Engineering and Science* **1960,** *23* (5), 22-36.

[16] Ramsden, J., *Nanotechnology: An introduction*. Elsevier Science: 2011.

[17] Binns, C., *Introduction to nanoscience and nanotechnology*. Wiley: 2010.

[18] Poole, C. P.; Owens, F. J., *Introduction to Nanotechnology*. John Wiley & Sons: 2003.

[19] Sabatier, P. A., Top-down and bottom-up approaches to implementation research: a critical analysis and suggested synthesis. *Journal of public policy* **1986,** *6* (1), 21-48.

[20] Chi, L., *Nanotechnology: Volume 8: Nanostructured surfaces*. John Wiley & Sons: 2010.

[21] Zhi, L.; Müllen, K., A bottom-up approach from molecular nanographenes to unconventional carbon materials. *Journal of Materials Chemistry* **2008,** *18* (13), 1472-1484.

[22] Stankovich, S.; Dikin, D. A.; Dommett, G. H.; Kohlhaas, K. M.; Zimney, E. J.; Stach, E. A.; Piner, R. D.; Nguyen, S. T.; Ruoff, R. S., Graphene-based composite materials. *Nature* **2006,** *442* (7100), 282-286.

[23] Huang, S. H.; Uppal, M.; Shi, J., A product driven approach to manufacturing supply chain selection. *Supply Chain Management: An International Journal* **2002,** *7* (4), 189-199.

[24] Lu, W.; Lieber, C. M., Nanoelectronics from the bottom up. *Nature materials* **2007,** *6* (11), 841-850.

[25] Budi, A.; Basile, A.; Opletal, G.; Hollenkamp, A. F.; Best, A. S.; Rees, R. J.; Bhatt, A. I.; O'Mullane, A. P.; Russo, S. P., Study of the initial stage of solid electrolyte interphase formation upon chemical reaction of lithium metal and N-Methyl-N-Propyl-Pyrrolidinium-Bis (Fluorosulfonyl) Imide. *The Journal of Physical Chemistry C* **2012,** *116* (37), 19789-19797.

[26] Balzani, V.; Credi, A.; Venturi, M., The bottom-up approach to molecular-level devices and machines. *Chem.-Eur. J.* **2002,** *8* (24), 5524-5532.

[27] Smeets, E. M.; Faaij, A. P.; Lewandowski, I. M.; Turkenburg, W. C., A bottom-up assessment and review of global bio-energy potentials to 2050. *Progress in Energy and combustion science* **2007,** *33* (1), 56-106.

[28] Bausch, A.; Kroy, K., A bottom-up approach to cell mechanics. *Nature Physics* **2006,** *2* (4), 231-238.

[29] Guido, N. J.; Wang, X.; Adalsteinsson, D.; McMillen, D.; Hasty, J.; Cantor, C. R.; Elston, T. C.; Collins, J., A bottom-up approach to gene regulation. *Nature* **2006,** *439* (7078), 856-860.

[30] Salata, O. V., Applications of nanoparticles in biology and medicine. *Journal of nanobiotechnology* **2004,** *2* (1), 3.

[31] Sackett, D. L. In *Evidence-based medicine*, Seminars in perinatology, Elsevier: 1997; pp 3-5.

[32] Hanrieder, J.; Nyakas, A.; Naessén, T.; Bergquist, J., Proteomic analysis of human follicular fluid using an alternative bottom-up approach. *Journal of proteome research* **2007,** *7* (01), 443-449.

[33] Chen, X.; Schluesener, H. J., Nanosilver: A nanoproduct in medical application. *Toxicology Letters* **2008,** *176* (1), 1-12.

[34] Solanki, A.; Kim, J. D.; Lee, K.-B., Nanotechnology for regenerative medicine: nanomaterials for stem cell imaging. **2008**.

[35] Goodsell, D. S., *Bionanotechnology: lessons from nature*. John Wiley & Sons: 2004.

[36] Chan, W. C., Bionanotechnology progress and advances. *Biology of Blood and Marrow Transplantation* **2006,** *12* (1), 87-91.

[37] Bellucci, S., *Nanoparticles and nanodevices in biological applications*. Springer: 2009.

[38] Vo-Dinh, T., *Nanotechnology in biology and medicine: methods, devices, and applications*. CRC Press: 2007.

[39] Niemeyer, C. M.; Mirkin, C. A., *Nanobiotechnology: Concepts, applications and perspectives*. Wiley: 2006.

[40] Mirkin, C. A.; Niemeyer, C. M., *Nanobiotechnology II: More concepts and applications*. Wiley: 2007.

[41] Seeman, N. C.; Belcher, A. M., Emulating biology: building nanostructures from the bottom up. *Proceedings of the National Academy of Sciences of the United States of America* **2002,** *99* (Suppl 2), 6451-6455.

[42] Vollath, D., *Nanomaterials: An introduction to synthesis, properties and applications*. Wiley: 2013.

[43] Hench, L. L.; West, J. K., The sol-gel process. *Chem. Rev.* **1990,** *90* (1), 33-72.

[44] Yang, Y.; Matsubara, S.; Xiong, L.; Hayakawa, T.; Nogami, M., Solvothermal synthesis of multiple shapes of silver nanoparticles and their SERS properties. *The Journal of Physical Chemistry C* **2007,** *111* (26), 9095-9104.

[45] Chou, K.-S.; Ren, C.-Y., Synthesis of nanosized silver particles by chemical reduction method. *Materials Chemistry and Physics* **2000,** *64* (3), 241-246.

[46] Thostenson, E. T.; Ren, Z.; Chou, T.-W., Advances in the science and technology of carbon nanotubes and their composites: a review. *Composites science and technology* **2001,** *61* (13), 1899-1912.

[47] Hahn, H., Gas phase synthesis of nanocrystalline materials. *Nanostructured Materials* **1997,** *9* (1), 3-12.

[48] Singh, A.; Viswanath, V.; Janu, V., Synthesis, effect of capping agents, structural, optical and photoluminescence properties of ZnO nanoparticles. *Journal of Luminescence* **2009,** *129* (8), 874-878.

[49] Mann, S., Biomimetic materials chemistry. *Biomimetic Materials Chemistry, by Stephen Mann (Editor), pp. 400. ISBN 0-471-18597-3. Wiley-VCH, November 1995.* **1995,** *1*.

[50] Bansal, V.; Bharde, A.; Ramanathan, R.; Bhargava, S. K., Inorganic materials using "unusual" microorganisms. *Advances in Colloid and Interface Science* **2012,** *179-182* (0), 150-168.

[51] Thakkar, K. N.; Mhatre, S. S.; Parikh, R. Y., Biological synthesis of metallic nanoparticles. *Nanomedicine: Nanotechnology, Biology and Medicine* **2010,** *6* (2), 257-262.

[52] Narayanan, K. B.; Sakthivel, N., Biological synthesis of metal nanoparticles by microbes. *Advances in colloid and interface science* **2010,** *156* (1), 1-13.

[53] Gericke, M.; Pinches, A., Biological synthesis of metal nanoparticles. *Hydrometallurgy* **2006,** *83* (1), 132-140.

[54] Barnes, W. L.; Dereux, A.; Ebbesen, T. W., Surface plasmon subwavelength optics. *Nature* **2003,** *424* (6950), 824-830.

[55] Kelly, K. L.; Coronado, E.; Zhao, L. L.; Schatz, G. C., The optical properties of metal nanoparticles: The influence of size, shape, and dielectric environment. *J. Phys. Chem. B* **2003,** *107* (3), 668-677.

[56] Kamat, P. V., Photophysical, photochemical and photocatalytic aspects of metal nanoparticles. *J. Phys. Chem. B* **2002,** *106* (32), 7729-7744.

[57] Rao, C. R.; Kulkarni, G. U.; Thomas, P. J.; Edwards, P. P., Metal nanoparticles and their assemblies. *Chemical Society Reviews* **2000,** *29* (1), 27-35.

[58] Mody, V. V.; Siwale, R.; Singh, A.; Mody, H. R., Introduction to metallic nanoparticles. *Journal of Pharmacy and Bioallied Sciences* **2010,** *2* (4), 282.

[59] Murphy, C. J.; Sau, T. K.; Gole, A. M.; Orendorff, C. J.; Gao, J.; Gou, L.; Hunyadi, S. E.; Li, T., Anisotropic metal nanoparticles: synthesis, assembly, and optical applications. *The Journal of Physical Chemistry B* **2005,** *109* (29), 13857-13870.

[60] Hiramatsu, H.; Osterloh, F. E., A simple large-scale synthesis of nearly monodisperse gold and silver nanoparticles with adjustable sizes and with exchangeable surfactants. *Chem. Mat.* **2004,** *16* (13), 2509-2511.

[61] Jana, N. R.; Gearheart, L.; Murphy, C. J., Seeding growth for size control of 5-40 nm diameter gold nanoparticles. *Langmuir* **2001,** *17* (22), 6782-6786.

[62] Skrabalak, S. E.; Chen, J.; Sun, Y.; Lu, X.; Au, L.; Cobley, C. M.; Xia, Y., Gold nanocages: synthesis, properties, and applications. *Accounts of chemical research* **2008,** *41* (12), 1587-1595.

[63] Wiley, B.; Sun, Y.; Mayers, B.; Xia, Y., Shape controlled synthesis of metal nanostructures: the case of silver. *Chem. Eur* **2005**, 454-463.

[64] García-Barrasa, J.; López-de-Luzuriaga, J. M.; Monge, M., Silver nanoparticles: synthesis through chemical methods in solution and biomedical applications. *Central European Journal of Chemistry* **2011,** *9* (1), 7-19.

[65] Nair, L. S.; Laurencin, C. T., Silver nanoparticles: Synthesis and therapeutic applications. *J. Biomed. Nanotechnol.* **2007,** *3* (4), 301-316.

[66] Xiong, Y. J.; Xia, Y. N., Shape-controlled synthesis of metal nanostructures: The case of palladium. *Adv. Mater.* **2007,** *19* (20), 3385-3391.

[67] Kim, S.-W.; Park, J.; Jang, Y.; Chung, Y.; Hwang, S.; Hyeon, T.; Kim, Y. W., Synthesis of monodisperse palladium nanoparticles. *Nano Lett.* **2003,** *3* (9), 1289-1291.

[68] Guo, J.; Wang, X.; Xu, B., One-step synthesis of carbon-onion-supported platinum nanoparticles by arc discharge in an aqueous solution. *Mater. Chem. Phys. In Press, Corrected Proof*.

[69] Paschos, O.; Choi, P.; Efstathiadis, H.; Haldar, P., Synthesis of platinum nanoparticles by aerosol assisted deposition method. *Thin Solid Films* **2008,** *516* (12), 3796-3801.

[70] Teng, X.; Liang, X.; Maksimuk, S.; Yang, H., Synthesis of porous platinum nanoparticles. *Small* **2006,** *2* (2), 249-253.

[71] Yu, X.; Li, Y.; Wlodarski, W.; Kandasamy, S.; Kalantar-zadeh, K., Fabrication of nanostructured TiO2 by anodization: A comparison between electrolytes and substrates. *Sensors and Actuators B: Chemical* **2008,** *130* (1), 25-31.

[72] Lee, J.-H.; Choi, H.-S.; Lee, J.-H.; Kim, Y.-J.; Suh, S.-J.; Chi, C.-S.; Oh, H.-J., Fabrication of titania nanotubular film with metal nanoparticles. *J. Cryst. Growth In Press, Corrected Proof*.

[73] Chen, X.; Mao, S. S., Titanium dioxide nanomaterials: synthesis, properties, modifications, and applications. *Chem. Rev.* **2007,** *107* (7), 2891-2959.

[74] Sondi, I.; Salopek-Sondi, B., Silver nanoparticles as antimicrobial agent: a case study on *E-coli* as a model for Gram-negative bacteria. *J. Colloid Interface Sci.* **2004,** *275* (1), 177-182.

[75] Selvakannan, P. R.; Swami, A.; Srisathiyanarayanan, D.; Shirude, P. S.; Pasricha, R.; Mandale, A. B.; Sastry, M., Synthesis of aqueous Au core–Ag shell nanoparticles using tyrosine as a pH-dependent reducing agent and assembling phase-transferred silver nanoparticles at the air–water interface. *Langmuir* **2004,** *20* (18), 7825-7836.

[76] Jana, N.; Gearheart, L.; Murphy, C. J., Wet chemical synthesis of silver nanrods and nanowires of controllable aspect ratio. *The Royal Society of Chemistry* **2001**, 617-618.

[77] Metraux, G. S.; Mirkin, C. A., Rapid thermal synthesis of silver nanoprisms with chemically tailorable thickness. *Adv. Mater.* **2005,** *17* (4), 412-+.

[78] Siekkinen, A. R.; McLellan, J. M.; Chen, J.; Xia, Y., Rapid synthesis of small silver nanocubes by mediating polyol reduction with a trace amount of sodium sulfide or sodium hydrosulfide. *Chemical Physics Letters* **2006,** *432* (4-6), 491-496.

[79] Smetana, A. B. Gram quantities of Silver and alloy nanoparticles: Synthesis through digestive ripening and the solvated metal atom dispersion (SMAD) method: Antimicobial properties, superlatteic self-assembly, and optical properties. Kansas State University, Manhattan, 2006.

[80] Eastman, C. M. Preparation and characterization of highly concentrated dispersions of uniform silver nanoparticles. CLARKSON UNIVERSITY, 2006.

[81] Eastman, C. M. Preparation and characterization of highly concentrated dispersions of uniform silver nanoparticles. Master, Clarkson University, 2005.

[82] Atiyeh, B. S.; Costagliola, M.; Hayek, S. N.; Dibo, S. A., Effect of silver on burn wound infection control and healing: review of the literature. *burns* **2007,** *33* (2), 139-148.

[83] Tian, J.; Wong, K. K.; Ho, C. M.; Lok, C. N.; Yu, W. Y.; Che, C. M.; Chiu, J. F.; Tam, P. K., Topical delivery of silver nanoparticles promotes wound healing. *ChemMedChem* **2007,** *2* (1), 129-136.

[84] Melaiye, A.; Youngs, W. J., Silver and its application as an antimicrobial agent. *Expert Opinion on Therapeutic Patents* **2005,** *15* (2), 125-130.

[85] Kim, J. S.; Kuk, E.; Yu, K. N.; Kim, J. H.; Park, S. J.; Lee, H. J.; Kim, S. H.; Park, Y. K.; Park, Y. H.; Hwang, C. Y.; Kim, Y. K.; Lee, Y. S.; Jeong, D. H.; Cho, M. H., Antimicrobial effects of silver nanoparticles. *Nanomed.-Nanotechnol. Biol. Med.* **2007,** *3* (1), 95-101.

[86] Li, P.; Li, J.; Wu, C.; Wu, Q.; Li, J., Synergistic antibacterial effects of β-lactam antibiotic combined with silver nanoparticles. *Nanotechnology* **2005,** *16* (9), 1912.

[87] Rai, M.; Yadav, A.; Gade, A., Silver nanoparticles as a new generation of antimicrobials. *Biotechnol. Adv.* **2009,** *27* (1), 76-83.

[88] Rosi, N. L.; Mirkin, C. A., Nanostructures in biodiagnostics. *Chem. Rev.* **2005,** *105* (4), 1547-1562.

[89] Pal, S.; Tak, Y. K.; Song, J. M., Does the antibacterial activity of silver nanoparticles depend on the shape of the nanoparticle? A study of the Gram-negative bacterium *Escherichia coli*. *Appl. Environ. Microbiol.* **2007,** *73* (6), 1712-1720.

[90] Raffi, M.; Hussain, F.; Bhatti, T.; Akhter, J.; Hameed, A.; Hasan, M., Antibacterial characterization of silver nanoparticles against *E. coli* ATCC-15224. *Journal of Materials Science and Technology* **2008,** *24* (2), 192-196.

[91] Choi, O.; Deng, K. K.; Kim, N.-J.; Ross Jr, L.; Surampalli, R. Y.; Hu, Z., The inhibitory effects of silver nanoparticles, silver ions, and silver chloride colloids on microbial growth. *Water research* **2008,** *42* (12), 3066-3074.

[92] Ahamed, M.; Karns, M.; Goodson, M.; Rowe, J.; Hussain, S. M.; Schlager, J. J.; Hong, Y., DNA damage response to different surface chemistry of silver nanoparticles in mammalian cells. *Toxicology and Applied Pharmacology* **2008,** *233* (3), 404-410.

[93] Jeng, H. A.; Swanson, J., Toxicity of metal oxide nanoparticles in mammalian cells. *Journal of Environmental Science and Health Part A* **2006,** *41* (12), 2699-2711.

[94] Hussain, S.; Hess, K.; Gearhart, J.; Geiss, K.; Schlager, J., In vitro toxicity of nanoparticles in BRL 3A rat liver cells. *Toxicology in vitro* **2005,** *19* (7), 975-983.

[95] Lewinski, N.; Colvin, V.; Drezek, R., Cytotoxicity of nanoparticles. *Small* **2008,** *4* (1), 26-49.

[96] Ahamed, M.; AlSalhi, M. S.; Siddiqui, M., Silver nanoparticle applications and human health. *Clinica chimica acta* **2010,** *411* (23), 1841-1848.

[97] Shahverdi, A. R.; Fakhimi, A.; Shahverdi, H. R.; Minaian, S., Synthesis and effect of silver nanoparticles on the antibacterial activity of different antibiotics against Staphylococcus aureus and Escherichia coli. *Nanomedicine: Nanotechnology, Biology and Medicine* **2007,** *3* (2), 168-171.

[98] Wolska, K. I.; Grzes, K.; Kurek, A., Synergy between novel antimicrobials and conventional antibiotics or bacteriocins. *Polish Journal of Microbiology* **2012,** *61* (2), 95-104.

[99] Naqvi, S. Z. H.; Kiran, U.; Ali, M. I.; Jamal, A.; Hameed, A.; Ahmed, S.; Ali, N., Combined efficacy of biologically synthesized silver nanoparticles and different antibiotics against multidrug-resistant bacteria. *International journal of nanomedicine* **2013,** *8*, 3187.

[100] Sekhon, B. S., Metalloantibiotics and antibiotic mimics—an overview. *Journal of Pharmaceutical Education and Research* **2010,** *1* (1), 1-20.

[101] Allahverdiyev, A. M.; Kon, K. V.; Abamor, E. S.; Bagirova, M.; Rafailovich, M., Coping with antibiotic resistance: combining nanoparticles with antibiotics and other antimicrobial agents. *Expert Review of Anti-infective Therapy* **2011,** *9* (11), 1035-1052.

[102] Che, C.-M.; Siu, F.-M., Metal complexes in medicine with a focus on enzyme inhibition. *Current opinion in chemical biology* **2010,** *14* (2), 255-261.

[103] Yu, J.; Patel, S. A.; Dickson, R. M., In vitro and intracellular production of peptide-encapsulated fluorescent silver nanoclusters. *Angewandte Chemie* **2007,** *119* (12), 2074-2076.

[104] Durán, N.; Marcato, P. D.; Durán, M.; Yadav, A.; Gade, A.; Rai, M., Mechanistic aspects in the biogenic synthesis of extracellular metal nanoparticles by peptides, bacteria, fungi, and plants. *Appl. Microbiol. Biotechnol.* **2011,** *90* (5), 1609-1624.

[105] Waldron, K. J.; Robinson, N. J., How do bacterial cells ensure that metalloproteins get the correct metal? *Nat. Rev. Microbiol.* **2009,** *7* (1), 25-35.

[106] Daima, H. K.; Selvakannan, P.; Kandjani, A. E.; Shukla, R.; Bhargava, S. K.; Bansal, V., Synergistic influence of polyoxometalate surface corona towards enhancing the antibacterial performance of tyrosine-capped Ag nanoparticles. *Nanoscale* **2014**.

[107] Quaroni, L.; Chumanov, G., Preparation of polymer-coated functionalized silver nanoparticles. *J. Am. Chem. Soc.* **1999,** *121* (45), 10642-10643.

[108] Cao, Y.; Jin, R.; Mirkin, C. A., DNA-modified core-shell Ag/Au nanoparticles. *J. Am. Chem. Soc.* **2001,** *123* (32), 7961-7962.

[109] Caruso, F., Nanoengineering of particle surfaces. *Adv. Mater.* **2001,** *13* (1), 11-22.

[110] Gaspard, J., Physisorption and chemisorption. In *Interfacial Aspects of Phase Transformations*, Springer: 1982; pp 103-118.

[111] Wang, X.; Liu, L.-H.; Ramström, O.; Yan, M., Engineering nanomaterial surfaces for biomedical applications. *Experimental Biology and Medicine* **2009,** *234* (10), 1128-1139.

[112] Niemann, M. U.; Srinivasan, S. S.; Phani, A. R.; Kumar, A.; Goswami, D. Y.; Stefanakos, E. K., Nanomaterials for hydrogen storage applications: a review. *Journal of Nanomaterials* **2008,** *2008*.

[113] Prescott, L. M.; Harley, J. P.; Klein, D. A., *Microbiology*. Boston, Mass: USA, 1999.

[114] Brogden, K. A., Antimicrobial peptides: pore formers or metabolic inhibitors in bacteria? *Nat. Rev. Microbiol.* **2005,** *3* (3), 238-250.

[115] Eckhardt, S.; Brunetto, P. S.; Gagnon, J.; Priebe, M.; Giese, B.; Fromm, K. M., Nanobio Silver: Its Interactions with Peptides and Bacteria, and Its Uses in Medicine. *Chem. Rev.* **2013**.

[116] Favor, L. J., *Bacteria*. Rosen Publishing Group: 2004.

[117] Beveridge, T. J., Use of the Gram stain in microbiology. *Biotechnic & Histochemistry* **2001,** *76* (3), 111-118.

[118] Gram, H., Uber die isolirte farbung der schizomyceten in schnitt-und trocken. *Fortschritte der Medizin* **1884,** *2*, 185-189.

[119] Salton, M., The relationship between the nature of the cell wall and the Gram stain. *Journal of general microbiology* **1963,** *30* (2), 223-235.

[120] Pommerville, J. C., *Fundamentals of microbiology*. Jones & Bartlett Learning: 2013.

[121] Garrett, R.; Grisham, C., *Biochemistry*. Cengage Learning: 2012.

[122] Wearing, J., *Bacteria: Staph, Strep, Clostridium, and other bacteria*. Crabtree Publishing Company: 2010.

[123] Fey, P. D.; Olson, M. E., Current concepts in biofilm formation of *Staphylococcus epidermidis*. *Future microbiology* **2010,** *5* (6), 917-933.

[124] O'gara, J. P.; Humphreys, H., Staphylococcus epidermidis biofilms: importance and implications. *J. Med. Microbiol.* **2001,** *50* (7), 582-587.

[125] Donnenberg, M. S., *Escherichia Coli: Virulence mechanisms of a versatile pathogen*. Academic Press: 2002.

[126] O'Brien, A. D.; Holmes, R. K., Shiga and Shiga-like toxins. *Microbiological Reviews* **1987,** *51* (2), 206.

[127] Boerlin, P.; McEwen, S. A.; Boerlin-Petzold, F.; Wilson, J. B.; Johnson, R. P.; Gyles, C. L., Associations between virulence factors of Shiga toxin-producing Escherichia coli and disease in humans. *Journal of Clinical Microbiology* **1999,** *37* (3), 497-503.

[128] Langer, R.; Tirrell, D. A., Designing materials for biology and medicine. *Nature* **2004,** *428* (6982), 487-492.

[129] Giljohann, D. A.; Seferos, D. S.; Daniel, W. L.; Massich, M. D.; Patel, P. C.; Mirkin, C. A., Gold nanoparticles for biology and medicine. *Angewandte Chemie International Edition* **2010,** *49* (19), 3280-3294.

[130] Jain, P. K.; Huang, X.; El-Sayed, I. H.; El-Sayed, M. A., Noble metals on the nanoscale: optical and photothermal properties and some applications in imaging, sensing, biology, and medicine. *Accounts of Chemical Research* **2008,** *41* (12), 1578-1586.

[131] Singh, M.; Singh, S.; Prasad, S.; Gambhir, I., Nanotechnology in medicine and antibacterial effect of silver nanoparticles. *Digest J. Nanomater. Biostructures* **2008,** *3* (3), 115-122.

[132] Kim, B. Y.; Rutka, J. T.; Chan, W. C., Nanomedicine. *New England Journal of Medicine* **2010,** *363* (25), 2434-2443.

[133] Li, W. R.; Xie, X. B.; Shi, Q. S.; Zeng, H. Y.; Ou-Yang, Y. S.; Chen, Y. B., Antibacterial activity and mechanism of silver nanoparticles on *Escherichia coli*. *Appl. Microbiol. Biotechnol.* **2010,** *85* (4), 1115-1122.

[134] Ip, M.; Lui, S. L.; Poon, V. K. M.; Lung, I.; Burd, A., Antimicrobial activities of silver dressings: an in vitro comparison. *J. Med. Microbiol.* **2006,** *55* (1), 59-63.

[135] Lara, H. H.; Ayala-Nunez, N. V.; Turrent, L. D. I.; Padilla, C. R., Bactericidal effect of silver nanoparticles against multidrug-resistant bacteria. *World J. Microbiol. Biotechnol.* **2010,** *26* (4), 615-621.

[136] Prabhu, S.; Poulose, E. K., Silver nanoparticles: mechanism of antimicrobial action, synthesis, medical applications, and toxicity effects. *International Nano Letters* **2012,** *2* (1), 1-10.

[137] Kane, R. S.; Stroock, A. D., Nanobiotechnology: Protein-nanomaterial interactions. *Biotechnol. Prog.* **2007,** *23* (2), 316-319.

[138] Nel, A. E.; Mädler, L.; Velegol, D.; Xia, T.; Hoek, E. M.; Somasundaran, P.; Klaessig, F.; Castranova, V.; Thompson, M., Understanding biophysicochemical interactions at the nano–bio interface. *Nature materials* **2009,** *8* (7), 543-557.

[139] Sarikaya, M.; Tamerler, C.; Jen, A. K.-Y.; Schulten, K.; Baneyx, F., Molecular biomimetics: nanotechnology through biology. *Nature materials* **2003,** *2* (9), 577-585.

[140] Yoshida, M.; Lahann, J., Smart nanomaterials. *ACS nano* **2008,** *2* (6), 1101-1107.

[141] Wang, P.; Wei, G.; Liu, X.; Ma, P. X., Bio-inspired nanomaterials. In *Scanning Microscopy for Nanotechnology*, Springer: 2007; pp 427-466.

[142] Rao, C. N. R.; Müller, A.; Cheetham, A. K., *Nanomaterials chemistry: recent developments and new directions*. John Wiley & Sons: 2007.

[143] You, C.-C.; Chompoosor, A.; Rotello, V. M., The biomacromolecule-nanoparticle interface. *Nano today* **2007,** *2* (3), 34-43.

Chapter II

Characterisation Techniques

2.1 Introduction

The study of nanoparticles in general and metal nanoparticles in particular is made possible only through the use of the latest technological discoveries in instrumentation techniques. High resolution electron microscopy allows scientists in this field to explore the structure, size, and shape of nanosized objects, with the latest instruments being able to resolve individual atoms and give information on the atomic structure of the crystal structure.[1] Even more impressive are spectroscopy probes that can be used in situ in the electron microscope to provide insight into the elemental composition and even chemical nature of the atoms within the particles themselves.

The main emphasis of this thesis is to develop Ag nanostructures and investigate their biological applications. Prior to antibacterial applications, all nanomaterials used in this thesis were characterised by Fourier transform infrared (FTIR) spectroscopy, X-ray photoelectron spectroscopy (XPS), UV-Visible absorption spectroscopy (UV-Vis), atomic absorption spectroscopy (AAS), transmission electron microscopy (TEM), scanning electron microscopy (SEM), dynamic light scattering (DLS) and X-ray diffraction (XRD) using general area detector diffraction system (GADDS).

This chapter is devoted to the physical principles and instrumentation of the various characterisation techniques used in this thesis which have been elaborated further below.

2.2 Fourier transform infrared spectroscopy (FTIR)

Fourier transform infrared spectroscopy is a vibrational spectroscopy technique that involves photons that induce transitions between vibrational states in molecules and solids. The infrared region of the electromagnetic spectrum broadens from 14,000 cm^{-1} to 10 cm^{-1}. The region of most significance for chemical analysis is between 4,000 cm^{-1} to 400 cm^{-1} which is known as the mid-infrared region. This region corresponds to changes in vibrational energies within molecules. As an infrared light beam interacts with the molecule, chemical bonds will stretch, contract and/or bend.[2]

In infrared spectroscopy, an IR photon hv is absorbed directly to induce a transition between two vibrational levels, E_n and $E_{n'}$, where

$$E_n = \left(n + \frac{1}{2}\right) h\nu_0 \tag{2.1}$$

The vibrational quantum number n= 0,1,2,... is a positive integer and v_0 is the characteristic frequency for a particular normal mode. In accordance with the selection rule $\Delta n = \pm 1$, infrared transitions are observed only between adjacent vibrational energy levels, hence have the frequency v_0.[2]

The classical method to perform infrared spectroscopy is to scan the frequency of the incoming light to enable the detector to record changes in the light intensity for those frequencies at which the sample absorbs energy. However, a major disadvantage of this method is that the detector cannot record any data. To overcome this deficiency, modern infrared spectrometers irradiate the sample with an extensive band of frequencies

simultaneously followed by a mathematical analysis of the signal output. This is called a *Fourier transformation*, where it is used to convert the detected signal back into the classical form of the spectrum. Thus the resulting signal is known as a Fourier transform infrared (FTIR) spectrum.

In contrast to classical spectrometers, where the spectral absorption of a sample is being scanned, FTIR spectroscopy is an interferometric method. A FTIR spectrometer consists in principle of an infrared source, an interferometer, the sample, and the infrared detector.

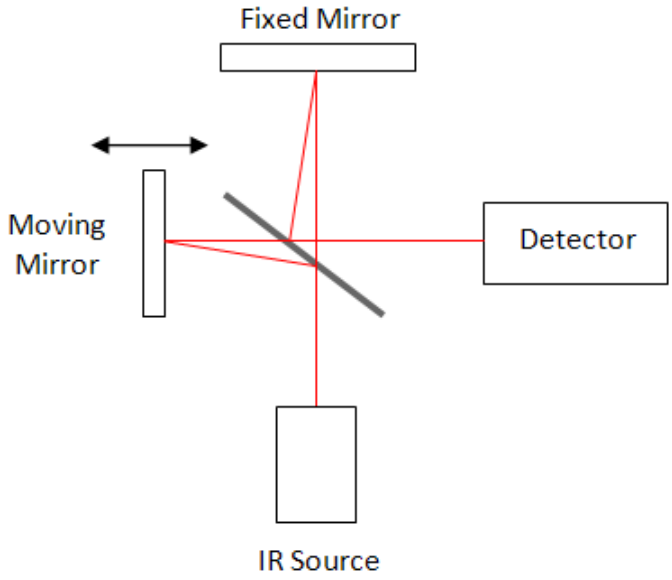

Figure 2.1- Schematic of a Fourier transform infrared spectrometer.

FTIR spectrometer attains infrared spectra by obtaining an interferogram of a sample signal with an interferometer. The interferometer is the heart of the spectrometer and consists of a beam splitter, a permanent mirror, and a moving mirror scanning back and forth. Hence, the spectrum is not directly measured but its interferogram is. This is when the infrared intensity reaches the detector as a function of the mirror position, as shown in Figure 2.1.

2.2.1 Attenuated total reflection infrared spectroscopy (ATR-IR)

Attenuated total reflection infrared (ATR-IR) spectroscopy is employed for the analysis of the surface of materials. It is also often suitable for characterisation of materials which are too condensed to be analysed by transmission spectroscopy. The experimental setup of the internal reflection technique is shown in Figure 2.2.

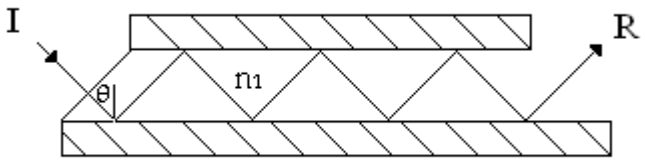

Figure 2.2- Attenuated total reflection experimental setup.

For ATR-IR, the infrared light passes through an optically dense crystal and reflects at the surface of the sample. According to Maxwell's theory, the propagating light passing through an optically thin, non-absorbing medium forms a standing wave, perpendicular to that of the total reflecting surface.[3] When the sample absorbs a fraction of this radiation, the propagating wave interacts with the sample and becomes attenuated. The reflectance *R* of the attenuated wave can be expressed as:

$$R = 1 - kd_e \tag{2.2}$$

Where d_e is the effective layer thickness and k is absorptivity of the layer. The loss of energy in the refractive wave is identified as *attenuated total reflectance*.

The depth of penetration of the IR radiation into the sample is dependent upon the angle of incidence, the frequency of incident light and refractive index difference between ATR element and the sample. The depth of penetration d_p is expressed by:

$$dp = \frac{\lambda_0}{2\pi_{n1}\left(\sin^2\theta - n^2{}_{21}\right)^{1/2}} \tag{2.3}$$

Where λ_0 is the wavelength of light in the internal reflection crystal, θ is the angle of incidence, and n_{21} is the reflective index ratio of the sample and crystal.

Characterisation of silver nanoparticles was achieved by using Perkin Elmer Spectrum 100 to define functional groups present. An initial background for energy match was run at 16 scans per spectrum. Spectra were obtained by accumulating 16 scans per spectrum in the ranges from 4000 cm^{-1} to 850 cm^{-1}.

2.3 X-ray photoelectron spectroscopy (XPS)

X-ray photoelectron spectroscopy (XPS) provides chemical information regarding the surface of a specimen. The XPS functions by bombarding a surface with x-rays and recording the energy of ejected electrons. These characteristic electrons are ejected from the top most layers of the surface, typically nanometres in depth, and are used to identify the source element and immediate environment of components. Thus the energy of electrons measured at the detector is used to distinguish which elements are present and how they are bound. This is described by binding energy (BE) in an XPS spectrum.[4]

When an x-ray of known energy $h\nu$ interacts with a surface, an electron is described as being ejected assigned E_B (binding energy) giving the following equation observing the conservation of energy:[4]

$$E_K = h\nu - E_B - E_W \qquad (2.4)$$

Where E_W is the work function of the x-ray photoelectron spectrometer, and not of the material. Equation 2.4 can thus be used to elucidate the element detected and the chemical nature in which it resides.

2.4 Ultraviolet visible spectroscopy (UV-Vis)

Ultraviolet-Visible spectroscopy (UV-Vis) is a reliable and accurate analytical technique that allows for the quantitative analysis of a material. Specifically, UV-Vis measures the absorption, transmission and emission of ultraviolet and visible light wavelengths by matter.[5]

When a beam of electromagnetic radiations strikes an object, it can be absorbed, transmitted, scattered, reflected or excite fluorescence. The processes of interest in the absorption spectroscopy are absorption and transmission. When a sample is observed for absorption, conditions are undertaken to maintain reflection, scatter and fluorescence to a minimum.[6] An optical spectrometer records the wavelengths at which absorption occurs as well as the degree of absorption at each wavelength. The energy associated with a given fragment of the spectrum is proportional to its frequency. The following equation depicts this correlation, which provides the energy carried by a photon of a given wavelength of radiation.

$$E = h\nu = \frac{hc}{\lambda} \tag{2.5}$$

Where E is the energy absorbed in an electronic transition, h is the Planck's constant, c is the speed of light and λ is the wavelength of the incident photon.

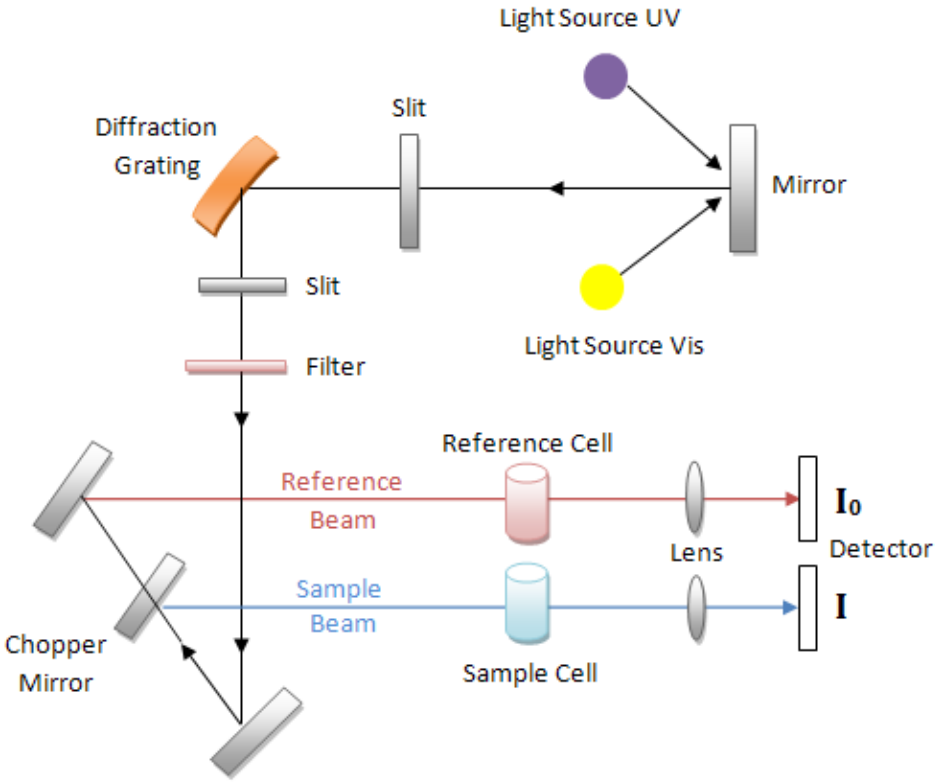

Figure 2.3- Components of a typical UV-Vis spectrometer.

The absorption of radiation in a sample follows the Beer-Lambert law which states that the concentration of a substance in a sample (thin film/solution) is directly proportional to the absorbance, *A*. As shown in the schematics of a spectrophotometer in Figure 2.3. I_0 is the intensity of the incident light at a given wavelength and I is the transmitted intensity.

$$A = -\log_{10}\left(\frac{I}{I_0}\right) \tag{2.6}$$

As part of this research, Varian UV-Visible Spectrophotometer Cary 50 BIO was used for optical characterization. The operating range of the equipment was 190-1000 nm, although in this work it was used to scan samples in the wavelength of 300-800 nm at a scan speed of 480 nm/min.

2.4.1 Surface plasmon resonance (SPR)

Surface plasmons are essentially the light waves that are trapped on the surface due to interactions with free electrons of the metal.[7] When metal nanoparticles are implanted in a dielectric medium and specimen are exposed to electromagnetic radiation, SPR absorption band is observed at a specific wavelength (Figure 2.4). This is chiefly dependent upon the nature of the metal, size and distribution of the particles including several other factors.[6]

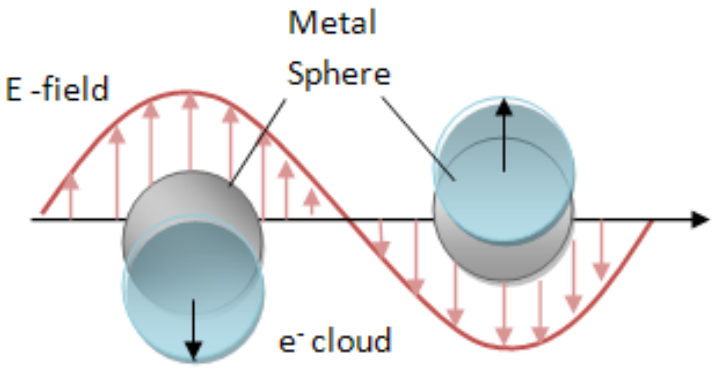

Figure 2.4- Schematic of SPR spectroscopy.

As the size of a particle is increased, the greater the number of electrons are involved, which will possess less displacement from the nuclear framework. If the formation of the particle is altered from a spherical shape, separate responses of the electrons for different directions of oscillation are apparent.[8] Therefore, SPR is found to be dependent on the size, shape and environment of particles. It can be used to determine size dispersity of particles in solution. A strong narrow absorption is representative of similar particles, while a broader, weaker band will be the result of the contribution of many particles over a large size distribution.[9-11]

2.5 Atomic absorption spectroscopy (AAS)

Atomic absorption spectroscopy (AAS) is an analytical procedure for the qualitative detection and quantitative determination of elements through the absorption of optical radiation by free atoms in the gas phase.[12]

Atomic absorption obeys the Beer Lambert law, which states that absorbance (denoted as *A,* negative logarithm of the transmission factor) is proportional to the concentration *c* of the absorbing substance and the thickness *d* of the absorbing layer:

$$A = -\log \frac{\phi_t(\lambda)}{\phi_i(\lambda)} = kcd \qquad (2.7)$$

Where Φ_t is the power of transmitted radiation and Φ_i is the power of incident radiation. Concentrations of samples were determined by Perkin Elmer Atomic Absorption Spectrometer 3110 (Cary 1).

2.6 Electron microscopy

Spectroscopic techniques can provide information on chemical nature of nanostructures, however, direct imagining of specimens can only be made possible via electron microscopes- transmission and scanning electron microscopes. Similar to light microscopy, where the resolution of the acquired image is dependent on the wavelength of light, electron microscopes uses beam of electrons to create such image. It is capable of much higher magnifications and has a greater resolving power than that of a light microscope, allowing one to see much smaller specimens in finer detail.

2.6.1 Transmission electron microscopy (TEM)

Transmission electron microscopy, as a high spatial resolution structure and chemical microanalysis tool, has proven to be powerful for the characterization of nanomaterials.[13] TEM explore the internal structure of solids to provide an

understanding of morphological fine structural details. A modern TEM provides the capability to directly image atoms in crystalline specimens at resolutions close to 0.1 nm, which is of the order of interatomic distances.

Electron beam instruments are operated under high vacuum to avoid dispersion of electrons from the air molecules due to high voltage. A TEM is operated under vacuum, equipped with an electron gun capable of accelerating electrons through a potential difference in the range of 60 to 400kV.

2.6.1.1 Image formation

TEM is simplified into a single-lens microscope, as shown in Figure 2.6, in which only a single objective lens is considered for imaging. The intermediate lenses and projection lenses are omitted. This is due to the resolution of the TEM being primarily determined by the objective lens.[14] The entrance surface of a thin foil specimen is illuminated by a parallel beam. The electron beam is diffracted by the lattices of the crystal, forming the Bragg beams that are propagated along different directions.[15] The electron interaction results in phase and amplitude changes in the electron wave that are determined by quantum mechanical diffraction theory.[16]

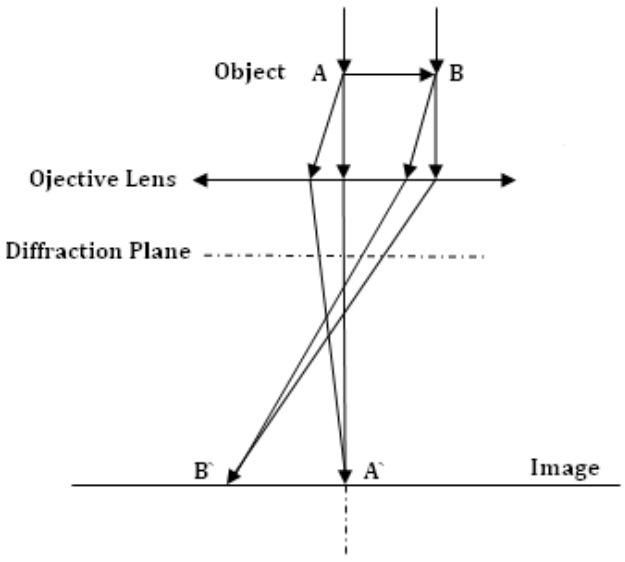

Figure 2.5- Schematic of a single-lens transmission electron microscope.

All TEM images in this thesis were obtained using a JEOL-1010 TEM operating at an accelerating voltage of 100kV. Samples were prepared by drop casting sample onto strong carbon coated 200 mesh copper grids and allowed to evaporate before TEM imaging.

2.6.2 Scanning electron microscope (SEM)

Scanning electron microscope provides observation and characterisation of heterogeneous organic and inorganic materials on a nanometre (nm) to micrometre (μm) scale. Similar to the TEM, electrons are used to form an image. The SEM has many advantages over traditional microscopes, by means of a larger depth of field, which allows more of a specimen to be focused at one time and the capability of obtaining three-dimensional images that are high in resolution. Additionally, closely spaced specimens can be magnified at higher levels with more control with the use of electromagnets rather than lenses.

When a specimen is irradiated with a finely focused electron beam, electrons may be swept in a raster pattern across the surface of the specimen to form images or may be static to obtain an analysis at one position. The types of signals producing this interaction include secondary and backscattering electrons, characteristic x-rays and photons of various energies.[17]

The imaging signals of greatest significance are the secondary and backscattered electrons as they vary primarily as a result of differences in surface topography. The secondary electron emission are the main means of viewing images in the SEM. Secondary electrons are predominately formed by collisions with the nucleus where substantial energy loss occurs or by the ejection of loosely bound electrons from the specimen atoms. The incident electron causes electrons to be emitted from the specimen

due to elastic and inelastic scattering interaction within the surface. High energy electrons that are ejected by an elastic collision of an incident electron are referred to backscattered electrons.[18]

SEM images presented within this thesis were obtained by using Philips XL30 SEM. Samples were drop cast on polished silicon wafers attached to SEM stub via carbon tape. The samples were then coated with a thin layer of platinum deposition via precision etching coating system (PECS), Gratan model 682 to minimise sample charging. The coatings were prepared at a rock angle of 20°, speed 40°/sec, rotation of 25 rpm and beam current of 5 KeV.

2.7 Dynamic light scattering (DLS)

Dynamic light scattering, also referred to as photon correlation spectroscopy is one of the most common techniques used for measuring the size distribution profile of colloidal particles. DLS measures Brownian motion and relates this to the size of the particles. Brownian motion is the random movement of particles due to the bombardment by the surrounding solvent molecules. Generally, DLS is correlated with the measurement of particles suspended within a liquid sample.

The larger the particle, the Brownian motion is slower and the smaller particles move rapidly by solvent molecules. Additionally, an accurately known temperature is crucial for DLS as knowledge of the viscosity is required. Temperature needs to be constant otherwise convection currents in the sample will cause non-random movements that will interrupt the correct interpretation of the size. The velocity of the Brownian motion is defined by a property known as the translational diffusion coefficient.[19, 20]

The size of a particle is calculated from the translation diffusion coefficient using the Stokes-Einstein equation:

$$d(H) = \frac{kT}{3\pi\eta D} \tag{2.8}$$

Where d(H) is the hydrodynamic diameter, d is the translational diffusion coefficient, k is Boltzmann's constant, T is absolute temperature and η is the viscosity.

The diameter measured in DLS is a value that refers to how a particle diffuses within the fluid and is referred to as a hydrodynamic diameter. The diameter obtained by this technique is the diameter of a sphere that has the same translational diffusion coefficient as the particle.

The translational diffusion coefficient is determined by not only the size of the core of the particle, but also on any surface structure as well as the concentration and type of ions in the medium. Factors that affect the diffusion speed of particles are ionic strength of medium, surface structure and non-spherical particles. Therefore, the hydrodynamic diameter measured in DLS can often be larger than that measured by electron microscopy.

All DLS measurements were carried out on an ALV 5022F Fast DLS particle sizing spectrometer at 22°C with a fixed angle of 90° on highly diluted aqueous samples.

2.8 X-ray diffraction (XRD) via general area detector diffraction system (GADDS)

X-ray diffraction (XRD) is a versatile, non-destructive technique that reveals in-depth information regarding the chemical composition and crystallographic structure of an unknown material.

When an X-ray beam interacts with an atom, radiation striking the material may be scattered or absorbed. X-rays, high energy electrons and neutrons are used to extract structural information of the crystal lattice. Incident radiations of sufficiently smaller

wavelength interact elastically with the regular arrays of atoms in a crystal lattice to yield a diffraction pattern.[21] Diffraction angles and the intensities in various diffracted beams are a receptive function of the crystal structure. The diffracted angles are dependent upon the lattice and the unit cell dimensions, while the diffracted intensities are dependent upon the atomic numbers of the constituent atoms and geometrical relationship with the lattice points.

A convenient form of the geometrical relationship determining the angular distribution of the peak intensities in the diffraction pattern is the Bragg's equation:[22]

$$n\lambda = 2d \sin\theta \tag{2.9}$$

Where n is an integer referring to the order of reflection, λ is wavelength of the radiation, d is the spacing between crystal lattice planes and θ is the angle of the incident beam.

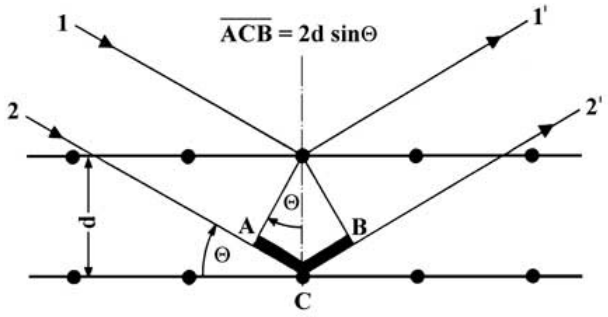

Figure 2.6- Schematic of Bragg's reflection from a crystal.

An X-ray diffractometer comprises of a source of X-rays, the X-ray generator, a diffractometer assembly, X-ray data collection and analysis system. The diffractometer assembly controls the alignment of the beam and the position and orientation of the specimen and detector.

2.8.1 General area detector diffraction system

GADDS is a micro X-ray diffraction system which utilizes a high sensitivity 2D area detector. GADDS has the capability to analyse a selected spot on the surface of a sample, where the instrument focuses an x-ray beam to a spot as small as 60 μm.[23] Samples are usually fixed on a moveable x,y,z stage and for the investigation of a specific area, the sample is orientated in the x-ray beam via a CAD camera and a laser beam.

Powder XRD data was obtained using Bruker Axis D8 Advance Powder Diffractometer with a GADDS micro diffraction instrument over a 2θ range of 15-85°.

2.9 Electrochemical studies using cyclic voltammetry

The oxidation and reduction involving electron transfer can be described as follows:

$$O + ne^- \longleftrightarrow R \tag{2.10}$$

where *O* is the oxidant and *R* is the reductant losing and gaining n electrons, *e*. However the more accurate definition of a REDOX reaction is a change in oxidation state with oxidants increasing whilst reductants decrease which occurs in covalent reactions where no electron transfer takes place.[24] Cyclic voltammetry (CV) techniques can be utilised to probe these REDOX reactions using a three-electrode conventional setup. This setup includes a working electrode, a reference electrode and a counter electrode with particular functions. The working electrode acts to probe the REDOX chemistry of an analyte by applying a potential whilst the reference electrode is a half-cell with a known stable potential and is used to reference said applied potential. A counter electrode is a stable material which is used to complete the current circuit with the working electrode. The current is measured between the working and counter electrodes, while the potential between the working and reference electrodes is applied.

When carrying out a cyclic voltammogram (CV), an initial potential is applied to the working electrode and is ramped positively at a sweep rate of 50 mV s^{-1} to a predetermined switching potential, at which the ramping direction is reversed. This is illustrated in Figure 2.7 where (A) shows the potential ramping profile whilst (B) shows the corresponding CV (current response) to the profile.[25]

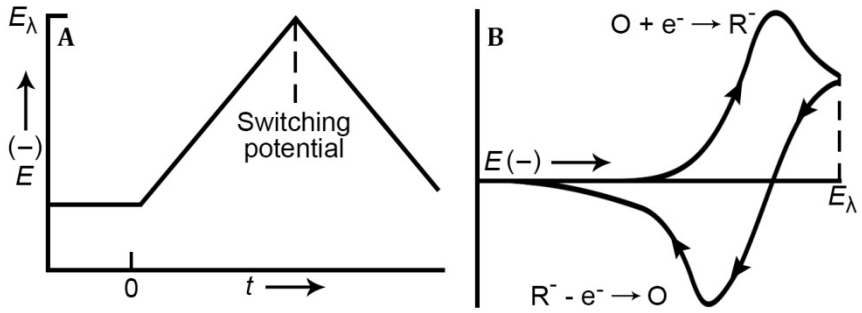

Figure 2.7- (A) Applied potential regime and (B) the corresponding cyclic voltammogram.

2.10 References

[1] Smetana, A. B. Gram quantities of Silver and alloy nanoparticles: Synthesis through digestive ripening and the solvated metal atom dispersion (SMAD) method: Antimicobial properties, superlatteic self-assembly, and optical properties. Kansas State University, Manhattan, 2006.

[2] Poole, C. P.; Owens, F. J., *Introduction to Nanotechnology*. Wiley: 2003; p 388.

[3] Urban, M. W., *Vibrational spectroscopy of molecules and macromolecules on surfaces* Wiley- Interscience: New York, 1993; p 384.

[4] Prutton, M.; Prutton, M., *Introduction to surface physics*. Clarendon Press Oxford: 1994.

[5] Thomas, M. J. K., *Ultraviolet and Visible Spectroscopy: Analytical Chemistry by Open Learning* 2nd ed.; Wiley: U.S.A, 1996.

[6] Raffi, M. Synthesis and Characterization of Metal Nanoparticles. Pakistan Institute Engineering and Applied Sciences, 2007.

[7] Barnes, W. L.; Dereux, A.; Ebbesen, T. W., Surface plasmon subwavelength optics. *Nature* **2003,** *424* (6950), 824-830.

[8] Mulvaney, P., Surface plasmon spectroscopy of nanosized metal particles. *Langmuir* **1996,** *12* (3), 788-800.

[9] Gollub, J. N.; Smith, D. R.; Vier, D. C.; Perram, T.; Mock, J. J., Experimental characterization of magnetic surface plasmons on metamaterials with negative permeability. *Phys. Rev. B* **2005,** *71* (19), 7.

[10] Taleb, A.; Petit, C.; Pileni, M. P., Optical properties of self-assembled 2D and 3D superlattices of silver nanoparticles. *Journal of Physical Chemistry B* **1998,** *102* (12), 2214-2220.

[11] Hutter, E.; Fendler, J. H., Exploitation of localized surface plasmon resonance. *Adv. Mater.* **2004,** *16* (19), 1685-1706.

[12] Seiler, H. G.; Sigel, A.; Sigel, H., *Handbook on Metals in Clinical and Analytical Chemistry*. CRC Press: 1994.

[13] Wang, Z. L., *Characterization of Nanophase Materials*. Wiley-VCH: New York, 2000; p 406.

[14] Buseck, P.; Cowley, J.; Eyring, L., *High-Resolution Transmission Electron Microscopy*. Oxford University Press: 1989.

[15] Zhang, J. Z., *Self-assembled nanostructures*. Kluwer Academic/Plenum Publishers: New York, 2003; p 316.

[16] Cowley, J. M., *Diffraction Physics*. 3rd ed.; North-Holland Physics Publishing: Amestadam, 1995.

[17] Goldstein, J., *Scanning electron microscopy and X-ray microanalysis*. 3rd ed.; New York : Kluwer Academic/Plenum: New York, 2003; p 689.

[18] Hawkes, P. W., *Advances in imaging and electron physics*. Elsevier Science: 2004.

[19] Berne, B. J.; Pecora, R., *Dynamic light scattering: With applications to chemistry, biology, and physics*. Dover Publications: 2000.

[20] Brown, W., *Dynamic light scattering: the method and some applications*. Clarendon Press: 1993.

[21] Warren, B. E., *X-ray Diffraction*. Dover Publications: New York, 1990; p 381.

[22] Cullity, B. D., *Elements of X-ray diffraction*. 2nd ed.; Addison-Wesley: USA, 1978.

[23] Helming, K.; Lyubchenko, M.; He, B.; Preckwinkel, U. In *A new method for texture measurements using a general area detector diffraction system*, J C P D S-Int Centre Diffraction Data: 2003; pp 99-102.

[24] McMurry, J., *Organic chemistry*. Brooks/Cole: 2012.

[25] Bard, A. J.; Faulkner, L. R., *Electrochemical methods: Fundamentals and applications*. Wiley: 2001.

Chapter III

Influence of the morphology of silver nanoparticles on antibacterial activity: spheres, cubes and prisms

3.1 Introduction

Due to the outbreak of infectious diseases caused by various pathogens and the development of antibiotic resistance, researchers are discovering new and effective antimicrobial agents.[1] Recently, nanoscale materials have emerged as novel antimicrobial agents owing to their inorganic nature, which are significantly different than traditional antibiotics that are mainly organic. Inorganic nanoparticles with antimicrobial activity are thus promising as a new class of biomedical materials to potentially overcome the rise of antibiotics resistance.[2] Nanostructured materials are attracting an immense deal of attention due to their potential for achieving specific processes and selectivity, particularly in biological and medical applications.[3]

Innovations in the past decade have revealed that size and shape of metal nanoparticles influence their electromagnetic, optical and catalytic properties.[4] Therefore, there has been an increase in research on the synthesis of metal nanostructures with interesting size and shape-dependent properties. These novel properties can be tailored by controlling their size, shape, composition, structure and

crystallinity. Emphasis is placed on shape control as this allows optical, electronic, magnetic, catalytic and other properties of the nanostructures to be altered for versatile applications.[5, 6] The synthesis and properties of various types of metal nanoparticles have been investigated. These include, gold,[7, 8] silver,[9] palladium,[10] platinum,[11] titanium etc.[12]

Among noble metals, silver has have been commonly studied for its diverse range of applications. Silver has been employed for centuries to fight infections and control spoilage.[13] The role of silver for medicinal applications has been extensive with time and today, silver is still used in the healthcare and pharmaceutical sector.[14] Microorganisms are less likely to develop resistance against silver as they do against narrow-targeting antibiotics. This is due to the metal attacking a wide range of targets in the organisms, leading to the requirement to develop a host of mutations simultaneously in pathogens to generate resistance. Hence, silver ions have been employed as an antibacterial component in dental resins,[15, 16] wound dressings,[17, 18] and coatings of medical devices.[14, 19]

Despite silver's extensive use throughout the history as an antimicrobial agent, the discovery and development of wonder drug penicillin caused a dramatic shift in the way bacterial infections were treated. This led to a significant decrease in the use of silver-based products for antimicrobial applications, and new silver-based products almost ceased to be developed. However, with the increase of resistant strains of bacteria due to heavy use of antibiotics and the need for an efficient universal disinfectant, the interest in the antimicrobial capability of silver-based products has once again renewed.[20]

To this end, the recent focus is shifting towards silver nanoparticles, which are being tested against common pathogens in the hope of finding a novel and effective

antimicrobial agent. It is notable that silver ions (Ag^+) are well known to possess strong inhibitory and antibacterial effects as well as a broad range of antimicrobial activities.[21-23] However, it is relatively recent that various researchers have started investigating the antimicrobial capabilities of silver nanoparticles (Ag^0). Most of these studies on Ag nanoparticles based antimicrobial agents have been restricted to the use of spherical Ag nanoparticles against Gram negative and or Gram positive bacteria.[2, 21, 23, 24] Relatively few reports have investigated shape-dependent antimicrobial efficacy of Ag nanoparticles. However, contamination of samples with different Ag shapes in such studies makes it difficult to precisely understand the role of Ag nanoparticle shape in causing antimicrobial activity.[22]

Considering that size as well as shape of Ag nanoparticles may have considerable effect on their properties, this chapter has undertaken the task of studying the shape-dependent antibacterial properties of Ag nanoparticles. The main focus on this chapter is to particularly investigate the comparison of different shapes of nanoparticles (spherical, cubic and prismatic) against representative strains of Gram negative and Gram positive bacteria.

3.2 Experimental

3.2.1 Synthesis of Ag nanospheres

Silver nanospheres were synthesised via a procedure outlined by Selvakannan *et al.*[25] whereby amino acid tyrosine was used as a reducing as well as capping agent in an alkaline environment. This procedure shows that amino acid tyrosine is an excellent reducing agent that is capable of reducing Ag^+ ions to yield highly stable monodispersed spherical silver nanoparticles. In brief, 10 mL of 10^{-3} M aqueous silver

sulphate (containing 2 x 10^{-3} M equivalent of Ag^+ ions) was prepared and added to 20 mL of 10^{-3} M aqueous solution of tyrosine. This solution was then diluted to 100 mL with Milli-Q water. To this solution, 1 mL of 10^{-1} M KOH was added and allowed to boil. Within 20 minutes the initial colourless solution changed into a light yellow colour which indicated the formation of silver nanoparticles. The solution was allowed to boil for a further 15 minutes for silver nanoparticles to grow and stabilise.

3.2.2 Synthesis of Ag nanocubes

Silver nanocubes were synthesised via a procedure outlined by Xia *et al*.[26] This synthesis was achieved by mediating a polyol process which is simple, robust and versatile in the formation of monodispersed silver nanocubes. In a typical experiment, silver cubes are produced by reducing $AgNO_3$ with ethylene glycol (EG) through the subsequent mechanism:

$$2HOCH_2\,CH_2\,OH \rightarrow 2CH_3CHO + 2H_2O \quad (3.1)$$

$$2Ag^+ + 2CH_3\,CHO \rightarrow CH_3\,CO-OCCH_3 + 2Ag^0 + 2H^+ \quad (3.2)$$

In brief, this method was adjusted through the modification of reaction conditions. Initially 30 mL of EG was heated and magnetically stirred for 1 hr. While the EG solution was heated, EG solutions containing $AgNO_3$ (48 mg mL^{-1}), polyvinylpyrrolidone (PVP) (20 mg mL^{-1}) and 3 mM Na_2S were prepared 45 minutes prior to injection. After an hour heating the EG solution, 400 µL of Na_2S, 7.5 mL PVP and 2.5 mL $AgNO_3$ solutions were injected into the initial EG solution. As soon as $AgNO_3$ was added, the colourless solution instantaneously turned purple/black, followed by a bright yellow colour. After 5 minutes into the reaction, the solution darkened to orange yellow. 10 minutes later, the final colour was an opalescent muddy brown indicating the formation of Ag nanocubes.

3.2.3 Synthesis of Ag nanoprisms

Silver nanoprisms were synthesised via a procedure outlined by Aherne *et al.*[27] by a reproducible seed-based thermal method. The method was modified through the adjustment of reaction conditions and included following steps:

3.2.3.1 Seed production:

Silver seeds were produced by combining aqueous trisodium citrate (5 mL, 2.5 mM), aqueous poly(sodium styrenesulphonate) (PSSS - 0.25 mL, 500 mgL^{-1}; Aldrich 1,000 kDa) and aqueous $NaBH_4$ (0.3 mL, 10 mM, freshly prepared) followed by addition of aqueous $AgNO_3$ (5 mL, 0.5 mM) at a rate of 2 mL min^{-1} while continuously stirred.

3.2.3.2 Nanoprism growth:

Nanoprisms were synthesised by increasing 5 times the concentration of the originally reported experiment; specifically, nanoprisms were produced by the combination of 10 mL Milli-Q water, 75 µL of aqueous ascorbic acid (50 mM), 400 µL seed solution, followed by the addition of 3 mL aqueous $AgNO_3$ (2.5 mM) solution at a rate of 1 mL min^{-1}. To stabilize the nanoprisms 0.5 mL of aqueous trisodium citrate (125 mM) was added after the experiment.

3.2.4 Quantification of Ag nanoparticles by atomic absorption spectroscopy (AAS)

For antibacterial applications, it is important to ascertain that nanoparticles used in experiments have the same concentration of silver. Therefore, all nanoparticles used in this study were analysed by AAS to determine the concentration of silver. Before AAS

analysis, all Ag nanoparticles were centrifuged three times against Milli-Q water for 15 minutes at 12,000 rpm to remove free Ag^+ ions.

Ag nanoparticles were initially dissolved in nitric acid and calibration standards were prepared using 1000 ppm stock solution of silver nitrate. Based on Ag standards, calibration graph was created and concentrations of Ag nanoparticles were determined. Samples were then diluted to desired concentrations for use.

3.2.5 Antibacterial applications

All antibacterial experiments were performed under sterile conditions in a laminar flow cabinet. Before the commencement of microbiological experiments, media cultures, glassware and pipette tips were sterilised by autoclaving at 121°C for 15 minutes. Gram negative *Escherichia coli* (*E. coli*) and Gram positive bacterium *Staphylococcus albus* (*S. albus*) were used as microorganisms for antibacterial applications.

3.2.5.1 Colony forming units (CFU) assay

To examine the bactericidal effect of silver nanoparticles against Gram negative and Gram positive bacteria, 10^4 colony forming units (CFU) of each bacteria were mixed with various Ag nanoparticles (spheres, cubes and prisms) in varying concentrations for 30 minutes in 1 mL volume. 100 µL of this was then plated on agar plates. These plates were then incubated for 24 hrs at 37°C and the numbers of colonies were counted. Colonies formed correspond to the number of viable bacteria in each suspension at the time of aliquot withdrawal.

3.2.5.2 Liquid broth growth kinetic assay

To examine the bacterial growth rate and to determine the kinetic growth curve in the presence of various shapes of Ag nanoparticles, *E. coli* and *S. albus* were grown in Luria-Bertani (LB) broth. Growth rates and bacterial concentrations were determined by measuring optical density (OD) at 600 nm at hourly intervals where OD of 0.1 corresponds to a concentration of 10^8 cells per cm^3. For these kinetic experiments, Ag nanoprisms were omitted, as the absorption for these nanostructures occurs in the same region (ca. 650 nm) which interferes with measurements.

7 mL of LB broth, 2 mL of Ag nanoparticles (10^{-3} M) and 1 mL of respective bacteria (10^8 cells/mL) were mixed in sterile vials with a final volume of 10 mL. Vials of the following contents were prepared for each microorganism:

1. Broth (for blank)
2. Broth + Bacteria
3. Broth + Bacteria + Ag nanospheres
4. Broth + Bacteria + Ag nanocubes

For each bacteria, there were 4 experiments conducted and each were in triplicates to test the statistical significance. Therefore, a total of 12 reactions were prepared for each bacterium. Growth rate of bacteria in the prepared reactions were monitored while incubating the reaction vessels on an orbital shaker at 37°C, and measuring the growth rate by using UV–Vis spectrophotometer at regular hourly intervals.

3.3 Results and discussion

3.3.1 UV-Visible spectroscopy studies of Ag nanoparticles

The optical absorption spectra of metal nanoparticles are dominated by surface plasmon resonance (SPR), which shifts to longer wavelengths with increasing particle size.[28] The shape and position of plasmon absorption of silver nanoclusters are highly dependent on the particle size, shape, dielectric environment and surface adsorbed species.[29] In Mie's theory,[30] only a single SPR band is expected to be present in the absorption of spherical nanoparticles, whereas anisotropic particles could give rise to two or more SPR bands depending on the shape of the particles. The number of SPR peaks increases as the symmetry of the nanoparticles decreases,[31] hence different shaped nanoparticles of silver may show one, two or more peaks.

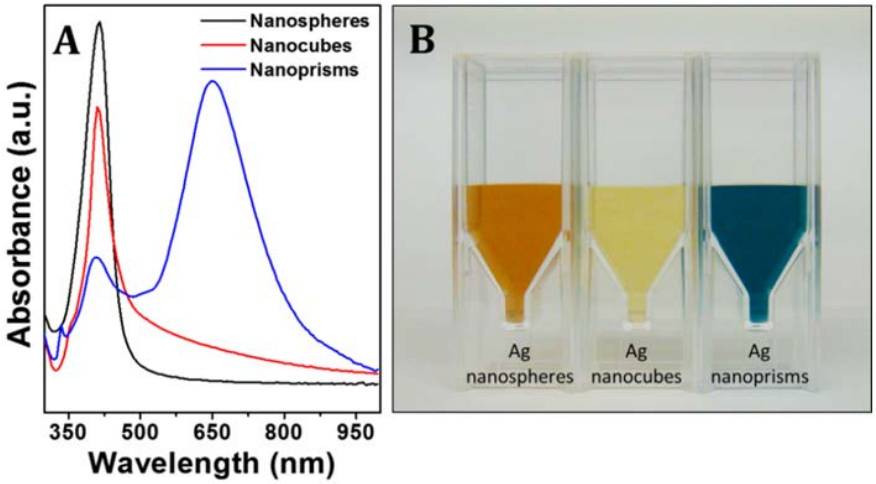

Figure 3.1- (A) UV-Visible spectra of Ag nanospheres, Ag nanocubes and Ag nanoprisms. (B) Photograph of Ag nanoparticles illustrating range of colours obtained.

The UV-Vis analysis of Ag nanoparticles reveals the SPR features of nanostructures that are in agreement with those from the previous studies (Figure 3.1).[25-27] The absorption spectrum of Ag nanospheres prepared by the reduction of tyrosine shows a

sharp SPR feature at 428 nm indicating monodispersity of the sample without any anisotropic features.[25]

Similarly, a SPR maximum of Ag nanocubes at 420 nm is consistent with that of previous studies wherein SPR maximum was found to blue-shift with the reduction in edge length and 40 nm sized nanocubes with rounded edges lead to SPR maximum at ca. 425 nm.[32] Conversely, Ag nanoprisms show three dominant SPR peaks in the UV-Vis spectrum that are typical of Ag nanoprisms, and arise due to in-plane dipolar excitation (most intense red-most band at 700 nm), in-plane quadrupole excitation (middle band at 400 nm), and out-of-plane quadrupole excitation (bluest resonance at 335 nm).[27, 33]

3.3.2 TEM and DLS measurements of Ag nanoparticles

Representative TEM images in Figure 3.2 of Ag nanospheres, nanocubes and nanoprisms reveal that well defined shapes are formed. Ag nanospheres, nanocubes and nanoprisms were synthesized using established chemical synthesis protocols that are known to predominately produce shape-selective, fairly monodispersed nanostructures in high yields. TEM images of Ag nanostructures used in this study show the well-formed Ag nanoparticles (Figure 3.2).

Furthermore, TEM analysis of all Ag nanostructures revealed that there was no aggregation in particles which is in agreement with UV-Vis spectroscopic analysis. Corresponding particle size histograms of respective 250-350 nanoparticles on TEM images were taken into account in each case to obtain particle size distribution. In case of Ag nanospheres, the reported values correspond to the nanoparticle diameter and in the case of Ag nanocubes and Ag nanoprisms, edge length is reported as a representative of nanoparticle size. The average particle diameter for each nanomaterial was calculated

along with standard distribution to be 21.8 ± 5.0 nm (diameter), 48.7 ± 9.3 nm (edge length) and 30.5 ± 10 nm (edge length) for spheres, cubes and prisms respectively.

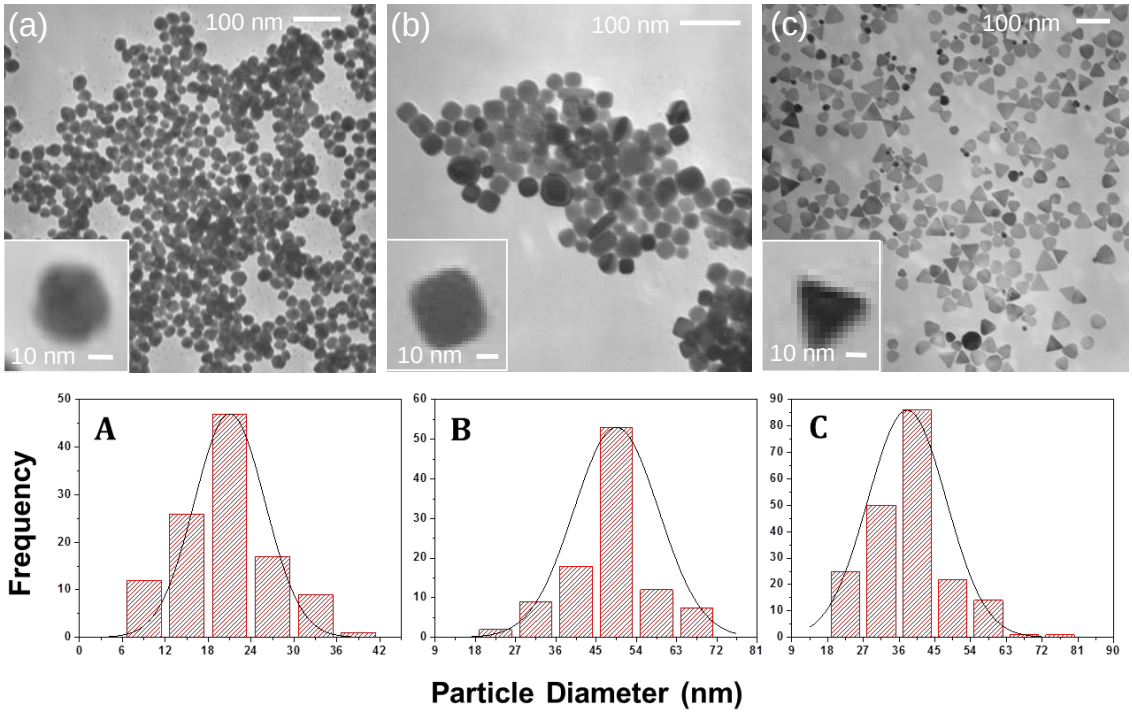

Figure 3.2- TEM images and corresponding particle size distribution histograms of (A) Ag nanospheres, (B) Ag nanocubes and (C) Ag nanoprisms.

Dynamic light scattering (DLS) is a well-established technique to determine the size distribution profile of nanoparticles that provides information about the hydrodynamic radii of nanoparticles in solution by measuring the time scale of light intensity fluctuations. Hence, to confirm the hydrodynamic radii of nanoparticles in solution, DLS analysis was carried out on all Ag nanostructures.

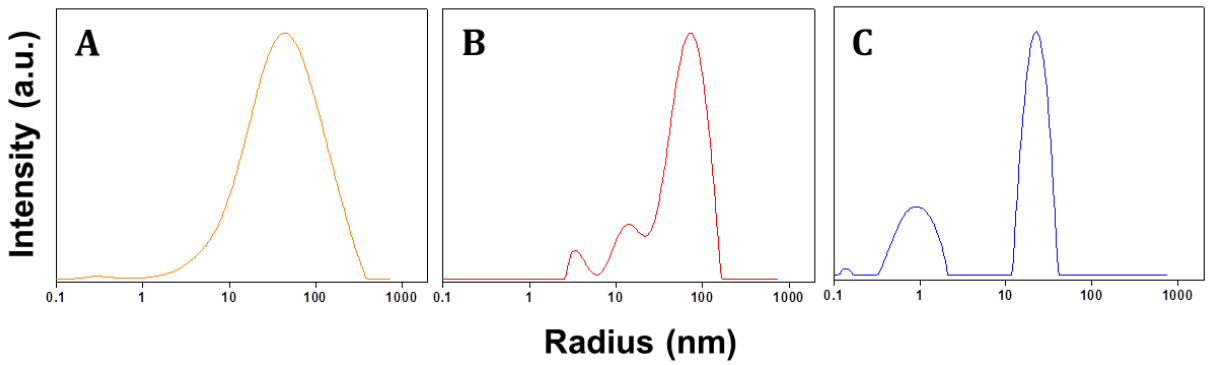

Figure 3.3- DLS size distribution profile of (A) Ag nanospheres, (B) Ag nanocubes and (C) Ag nanoprisms.

DLS measurements in Figure 3.3 revealed that the trend in change of the average hydrodynamic radius corroborates with TEM diameter measurements. The average hydrodynamic radius was 41.4 nm in Ag nanospheres (equivalent to hydrodynamic diameter 82 nm), 69.6 nm (equivalent to hydrodynamic diameter 140 nm) in Ag nanocubes and 22.8 nm (equivalent to hydrodynamic diameter 45 nm) in Ag nanoprisms. Although DLS reveals a significantly higher particle size than those measured using TEM, this is expected because TEM reveals the physical size of high contrasting Ag component while DLS reveals hydrodynamic size taking surface capping into account.

3.3.3 X-ray diffraction (XRD) studies of Ag nanoparticles

Silver crystallites are in a cubic packed structure (FCC- face centred cubic), wherein the unit cell structure consists of the same length in all sides and all the faces are perpendicular to one another (Figure 3.4A). Silver atoms are present at each corner and in the centre of each face of the unit cell. Therefore, this unit cell is referred to as a face-centered cubic (fcc) unit cell.

Structural information of Ag nanostructures were obtained by XRD using a general area detector diffraction system (GADDS) (Figure 3.4B). XRD patterns of Ag nanostructures confirm highly crystalline silver nanoparticles. Ag nanospheres showed an XRD pattern typical of face-centered cubic (fcc) silver with a predominant (111) Bragg reflection.[34] In the case of Ag nanocubes, (200) peak is significantly stronger relative to the (111) that is expected from a sample rich is Ag nanocubes since most of the cubes will tend to align flat on the substrate with their surface bound (100) planes being oriented parallel to the substrate.[32] Ag nanoprisms showed an XRD pattern typical of

flat-lying Ag nanoprisms predominantly covered by (111) fcc faces.[27] The (311) plane observed in the XRD pattern of Ag nanoprisms is also typically observed in flat fcc metal nanostructures, thus confirming the flat sheet-like morphology of Ag nanoprisms.[27] Additionally, two further peaks corresponding to reflections that were recently predicted to arise from a hexagonally closed pack (hcp) arrangement of Ag atoms was observed (dotted lines in Figure 3.4B). The hexagonal arrangement of Ag atoms is believed to propagate perpendicular to the flat (111) face of the nanoprism, resulting in a layered defect structure within the nanoprism.[27]

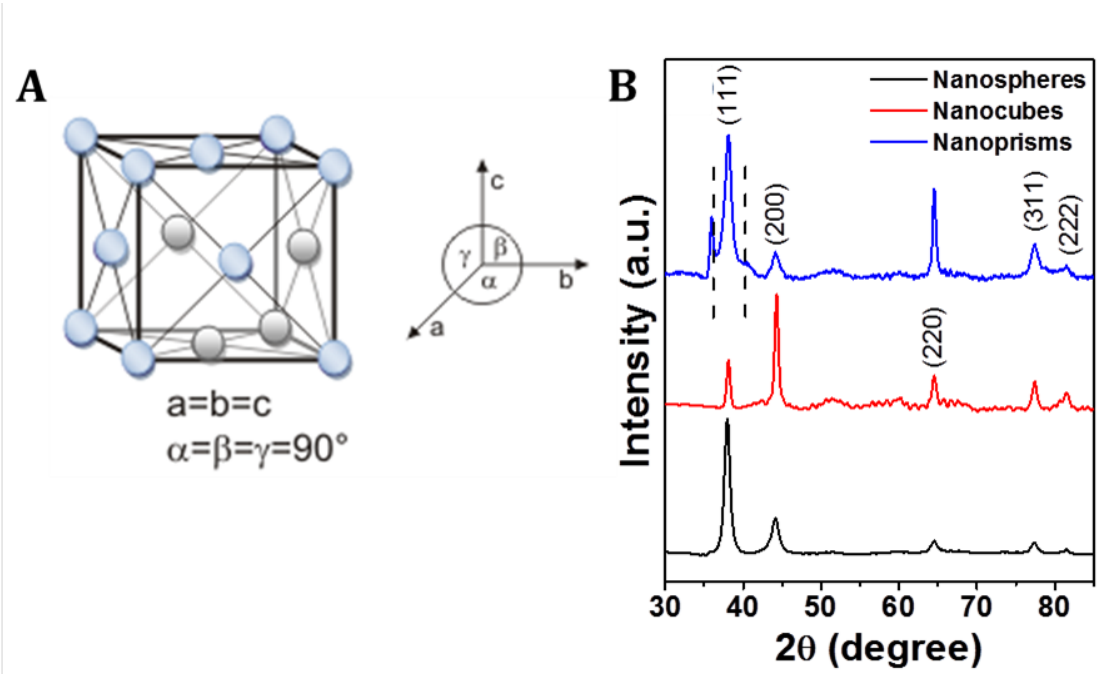

Figure 3.4- (A) Schematic of fcc crystal structure. (B) XRD patterns of Ag nanospheres, nanocubes and nanoprisms. XRD patterns have been shifted vertically for clarity with Bragg reflections corresponding to fcc Ag indicated. The dotted lines correspond to reflections corresponding to hcp Ag.

3.3.4 FTIR analysis of Ag nanoparticles

3.3.4.1 FTIR analysis of Ag nanospheres

The structure of the amino acid tyrosine used during the synthesis of Ag nanospheres is shown in Figure 3.5. Tyrosine consists of three main functional groups: phenolic, amine and carboxylic.

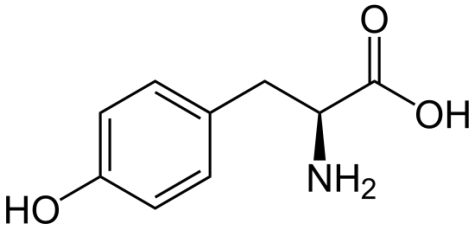

Figure 3.5- Functional groups within tyrosine molecule.

Tyrosine was used as a reducing agent under alkaline conditions to reduce Ag^+ ions for the synthesis of stable Ag nanospheres in aqueous solution. Ag^+ ion reduction occurs at high alkaline pH, therefore tyrosine is a pH-dependent reducing agent. The pH -dependent reducing ability of tyrosine is shown to arise due to ionization of the phenolic group of tyrosine at high pH which by electron transfer to silver ions, is transformed to quinone (Figure 3.6).[25]

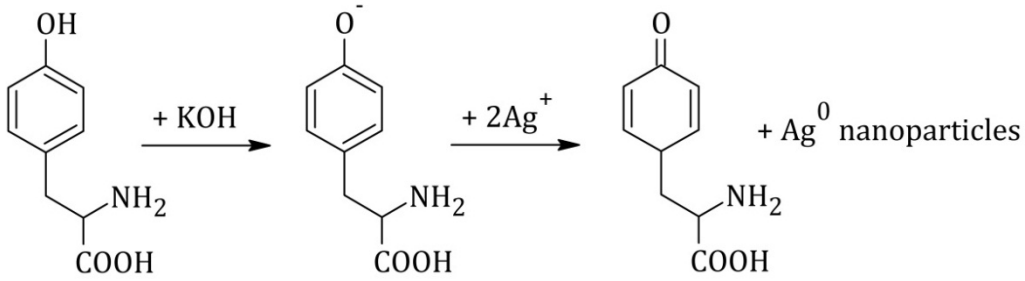

Figure 3.6-Mechanism of reduction of Ag^+ ions to Ag nanoparticles.

FTIR studies of pure tyrosine and Ag nanospheres (Figure 3.7) reveal different functional groups present within the molecules. Table 3.1 summarises the different vibrational bands present in tyrosine and Ag nanospheres. From the peaks observed, the carbonyl stretching from the carboxylate in tyrosine occurs from 1609 cm^{-1} in the case of

pure tyrosine. However, there is an apparent shift in vibrational frequency towards 1624 cm^{-1} after oxidation of tyrosine (Figure 3.7). Notably, this shift in the vibrational frequency of carbonyl stretching has been previously attributed to the formation of a quinone type structure due to the oxidation of the phenolic group in tyrosine.[25]

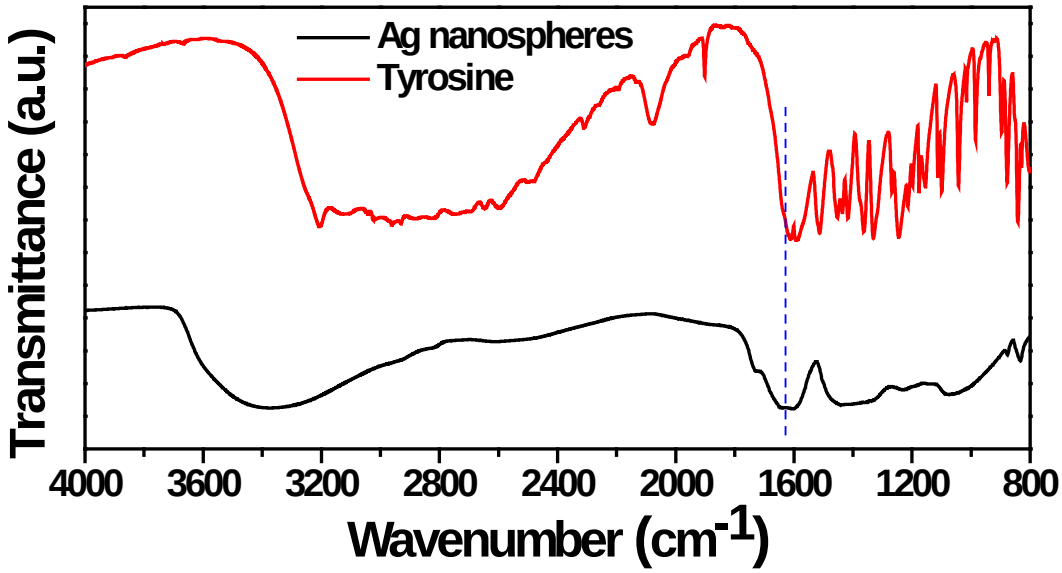

Figure 3.7- FTIR spectra of pure tyrosine and tyrosine-reduced Ag nanospheres.

The broad O-H peak in the tyrosine reduced Ag nanospheres at 3400 cm^{-1} to 3200 cm^{-1} is due to water molecules apparent in the sample. Absence of vibration signals of N-H bend and C-O stretch in Ag nanospheres compared to pure tyrosine suggests those functional groups have been involved and/or utilized during synthesis of Ag nanoparticles.

Table 3.1- Summary of functional groups in tyrosine and tyrosine-reduced Ag nanospheres.

Wavenumber (cm^{-1})	Bond	Functional group	Appearance
Tyrosine			
3640 - 3200	H- bonded	Phenolic vibrations	Broad
1609	C=O stretch	Carboxylic acid	Narrow and sharp
1591	N-H bend	1 ° amine	Narrow and sharp
1450 - 1300	C-H stretch	Alkanes	Narrow
Tyrosine-reduced Ag nanospheres			
3400 - 3200	O-H stretch	Hydroxyl	Broad
1624	C=O stretch	Carboxylate ion	Narrow and sharp

3.3.4.2 FTIR analysis of Ag nanocubes

Silver nanocubes were synthesized via a polyol-mediated process. The primary reaction of this process involves the reduction of an organic salt (the precursor) by polyol at an elevated temperature.[35] Polyvinylpyrrolidone (PVP) is normally added as a stabilizer to prevent agglomeration of the colloidal particles. The structure of the precursors used in this study has been shown in Figure 3.8. Table 3.2 provides a summary of the different vibrational bands present in PVP, EG, Ag nanocubes, and washed Ag nanocubes respectively.

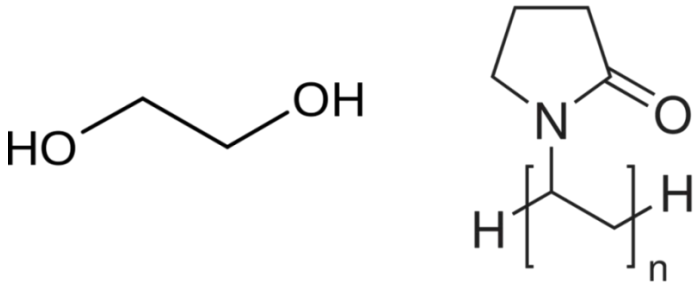

Figure 3.8- Structure of precursors EG (left) and PVP (right) employed for Ag nanocubes synthesis.

FTIR spectra of precursors and Ag nanocubes are shown in Figure 3.9. The precursors for FTIR studies were PVP and EG. The polyol process is based on EG, which serves as an excellent solvent for PVP due to its relatively high dielectric constant.[36, 37] At high temperatures, EG can reduce Ag^{+} ions into Ag atoms and thereby induce the nucleation and growth of silver nanostructures in the solution phase. PVP plays a critical role in the formation of nanostructures, possessing efficient stability and size/shape uniformity.

From the comparison between the FTIR spectra of precursors and Ag nanocubes (Figure 3.9), it can be seen that all spectra possess a broad hydroxyl vibrational signal at ca. 3600 cm^{-1} to 3000 cm^{-1} due to water molecules within the sample. The frequencies

from 3000 cm^{-1} to 2800 cm^{-1} indicate C-H stretching vibration modes of alkanes within PVP, EG, and Ag nanocubes.

It is also evident from Figure 3.9 that PVP plays a critical role in the formation of silver nanocubes, as is clear from the comparison of the spectra of PVP and Ag nanocubes washed (peak shift and sharpening ca. 1600 cm^{-1}). PVP molecules have been shown to preferentially adsorb onto the surface of silver particles, thus stabilizing the small single crystal Ag seeds.[32, 36] This also supports that EG acts as a solvent during the synthesis of Ag nanocubes, while PVP acts as a shape promoting and stabilizing agent, which leads to the formation of Ag nanocubes.

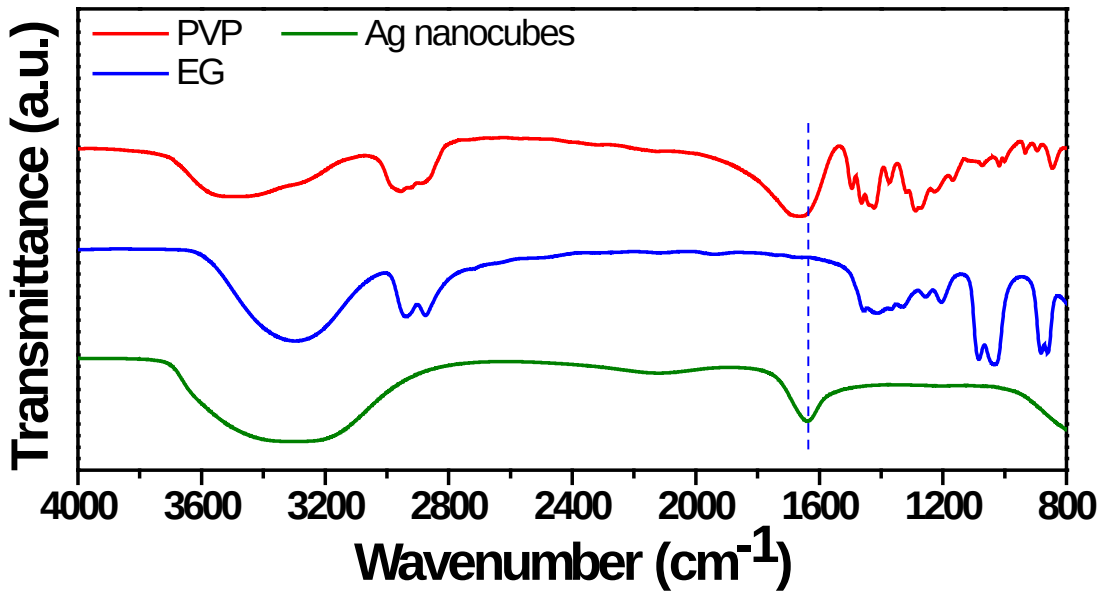

Figure 3.9- FTIR spectra of Ag nanocubes, EG and PVP.

Table 3.2- Summary of functional groups in PVP, EG and Ag nanocubes.

Wavenumber (cm^{-1})	Bond	Functional group	Appearance
Polyvinylpyrrolidone			
3400 - 3600	O–H stretch	Hydroxyl	Broad
2900 - 2800	C–H stretch	Alkane	Broad
1660	C= O stretch	Aromatic ketone	Broad
1470 - 1450	C H bend	Alkane	Medium
1250 - 1020	C–N stretch	Aliphatic amine	Medium
900 - 800	Vinyl	Monosubstituted alkene	Medium
Ethylene glycol			
3300	O-H stretch	Hydroxyl	Broad
2900 - 2800	C-H stretch	Alkane	Medium
1470 - 1450	C-H bend	Alkanes	Medium
1110 - 1000	C–O stretch	Primary alcohol	Strong
Ag nanocubes			
3600 - 3000	O-H stretch	Hydroxyl	Broad
1660	C=O stretch	Aromatic ketone	Broad

3.3.4.3 FTIR analysis of Ag nanoprisms

Silver nanoprism synthesis is a seed-based thermal synthetic procedure that selectively produces Ag nanoprisms in a rapid and reproducible manner at room temperature. This method involves the silver seed catalysing a reduction of Ag^{+} by ascorbic acid. One of the key precursors for production of high quality Ag nanoprisms is the use of PSSS, which is used as a stabiliser in the seed production stage. The structures of PSSS and ascorbic acid are shown below in Figure 3.10.

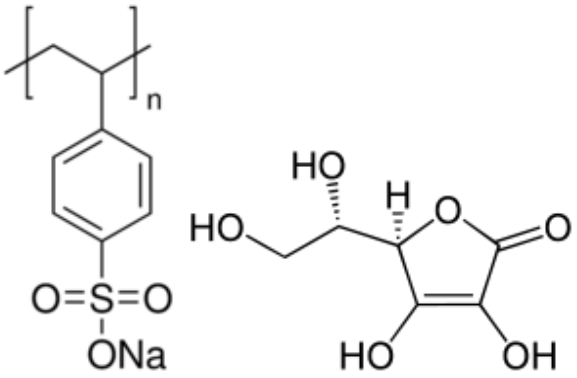

Figure 3.10- Structure of precursors, PSSS (left) and ascorbic acid (right) employed for Ag nanoprisms synthesis.

Illustrated in Figure 3.11 is the FTIR spectra of precursors used in the synthesis, Ag seed as well as Ag nanoprisms. The frequencies observed at 1700 cm^{-1} to 1560 cm^{-1} in the case of PSSS are aromatic alkenes with HC=CH stretching. Since PSSS is used in the synthesis of Ag seeds, a shift at 1635 cm^{-1} in the case of Ag seeds is apparent. This shift suggests binding of PSSS to seed Ag nanoparticles. Similarly, a shoulder peak can be observed in the case of Ag nanoprisms at 1635 cm^{-1}. Therefore, direct evidence for the utilisation of PSSS and the Ag seed during the synthesis of Ag nanoprisms is observed.

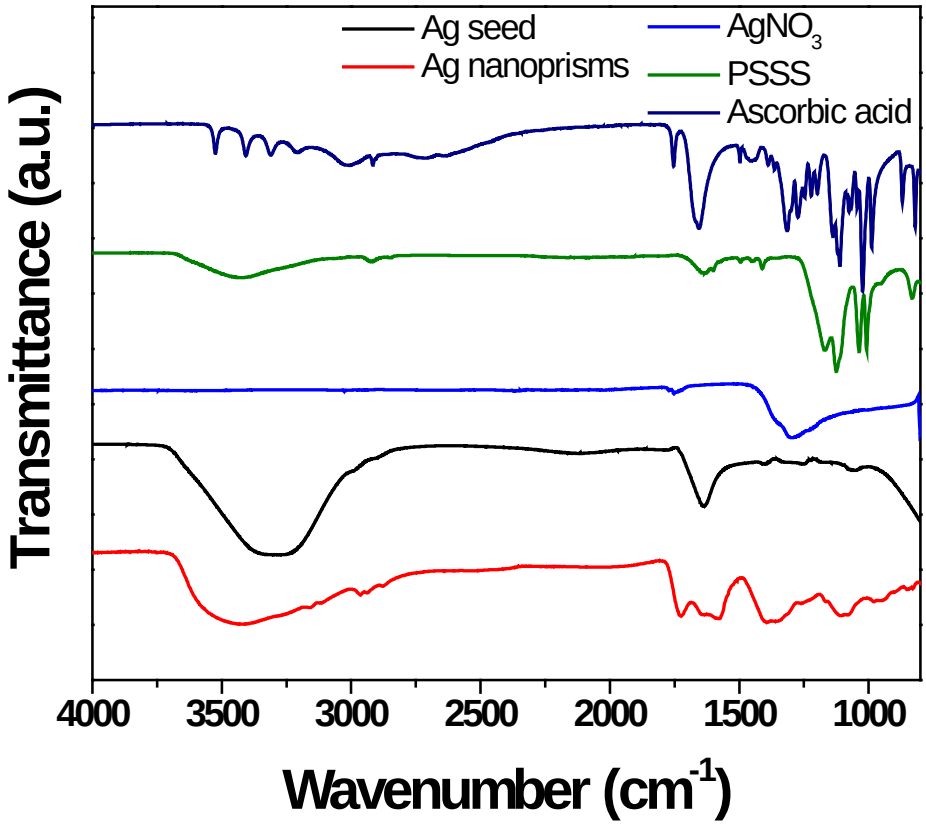

Figure 3.11- FTIR spectra of precursors, Ag seed and Ag nanoprisms.

It is also evident that ascorbic acid plays a vital role in the formation of Ag nanoprisms with a peak at ca. 1750 cm^{-1} within the ascorbic acid spectrum representing C=O, and a shift in the frequency to ca. 1726 cm^{-1} in the Ag nanoprisms spectrum. Moreover, nitrate frequencies at 1398 cm^{-1} and 1356 cm^{-1} present in

Ag nanoprisms suggests that $AgNO_3$ have also been involved and NO_3^- potentially remain bound to Ag nanoprisms post synthesis.

Broad O-H peaks at ca. 3600 cm^{-1} to 3000 cm^{-1} are present in ascorbic acid, Ag seed and Ag nanoprisms which are attributed to water molecules apparent within the samples. Table 3.3 provides a summary of the various vibrational bands present in all the precursors used in the synthesis as well as Ag seed and Ag nanoprisms.

Table 3.3- Summary of functional groups in ascorbic acid, PSSS, $AgNO_3$, Ag seed and Ag nanoprisms.

Wavenumber (cm^{-1})	Bond	Functional group	Appearance
Ascorbic acid			
3550 - 2950	O–H stretch	Hydroxyl	Broad
1750	C=O	Aldehyde/Ketone	Weak
1660	C=C stretch	Aromatic ketone	Strong
1443	C-H scissor	Alkane	Weak
1300	C–H bend	Alkane	Medium
PSSS			
3600 - 3100	R–SO_3stretch	Ionic sulphonate	Sharp
1700 - 1560	HC=CH stretch	Aromatic alkene	Weak
$AgNO_3$			
1296	NO_3	Nitrate	Broad
Ag seed			
3600 - 3000	O-H stretch	Hydroxyl	Broad
1635	HC=CH stretch	Aromatic alkene	Broad
Ag nanoprisms			
3600 - 3000	O–H stretch	Hydroxyl	Broad
1726	C=O	Aldehyde/Ketone	Medium
1635	HC=CH stretch	Aromatic alkene	Shoulder
1584	CO-NH_x	Amide	Shoulder
1398	NO_3	Nitrate	Broad
1356	NO_3	Nitrate	Broad

3.3.5 Antibacterial study of Ag nanoparticles against microorganisms

3.3.5.1 Colony count studies

Colony count method was empolyed to investigate the antibacterial effects of Ag nanoparticles against different bacterial strains. To evaluate the effects of Ag nanoparticles on bacteria, various concentrations of Ag^0 nanoparticles ranging from 0.1 mM to 1 mM were tested against 10^3 colony forming units (CFU) of bacteria. During CFU assays, Ag nanoparticles demonstrated antibacterial activity against both Gram negative and Gram positive bacteria as shown in Figure 3.12A and B.

In the case of Ag nanoparticles against Gram negative bacteria *E. coli* as shown in Figure 3.12A, all nanostructures (prisms, spheres and cubes) showed a consistent trend of increasing cell death across the various concentrations from low to high. Ag nanoprisms exhibited the least percentage cell death compared to Ag nanocubes which displayed the highest cell death in most concentrations. Similarly, Ag nanospheres possessed comparable trends to that of Ag nanocubes with little percentage differences in cell death across the range of concentrations.

Similarly, in case of Gram positive bacteria *S. albus* (Figure 3.12B), Ag nanoprisms once again showed the least and limited inhibitory effect in the lower concentrations of 0.1 mM and 0.2 mM and mild effects in higher concentration with only ca. 30% cell death. Since Ag nanoprisms are expected to be highly rich in (111) crystal planes followed by that in nanospheres and nanocubes, this observation suggests that crystallography of Ag nanoparticles might play some role in assigning activity against Gram positive bacteria.

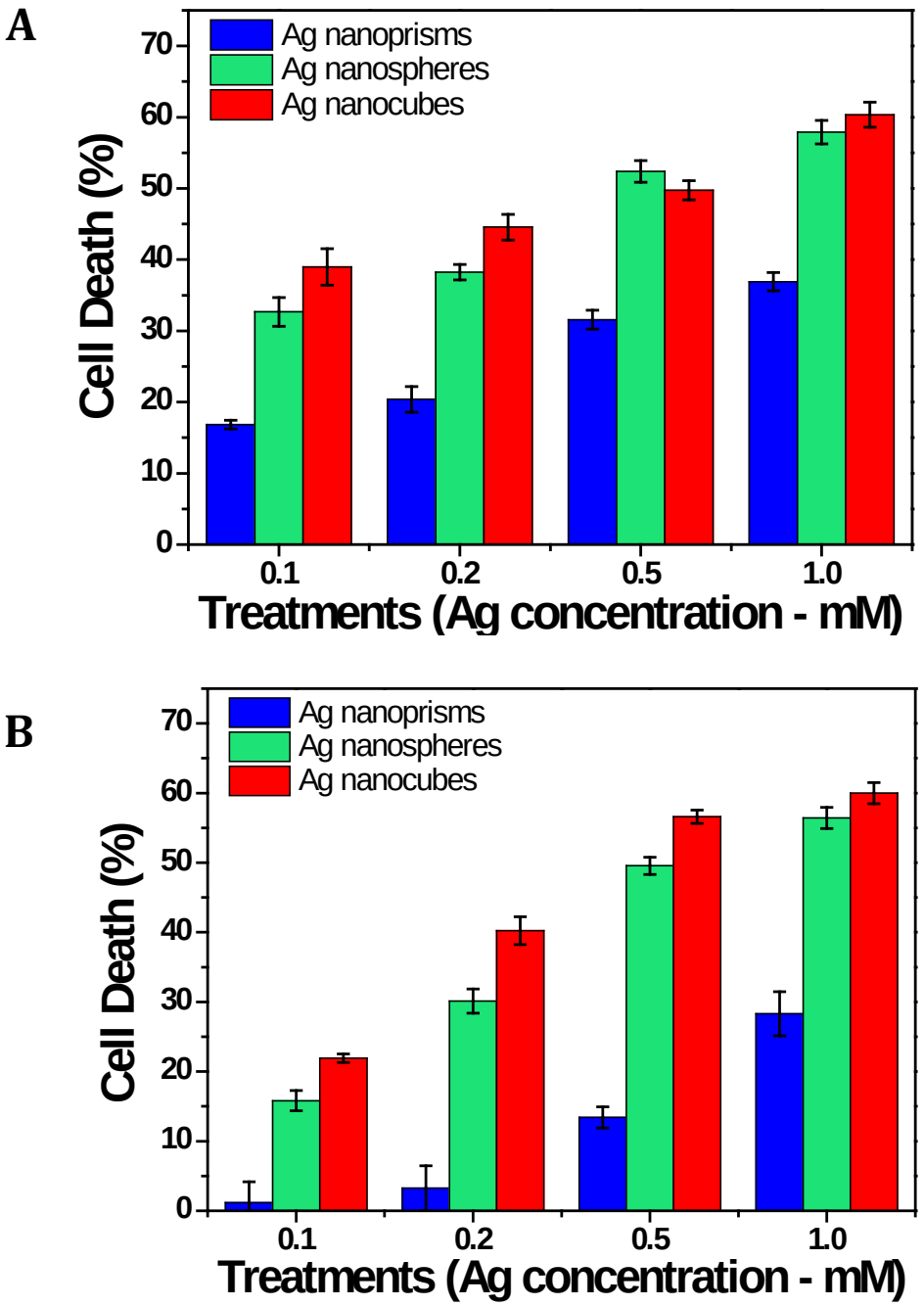

Figure 3.12- CFU expressed in percentage cell death (A) Ag nanoparticles against Gram negative *E. coli* and (B) Ag nanoparticles against Gram positive *S. albus.*

Therefore, it can be inferred from the CFU assay that Ag nanocubes perform significantly better than Ag nanoprisms and nanospheres in terms of antibacterial activity against both Gram negative and Gram positive bacteria. These findings suggest that different shape of Ag nanoparticles can considerably influence their antibacterial

behaviour and via controlling the shape of Ag nanoparticles, it might also be possible to control the growth of both Gram negative and Gram positive bacterial species.

3.3.5.2 Antibacterial growth kinetics studies

Although bacterial growth on agar plates is commonly employed for distinguishing antibacterial properties of various materials, LB broth (liquid) assay provides a better qualitative estimation and kinetics of antibacterial activity. Therefore, LB broth assays (Figure 3.13) were also performed to compare the antibacterial capabilities of Ag nanospheres and Ag nanocubes against Gram negative *E. coli* and Gram positive *S. albus*, which further supported the results obtained from CFU assay. However, as Ag nanoprisms absorb at ca. 600 nm, they were not included in this study. The comparison of Ag nanospheres and nanocubes using growth kinetics studies was important as they show relatively less difference in activity profile during CFU assay, in comparison to Ag nanoprisms that were significantly less effective.

The dynamics of bacterial growth in the presence and absence of Ag nanoparticles was monitored in liquid LB broth (initial bacterial concentration, 10^6 CFU ml^{-1}) with 0.1 mM final effective concentration of Ag nanoparticles in 1 mL reaction volume for 10^6 starting bacterial population.

It is apparent from the comparison of curves in Figure 3.13 that the Ag nanoparticles in liquid medium caused a growth delay in all cases of bacterial species (red and blue curves in Figure 3.13). From the growth curves of Gram negative bacteria it is also evident that Ag nanocubes are significantly more effective than Ag nanospheres. In the case of *E. coli,* Ag nanocubes exhibited cytotoxicity (cell death), clearly indicated by the negative gradient. The decline in the number of cells at the later time points in case of

Ag nanocubes therefore indicates cytolytic activity of Ag nanocubes. Whereas Ag nanospheres could only exhibit growth inhibition within this time frame.

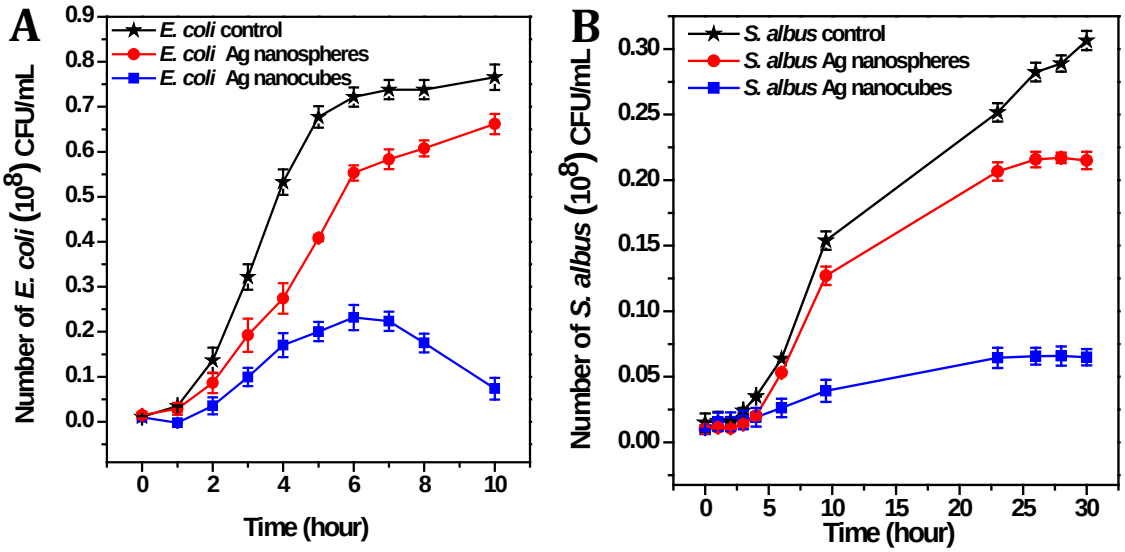

Figure 3.13- Growth kinetic profiles of (A) *E. coli* and (B) *S. albus.*

Interestingly, Ag nanocubes were found to be significantly more effective in delaying the growth of Gram positive bacteria *S. albus* as evident in Figure 3.13B. The difference between the control and Ag nanospheres curves were not that significant compared to the effectiveness of Ag nanocubes. Therefore, Ag nanocubes are definitely more effective than Ag nanospheres as they are found to intensively delay the growth of Gram positive bacteria.

3.3.6 SEM of bacterial cells after treatment of Ag nanostructures

To understand the behaviour of bacteria on exposure to Ag nanoparticles, scanning electron microscopy (SEM) images of bacteria before and after exposure to Ag nanoparticles were obtained as shown in Figures 3.14 and 3.15. In the case of *E.* coli, Figure 3.14A shows untreated cells which appear smooth. When cells are exposed to Ag nanostructures (Figures 3.14B and D), cell walls show signs of rupture. In comparison to untreated *E. coli* cells against treated cells with Ag nanoparticles, the images reveal

distinct changes in cell morphology, with pitting occurring where Ag nanoparticles are present. It is evident that there is a breakdown of cells as well as aggregation of Ag nanoparticles with the treatment of Ag nanocubes (Figure 3.14C). In the case of Ag nanospheres and Ag nanoprisms (Figure 3.14 B and D) exposure to *E. coli* promotes breakdown of the cell wall with less Ag nanoparticle aggregation observed on the bacterial surface in the case of Ag nanoprisms.

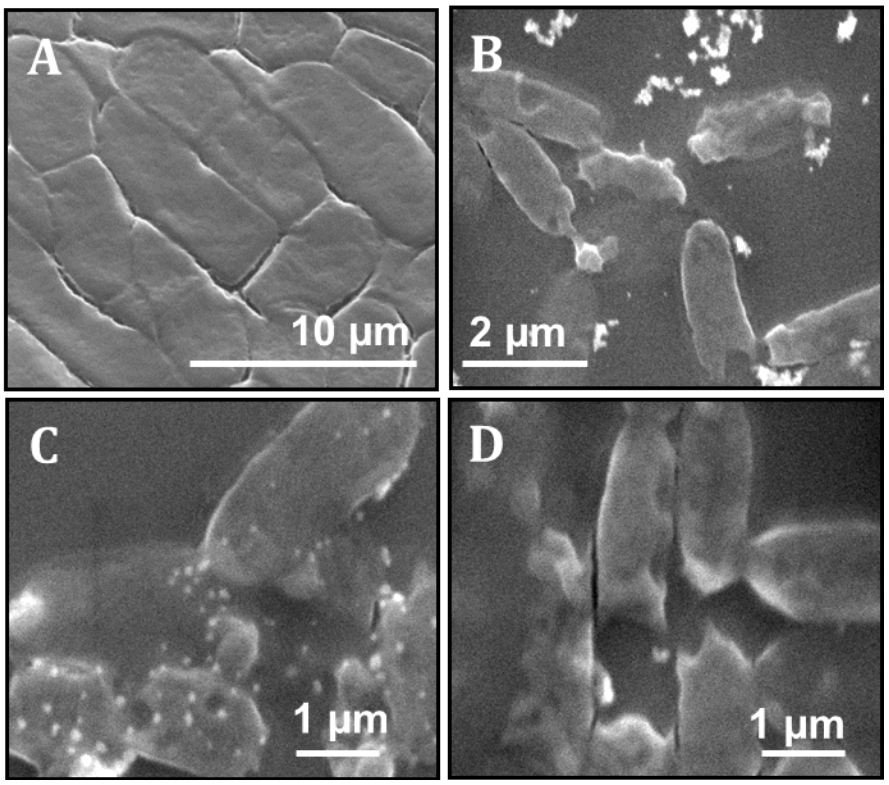

Figure 3.14- SEM micrographs of *E. coli* cells (A) untreated cells and after treatments with (B) Ag nanospheres, (C) Ag nanocubes and (D) Ag nanoprisms.

After the exposure of Ag nanoparticles the components of *E. coli* bacterial cell wall are damaged causing *E. coli* to migrate from their original close arrangement. This confirms that shape-dependent Ag nanostructures have substantial influence on *E. coli* bacterial cell morphology. These observations reveal that in the case of Gram negative bacteria *E. coli*, shape-dependent Ag nanostructures exhibit toxic effects.

In the case of *S. albus*, upon treatment of Ag nanostructures there is a clear morphological change in contrast to untreated *S. albus* cells (Figure 3.15A). The cell wall

observed in Figure 3.15B with the treatment of Ag nanospheres reveals comprehensive breakdown and damage to the bacterial cell integrity. Furthermore, it could be seen that treated *S. albus* upon exposure of Ag nanocubes (Figure 3.15C) showed cells dissolving and their cellular components being released. Additionally, the components of *S. albus* bacteria cell wall displayed disorganised and scattered arrangement after the exposure of Ag nanoprisms in Figure 3.15D.

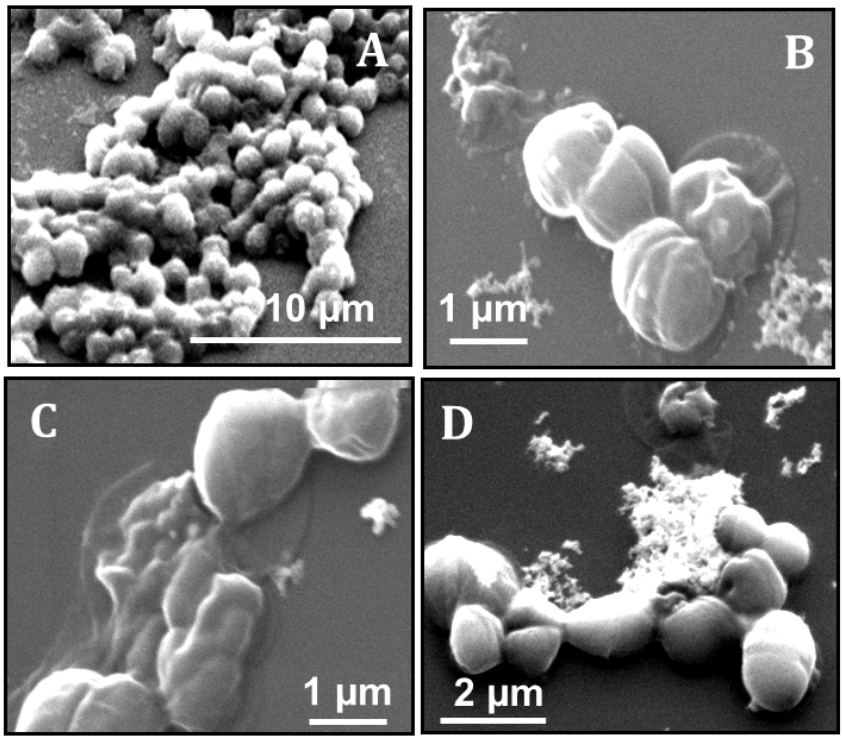

Figure 3.15- SEM micrographs of *S. albus* cells (A) untreated cells and after treatments with (B) Ag nanospheres, (C) Ag nanocubes and (D) Ag nanoprisms.

It has been documented in literature that nanomaterials and heavy metal cations such as Ag^+ ions can play a vital role in the bacterial cell's function.[38, 39] It has been hypothesised that Ag^+ ions can affect the function of membrane bound enzymes and proteins. This interaction causes cellular distortion and a loss of viability.[40] Reports on the mechanism of inhibitory action of silver ions on microorganisms demonstrate that upon Ag^+ treatment, DNA loses its replication ability and expression of ribosomal subunit

proteins. Furthermore, other cellular proteins and enzymes essential to adenosine triphosphate (ATP) production becomes inactivated.[23, 38, 41-44]

However, the exact mechanism of bacterial actions of Ag nanoparticles employed to cause antibacterial effect is still not well understood. In previous findings Ag nanoparticles displayed interaction between constituents of bacterial membrane which resulted in structural changes and destruction to membranes, consequently leading to cell death.[21, 45] From antibacterial applications and SEM imaging of bacterial cells, it is evident that Ag nanostructures cause irreversible bacterial damage to the cell wall and result in ultimate cell death by disrupting the bacterial integrity.

From this study we can speculate that the action of Ag nanoparticles is fairly similar to that of silver ions. It may be proposed that when a bacterial cell is in contact with Ag nanoparticles silver ions are released due to nanoparticle oxidation which inhibits respiratory enzymes, facilitating the generation of reactive oxygen species and consequently damaging the cell. Additionally, Ag nanoparticles have the ability to anchor to the bacterial cell wall and subsequently penetrate through it thereby causing structural changes in the cell membrane as depicted in SEM images.

Based on the observed antibacterial activity and existing literature, Figure 3.16 exhibits various mechanisms by which Ag nanostructures may pose antibacterial activity towards Gram negative and Gram positive bacteria. The schematic illustrates Ag nanostructures interacting with the cell membrane as well as components within each bacterial cell.

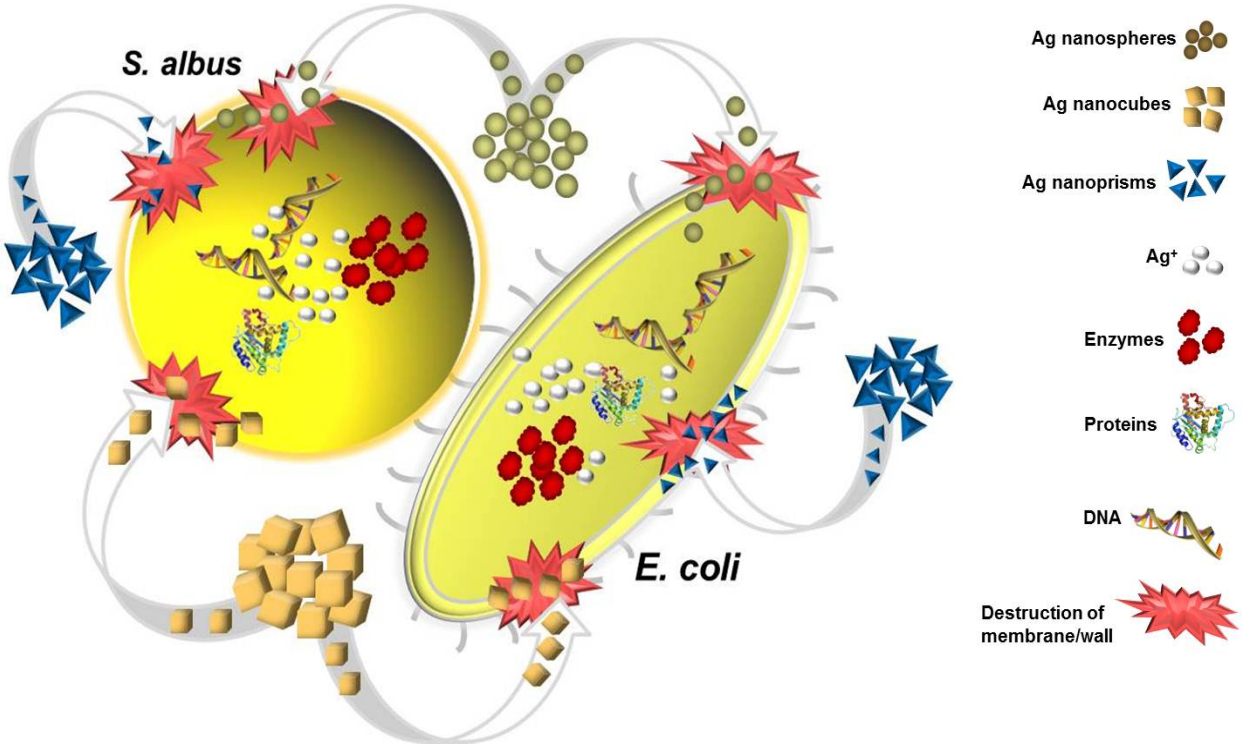

Figure 3.16- Schematic illustration of potential mechanisms of antibacterial activity of Ag nanostructures against *E. coli* and *S. albus.*

3.4 Conclusions

This study shows that Ag nanoparticles exhibit a shape-dependent antibacterial behaviour against bacterial species. Overall, Ag nanoparticles were found to be active against both Gram negative and Gram positive bacterial species. Moreover, among different shapes of Ag nanoparticles explored, Ag nanocubes performed significantly better than Ag nanospheres and nanoprisms, in that order in terms of antibacterial activity against both Gram negative and Gram positive bacteria. This is a significant finding considering that Ag nanocubes have not so far been studied for antibacterial studies, and most of the Ag based nanomaterials reported so far in the literature demonstrate antibacterial activity mainly against Gram negative bacteria. Hence, Ag nanocubes can potentially be utilized in the future for controlling the growth of pathogenic Gram positive bacterial species.

3.5 References

[1] Rai, M.; Yadav, A.; Gade, A., Silver nanoparticles as a new generation of antimicrobials. *Biotechnol. Adv.* **2009,** *27* (1), 76-83.

[2] Kim, J. S.; Kuk, E.; Yu, K. N.; Kim, J. H.; Park, S. J.; Lee, H. J.; Kim, S. H.; Park, Y. K.; Park, Y. H.; Hwang, C. Y.; Kim, Y. K.; Lee, Y. S.; Jeong, D. H.; Cho, M. H., Antimicrobial effects of silver nanoparticles. *Nanomed.-Nanotechnol. Biol. Med.* **2007,** *3* (1), 95-101.

[3] Rai, M. K.; Deshmukh, S. D.; Ingle, A. P.; Gade, A. K., Silver nanoparticles: the powerful nanoweapon against multidrug-resistant bacteria. *Journal of Applied Microbiology* **2011,** *112* (5), 841-852.

[4] Burda, C.; Chen, X. B.; Narayanan, R.; El-Sayed, M. A., Chemistry and properties of nanocrystals of different shapes. *Chem. Rev.* **2005,** *105* (4), 1025-1102.

[5] Kelly, K. L.; Coronado, E.; Zhao, L. L.; Schatz, G. C., The optical properties of metal nanoparticles: The influence of size, shape, and dielectric environment. *J. Phys. Chem. B* **2003,** *107* (3), 668-677.

[6] Kamat, P. V., Photophysical, photochemical and photocatalytic aspects of metal nanoparticles. *J. Phys. Chem. B* **2002,** *106* (32), 7729-7744.

[7] Hiramatsu, H.; Osterloh, F. E., A simple large-scale synthesis of nearly monodisperse gold and silver nanoparticles with adjustable sizes and with exchangeable surfactants. *Chem. Mat.* **2004,** *16* (13), 2509-2511.

[8] Jana, N. R.; Gearheart, L.; Murphy, C. J., Seeding growth for size control of 5-40 nm diameter gold nanoparticles. *Langmuir* **2001,** *17* (22), 6782-6786.

[9] Wiley, B.; Sun, Y. G.; Mayers, B.; Xia, Y. N., Shape-controlled synthesis of metal nanostructures: The case of silver. *Chem.-Eur. J.* **2005,** *11* (2), 454-463.

[10] Xiong, Y. J.; Xia, Y. N., Shape-controlled synthesis of metal nanostructures: The case of palladium. *Adv. Mater.* **2007,** *19* (20), 3385-3391.

[11] Lim, B. W.; Lu, X. M.; Jiang, M. J.; Camargo, P. H. C.; Cho, E. C.; Lee, E. P.; Xia, Y. N., Facile synthesis of highly faceted multioctahedral Pt nanocrystals through controlled overgrowth. *Nano Lett.* **2008,** *8* (11), 4043-4047.

[12] Yu, X. F.; Li, Y. X.; Wlodarski, W.; Kandasamy, S.; Kalantar-Zadeh, K., Fabrication of nanostructured TiO_2 by anodization: A comparison between electrolytes and substrates. *Sens. Actuator B-Chem.* **2008,** *130* (1), 25-31.

[13] Nair, L. S.; Laurencin, C. T., Silver nanoparticles: Synthesis and therapeutic applications. *J. Biomed. Nanotechnol.* **2007,** *3* (4), 301-316.

[14] Chen, X.; Schluesener, H. J., Nanosilver: A nanoproduct in medical application. *Toxicology Letters* **2008,** *176* (1), 1-12.

[15] Kassaee, M. Z.; Akhavan, A.; Sheikh, N.; Sodagar, A., Antibacterial effects of a new dental acrylic resin containing silver nanoparticles. *J. Appl. Polym. Sci.* **2008,** *110* (3), 1699-1703.

[16] Ahn, S. J.; Lee, S. J.; Kook, J. K.; Lim, B. S., Experimental antimicrobial orthodontic adhesives using nanofillers and silver nanoparticles. *Dent. Mater.* **2009,** *25* (2), 206-213.

[17] Maneerung, T.; Tokura, S.; Rujiravanit, R., Impregnation of silver nanoparticles into bacterial cellulose for antimicrobial wound dressing. *Carbohydrate Polymers* **2008,** *72* (1), 43-51.

[18] Ip, M.; Lui, S. L.; Poon, V. K. M.; Lung, I.; Burd, A., Antimicrobial activities of silver dressings: an in vitro comparison. *J. Med. Microbiol.* **2006,** *55* (1), 59-63.

[19] Bosetti, M.; Masse, A.; Tobin, E.; Cannas, M., Silver coated materials for external fixation devices: in vitro biocompatibility and genotoxicity. *Biomaterials* **2002,** *23* (3), 887-892.

[20] Andersson, D. I.; Hughes, D., Antibiotic resistance and its cost: is it possible to reverse resistance? *Nat. Rev. Microbiol. 8* (4), 260-271.

[21] Sondi, I.; Salopek-Sondi, B., Silver nanoparticles as antimicrobial agent: a case study on *E-coli* as a model for Gram-negative bacteria. *J. Colloid Interface Sci.* **2004,** *275* (1), 177-182.

[22] Pal, S.; Tak, Y. K.; Song, J. M., Does the antibacterial activity of silver nanoparticles depend on the shape of the nanoparticle? A study of the Gram-negative bacterium *Escherichia coli*. *Appl. Environ. Microbiol.* **2007,** *73* (6), 1712-1720.

[23] Li, W. R.; Xie, X. B.; Shi, Q. S.; Zeng, H. Y.; Ou-Yang, Y. S.; Chen, Y. B., Antibacterial activity and mechanism of silver nanoparticles on *Escherichia coli*. *Appl. Microbiol. Biotechnol.* **2010,** *85* (4), 1115-1122.

[24] Panacek, A.; Kvitek, L.; Prucek, R.; Kolar, M.; Vecerova, R.; Pizurova, N.; Sharma, V. K.; Nevecna, T.; Zboril, R., Silver colloid nanoparticles: Synthesis, characterization, and their antibacterial activity. *J. Phys. Chem. B* **2006,** *110* (33), 16248-16253.

[25] Selvakannan, P. R.; Swami, A.; Srisathiyanarayanan, D.; Shirude, P. S.; Pasricha, R.; Mandale, A. B.; Sastry, M., Synthesis of aqueous Au core–Ag shell nanoparticles using tyrosine as a pH-dependent reducing agent and assembling phase-transferred silver nanoparticles at the air–water interface. *Langmuir* **2004,** *20* (18), 7825-7836.

[26] Siekkinen, A. R.; McLellan, J. M.; Chen, J. Y.; Xia, Y. N., Rapid synthesis of small silver nanocubes by mediating polyol reduction with a trace amount of sodium sulfide or sodium hydrosulfide. *Chem. Phys. Lett.* **2006,** *432* (4-6), 491-496.

[27] Aherne, D.; Ledwith, D. M.; Gara, M.; Kelly, J. M., Optical properties and growth aspects of silver nanoprisms produced by a highly reproducible and rapid synthesis at room temperature. *Adv. Funct. Mater.* **2008,** *18* (14), 2005-2016.

[28] Brause, R.; Moeltgen, H.; Kleinermanns, K., Characterization of laser-ablated and chemically reduced silver colloids in aqueous solution by UV/VIS spectroscopy and STM/SEM microscopy. *Applied Physics B: Lasers and Optics* **2002,** *75* (6), 711-716.

[29] Mulvaney, P., Surface plasmon spectroscopy of nanosized metal particles. *Langmuir* **1996,** *12* (3), 788-800.

[30] Mie, G., *Contributions to the optics of turbid media: Particularly of colloidal metal solutions*. H.M. Stationery Office: 1976.

[31] Sosa, I. O.; Noguez, C.; Barrera, R. G., Optical properties of metal nanoparticles with arbitrary shapes. *The Journal of Physical Chemistry B* **2003,** *107* (26), 6269-6275.

[32] Siekkinen, A. R.; McLellan, J. M.; Chen, J.; Xia, Y., Rapid synthesis of small silver nanocubes by mediating polyol reduction with a trace amount of sodium sulfide or sodium hydrosulfide. *Chem. Phys. Lett.* **2006,** *432* (4-6), 491-496.

[33] Hao, E.; Schatz, G.; Hupp, J., Synthesis and Optical Properties of Anisotropic Metal Nanoparticles. *J. Fluoresc.* **2004,** *14* (4), 331-341.

[34] Selvakannan, P. R.; Swami, A.; Srisathiyanarayanan, D.; Shirude, P. S.; Pasricha, R.; Mandale, A. B.; Sastry, M., Synthesis of Aqueous Au Coreâ˜Ag Shell Nanoparticles Using Tyrosine as a pH-Dependent Reducing Agent and Assembling Phase-

Transferred Silver Nanoparticles at the Airâ^'Water Interface. *Langmuir* **2004,** *20* (18), 7825-7836.

[35] Sun, Y.; Mayers, B.; Xia, Y., Transformation of silver nanospheres into nanobelts and triangular nanoplates through a thermal process. *Nano Letters* **2003,** *3*, 675-679.

[36] Wiley, B.; Sun, Y.; Mayers, B.; Xia, Y., Shape controlled synthesis of metal nanostructures: the case of silver. *Chem. Eur* **2005**, 454-463.

[37] Yu, D. B.; Yam, V. W. W., Controlled synthesis of monodisperse silver nanocubes in water. *J. Am. Chem. Soc.* **2004,** *126* (41), 13200-13201.

[38] Feng, Q.; Wu, J.; Chen, G.; Cui, F.; Kim, T.; Kim, J., A mechanistic study of the antibacterial effect of silver ions on *Escherichia coli* and *Staphylococcus aureus*. *Journal of biomedical materials research* **2000,** *52* (4), 662-668.

[39] Kumar, R.; Münstedt, H., Silver ion release from antimicrobial polyamide/silver composites. *Biomaterials* **2005,** *26* (14), 2081-2088.

[40] Clement, J. L.; Jarrett, P. S., Antibacterial silver. *Met Based Drugs* **1994,** *1* (5-6), 467-482.

[41] Eckhardt, S.; Brunetto, P. S.; Gagnon, J.; Priebe, M.; Giese, B.; Fromm, K. M., Nanobio Silver: Its Interactions with Peptides and Bacteria, and Its Uses in Medicine. *Chem. Rev.* **2013**.

[42] Hajipour, M. J.; Fromm, K. M.; AkbarAshkarran, A.; Jimenez de Aberasturi, D.; Larramendi, I. R. d.; Rojo, T.; Serpooshan, V.; Parak, W. J.; Mahmoudi, M., Antibacterial properties of nanoparticles. *Trends in Biotechnology* **2012**.

[43] Auffan, M.; Rose, J.; Bottero, J.-Y.; Lowry, G. V.; Jolivet, J.-P.; Wiesner, M. R., Towards a definition of inorganic nanoparticles from an environmental, health and safety perspective. *Nat. Nanotechnol.* **2009,** *4* (10), 634-641.

[44] Bhabra, G.; Sood, A.; Fisher, B.; Cartwright, L.; Saunders, M.; Evans, W. H.; Surprenant, A.; Lopez-Castejon, G.; Mann, S.; Davis, S. A.; Hails, L. A.; Ingham, E.; Verkade, P.; Lane, J.; Heesom, K.; Newson, R.; Case, C. P., Nanoparticles can cause DNA damage across a cellular barrier. *Nat. Nanotechnol.* **2009,** *4* (12), 876-883.

[45] Xiu, Z.; Zhang, Q. B.; Puppala, H. L.; Colvin, V. L.; Alvarez, P. J., Negligible particle-specific antibacterial activity of silver nanoparticles. *Nano Lett.* **2012**.

Chapter IV

Influence of synergism between antibiotics and silver nanoparticles on antibacterial activity: ampicillin, penicillin G and polymyxin B

4.1 Introduction

Antibiotics are molecules that inhibit microbes, both bacteria and fungi from growth inhibition or outright cell killing. Generally, antibiotics are divided into two broad groups of selective toxicity according to their biological effect on microorganisms: antibiotics that prevent bacteria from growing are known as *bacteriostatic*, and ones that cause bacterial cell death are *bactericidal*. Certain antibiotics can display bacteriostatic activity in some circumstances and bactericidal activity in others, with sufficient damage to one or more metabolic pathways or cellular structures.[1]

Antibiotic agents can either be natural products or man-made synthetic chemicals designed to selectively block specific crucial metabolic pathways in microbial cells selectivity.[2] Majority of antibiotics introduced into human clinical use to treat infectious disease have been natural products. This aspect of antibiotic discovery is underpinned by

one microorganism in a specific habitat and set of environmental conditions to disturb neighbouring microbes, either to regulate their growth or to activate their elimination.[3]

The range of bacteria or other microorganisms that is affected by a certain antibiotic is expressed as its spectrum of action. When antibiotics are effective against prokaryotes to kill or inhibit a wide array of Gram positive and Gram negative bacteria, they are known to be of *broad spectrum*. If effectiveness is primarily against either Gram positive or Gram negative bacteria, they are of *narrow spectrum*. Additionally, if effective against a single organism or disease, they are referred to as *limited spectrum*. A medically useful antibiotic should have as many of these characteristic as possible:[4]

- Possess a wide spectrum of activity with the ability to destroy or inhibit many different species of pathogenic organisms
- Nontoxic to the host and without undesirable side effects
- Non-allergenic to the host
- Inexpensive and easy to produce
- Chemically-stable (long shelf life)
- Least chance of microbial resistance
- Microbial resistance is uncommon and unlikely to develop

The first antibiotic was penicillin, which was discovered in 1928 and then followed by penicillin-related antibiotics such as ampicillin, amoxicillin and benzylpenicillin which are extensively used today to treat various infections and diseases. However complete elimination of bacteria is somewhat impossible as they eventually become resistant to antibiotics.[5]

Antibiotic resistance is a natural phenomenon. When antibiotics are utilised, bacteria that show resistance have a greater chance of survival than those that are

susceptible. Susceptible bacteria are killed or inhibited by an antibiotic, resulting in a selective pressure whereby antibiotic-resistant bacteria are allowed to survive and multiply. Some bacteria are naturally resistant to certain types of antibiotics, and may also become resistant in two ways: genetic mutation or by acquiring resistance from another bacterium.[6-8] Figure 4.1 illustrates how antibiotic resistance spreads in day to day life from humans and animals.

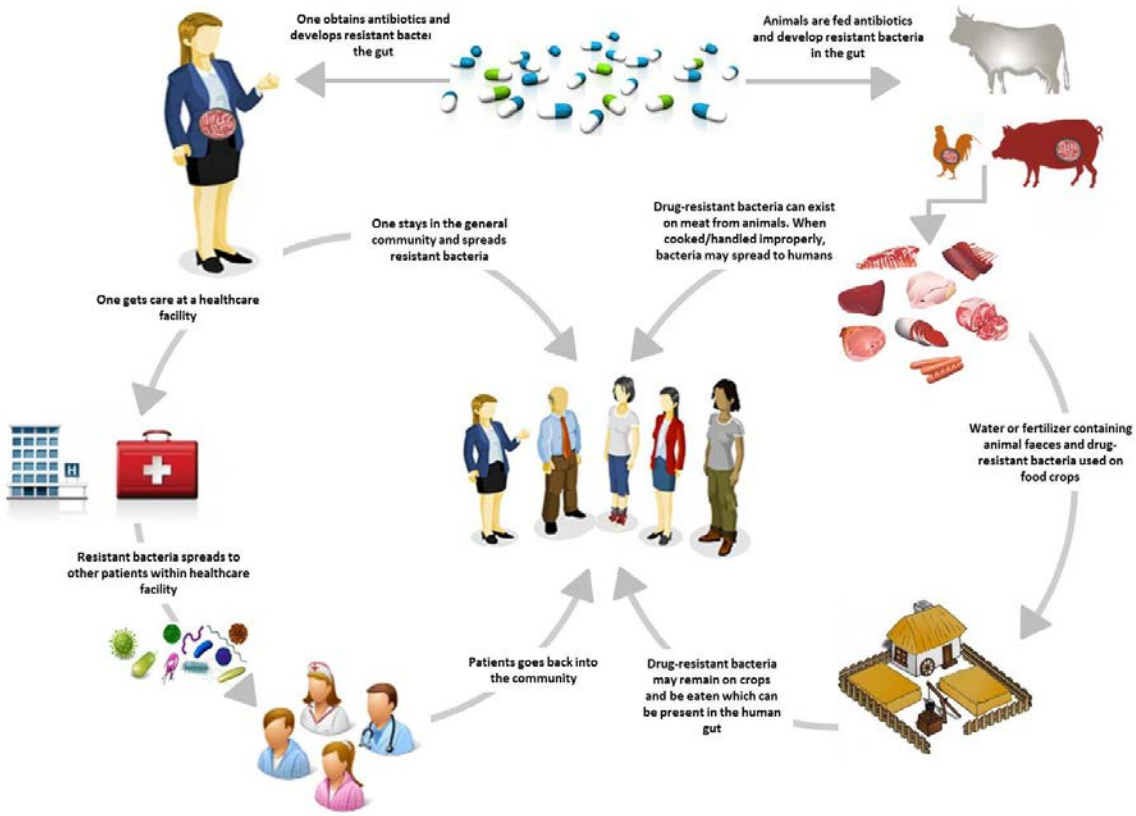

Figure 4.1- Schematic representation of antibiotic resistance scheme.

Different genetic mutations yield diverse types of resistance. Some mutations enable the bacteria to produce effective enzymes that inactivate antibiotics, while other mutations eliminate the cell target that the antibiotics attack. A mechanism responsible for removing compounds such as neurotransmitters, toxic substances and antibiotics out of the cell is known as active efflux. The system functions via an energy dependent mechanism to pump out unwanted toxic wastes through efflux pumps. These pumps are

protein transporters localised in the cytoplasmic membrane in cells. However, the impact of efflux mechanisms on antimicrobial resistance is relatively vast. This may attribute to genetic elements encoded on chromosomes and plasmids. Antibiotics can act as inducers and regulators of some efflux pumps causing over-expression of several efflux pumps in a given bacterial species. However this can lead to a broad spectrum of resistance when shared across species.[9, 10]

Consequently, the extensive use of antibiotics has led to a worldwide escalation of bacterial resistance and spread of many pathogens which is a serious concern for modern day medicine. High prevalence of multidrug-resistant bacteria among bacteria-based infections decreases effectiveness of current treatments and causes millions of deaths.[11, 12] Antibiotics are also commonly found in food of animals to prevent, control and treat disease, and to promote the growth of food-producing animals. The foremost problem is that bacteria and other microbes that cause infections are remarkably resilient and have developed several ways to resist antibiotics and other antimicrobial drugs. Moreover, resistance is due to increasing use and misuse of existing antibiotics in human and veterinary medicine as well as in agriculture. Other factors contributing to the development of antimicrobial resistance are:[13, 14]

- Single mode of action of particular antibiotics
- Evolving microorganisms themselves, escalation of emerging and re-emerging infectious diseases
- Combination of increased pressure of antibiotic selections
- Decline in the development of new antibiotics

Bacteria can obtain antibiotic resistance genes from other microorganisms in several ways by conjugation. This allows bacteria to transfer genetic material including

genes encoding resistance to antibiotics from one bacterium to another. Bacteriophages provide an additional mechanism for passing resistance traits between microorganisms. The resistance traits from one bacterium are embedded into the head portion of the virus. The virus then transfers the resistance traits into any new bacteria it attacks. Bacteria also have the capacity to obtain deoxyribonucleic acid (DNA) from their surrounding environment.[15] Hence, any bacteria that attain resistance genes, whether by spontaneous mutation or genetic exchange with other bacteria have the ability to resist one or more antibiotics. Since bacteria can accumulate multiple resistance traits over time, they may become resistant to different categories of antibiotics.

The bacterial resistance to antibiotics has been attempted to be resolved by discovering new antibiotics and chemically modifying existing antimicrobial drugs. However, it is difficult for new antimicrobial drugs to catch up to the microbial pathogen's fast and frequent development of resistance in a timely manner. This challenging and dynamic array of infectious diseases and the emergence of bacterial strains resistant to current antibiotics, demand for a long term solution to this ever growing problem.[16-18]

One of the promising approaches in addressing this challenge lies in exploring antimicrobial nanomaterials, to which microbial pathogens may not be able to develop resistance due to multiple mechanisms of action and novel nanosized platforms for efficient antibiotics delivery.[19, 20] It has been suggested in recent studies that some metal nanomaterials are known to possess antimicrobial activities to control infectious diseases. Moreover, metallic nanoparticles offer many distinctive advantages in reducing toxicity, overcoming resistance and lower costs when compared to conventional antibiotics. Owing to their small sizes and higher surface to volume ratio, metallic

nanoparticles have an enlarged contact surface area with microorganisms. This trait enhances biological and chemical activity, which contributes towards potent antibacterial properties. In addition to this property, metal nanoparticles have the ability to target various bacterial structures as shown in the previous chapter. Nanoparticles can disturb functions of cell membranes, causing permeability and interference with metabolic processes.

Recent studies have shown that combined use of nanoparticles with antibiotics makes it possible to reduce the toxicity of both agents towards mammalian cells while synergistically enhancing their antimicrobial activity. Investigations of interactions of antibiotics with silver nanoparticles are the most common among studies dedicated to examination of combined action of metallic nanoparticles with antibiotics. However, most of these studies are mainly focused on broad spectrum of antibiotics.[21-24] The variety of novel antimicrobials which show synergy with classic antibiotics is limited with many of these compounds used as an alternative to conventional treatments and agriculture. However, their widespread application is limited, primarily due to their mechanisms of action have not been fully characterised and understood.[22-24]

Since it has been shown in the previous chapter that Ag nanoparticles exhibit antibacterial activities against both Gram negative and Gram positive bacteria, this chapter will explore the synergistic effects of Ag nanoparticles when combined with antibiotics. The major focus on this chapter is primarily on tyrosine reduced Ag nanospheres combined with both broad and narrow spectrums of antibiotics. The bactericidal antibiotics selected for this study were ampicillin, penicillin G and polymyxin B.

4.1.1 Ampicillin

Ampicillin, commonly known as broad-spectrum aminopenicillin is a β-lactam (beta-lactam) antibiotic which belongs to the broad class of antibiotics and has been extensively used to treat bacterial infections. Since it is classified to be in the broad spectrum, ampicillin is effective against Gram negative as well as Gram positive organisms. Aminopenicillins were created by joining penicillin to an amino group or side chain. Addition of the side chains significantly changed the activity of the antibiotic drug against some bacteria.

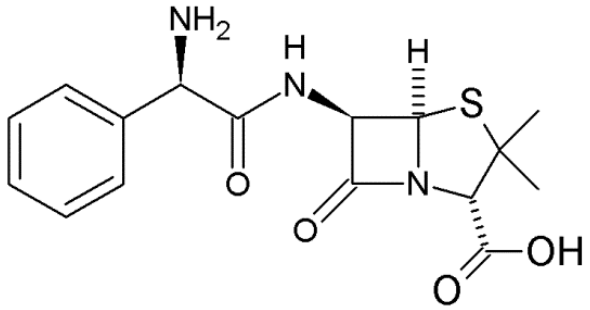

Figure 4.2- Chemical structure of ampicillin.

4.1.2 Penicillin G

Penicillin G, also known as benzylpenicillin is a derivative from penicillin. Penicillin G possesses a narrow spectrum of effectiveness against microorganisms, mainly against Gram positive bacteria. The structure of penicillin G is shown in Figure 4.3.

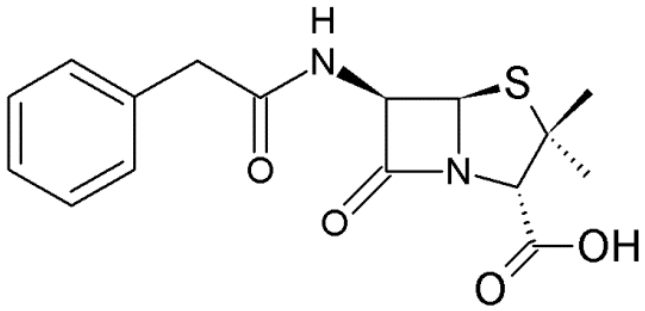

Figure 4.3- Chemical structure of penicillin G.

4.1.3 Polymyxin B

Polymyxin B is a lipopeptide antibiotic isolated from *Bacillus polymyxa*. Its basic structure consists of a polycatonic peptide ring and a tripeptide side chain with a fatty acid tail as shown in Figure 4.4. This antibiotic has a narrow spectrum and is active against most Gram negative bacteria.

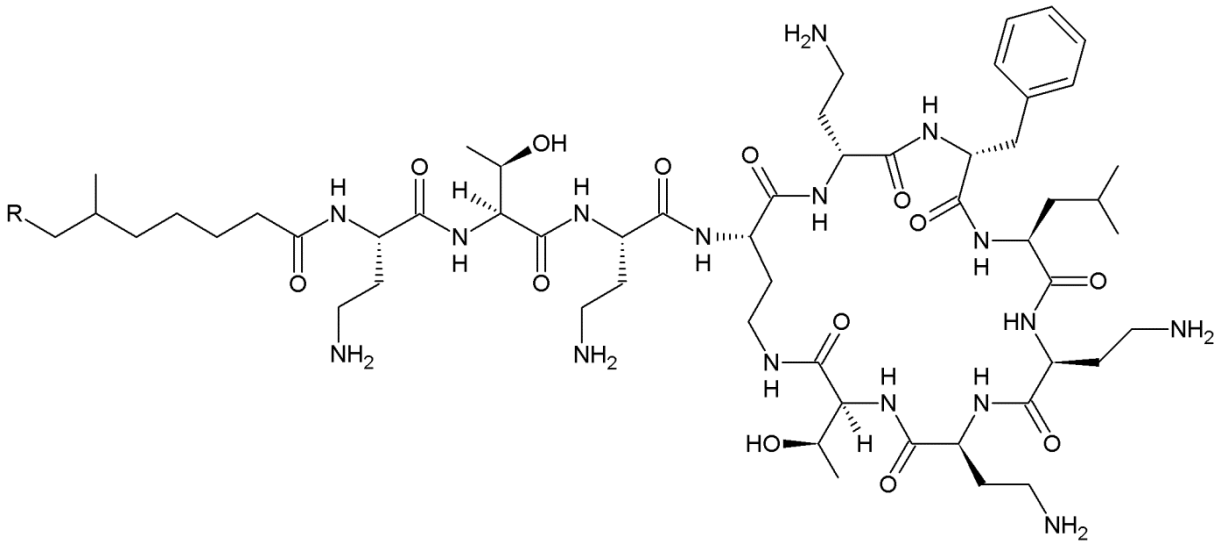

Figure 4.4- Chemical structure of polymyxin B.

4.2 Experimental

4.2.1 Synthesis of Ag nanospheres

Tyrosine reduced Ag nanospheres were synthesised as discussed in Chapter III, with slight modifications. In brief, 10 ml of 10^{-3} M aqueous silver nitrate was prepared and added to 10 ml of 10^{-3} M aqueous solution of tyrosine. This solution was then diluted to 100 mL with Milli-Q water. To this solution, 1 mL of 10^{-1} M KOH was added and was allowed to boil. Within 20 minutes the final colourless solution changed into a light yellow colour which indicated the formation of silver nanoparticles. The solution was allowed to boil for a further 15 minutes for silver nanoparticles to grow and stabilise.

4.2.2 Antibacterial study

All antibacterial experiments were performed under aseptic conditions in a laminar flow cabinet. Before the commencement of microbiological experiments, media cultures, glassware and pipette tips were sterilised by autoclaving at 121°C for 15 minutes. *Escherichia coli* was chosen as Gram negative representative and Gram positive bacterium *Staphylococcus albus* was another candidate for antibacterial studies. Antibiotics used were ampicillin, penicillin G and polymyxin B.

4.2.2.1 Colony forming units (CFU) assay

Colony forming units assay was used to examine the synergistic effects of antibiotics with Ag nanospheres for bactericidal activity against Gram negative and Gram positive bacteria. 10^4 CFU of each bacterium were mixed with appropriate proportion of antibiotics causing 20% cell death and different concentrations of nanoparticles in a total of 1 mL volume. 100 µL of this was then plated on agar plates and were incubated for 24 hrs at 37°C and the numbers of colonies were counted.

In order to screen the optimum concentration of antibiotics needed for further studies, preliminary experiments were conducted to determine the amount of antibiotics needed to yield ca. 20% cell death. Stock solutions of antibiotics were prepared and from this, various aliquots were taken and mixed with 10^4 bacteria in 1 mL volume tissue culture wells as shown in Table 4.1. From each well, 100 µL were plated onto agar plates with 1 hr exposure. Plates were then incubated for 24 hrs at 37°C and the numbers of colonies were counted. Colonies formed correspond to the number of viable bacteria in each suspension at the time of aliquot withdrawal.

Table 4.1- Optimum concentration of antibiotics needed for further studies.

Antibiotics	*E. coli* culture		*S. albus* culture	
	Stock Solution	Aliquot for 20% cell death	Stock Solution	Aliquot for 20% cell death
Ampicillin (+, -)	1 mg / mL	50 µL	1 mg / 5 mL	10 µL
Penicillin G (+)	-	-	1 mg / 5 mL	2 µL
Polymyxin B (-)	0.0125 mg / mL	10 µL	-	-

Subsequently, each aliquot of antibiotics as determined in Table 4.1 was combined with different concentrations of Ag nanospheres such as 0.5 mM, 1 mM, 1.5 mM and 2.0 mM and were tested for their synergistic effects on both Gram positive and Gram negative bacteria via CFU assay. It may be noted that while further discussed nanoparticle characterisation aspect investigates only nanoparticles conjugated to antibiotics (through removal of free antibiotic in nanoparticle solution by centrifugation), the antibacterial tests took both free and conjugated antibiotics into account as per the above Table 4.1.

4.3 Results and discussion

4.3.1 UV-Visible spectral studies of antibiotics and Ag nanoparticles

UV-Vis spectra shown in Figure 4.5, display the absorbance of antibiotics with and without the addition of Ag nanoparticles (AgNPs). Initially, antibiotics without the addition of Ag nanoparticles were characterised by UV-Vis (dotted lines) followed by the combination of Ag nanoparticles and antibiotics (solid lines).

As illustrated in the UV-vis spectra, a strong absorbance peak was centered at ca. 320 nm for ampicillin (AMP) and penicillin G (PCG). However in the case of polymyxin B (PMB), only a weak peak was observed in this region while a shoulder observed at ca. 280 nm attributed to its peptide nature. Tyrosine reduced Ag nanoparticles showed a peak maximum at ca. 413 nm. Upon conjugation of antibiotics,

the surface plasmon resonance (SPR) peak maxima of Ag shifted to ca. 419, 421 and 441 nm in case of AMP, PCG and PMB respectively. These shifts in Ag SPR peak maxima supports successful binding of antibiotics to the Ag nanoparticle surface.

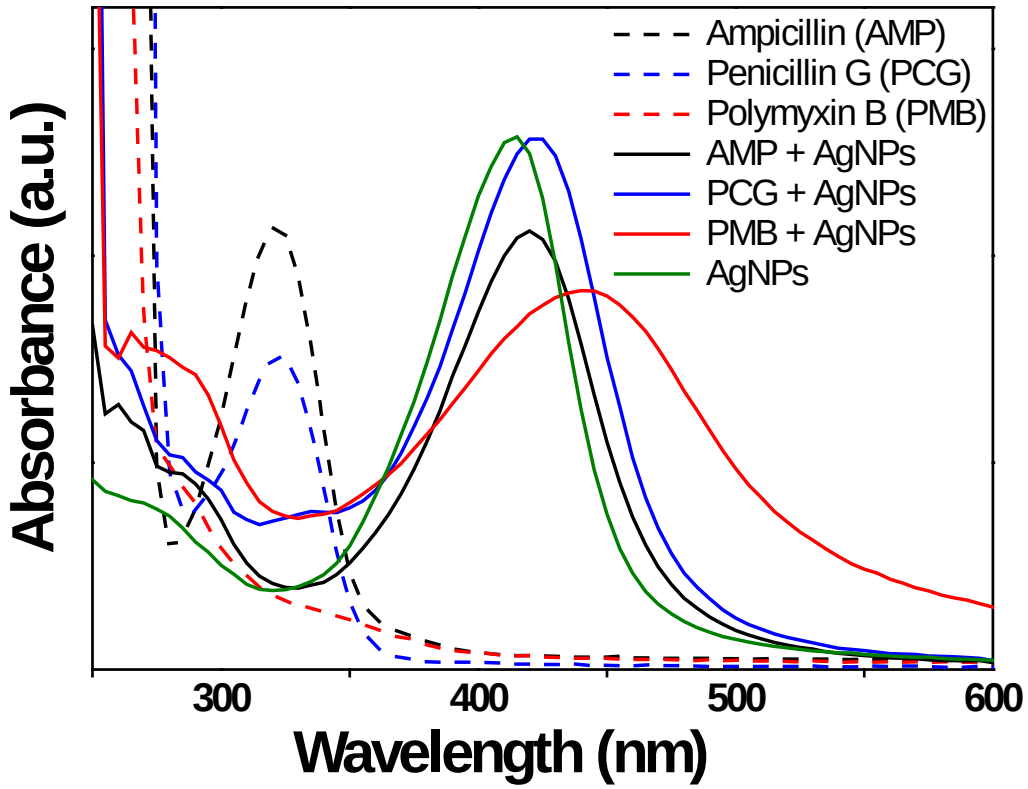

Figure 4.5- UV-Visible absorbance studies on pristine antibiotics on its own and antibiotics combined with Ag nanoparticles.

4.3.2 TEM and DLS studies of antibiotics combined with Ag nanoparticles

Illustrated in Figure 4.6 are TEM images of Ag nanoparticles combined with various antibiotics with corresponding particle size histograms. Images reveal that these particles are quasi spherical in shape with low polydispersity. The pristine tyrosine reduced Ag nanoparticles were found to be of ca. 21.8 ± 5.0 nm in diameter as shown in previous Chapter III. The average particle diameter for each nanomaterial after antibiotic exposure was calculated along with the standard deviation of ca. 22.1 ± 8.2 nm, 21.7 ± 7.7 nm and 23.4 ± 7.1 nm for Ag nanoparticles combined with ampicillin, penicillin G and polymyxin B respectively. The nanomaterials are relatively similar in sizes and

there were no signs of aggregation post antibiotic exposure which is consistent with UV-Vis spectroscopic observation.

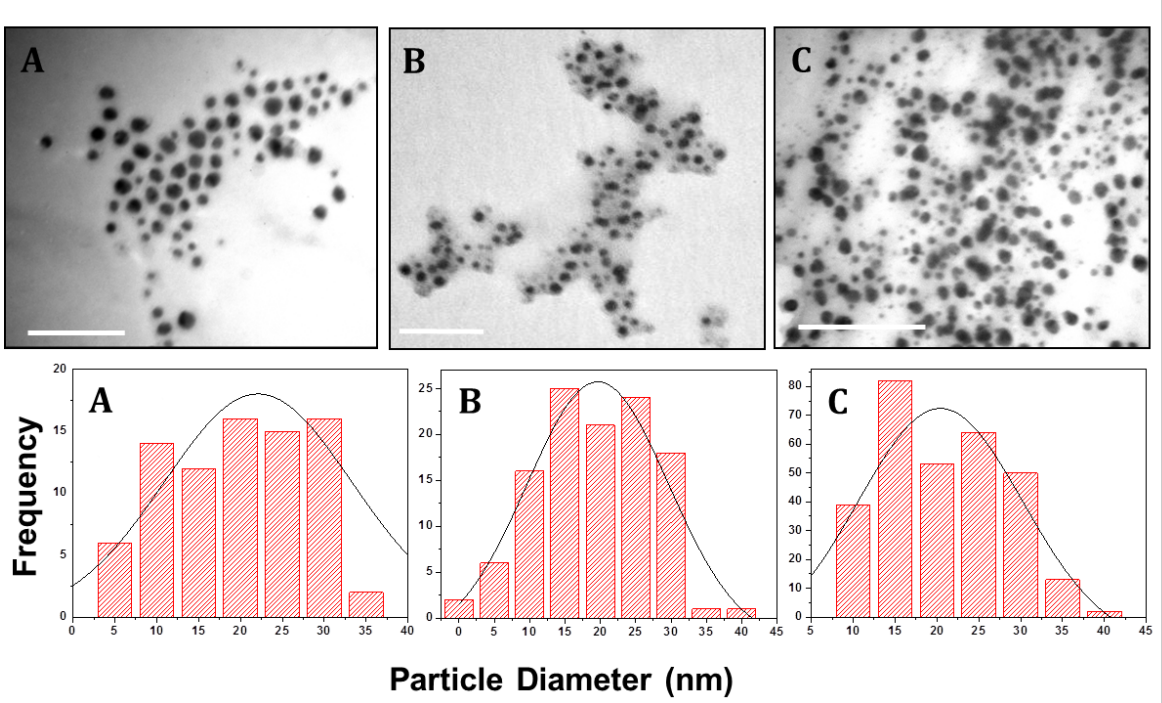

Figure 4.6- TEM images and corresponding particle size distribution histograms of (A) AgNPs+AMP (B) AgNPs+PCG and (C) AgNPs+PMB. (Scale bars corresponds to 200 nm)

Additionally, DLS analysis was carried out on these nanomaterials to substantiate TEM results. DLS contributes information on the hydrodyanmic radii of nanoparticles in solution by measuring the time scale of light intensity fluctuations. DLS measurements in Figure 4.7 reveal the average hydrodynamic radius was 33.1 nm (equivalent to hydrodynamic diameter 66.2 nm) in the case of AgNPs+AMP, 28.5 nm (equivalent to hydrodynamic diameter 57.0 nm) for AgNPs+PCG and 35.7 nm (equivalent to hydrodynamic diameter 71.4 nm) for AgNPs+PMB. In comparison, as shown in Chapter III, pristine tyrosine reduced Ag nanoparticles had a hydrodynamic radius of 41.4 nm (equivalent to hydrodynamic diamter 82.8 nm). Since the hydrodynamic diameter is typically larger than the TEM determined diameter by an offset that is a function of surface capping agent, reduction in hydrodynamic diameter of

Ag nanoparticles after exposure to antibiotics suggest a ligand exchange between tyrosine and antibiotics.

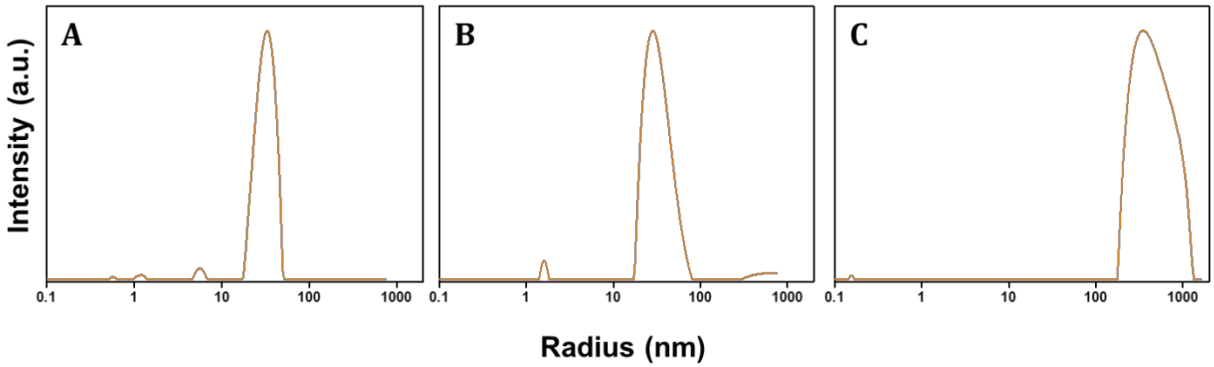

Figure 4.7- DLS size distribution of (a) AgNPs+AMP (b) AgNPs+PCG and (c) AgNPs+PMB.

4.3.3 FTIR analysis of antibiotics combined with Ag nanoparticles

FTIR spectroscopic analysis of Ag nanoparticles, various antibiotics and Ag nanoparticles combined with antibiotics was carried out to understand how antibiotics are interacting and binding with Ag nanoparticles. FTIR analysis is also beneficial as it provides evidence on the surface chemistry of these particles. Figure 4.8 reveals different functional groups present within each antibiotic and Table 4.2 provides a summary of functional groups present in each nanoparticle and antibiotic combination. The spectra of Ag nanoparticles combined with ampicillin, and pure ampicillin are similar suggesting that Ag nanoparticles are completely capped with the antibiotic without any perturbation of antibiotic structure while sharing spectral bands at frequencies 1765 cm^{-1} representing C=O stretch, and 1700 cm^{-1} to 1450 cm^{-1} with C=C stretching of aromatic rings. Similarly, frequencies at 1393 cm^{-1} and 1280 cm^{-1} corresponds to aromatic rings with C-O stretching.[25-27]

In the case of pure penicillin G, the C=O stretch at ca. 1792 cm^{-1} shifted to ca. 1773 cm^{-1} when combined with Ag nanoparticles. Similarly, aromatic rings with C=C stretching at ca. 1516 cm^{-1} and 1322 cm^{-1} were shifted to ca. 1499 cm^{-1} and 1311 cm^{-1},

respectively when combined with Ag nanoparticles. These shifts suggest that there is interaction between penicillin G and the metal surface through the C=C bond.[26, 28]

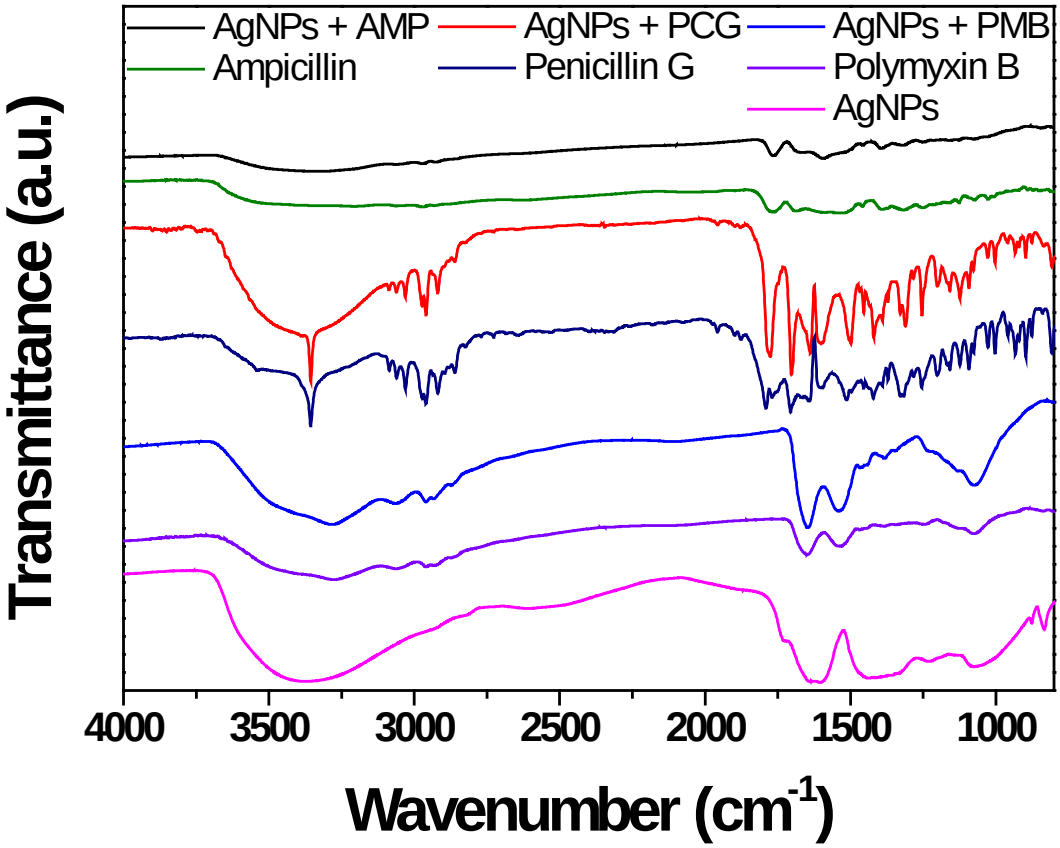

Figure 4.8- FTIR spectral analysis of Ag nanoparticles and antibiotics.

In the spectrum for pure polymyxin B, bands at ca. 1649 cm^{-1} and 1539 cm^{-1} are attributed to the amide I and II vibrational modes.[26, 29, 30] These frequencies were slightly shifted to ca. 1647 cm^{-1} and 1536 cm^{-1} upon exposure to Ag nanoparticles. The shifts indicate the binding of polymyxin B on Ag nanoparticles. Additionally, broad O-H peaks ca. 3650 cm^{-1} to 2800 cm^{-1} are present in all cases of antibiotics and when antibiotics are combined with Ag nanoparticles. These peaks are attributed to water molecules apparent within the samples.

Table 4.2- Summary of functional groups in Ag nanoparticles and antibiotics combined with Ag nanoparticles.

Wavenumber (cm^{-1})	Bond	Functional group	Appearance
AgNPs with Ampicillin			
3650 - 2800	O-H stretch	Hydroxyl	Broad
1765	C=O stretch	Aldehyde/Ketone	Weak
1700 - 1450	C=C stretch	Aromatic rings	Weak
1393	C–O stretch	Aromatic rings	Weak
1280	C–O stretch	Aromatic rings	Weak
Ampicillin			
3650 - 2800	O–H stretch	Hydroxyl	Broad
1765	C=O stretch	Aldehyde/Ketone	Weak
1700 - 1450	C-C stretch	Aromatic rings	Weak
1393	C-O stretch	Aromatic rings	Weak
1280	C-O stretch	Aromatic rings	Weak
AgNPs with Penicillin G			
3356	N–H stretch	Amine	Narrow and sharp
3088 - 2858	C–H stretch	Alkane	Broad
1773	C=O stretch	Aldehyde/Ketone	Medium
1604	C=O stretch	Aromatic rings	Medium
1499	C=C stretch	Aromatic rings	Medium
1311	C=C stretch	Aromatic rings	Medium
3356	N–H stretch	Amine	Narrow and sharp
AgNPs with Penicillin G			
3088 - 2858	C–H stretch	Alkane	Broad
1792	C=O stretch	Aldehyde/Ketone	Medium
1604	C=O stretch	Aromatic rings	Medium
1516	C=C stretch	Aromatic rings	Medium
1322	C=C stretch	Aromatic rings	Medium
AgNPs with Polymyxin B			
3650 - 3150	O–H stretch	Hydroxyl	Broad
1647	N–H stretch	Amide	Medium
1539	N–H stretch	Amide	Medium
Polymyxin B			
3650 - 3150	O–H stretch	Hydroxyl	Broad
1649	N–H stretch	Amide	Medium
1536	N–H stretch	Amide	Medium
AgNPs			
3400 - 3200	O–H stretch	Hydroxyl	Broad
1638	C=O stretch	Carboxylate ion	Narrow and sharp

4.3.4 X-ray photoelectron spectroscopy (XPS) of antibiotics combined with Ag nanoparticles

The X-ray photoelectron spectra for C 1s, N 1s and O 1s core level binding energies (BEs) of silver nanoparticles that were synthesised by tyrosine mediated reduction of silver ions are shown in Figure 4.9. These are in close agreement with the BE's of silver nanoparticles previously reported.[31] The C 1s spectrum was deconvoluted into three chemically different components, which were assigned to the aromatic carbon (285.04 eV), carbon bound to the quinone oxygen (286.74 eV) and the carbon in carboxylate ion (288.53 eV) that bind with the silver metal nanoparticle. The N 1 s spectra was deconvoluted into two chemically different nitrogen peaks at 400.17 eV and 399.25 eV, which correspond to the amine groups bound to the silver nanoparticles and free amine groups respectively. Amine groups were shown to bind with nanoparticles, therefore these groups may have competitive binding with silver nanoparticles such as carboxylate groups. The O 1s spectrum was resolved into three major components with BE of 531.72, 532.93 and 536.13 eV. The peaks at 531.72 and 532.93 eV are representative of the carboxylate oxygen and the semiquinone group respectively. The high BE O 1s peak at 536.13 eV is indicative of the presence of nitrate ions that are coming from the silver nitrate precursor, which are usually present along with nanoparticles for stabilisation because complete removal of these ions and molecules typically results in the aggregation of nanoparticles.[31]

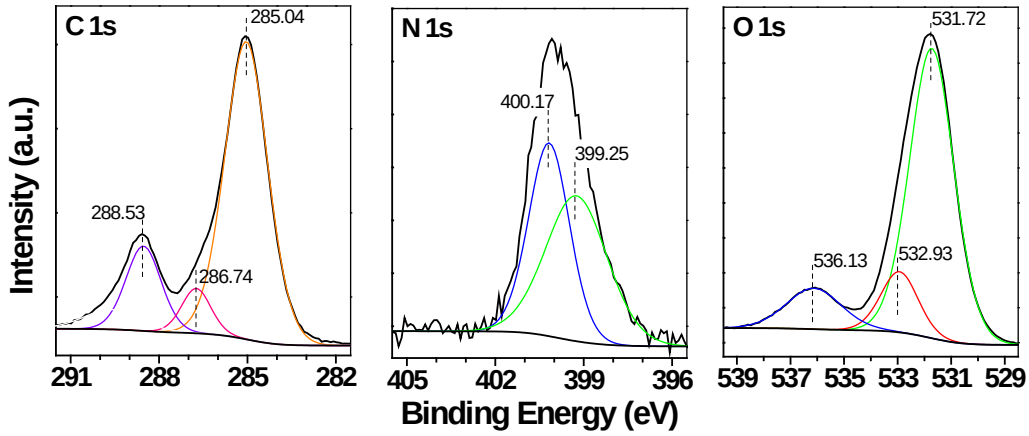

Figure 4.9- XPS spectra of tyrosine reduced Ag nanoparticles.

The antibiotic ampicillin was added to these nanoparticles and X-ray photoelectron spectroscopy was used to determine the binding of antibiotic with Ag nanoparticles to identify which functional groups of ampicillin take part in binding. Shown in Figure 4.9 are the 1s core level spectra for carbon, nitrogen and oxygen of ampicillin as well as Ag nanoparticles bound with ampicillin molecules. The C 1s spectra was fitted with three chemically distinct carbon species and their BEs were observed at 285.02, 286.55 and 288.18 eV, respectively. These three chemical states of carbon were assigned to the aromatic carbon, carbon that bound to the amine groups and carboxylic acid carbon. The spectra for ampicillin is presented in Figure 4.10. The N 1s spectrum for ampicillin shows an intense peak at 400.16 eV, which was assigned to secondary amine nitrogen group. The higher N 1s binding energy component observed at 402.11 eV represents the primary amine group and the weak component at 398.7 eV can be assigned to the nitrogen in a cyclic structure. O 1s core level spectrum shows two intense chemically different oxygen species, representing the carbonyl oxygen (532.77 eV) and carboxylate oxygen (532.13 eV). A weak O 1s component observed at 534.87 eV was assigned to the carbonyl oxygen present in the four membered ring.

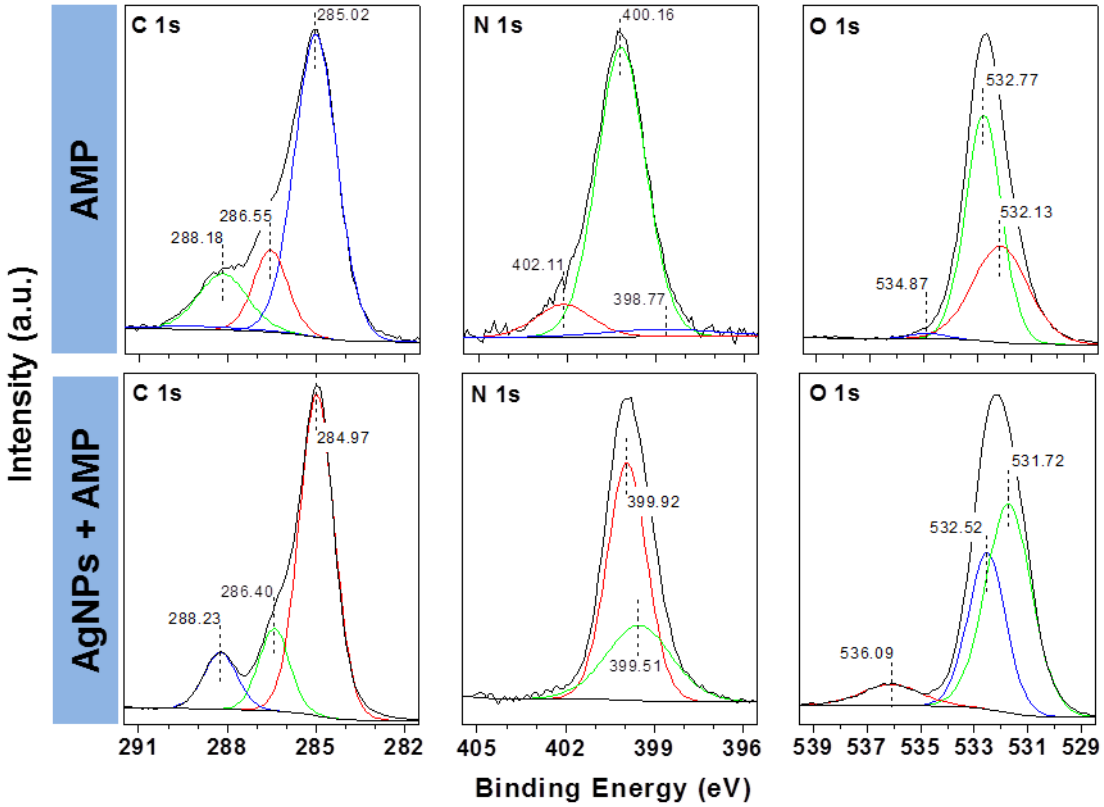

Figure 4.10- XPS spectra of ampicillin and Ag nanoparticles with ampicillin coverage.

Significant changes in the BEs of the different components of 1s core level spectra of carbon, nitrogen and oxygen after ampicillin functionalisation with Ag nanoparticles are observed. In the case of tyrosine mediated synthesis of Ag nanoparticles (Figure 4.9), BE of the carboxylate carbon that was bound to the Ag nanoparticles surface appeared at 288.53 eV, however after functionalisation with ampicillin, the BE was shifted to 288.23 eV. This BE value was found to be very close to the carboxylic acid C 1s binding energy of free ampicillin. Moreover, the BEs associated with the carbon that is bound with the amine groups decreased to 286.40 eV. N 1s binding energies of tyrosine reduced Ag nanoparticles and the free ampicillin were shifted from 400.17 eV to 399.92 eV, and this lowering of BE indicated that the amine groups were no-longer protonated. The O 1s binding energy associated with carboxyl oxygen remains at 531.72 eV and the appearance of new O 1s peak at 532.52 eV was observed after ampicillin addition to

Ag nanoparticles. All these changes clearly indicated that ampicillin bind with the Ag nanoparticles through its carboxylic acid group, by partially replacing tyrosine from the nanoparticles surface. Therefore, XPS analysis further supports DLS observations, which indicated ligand exchange between tyrosine and antibiotics. Since both tyrosine and ampicillin have carboxylic acid groups and they can bond with the nanoparticles surface, the probable mode of binding of ampicillin with Ag nanoparticles is shown in Figure 4.11.

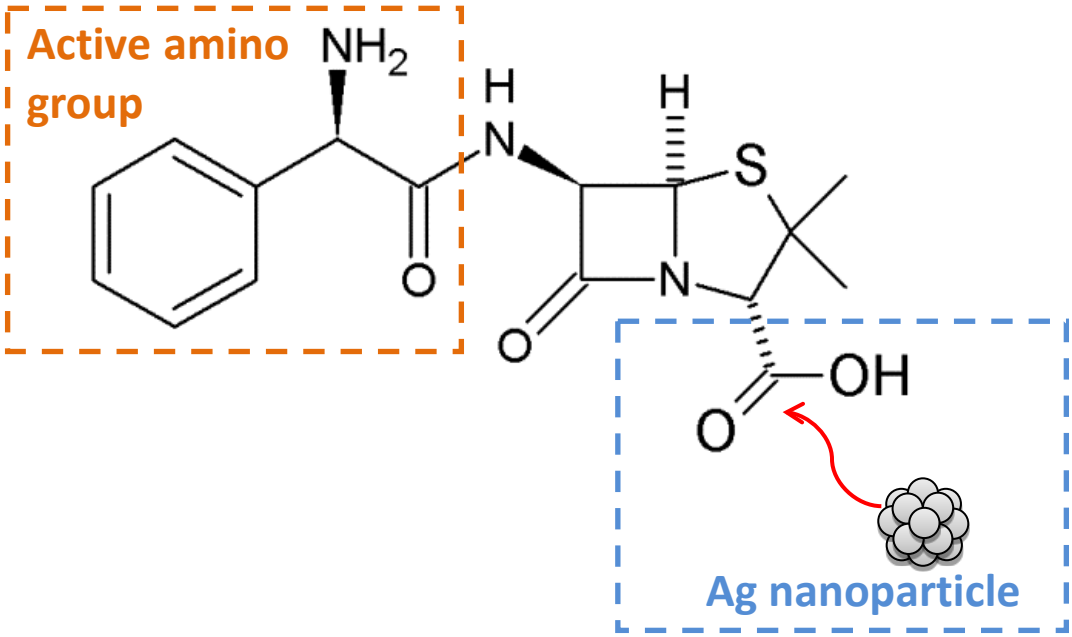

Figure 4.11- Scheme illustrating the structure of Ag nanoparticle with bound ampicillin antibiotic.

Illustrated in Figure 4.12 is the XPS core level spectra of penicillin G and after its functionalisation with Ag nanoparticles. The C 1s spectra of penicillin G was deconvoluted into three chemically distinct carbon species and their BEs were observed at 285.01, 286.34 and 288.03 eV respectively. These three chemical states of carbon were assigned to the aromatic carbon, amine groups bearing carbon and carbon in the carboxylic acid functional group. The N 1s spectrum for ampicillin shows a major peak at 400.00 eV, which was assigned to the secondary amine nitrogen group. Another N 1s component fitted at 399.34 eV was assigned to the nitrogen present in the cyclic structure. O 1s core

level spectrum shows three chemically distinct species, representing the carbonyl oxygen (532.03 eV), carboxylate oxygen (531.14 eV) and the carbonyl oxygen present in the four membered ring (535.69 eV).

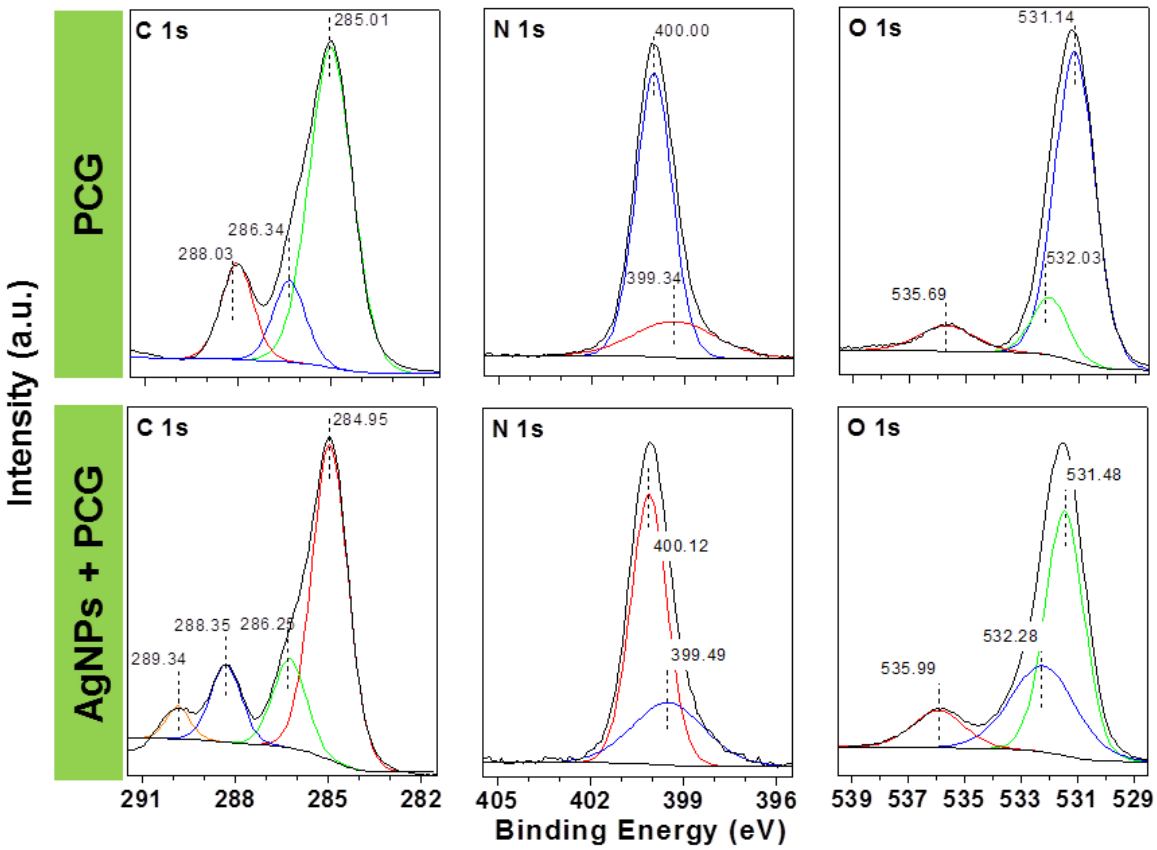

Figure 4.12- XPS spectra of penicillin G and Ag nanoparticles with penicilin G coverage.

Like the previous case, XPS spectra of penicillin G after its binding with Ag nanoparticles have shown significant changes. In the case of tyrosine mediated synthesis of Ag nanoparticles (Figure 4.9), BE of the carboxylate carbon that was bound to the Ag nanoparticles surface appeared at 288.53 eV, while pure penicillin G showed the carboxylic carbon BE at 288.03 eV. After penicillin G functionalisation of the Ag nanoparticles, both these carboxylate carbon binding energies shifted to 289.34 eV and 288.35 eV respectively. These results clearly indicate that carboxylic groups present in both tyrosine and penicillin G are bound to the Ag nanoparticles surface. Major changes were seen in the O 1s spectrum, wherein carboxylic acid group oxygen binding energies

were shifted to 531.48 eV with clear signature of carboxylic acid group binding with Ag nanoparticles. The BE of the carbonyl group present in the four membered ring shifted from 535.69 eV to 535.99 eV, which is again due to the proximity of this functional group to the Ag nanoparticles surface owing to the binding of carboxylic acid group with the Ag nanoparticles. In the case of N 1s spectra, the BE of the nitrogen present in the four membered ring only was shifted to 399.49 eV, which is again due to the proximity of the four membered ring to the Ag nanoparticles surface. Penicillin G and ampicillin differ only in the number of amine groups (additional groups in ampicillin), therefore their mode of binding is almost similar. They both bind with the Ag nanoparticles through their carboxylic acid groups by partially replacing tyrosine molecules from the Ag nanoparticles surface. The probable mode of binding of penicillin G with the Ag nanoparticle is given in the following Figure 4.13.

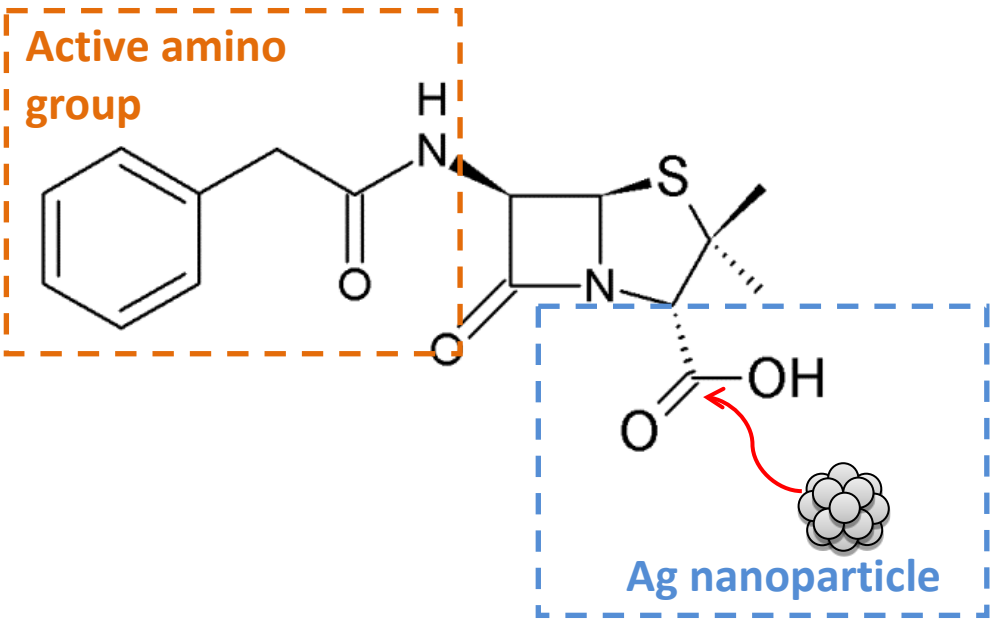

Figure 4.13- Scheme illustrating the structure of the Ag nanoparticle with bound penicillin G.

Polymyxin B is a larger antibiotic, structurally different from penicillin G and ampicillin (Figure 4.14). The C 1s spectra of polymyxin B was deconvoluted into three chemically distinct carbon species and their BEs were observed at 284.98, 286.38 and

288.07 eV respectively. These three chemical states of carbon were assigned to the aromatic carbon, amine/hydroxyl groups bearing carbon and carbon in the carbonyl group of the amide functional group. The N 1s spectrum for polymyxin B shows a major peak at 400.01 eV, which was assigned to the amide nitrogen groups. Additionally two N 1s components fitted at 401.40 and 401.94 eV were assigned to the primary amine group nitrogen present in the decapeptide and tail of the polymyxin B respectively. O 1s core level spectrum was deconvoluted into two chemically distinct O components, representing the carbonyl oxygen (531.41 eV) present in the amide groups and alcohol functional groups (533.21 eV).

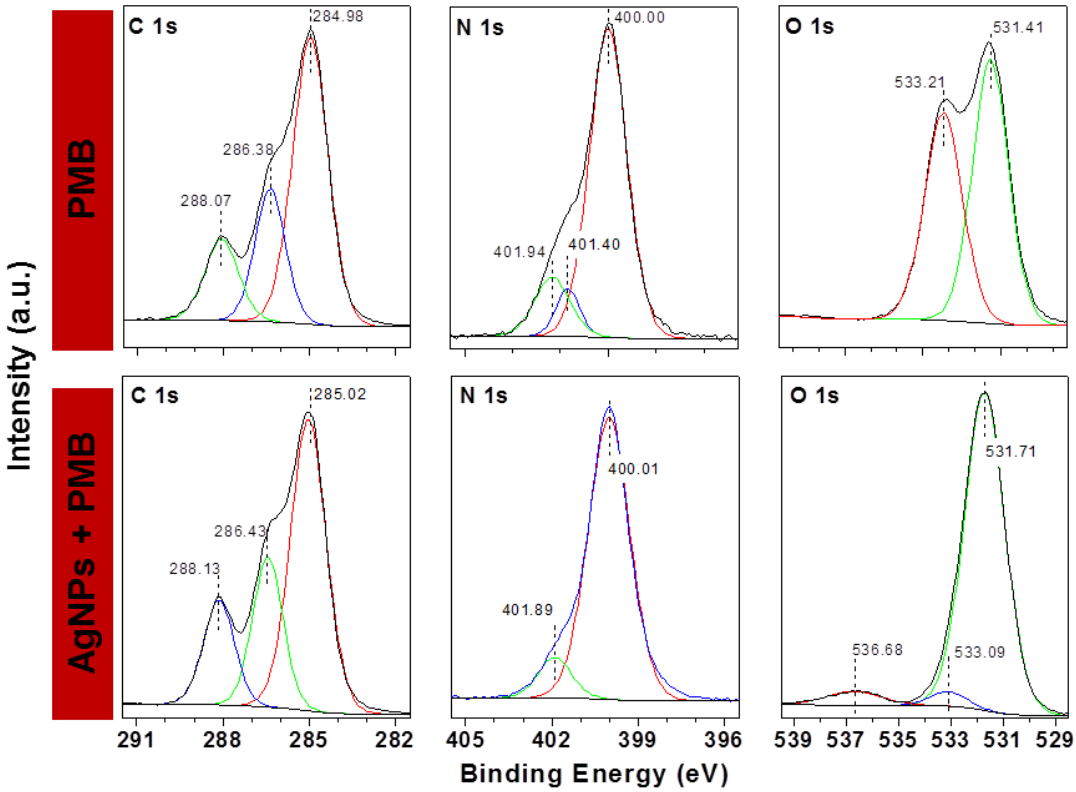

Figure 4.14- XPS spectra of polymyxin B and Ag nanoparticles with polymyxin B coverage.

Unlike the previous two antibiotics, they are minor changes observed in the C 1s and N 1s core level spectrum of the nanoparticles. The larger structure of decapeptide and associated steric hindrance tends to avoid this group binding with the

Ag nanoparticles by replacing the tyrosine molecules from its surface. This minimal replacement of tyrosine molecules bound onto Ag nanoparticle surface is further reflected from DLS analysis. DLS revealed that while ampicillin and penicillin G caused significant reduction in hydrodynamic diameters, only limited reduction in the DLS size of Ag nanoparticles was observed during polymyxin B functionalisation. Moreover, significant changes are observed in the O 1s binding energies after addition of polymyxin B to Ag nanoparticles. In particular, the BE component corresponding to the hydroxyl/alcohol groups diminished its intensity. This indicates that polymyxin B can bind through the alcohol functional groups present in the long chain attached to the decapeptide. This would be beneficial as the antibiotic component is undisturbed and the probable mode of binding is given below in Figure 4.15.

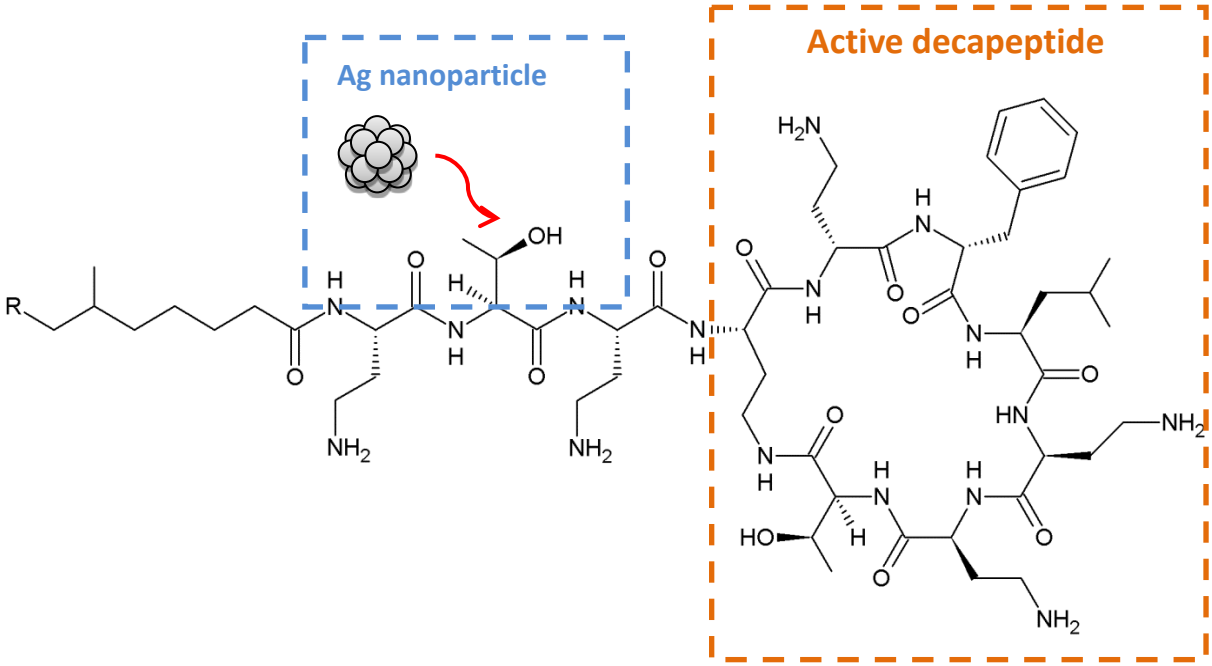

Figure 4.15- Scheme illustrating the structure of the Ag nanoparticle with bound polymyxin B.

Shown in Figure 4.16 are the Ag $3d_{5/2}$ and $3d_{3/2}$ spin-orbit components of the Ag scan. The tyrosine reduced Ag nanoparticles exhibit two chemically distinct peaks in the Ag $3d_{5/2}$ region at 367.88 and 369.18 eV which have been previously assigned to silver

metal and unreduced silver cations, respectively.[31] The presence of silver cations in this spectrum suggests that unreduced silver ions remain bound to the nanoparticle surface. Each of the Ag nanoparticles with bound antibiotics display peaks at ca. 368.3 and 374.3 eV representing Ag^0, higher than the initial silver binding energy. This is a clear indication that the chemical environment of Ag nanoparticles has been changed as a result of antibiotic binding.

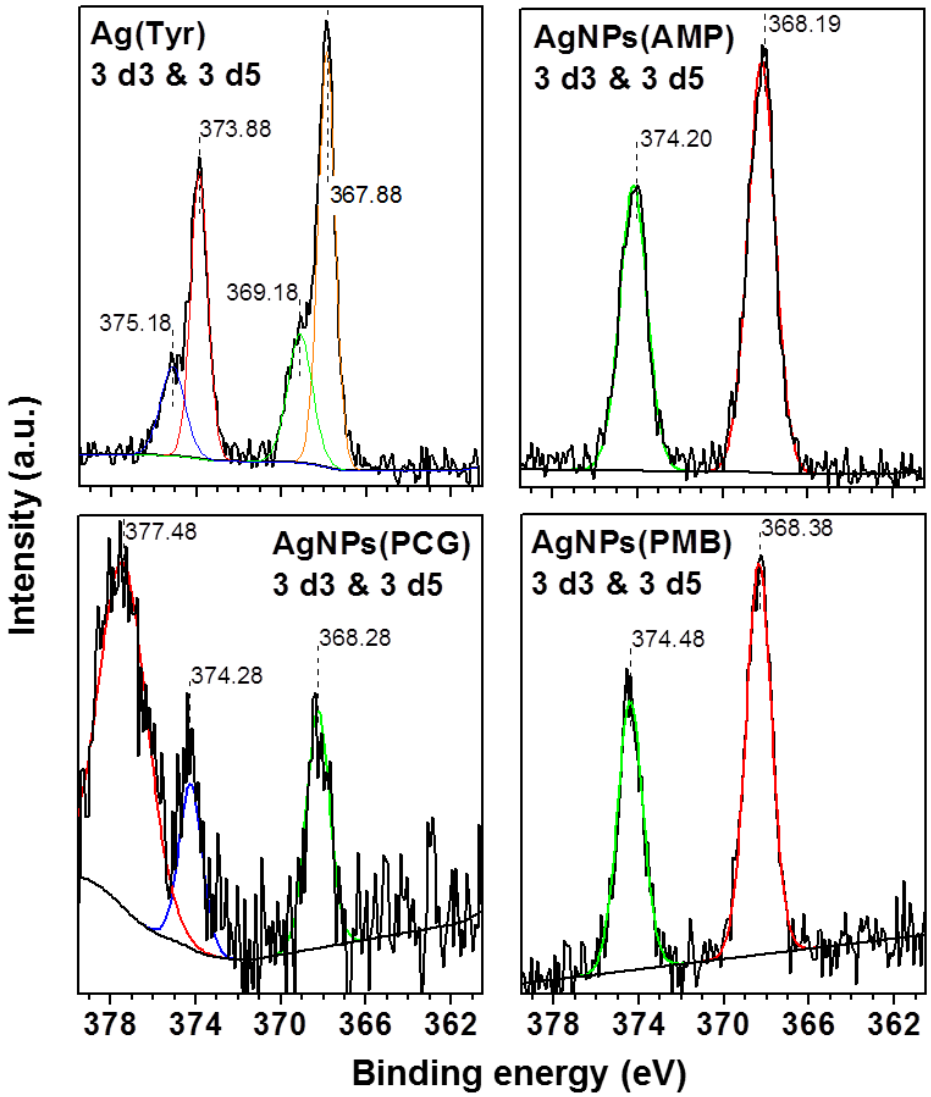

Figure 4.16- Ag nanoparticles prepared with tyrosine coated with ampicillin, penicillin G and polymyxin B.

4.3.5 Antibacterial assays of antibiotics and Ag nanoparticles

Colony count method was used to investigate the synergistic effects of Ag nanoparticles combined with antibiotics against Gram positive and Gram negative bacteria. Since all antibiotic concentrations were set at a constant cell death of 20%, to achieve synergism, the percentage cell death of antibiotics combined with Ag nanoparticles needs to be greater than the sum of the individual cell death (CD) percentage of antibiotics and Ag nanoparticles (i.e., CD% AgNPs/Antibiotics combined > CD% antibiotics + CD% AgNPs).

4.3.5.1 Synergistic effects of ampicillin combined with Ag nanoparticles

In the case of Ag nanoparticles combined with ampicillin, synergistic effects were tested against both Gram negative and Gram positive bacteria as ampicillin is of broad spectrum range. Illustrated in Figure 4.17A is the antibacterial profile of Ag nanoparticles combined with ampicillin against *E. coli*. Evidence of synergistic effects can be observed across all concentrations of silver, particularly higher synergism is demonstrated at lower concentrations. When 0.1 mM of silver was used, the sum of the individual percentage cell death of ampicillin and Ag nanoparticles was ca. 54% (20% cell death of ampicillin + 34% cell death of AgNPs); however the combined effects of Ag nanoparticles with ampicillin exhibited ca. 77% cell death. This gives an additional effect of ca. 23% and an overall synergistic enhancement of ca. 43% (23/54×100). The same trend occurs at 0.2 mM concentration where there is an additional effect of ca. 26% and synergism enhancement of 43%. As concentration of silver increases to 0.5 mM, the synergistic enhancement decreases to ca. 21% and thereafter ca. 18% for the highest concentration at 1.0 mM.

Conversely, in the case of Ag nanoparticles combined with ampicillin against *S. albus* as shown in Figure 4.17B, at the lowest concentration of 0.1 mM, the synergistic enhancement achieved was ca. 49%. It was then decreased to ca. 17% synergism at 0.2 mM of silver concentration. As the concentrations increased to 0.5 mM and 1.0 mM, limited synergistic effects were apparent, at only 3-4% enhancement. Table 4.3 displays a summary of the synergistic effects between the studies of *E. coli* and *S. albus*.

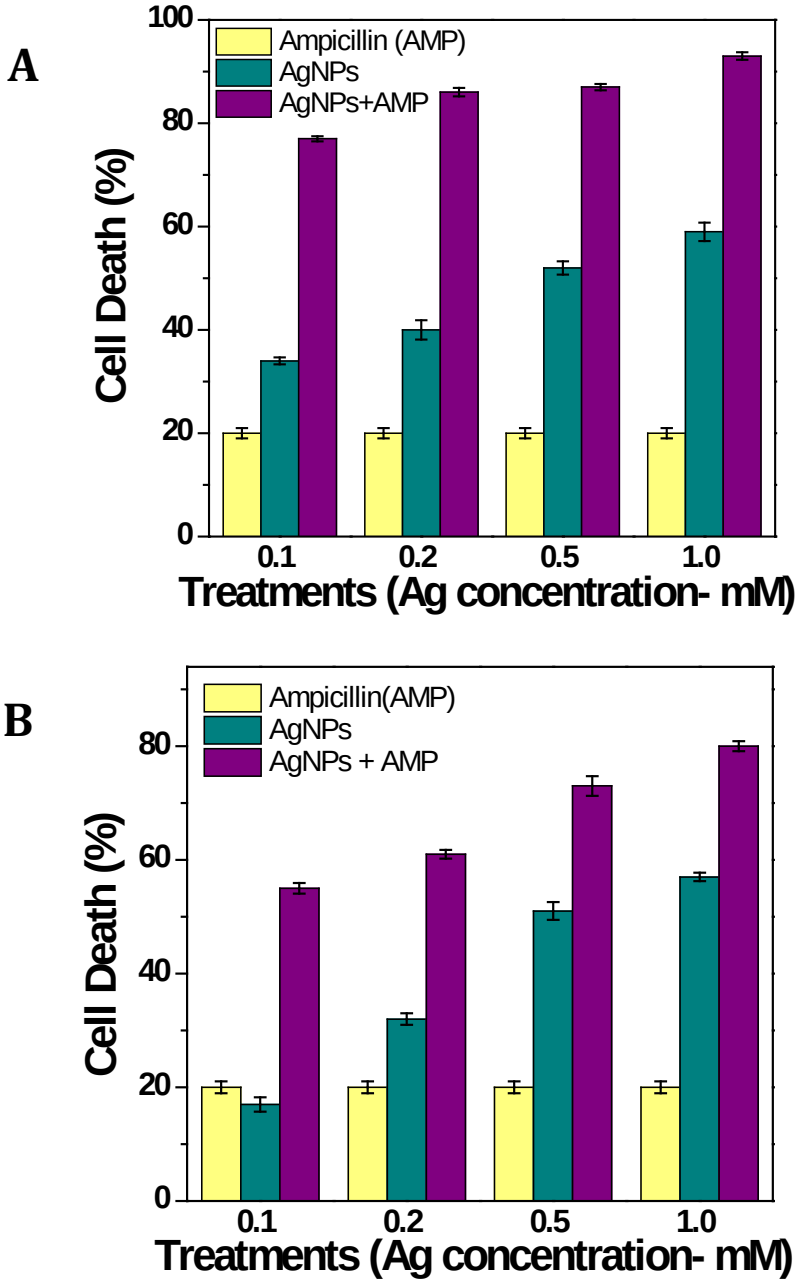

Figure 4.17- Synergistic effects of Ag nanoparticles and ampicillin against (A) *E. coli* and (B) *S. albus.*

4.3.5.2 Synergistic effects of penicillin G or polymyxin B combined with Ag nanoparticles

Synergistic effects of penicillin G was tested only against Gram positive bacteria *S. albus* as it is of narrow spectrum antibiotic (Figure 4.18). All concentrations demonstrated synergistic effects, with the lowest concentration of 0.1 mM exhibiting the highest outcome. At 0.1 mM of silver, the individual sum of percentage cell death of penicillin G and Ag nanoparticles demonstrated ca. 37%, and the combined effect displayed ca. 69% cell death which suggests a significant synergistic enhancement of ca. 87%. As the concentration of silver increases, the synergistic effects decrease to 42% (for 0.2 mM Ag), 14% (0.5 mM Ag) and 10% (1.0 mM Ag). At higher concentrations, Ag nanoparticles itself exhibits significant antibacterial effects therefore at those concentrations, the synergism between antibiotics and Ag nanoparticles becomes less effective compared to lower concentrations.

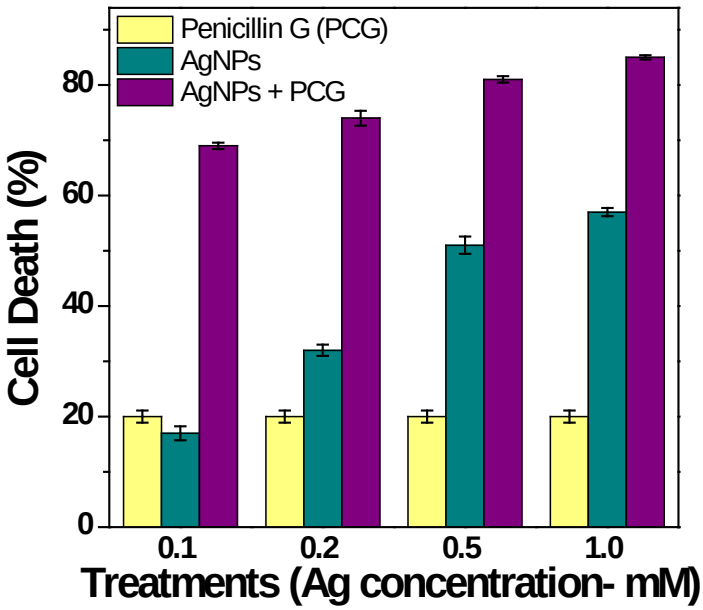

Figure 4.18- Synergistic effects of Ag nanoparticles and penicillin G against *S. albus.*

Similar outcomes were achieved in the case of Ag nanoparticles combined with Gram negative specific polymyxin B where synergistic effects profile was tested against Gram negative bacteria *E. coli*. Again, as illustrated in Figure 4.19, at lower concentrations of silver, synergism is clearly evident. When 0.1 mM silver was used, the individual sum of percentage cell death of polymyxin B and Ag nanoparticles achieved was ca. 54% compared to 100% cell death when Ag nanoparticles and polymyxin B were combined. This produces an additional effect of ca. 46% and a high synergistic enhancement of ca. 85%. The percentage cell death of Ag nanoparticles combined with antibiotics is ca. 100% across all four concentrations.

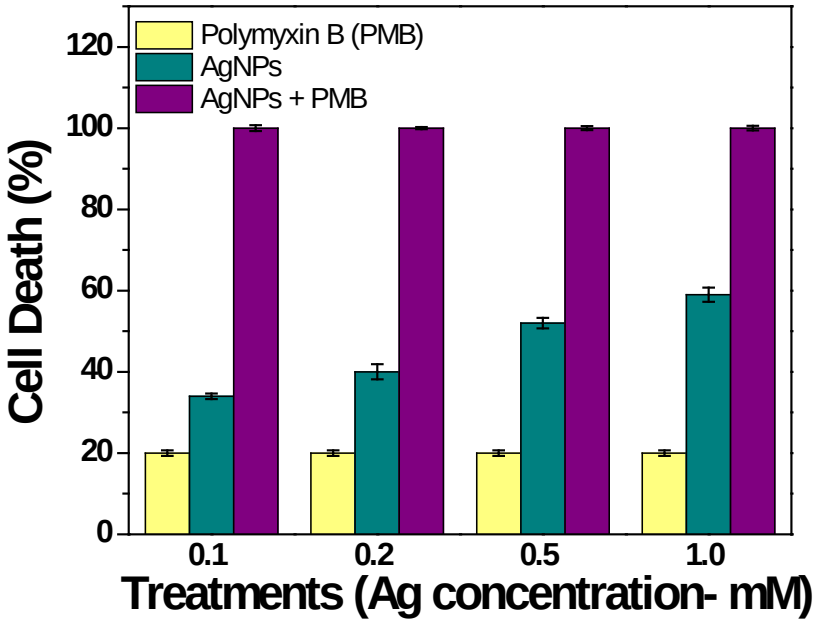

Figure 4.19- Synergistic effects of Ag nanoparticles and polymyxin B against *E. coli*.

Similar to all other antibiotics, as the silver concentration increases, the synergistic effect appears to decrease. This is shown clearly in Table 4.3 which summarises all the synergistic effects of each antibiotic combination. It can be demonstrated that the lower the silver concentration, the better the synergistic enhancements across all antibiotic combinations. The highest synergism was demonstrated in 0.5 mM for polymyxin B against *E. coli* at ca. 85% and for penicillin G

against *S. albus* at ca. 87%, whereas, the similar concentration of Ag nanoparticles in case of broad spectrum ampicillin caused only 43% and 49% synergistic enhancements in case of *E. coli* and *S. albus*, respectively.

Table 4.3- Summary of synergistic effects of each antibiotic combination.

Concentration (mM)	Percentage cell death (%)					Synergistic enhancement of activity (%)*
	Antibiotic (A)	AgNPs (B)	Individual AgNPs + Antibiotics (A+B)	AgNPs-Antibiotics combined (C)	Additional effect [C-(A+B)]	
Ampicillin against *E. coli*						
0.1	20	34	54	77	23	43
0.2	20	40	60	86	26	43
0.5	20	52	72	87	15	21
1.0	20	59	79	93	14	18
Ampicillin against *S. albus*						
0.1	20	17	37	55	18	49
0.2	20	32	52	61	9	17
0.5	20	51	71	73	2	3
1.0	20	57	77	80	3	4
Penicillin G against *S. albus*						
0.1	20	17	37	69	32	87
0.2	20	32	52	74	22	42
0.5	20	51	71	81	10	14
1.0	20	57	77	85	8	10
Polymyxin B against *E. coli*						
0.1	20	34	54	100	46	85
0.2	20	40	60	100	40	67
0.5	20	52	72	100	28	39
1.0	20	59	79	100	21	27

* $\frac{[C-(A+B)]}{(A+B)} \times 100$

4.3.6 SEM of bacteria cells after treatment of Ag nanoparticles and antibiotics

Physical composition of bacterial cell is essential for its survival and to overcome environmental changes and stress. Hence, the morphological changes that occur in the bacterial cells after exposure to Ag nanoparticles, antibiotics, and Ag nanoparticles combined with antibiotics are illustrated in Figure 4.20-4.23.

As mentioned previously, ampicillin is a broad spectrum antibiotic which targets Gram negative and Gram positive bacteria. In the study of ampicillin, SEM images of bacteria cells without treatment and those treated with Ag nanoparticles and ampicillin are demonstrated below in Figure 4.20.

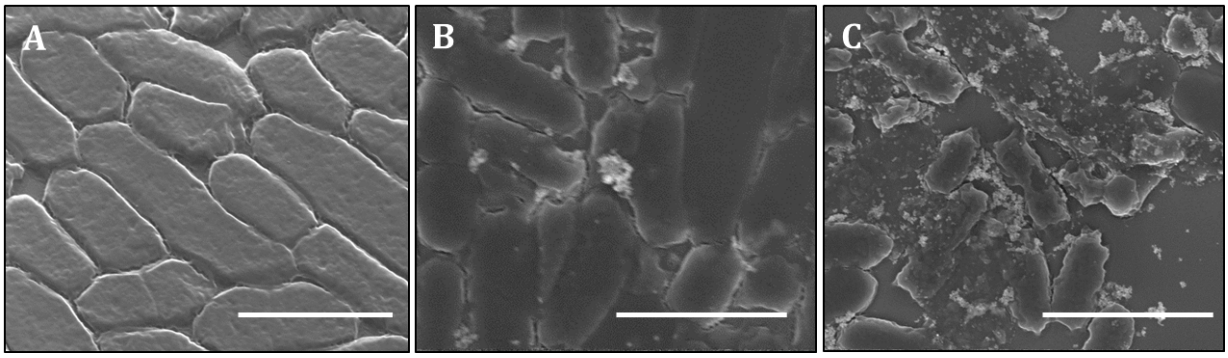

Figure 4.20- SEM images of *E. coli* (A) untreated, (B) treatment with ampicillin and (C) treatment with Ag nanoparticles combined with ampicillin. (Scale bars corresponds to 5 μm)

The SEM images of rod-shaped *E. coli* untreated (Figure 4.20A) and those treated with ampicillin on its own (Figure 4.20B) reveal negligible morphological changes, especially in the cell membrane integrity. It is evident that there is initial cell wall interaction with ampicillin by itself where the bacterial cell edges are roughening, which suggests the disruption of cellular component especially membrane change in morphology. This observation of slight modification in the bacterial cell also supports the results obtained in the antibacterial CFU assay where ampicillin only exhibiting ca. 20% cell death.

Upon exposure of Ag nanoparticles combined with ampicillin (Figure 4.20C), SEM images illustrated distinct morphological changes in *E. coli*. This change is indicative of significant damage to bacterial cell integrity. The combined effect of Ag nanoparticles and ampicillin on *E. coli* is evident where further damage of cells is seen compared to ampicillin on its own. Furthermore, the bacterial cells are completely fragmented and the dissolving of the bacterial cell walls is evident. These disintegrated cells provide distinct evidence that there are distinct changes in the morphology of the cells.

Figure 4.21 displays SEM images of *S. albus* bacterial cells with and without the treatment of ampicillin and combined Ag nanoparticles and ampicillin. The control image of *S. albus* without exposure (Figure 4.21A) is arranged in grape-like clusters. Upon treatment of ampicillin, cells become fused together as illustrated in Figure 4.21B and this provides evidence of some interaction between ampicillin and bacterial cells. The combined effects of Ag nanoparticles and ampicillin exposed to *S. albus* are illustrated in Figure 4.21C. As evident in the image, the cell wall components appeared to be exfoliating and a change in morphology is apparent.

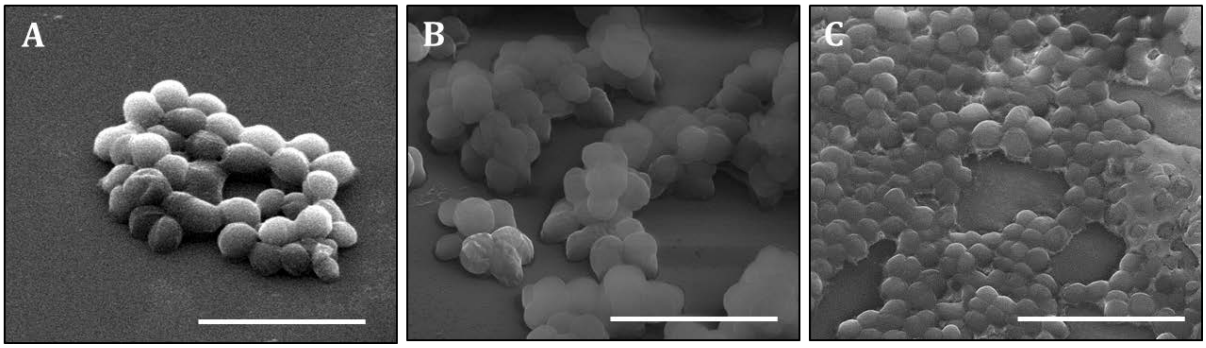

Figure 4.21- SEM images of *S. albus* (A) untreated, (B) treatment with ampicillin and (C) treatment with Ag nanoparticles combined with ampicillin. (Scale bars corresponds to 5 μm)

In contrast, for the case of penicillin G (narrow spectrum) against *S. albus*, similar outcomes are observed as shown in Figure 4.22. Similarly, when *S. albus* is treated only with penicillin G, bacterial cells appeared to be once again fused together and cell

surfaces were peeling (Figure 4.22B). When Ag nanoparticles are combined with penicillin G (Figure 4.22C), *S. albus* cells are dissolved and cellular components appeared to be disintegrated. After treatments, the cell wall components are disorganised and scattered from the original ordered close packed smooth arrangement.

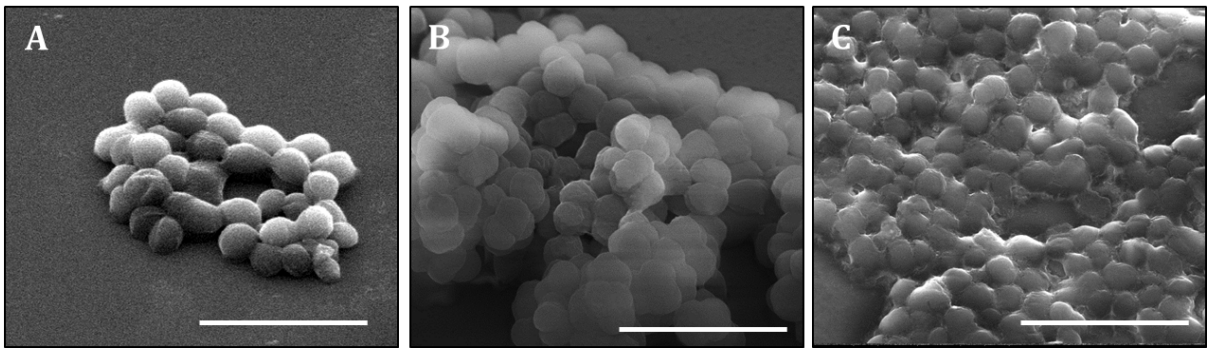

Figure 4.22- SEM images of *S. albus* (A) untreated, (B) treatment with penicillin G and (C) treatment with Ag nanoparticles combined with penicillin G. (Scale bars corresponds to 5 μm)

Illustrated in Figure 4.23, is the profile for polymyxin B (narrow spectrum) against *E. coli*. When cells are untreated, they are well intact rod-shaped structures as it is apparent in Figure 4.23A. When cells are exposed to only polymyxin B, there is evident of change in morphology. There is clear indication of cell wall breakdown, whereby *E. coli* cells appeared to be dissolving and denaturing as observed in Figure 4.23B. In contrast Figure 4.23C depicts that when these cells are exposed to Ag nanoparticles combined with polymyxin B, there is a significant alteration in the cell morphology. Bacterial cells are dissolved and disorganised from their original arrangement to an extent that cell debris is clearly visible. Thus confirming that Ag nanoparticles combined with polymyxin B had significant influence on *E. coli* bacterial cell morphology compared to polymyxin B on its own.

In all cases of the change of morphology and disintegration caused by Ag nanoparticles and antibiotics to bacterial cells, it can be observed that cell wall plays a vital role in the survival of these bacterial cells. Treatment of bacterial cells resulted in

reduction in the initial cell thickness as well as roughening of the cell which caused the disruption of the cell wall and membrane.

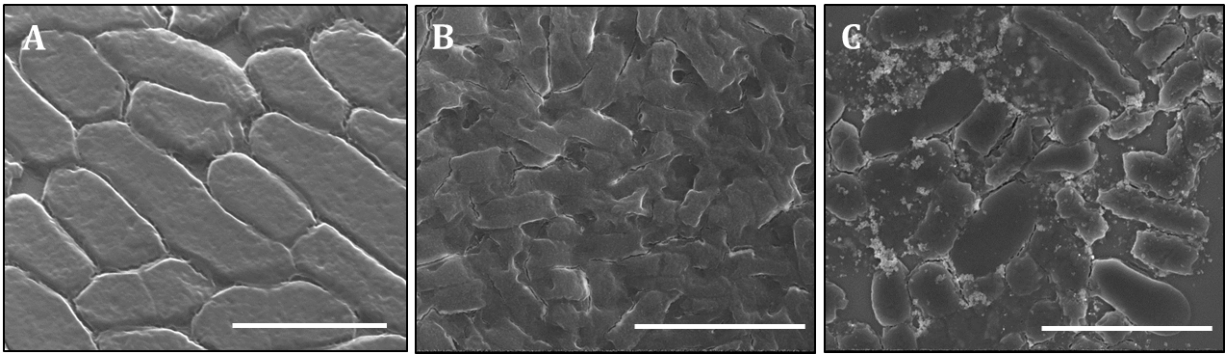

Figure 4.23- SEM images of *E. coli* (A) untreated, (B) treatment with polymyxin B and (C) treatment with Ag nanoparticles combined with polymyxin B. (Scale bars corresponds to 5 μm)

From antibacterial studies and SEM imaging of bacterial cells, it is clear that Ag nanoparticles combined with antibiotics has synergistic effects which cause significant irreversible bacterial cell damage and ultimately cell death by disruption of the cell wall and membrane when compared with antibiotics on its own.

4.3.7 Mechanism of action

As mentioned previously, antibacterial antibiotics are commonly determined based on their mechanisms of action, chemical structure, or spectrum of activity. They generally target bacterial functions or growth processes. Those that target the bacterial cell wall or cell membrane or interfere with essential bacterial enzymes have bactericidal activities.

Gram negative and Gram positive bacteria both have a peptidoglycan layer as part of their cell wall structure. The peptidoglycan layer is substantially thicker and multilayered in Gram positive bacteria. The peptidoglycan with orthogonal glycan and peptide strands undergo enzymatic cross-linking of the glycan strands by transglycosylase action and the peptide strands by the transpeptidase action. The peptide cross-links introduce covalent connectivity to the interlacing, transmit mechanical

strength and provide the major structure barrier to osmotic pressure forces that could kill the bacteria. Antibiotics that affect bacterial cell wall inhibit enzymes or seize substrates involved in peptidoglycan assembly and cross-linking.[32]

In the case of ampicillin, the amino group present helps penetrate the outer membrane of Gram negative bacteria. Ampicillin acts as a competitive inhibitor of the enzyme transpeptidase which is needed to form the cell wall. The final stages of bacterial cell wall synthesis in binary fission are also inhibited and leads to cell lysis.

Similarly, penicillin G binds at the active site of the transpeptidase enzyme that cross-links the peptidoglycan strands in Gram positive bacteria. It does this by mimicking the D-alanyl-D-alanine enzyme residues that would generally bind to this site. Penicillin G irreversibly inhibits the enzyme transpeptidase by reacting with a serine residue in the transpeptidase. This reaction is irreversible and hence the growth of the bacterial cell wall is inhibited.[33]

Polymyxin B is a cationic antibiotic that consists of a cyclic decapeptide molecule which is positively charged and linked to a fatty acid chain. Bactericidal effect of polymyxin B is via binding to the bacterial cell membrane and disrupting its permeability which results in leakage of intracellular components. Antiendotoxin activity is also apparent in polymyxin B; these agents are rapidly bactericidal against many Gram negative bacteria. Therefore, polymyxin B acts primarily on the Gram negative cell wall, leading to rapid permeability changes in the cytoplasmic membrane and ultimately cell death.[34-37] Additionally, a study has found that drug entry into the cell is not essential, as polymyxin B can inhibit the growth and respiration via interacting with the outer surface of the cells. It was projected that perturbation of the outer membrane structure indirectly affected the selective permeability of the inner membrane and

inhibited respiration.[38] Since all of the antibiotics employed in this study act on bacterial cell wall, it is not surprising that in the presence of antibiotics, nanoparticle uptake may be significantly enhanced. This is most likely the dominant reason for large synergistic enhancement observed when nanoparticles are jointly used with antibiotics.

4.4 Conclusions

Ag nanomaterials are known for their biological applications due to their high surface area to volume ratio. Ag nanoparticles have been employed as potent antibacterial agents to overcome resistance. Of many different approaches to overcome antimicrobial resistance, using Ag nanoparticles as antibiotics carriers seems to hold highest promise. Hence, this chapter has demonstrated that antibiotics bound onto Ag nanoparticles as well as those present freely around nanoparticles revealed noteworthy influence on antibacterial activities.

Additionally, traditional antibiotics with various spectrums were employed as functional fragments to influence antibacterial potential on the surface of Ag nanoparticles.

Furthermore, this chapter provides strong evidence that antibiotic combined Ag nanoparticles provide synergistic effects and employ a physical mode of action against bacterial cells causing cell wall cleavage and cell lysis. Although Ag nanoparticles combined with antibiotics may not replace antibiotics, but they may become valuable antibiotic complements by preventing the development of resistance.

4.5 References

[1] Prescott, L. M.; Harley, J. P.; Klein, D. A., *Microbiology*. Boston, Mass: USA, 1999.

[2] Udall, K. G., *Nature's antibiotics*. Woodland Publishing, Incorporated: 1998.

[3] Drlica, K. S.; Perlin, D. S., *Antibiotics: An overview*. Pearson Education: 2011.

[4] Berlatsky, N., *Antibiotics*. Greenhaven Press(CA): 2011.

[5] Scott, G. M.; Kyi, M. S., *Handbook essential antibiotics*. Taylor & Francis: 2001.

[6] Amábile-Cuevas, C. F., *Antimicrobial resistance in bacteria*. Horizon Bioscience: 2007.

[7] Drlica, K. S.; Perlin, D. S., *Antibiotic resistance: Understanding and responding to an emerging crisis*. Pearson Education: 2010.

[8] Walsh, C., *Antibiotics: Actions, Origins, Resistance*. ASM Press: 2003.

[9] Webber, M.; Piddock, L., The importance of efflux pumps in bacterial antibiotic resistance. *Journal of Antimicrobial Chemotherapy* **2003,** *51* (1), 9-11.

[10] Poole, K., Efflux pumps as antimicrobial resistance mechanisms. *Annals of medicine* **2007,** *39* (3), 162-176.

[11] Leeb, M., Antibiotics: a shot in the arm. *Nature* **2004,** *431* (7011), 892-893.

[12] Norrby, S. R.; Nord, C. E.; Finch, R., Lack of development of new antimicrobial drugs: a potential serious threat to public health. *The Lancet infectious diseases* **2005,** *5* (2), 115-119.

[13] Cohen, M. L., Changing patterns of infectious disease. *Nature* **2000,** *406* (6797), 762-767.

[14] Rice, L. B., The clinical consequences of antimicrobial resistance. *Current opinion in microbiology* **2009,** *12* (5), 476-481.

[15] Sköld, O., *Antibiotics and antibiotic resistance*. Wiley: 2011.

[16] Guilfoile, P.; Alcamo, I. E.; Heymann, D. L., *Antibiotic-resistant bacteria*. Chelsea House: 2007.

[17] Symposium, C. F., *Antibiotic resistance: Origins, evolution, selection and spread*. Wiley: 2008.

[18] Wolska, K. I.; Grzes, K.; Kurek, A., Synergy between novel antimicrobials and conventional antibiotics or bacteriocins. *Polish Journal of Microbiology* **2012,** *61* (2), 95-104.

[19] Huh, A. J.; Kwon, Y. J., "Nanoantibiotics": A new paradigm for treating infectious diseases using nanomaterials in the antibiotics resistant era. *Journal of Controlled Release* **2011,** *156* (2), 128-145.

[20] Taylor, P. W.; Stapleton, P. D.; Paul Luzio, J., New ways to treat bacterial infections. *Drug Discovery Today* **2002,** *7* (21), 1086-1091.

[21] Fayaz, A. M.; Balaji, K.; Girilal, M.; Yadav, R.; Kalaichelvan, P. T.; Venketesan, R., Biogenic synthesis of silver nanoparticles and their synergistic effect with antibiotics: a study against gram-positive and gram-negative bacteria. *Nanomedicine: nanotechnology, biology, and medicine* **2009,** *6* (1), 103.

[22] Li, P.; Li, J.; Wu, C.; Wu, Q.; Li, J., Synergistic antibacterial effects of β-lactam antibiotic combined with silver nanoparticles. *Nanotechnology* **2005,** *16* (9), 1912.

[23] Rajawat, S.; Qureshi, M. S., Comparative study on bactericidal effect of silver nanoparticles, synthesized using green technology, in combination with antibiotics on *Salmonella Typhi*. *Journal of Biomaterials and Nanobiotechnology* **2012,** *3*, 480-485.

[24] Shahverdi, A. R.; Fakhimi, A.; Shahverdi, H. R.; Minaian, S., Synthesis and effect of silver nanoparticles on the antibacterial activity of different antibiotics against Staphylococcus aureus and Escherichia coli. *Nanomedicine: Nanotechnology, Biology and Medicine* **2007,** *3* (2), 168-171.

[25] Chamundeeswari, M.; Sobhana, S.; Jacob, J. P.; Kumar, M. G.; Devi, M. P.; Sastry, T. P.; Mandal, A. B., Preparation, characterization and evaluation of a biopolymeric gold nanocomposite with antimicrobial activity. *Biotechnology and applied biochemistry* **2010,** *55* (1), 29-35.

[26] Linstrom, P. J.; Mallard, W., NIST Chemistry webbook; NIST standard reference database No. 69. **2001**.

[27] Siaka, A.; Nnabuk, E.; Idris, S.; Magaji, L.; Muhammad, A., Ftir spectroscopic information on the corrosion inhibition potentials of amoxicillin in hcl solution. *Continental Journal of Engineering Sciences* **2012,** *7* (1).

[28] Siaka, A.; Edd, N.; Idris, S.; Magaji, L., Experimental and computational study of corrosion potentials of penicillin G. *Research Journal of Applied Sciences* **2011,** *6* (7), 487-493.

[29] Uzarski, J. R.; Tannous, A.; Morris, J. R.; Mello, C. M., The effects of solution structure on the surface conformation and orientation of a cysteine-terminated antimicrobial peptide cecropin P1. *Colloids and Surfaces B: Biointerfaces* **2008,** *67* (2), 157-165.

[30] Mohorčič, M.; Jerman, I.; Zorko, M.; Butinar, L.; Orel, B.; Jerala, R.; Friedrich, J., Surface with antimicrobial activity obtained through silane coating with covalently bound polymyxin B. *Journal of Materials Science: Materials in Medicine* **2010,** *21* (10), 2775-2782.

[31] Selvakannan, P. R.; Swami, A.; Srisathiyanarayanan, D.; Shirude, P. S.; Pasricha, R.; Mandale, A. B.; Sastry, M., Synthesis of aqueous Au core−Ag shell nanoparticles using tyrosine as a pH-dependent reducing agent and assembling phase-transferred silver nanoparticles at the air−water interface. *Langmuir* **2004,** *20* (18), 7825-7836.

[32] Franklin, T. J.; Snow, G. A., *Biochemistry and molecular biology of antimicrobia drug action*. Springer: 2005.

[33] Waxman, D. J.; Strominger, J. L., Penicillin-binding proteins and the mechanism of action of beta-lactam antibiotics. *Annual review of biochemistry* **1983,** *52* (1), 825-869.

[34] DaugelaviÄius, R.; Bamford, D. H., Stages of polymyxin B interaction with the *Escherichia coli* cell envelope. *Antimicrobial agents and chemotherapy* **2000,** *44* (11), 2969-2978.

[35] Yuan, Z.; Tam, V. H., Polymyxin B: a new strategy for multidrug-resistant gram-negative organisms. **2008**.

[36] Zavascki, A. P.; Goldani, L. Z.; Li, J.; Nation, R. L., Polymyxin B for the treatment of multidrug-resistant pathogens: a critical review. *Journal of Antimicrobial Chemotherapy* **2007,** *60* (6), 1206-1215.

[37] Teuber, M.; Bader, J., Action of polymyxin B on bacterial membranes. *Archives of microbiology* **1976,** *109* (1-2), 51-58.

[38] LaPorte, D. C.; Rosenthal, K. S.; Storm, D. R., Inhibition of Escherichia coli growth and respiration by polymyxin B covalently attached to agarose beads. *Biochemistry* **1977,** *16* (8), 1642-1648.

Chapter V

Influence of surface corona of silver nanoparticles on antibacterial activity: tyrosine, curcumin and epigallocatechin gallate

5.1 Introduction

Antioxidants are substances that when present in foods or in the body at low concentrations can distinctly delay or prevent the oxidation of proteins, carbohydrates, lipids and DNA. They may act by decreasing oxygen concentration, intercepting singlet oxygen, preventing first-chain initiation by scavenging initial radicals such as hydroxyl radicals, binding metal ion catalysts, decomposing primary products to non-radical compounds and chain-breaking to prevent continued hydrogen abstraction from substrates.[1-6] Moreover, it is imperative to recognise various herbs, spices and plant sources that produce powerful antioxidants as phytochemical elements in seeds, stems, fruits and in leaves. These naturally occurring antioxidants are already within the human food chain and have been proven to be nontoxic to living organisms and to the environment for thousands of years.[7-9]

Natural antioxidants from dietary sources include phenolic and polyphenolic compounds,[10, 11] chelators,[12, 13] antioxidant vitamins and enzymes[14] as well as carotenoids and carnosine.[8, 15] Phenolic compounds are a large group of the secondary metabolites produced by higher plants. They are distinguished into classes based on their structure and subcategorised according to the number and position of hydroxyl group and the presence of other constituents. Polyphenols are regular components of our diets and serve as a role in the prevention of degenerative diseases such as cancer and cardiovascular diseases.[16] Researchers and food manufacturers have become progressively interested in polyphenols, the foremost reason for this growing interest is the recognition of the antioxidant properties associated with polyphenols.[17] Moreover, polyphenols constitute the active substances found in medicinal plants; modulate the activity of an extensive array of enzymes and cell receptors.[18]

Currently, there is an increasing need to develop environmentally sustainable nanoparticle synthesis routes that do not exhibit toxic chemicals. As a result, scientists have explored the field of biological systems in the synthesis and assembly of nanoparticles. These inspirations of green chemistry includes but not limited to employment of bacteria,[19, 20] fungi[21, 22] and phytochemicals to produce nanoparticles.[23, 24] Biological methods are considered as a safe and ecologically sound alternative to conventional physical and chemical routes.[25-27] In this chapter, three different phenolic compounds consisting of one or multiple phenolic groups are adopted for the synthesis of Ag nanoparticles; namely tyrosine, curcumin and epigallocatechin gallate (EGCG). Additionally, these phenolic compounds are utilised as a reducing as well as a capping agent during the synthesis.

Tyrosine or 4-hydroxyphenylalanine is an essential aromatic amino acid that is derived from phenylalanine by hydroxylation in the para position. This amino acid acts as one of the building blocks of protein. Tyrosine can be synthesised in the body from phenylalanine, found in high protein packed produces, in plants and most microorganisms. The structure of tyrosine is shown below in Figure 5.1 consisting of one phenolic group.

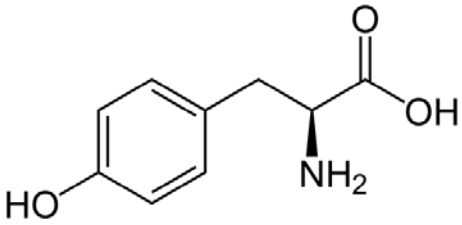

Figure 5.1- Chemical structure of tyrosine.

The polyphenol curcumin is the active ingredient found in the traditional herbal remedy and dietary spice turmeric, also known as *Curcuma longa*. Turmeric is a member of the *Curcuma* botanical group, which is part of the ginger family of herbs. Grounded turmeric produces a vibrant yellow-orange colour from a naturally occurring pigment in the Curcuma longa tuber; this pigment is the source of curcumin. The warm yellow spice, derived from the rhizome of the plant (Figure 5.2), has a long history of use in traditional Chinese and Indian medicines, asian cooking, cosmetics and fabric dying for more than 2000 years.[28-31]

Figure 5.2- *Curcuma longa* plant, turmeric and grounded curcumin.

The use of curcumin as an ancient remedy continues today in India where a bandage of turmeric paste is used to treat infections, wound dressings, burns, acne and different skin diseases.[31] In food and manufacturing, curcumin is presently used in perfumes as a naturally yellow colouring agent, as well as a food additive to flavour various types of curries and mustards.[32, 33]

Recent emphasis on employing the use of natural and complementary medicines in Western medicine has diverted the attention of the scientific community to this ancient remedy. Researchers have revealed that curcumin possesses an extensive range of beneficial properties, including antimicrobial,[34-36] anti-inflammatory,[37-39] antioxidant,[40-42] anti-carcinogenic, chemopreventive and chemotherapeutic activity.[43-46] Curcumin is a free radical scavenger and hydrogen donor which exhibits antioxidant activity. Sharma *et al.* observed that the phenolic hydroxyl groups are essential for antioxidant activity.[47] Illustrated in Figure 5.3 is the structure of curcumin, consisting of two phenolic groups.

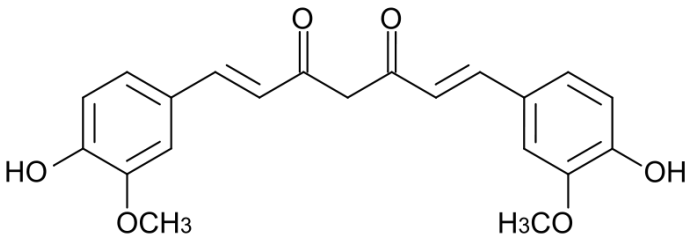

Figure 5.3- Chemical structure of curcumin.

Epigallocatechin gallate (EGCG), the main and the most essential polyphenol in green tea is a common phytochemical that is claimed to have many potential health benefits.[48] These include prevention of cardiovascular disease,[49] anti-inflammatory properties,[50] antioxidant,[51-53] antibacterial[54, 55] and anti-carcinogenic properties.[56-58] It has been proposed that many of the health benefits of green tea are due to the catechins, in particular EGCG to trap reactive oxygen species (ROS).[59, 60] Cancer

preventative properties of EGCG have also received recognition as various mechanisms for the preventive effect were suggested. These include antioxidant activity, direct binding to specific carcinogens and induction of apoptosis.[61, 62] As shown in Figure 5.4 is the structure of EGCG which consists of eight phenolic groups.

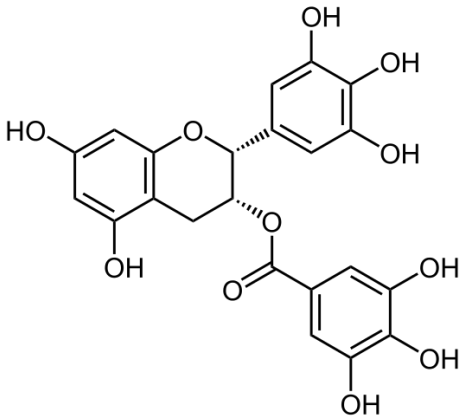

Figure 5.4- Chemical structure of EGCG.

Polyphenols possess strong antioxidant properties and has been documented comprehensively.[63-67] The typical mode of action for polyphenols is mainly due to their ability to donate hydrogen atoms (5.1) or electrons (5.2).[63, 68, 69]

$$R^{\bullet} + ArOH \rightarrow RH + ArO^{\bullet} \quad (5.1)$$

$$R^{\bullet} + ArOH \rightarrow R^{-} + ArOH^{\bullet +} \quad (5.2)$$

In the hydrogen-atom transfer (HAT) mechanism in Equation 5.1, the free radical ($R^{\bullet}$) removes a hydrogen atom from the phenolic antioxidant (ArOH) and becomes a free radical ($ArO^{\bullet}$) itself. This transfer is through homolytic rupture of the O-H bond. The formation and stability of $ArO^{\bullet}$ is highly dependent upon the structural features of the ArOH compound. The most crucial determining factors are:

- Presence, number and relative positions of additional phenolic hydroxyl groups,
- Involvement in the formation of intramolecular hydrogen bonds

- Conformation dependent possibility of allowing electronic delocalisation throughout the largest part of the molecule

All these factors affect the bond dissociation energy (BDE) of the phenolic O-H bond, where the weaker the O-H bond, the easier the H-atom transfer will be.

The second mechanism is the single-electron transfer (SET) displayed in Equation 5.2 from ArOH to a free radical $R^{\bullet}$ with formation of a stable radical cation $ArOH^{\bullet+}$. The ionisation potential (IP) of ArOH is another essential physicochemical parameter for evaluating the antioxidant efficacy of plant polyphenols where the lower the IP, the easier the electron abstraction.

The BDE and IP of polyphenols provide interesting information about the efficiency and the activity of the phenolic antioxidants. The following Table 5.1 provides the list of BDEs and IPs for the phenolic compounds used in this chapter from the literature. Thus, it is expected that the antibacterial activity of Ag nanoparticles may be improved by using phytochemicals such as curcumin and EGCG as reducing and capping agents.

Table 5.1- BDE and IP of phenolic compounds found in literature.

Phenolic Compound	BDE (kJ/mol)	IP (eV)
Tyrosine	350[70]	8.0[71]
Curcumin	348[72]	7.5[72]
EGCG	294[73]	7.1[74]

5.2 Experimental

5.2.1 Synthesis of tyrosine reduced Ag nanoparticles

Tyrosine reduced Ag nanospheres were synthesised as discussed previously in Chapter III.

5.2.2 Synthesis of curcumin reduced Ag nanoparticles

In a typical experiment, 10 mL of 10^{-3} M aqueous silver sulphate (containing 2×10^{-3} M equivalent of Ag^{+} ions) was prepared and added to 20 mL of 10^{-3} M aqueous solution of curcumin. This solution was then diluted to 100 mL with Milli-Q water. To this solution, 1 mL of 10^{-1} M KOH was added and was allowed to boil. Within 15 min, the final colourless solution changed into yellow in colour which indicates the formation of nanoparticles. Curcumin reduced Ag nanoparticles were also synthesised with a mole ratio of 1:2 (Curcumin: Ag), wherein while concentration of Ag^{+} ions were kept constant, the amount of curcumin was reduced to 50%.

5.2.3 Synthesis of EGCG reduced Ag nanoparticles

In a typical experiment, 20 mL of 10^{-3} M aqueous silver sulphate was prepared and added to 10 ml of 10^{-3} M aqueous solution of EGCG. This solution was then diluted to 100 mL with Milli-Q water. To this solution, 1 mL of 10^{-1} M KOH was added and was allowed to boil. Within 15 min, the final colourless solution changed into green/yellow in colour which indicates the formation of nanoparticles. EGCG reduced Ag nanoparticles were also synthesised with mole ratio of 1:3 (EGCG: Ag) and 1:8 (EGCG: Ag), wherein with a constant amount of Ag^{+} ions, the amount of EGCG was reduced to one-third and one-eighth respectively.

5.2.4 Processing of Ag nanoparticles by concentration and dialysis

All six nanoparticle solutions were dialysed overnight against deionised water using 12 kDa dialysis membranes to remove free ions. Samples were then rotary evaporated to concentrate the nanoparticle solutions by ten times. After concentration and dialysis, all Ag nanoparticles remained stable with an indication that they were

strongly capped with their precursors. The solutions were stable under standard laboratory conditions at room temperature and used for further characterisation and biological applications.

5.2.5 Quantification of Ag nanoparticles by atomic absorption spectroscopy (AAS)

Before the utilisation of further applications, AAS was used to determine the concentration of silver within each sample. Ag nanoparticles were initially dissolved in nitric acid and calibration standards were prepared using standard silver nitrate solution. Based on silver standards, a calibration graph was created and concentrations of silver within each sample were determined. Samples were then diluted to desired concentration for use.

5.2.6 Antibacterial applications

All antibacterial experiments were performed under aseptic conditions in a laminar flow cabinet. Before the commencement of microbiological experiments, media cultures, glassware and pipette tips were sterilised by autoclaving at 121°C for 15 minutes. Gram negative *Escherichia coli* (*E. coli*) and Gram positive bacterium *Staphylococcus albus* (*S. albus*) were used as microorganisms for antibacterial applications.

5.2.6.1 Colony forming units (CFU) assay

To examine the bactericidal effect of silver nanoparticles against Gram negative and Gram positive bacteria, 10^4 colony forming units (CFU) of each bacteria were mixed with various Ag nanoparticles in varying concentrations for 30 minutes in 1 mL volume.

100 μL of this was then plated on agar plates. These plates were then incubated for 24 hrs at 37°C and the numbers of colonies were counted. Colonies formed correspond to the number of viable bacteria in each suspension at the time of aliquot withdrawal.

5.3 Results and discussion

5.3.1 UV-Visible spectral studies of functionalised Ag nanoparticles

Reduction of aqueous Ag^+ ions during exposure to curcumin and EGCG can be revealed by UV-Vis spectroscopy. It is known that Ag nanoparticles exhibits yellow colour due to the excitation of surface plasmon vibrations (SPR) in metal nanoparticles.[75, 76] The SPR band for spherical Ag nanoparticles appears in the range of 380 nm to 440 nm in aqueous solutions. UV-Visible absorption spectra of Ag nanoparticles functionalised with tyrosine, curcumin and EGCG were obtained (Figure 5.5). It may be noted that in all the cases, the amount of Ag^+ ions used for nanoparticle synthesis is the same, while 1:1, 1:2, 1:3 and 1:8 phenolic Ag nanoparticles ratios correspond to increasingly less molar amounts of phenolic compounds with respect to constant 0.1 mM Ag_2SO_4.

In Figure 5.6, UV-Vis spectra have been separated according to their functionalised groups. A sharp SPR band for spherical tyrosine reduced Ag nanoparticles occur at ca. 417 nm in aqueous medium. For curcumin reduced Ag nanoparticles, SPR bands centred around 421 nm (1:1) is observed and as the amount of curcumin is decreased, there is an apparent shift to ca. 412 nm. There is also a noticeable decrease in intensity in the Ag SPR peak for C1:Ag2 which includes less curcumin, suggesting that there is not enough reducing agent (curcumin) available to reduce all of the Ag^+ ions.

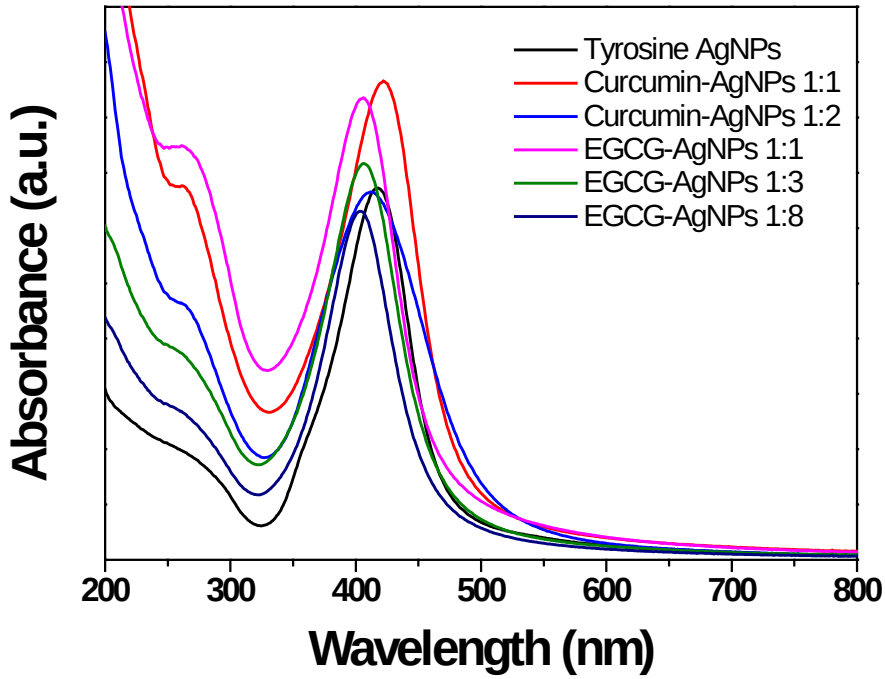

Figure 5.5- UV-Visible spectra of tyrosine, curcumin and EGCG reduced Ag nanoparticles in different mole ratios.

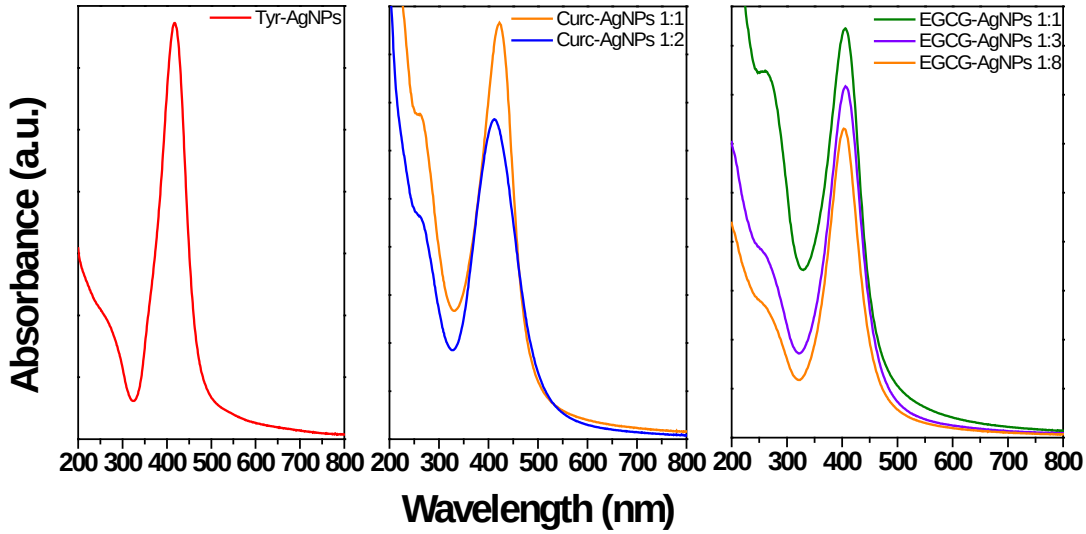

Figure 5.6- UV-Visible spectra of functionalised Ag nanoparticles separated for clarity.

Similarly, at equimolar (1:1) concentration of EGCG reduced Ag nanoparticles, SPR bands are observed at ca. 406 nm. As the amount of EGCG is decreased, the peak at ca. 406 nm shifted to 404 nm for (1 EGCG: 3 Ag) and (1 EGCG: 8 Ag) with a decrease of intensity. Again, the intensities of the ratios decrease as less EGCG is apparent within the sample, suggesting the lack of enough reducing agent to allow complete reduction of Ag^{+} ions.

5.3.2 Silver reducing capabilities of phenolic compounds via AAS

Dialysed solutions were analysed by AAS to determine the concentration of silver after functionalised nanoparticle reduction. During the synthesis of each sample, the amount of precursor capping and reducing agent i.e. tyrosine, curcumin and EGCG, was decreased according to their phenolic group present within their structure. For example, in the case of amino acid tyrosine, only one active phenolic group is present, therefore an equimolar ratio of 1:1 (Tyr:Ag) was studied. As for the structure of curcumin, two phenolic groups are present hence ratios of 1:1 and 1:2 were studied. EGCG on the other hand consists of multiple phenolic groups, leading ratios of 1:1, 1:3 and 1:8 to be synthesised. During the synthesis, since 0.1 mM Ag_2SO_4 was employed, it corresponds to 0.2 mM Ag^+ ions that remained constant for all six nanoparticle solutions. Illustrated below in Table 5.2, depicts the concentrations of silver present before and after synthesis according to AAS analysis.

Table 5.2- Concentrations of silver and phenolic compounds and their reducing capabilities.

System	Ag (mM)	Phenolic compounds (mM)	AgNPs (mM)	Efficiency (%)
Tyr-AgNPs 1:1	0.2	0.2	0.172	86
Curc-AgNPs 1:1	0.2	0.2	0.178	89
Curc-AgNPs 1:2	0.2	0.1	0.180	90
EGCG-AgNPs 1:1	0.2	0.2	0.143	72
EGCG-AgNPs 1:3	0.2	0.07	0.142	71
EGCG-AgNPs 1:8	0.2	0.025	0.147	74

From Table 5.2, it can be observed that among different reducing agents, EGCG provided the least amount of silver content in Ag nanoparticles from 71-74% efficiency across different concentrations of EGCG, while tyrosine could reduce Ag^+ ions with 86% efficiency. Overall, the highest silver nanoparticle concentrations attained were from curcumin for both ratios of 1:1 and 1:2 with ca. 90% reduction efficiency. Therefore, of all three phenolic compounds, curcumin shows the best Ag^+ ion reducing capability.

Although the ratios of phenolic compounds to silver were decreased, the reducing capabilities within each sample did not significantly differ. This suggests that more than one phenolic group present in curcumin and EGCG structure can simultaneously participate in reduction of Ag^+ ions.

5.3.3 TEM and DLS measurements of functionalised Ag nanoparticles

Illustrated in Figure 5.7 are TEM images and particle size distribution histograms of functionalized Ag nanoparticles with their respective mole ratios. Influence of the amount of capping agent used during synthesis can determine the surface modifications on particle size and distribution. Tyrosine reduced Ag nanoparticles (Figure 5.7A) are quasi spherical in appearance with an average particle diameter of ca. 21.8 nm and standard deviation of 5.0 nm.

Curcumin reduced Ag nanoparticles are spherical in shape in both mole ratios (Figure 5.7B and 5.7C). As the ratio of curcumin decreases, the average size diameter is increased. The average particle diameter for each curcumin reduced Ag nanoparticle was calculated along with standard deviation to be ca. 14.5 nm ± 5.6 nm and ca. 15.2 nm ± 5.6 nm for curcumin reduced Ag nanoparticles 1:1 and curcumin reduced Ag nanoparticles 1:2, respectively.

EGCG reduced Ag nanoparticles portrayed similar trends in the increase of particle size diameter as the ratio of EGCG decreases (Figure 5.7D-F). These spherical particles become aggregated at the highest mole ratio of 1:8. This may be due to a reduction in the amount of EGCG available as a capping agent post reduction of Ag^+ ions. The average diameter for each EGCG reduced Ag nanoparticle was ca. 10.5 nm ± 7.4 nm, ca. 11.8 ±7.2 nm and ca. 24.1 nm ± 16.4 nm for EGCG reduced Ag nanoparticles at 1:1, 1:3

and 1:8 mole ratios respectively. According to Ejima *et al.*, it was found that the increase in salt concentration affects the morphology of nanomaterials.[77] In that study, with an increasing metal ion concentration with respect to a polyphenol as a reducing agent, larger film assembly and increase of roughness was observed. Similarly, in this study while overall Ag^{+} ion remain constant, the Ag_2SO_4 concentration has been artificially increased with respect to relative amount of EGCG present.

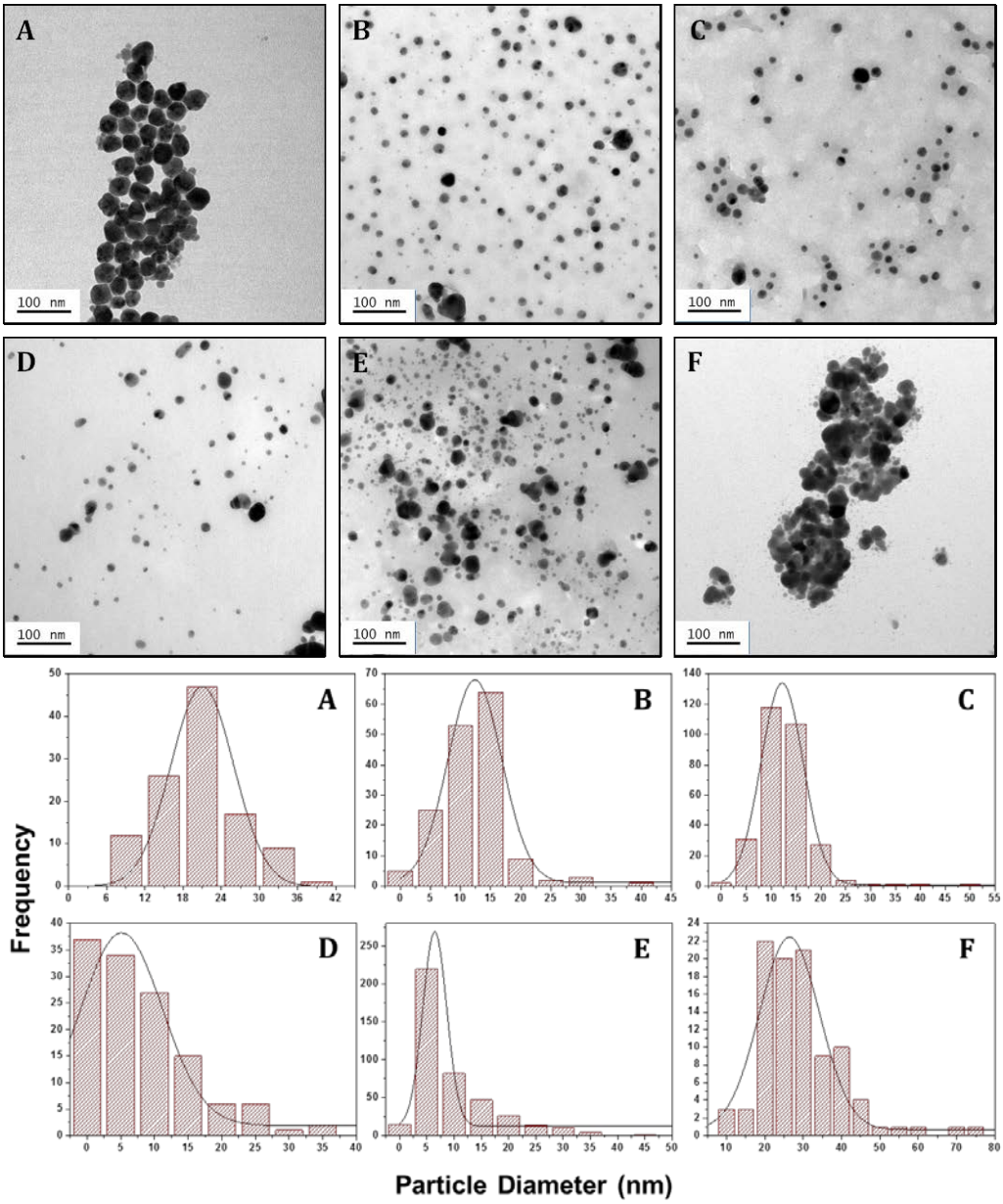

Figure 5.7- TEM images and corresponding particle size distribution histograms of functionalised Ag nanoparticles at various mole ratios: (A) tyrosine Ag nanoparticles, (B) curcumin Ag nanoparticles 1:1, (C) curcumin Ag nanoparticles 1:2, (D) EGCG Ag nanoparticles 1:1, (E) EGCG Ag nanoparticles 1:3 and (F) EGCG Ag nanoparticles 1:8.

Alternatively, size distribution of the functionalised Ag nanoparticles was also investigated via dynamic light scattering (DLS). DLS provides information on the hydrodynamic radii of nanoparticles in solution by measuring the time sale of light intensity fluctuations. DLS measurements in Figure 5.8 provided the trend in change of the average hydrodynamic radius for each mole ratio. The average hydrodynamic radius for tyrosine reduced Ag nanoparticles was 41.4 nm (equivalent to hydrodynamic diameter 82.8 nm).

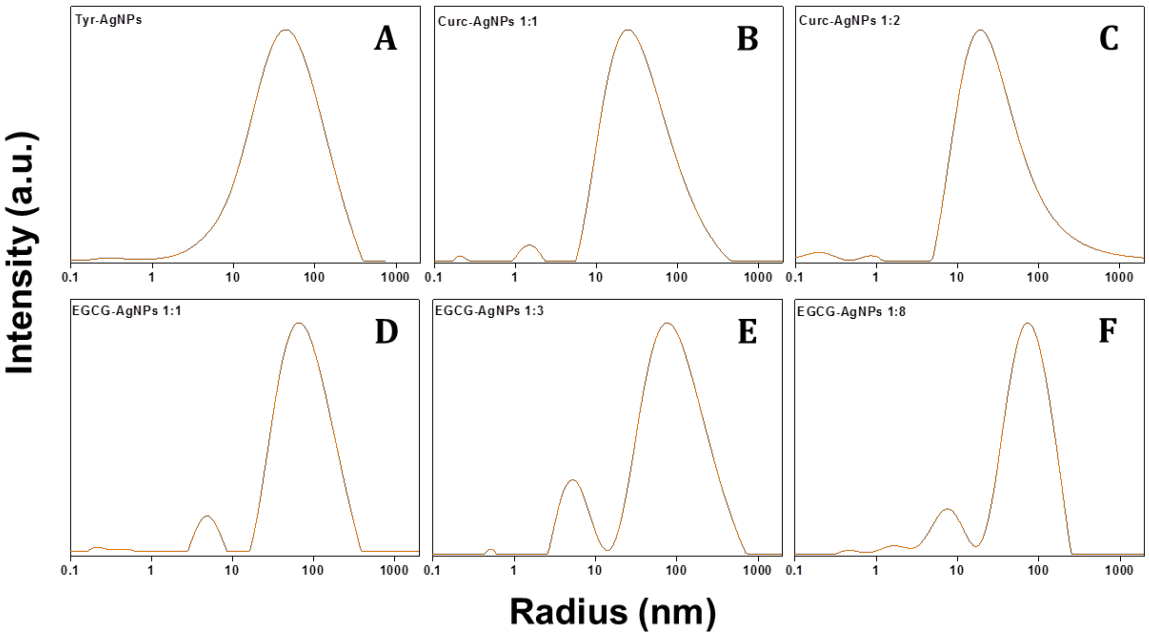

Figure 5.8- DLS size distribution profile of (A) tyrosine Ag nanoparticles, (B) curcumin Ag nanoparticles 1:1, (C) curcumin Ag nanoparticles 1:2, (D) EGCG Ag nanoparticles 1:1, (E) EGCG Ag nanoparticles 1:3 and (F) EGCG Ag nanoparticles 1:8.

In the case of curcumin reduced Ag nanoparticles, at equimolar ratio the average hydrodynamic radius was 25.1 nm (equivalent to hydrodynamic diameter 50.2 nm) and at 1:2 mole ratio, the average hydrodynamic radius was 18.8 nm (equivalent to hydrodynamic diameter 37.6 nm). Moreover, as for EGCG reduced Ag nanoparticles, the equivalent trend of increase of hydrodynamic radius are observed as the mole ratio rises. The average hydrodynamic radius was 65.7 nm (equivalent to hydrodynamic diameter

131.4 nm) for equimolar ratio, 75.6 nm (equivalent to hydrodynamic diameter 151.2 nm) for 1:3 mole ratio and 75.6 nm (equivalent to hydrodynamic diameter 151.2nm) for 1:8 mole ratio.

5.3.4 X-ray diffraction (XRD) studies of functionalised Ag nanoparticles

Silver crystallises in a cubic close packed structure. The unit cell for this structure is cubic consisting of the same length and all faces are perpendicular to each other. Silver atoms are present at each corner as well as in the centre of each face of the unit cell. This unit cell is also known as a face-centered cubic (FCC) unit cell. Structural information of functionalised Ag nanoparticles were attained via XRD using a general area detector diffraction system (GADDS) as shown in Figure 5.9.

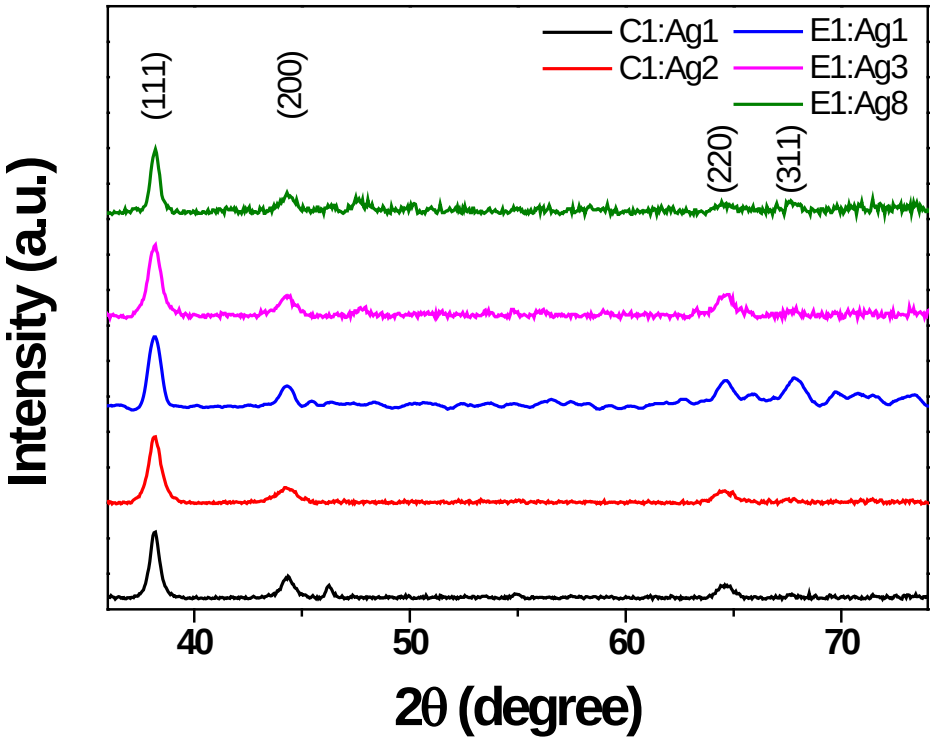

Figure 5.9- XRD patterns of functionalised Ag nanoparticles.

Diffraction patterns of functionalised Ag nanoparticles confirmed the crystalline structure of silver nanoparticles and are normalised to the (111) peak. All peaks in the XRD pattern can be readily indexed to a face-centered cubic structure of silver. Curcumin

reduced Ag nanoparticles in all mole ratios displayed characteristic (111), (200) and (220) peaks which represents the FCC silver plane in Bragg's Law. In the case of EGCG reduced Ag nanoparticles, the same (111), (200) and (220) peaks of silver are shown. Additionally, an extra peak at (311) plane of silver FCC is apparent across all mole ratios, however intensity decreases as mole ratios rises to 1:8. The XRD pattern of tyrosine reduced Ag nanoparticles is provided in Chapter III.

5.3.5 FTIR analysis to understand surface corona of functionalised Ag nanoparticles

Tyrosine reduced Ag nanoparticle FTIR can be found in Chapter III.

5.3.5.1 FTIR analysis of curcumin-reduced Ag nanoparticles

The molecule of curcumin as shown in Figure 5.10, have an alternating conjugated symmetrical structure with single (-C-C-) and double (-C=C-) bonds. There are two benzene rings, two methoxy and predominantly two hydroxyl functional groups. Curcumin can also exist in two tautomeric forms in the central part of the molecule; keto with two C=O groups, and a C=O and C-OH group for enol form.

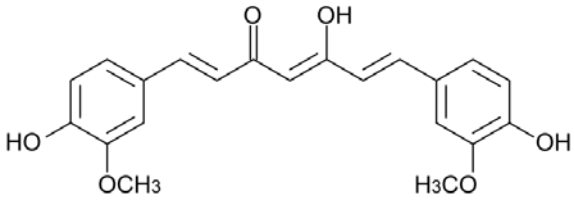

Figure 5.10- Chemical structure of curcumin.

The FTIR spectrum of curcumin and curcumin reduced Ag nanoparticles are shown in Figure 5.11. In the case of curcumin alone, the highest frequency region for both phenolic OH vibrations were calculated at 3595 cm^{-1} by *Kolevet et al.*,[78] however in practice this band could be shifted towards the negative scale due to intramolecular and

intermolecular hydrogen bonding and this can be seen in Figure 5.11, with a weak sharp peak at ca. 3509 cm^{-1}. Towards the middle region, a sharp peak at ca. 1627 cm^{-1} has a predominately mixed C=C and C=O character of the benzene ring. The observed shoulder peak at ca. 1602 cm^{-1} is attributed to the symmetric aromatic ring stretching vibrations $C=C_{ring}$. The medium intensity peak at ca. 1506 cm^{-1} is assigned to the C=O. Most bands in the frequency region 1400 cm^{-1} to 1490 cm^{-1} are highly mixed with one clear band at ca. 1428 cm^{-1}. This band corresponds to deformation vibrations of the two methyl groups. In-plane deformation vibrations of CCH of phenyl rings and skeletal in-plane formations are observed at ca. 1274 cm^{-1} and ca. 1182 cm^{-1} respectively. In the range of 1320 cm^{-1} to 1200 cm^{-1}, the observed bands at 1315 cm^{-1} and 1204 cm^{-1} are attributed to C-O and C=C-H of interring chain respectively. In this fragment the vibrations of the phenyl group are intensely mixed with skeletal groups. Therefore a prominent peak at ca. 1152 cm^{-1} corresponds to C-O-C vibration. The band at ca. 1024 cm^{-1} is attributed to the C-H out of plane vibration of the aromatic ring.

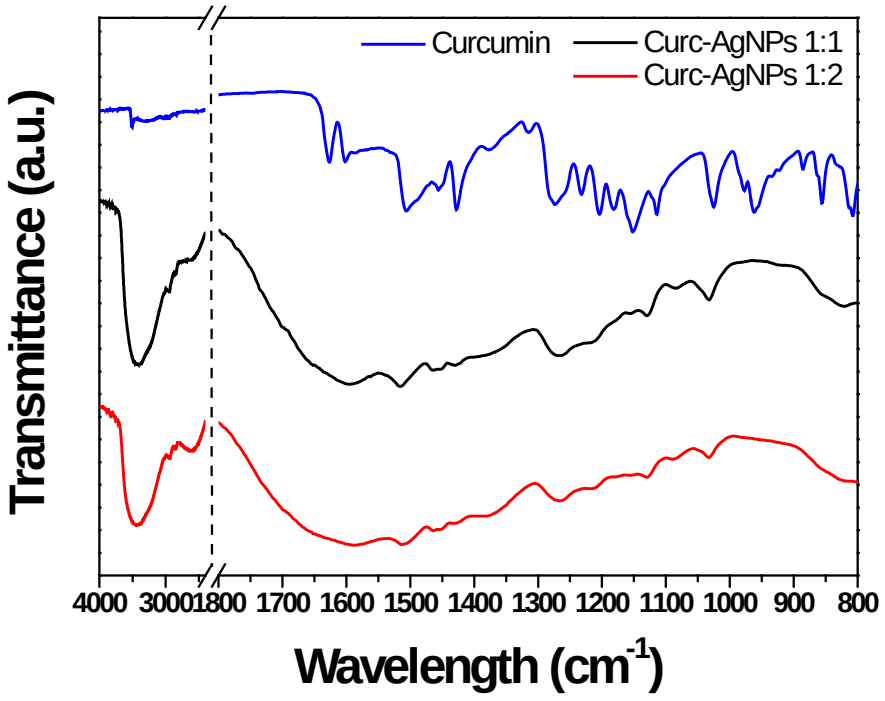

Figure 5.11- FTIR spectra of pure curcumin and curcumin reduced Ag nanoparticles at various mole ratios.

When curcumin is used to reduce silver ions to form Ag nanoparticles, several bands representing curcumin were shifted from their original positions according to the IR spectrum. There is an increase in intensity for the hydroxyl vibration for Curc-AgNPs 1:1 and Curc-AgNPs 1:2 with a slight shift at ca. 3430 cm^{-1} and ca. 3432 cm^{-1} respectively.

The assignment of the ketone functional group C=O was shifted from the original spectrum to ca. 1514 cm^{-1} for Curc-AgNPs 1:1 and ca. 1512 cm^{-1} for Curc-AgNPs 1:2. The intensities of these peaks have also been diminished upon binding of curcumin to Ag nanoparticles during synthesis.

The phenolic groups in Curc-AgNPs 1:1 and Curc-AgNPs 1:2 were also shifted to ca. 1272 cm^{-1} and ca. 1268 cm^{-1}. The ether vibration for both ratios shifted to ca. 1130 cm^{-1} from the original curcumin spectrum at ca. 1152 cm^{-1}. Similarly, the C-H vibration of the aromatic ring were shifted to ca. 1034 cm^{-1} and ca. 1032 cm^{-1} for Curc-AgNPs 1:1 and Curc-AgNPs 1:2. A summary of the various vibrational bands and functional groups present for curcumin and curcumin reduced Ag nanoparticles is provided in Table 5.3.

Table 5.3- Summary of functional groups in curcumin and curcumin reduced Ag nanoparticles.

Wavenumber (cm^{-1})	Bond	Functional group	Appearance
	Curcumin		
3509	O-H stretch	Hydroxyl	Weak
1627	C=O stretch	Aromatic	Sharp
1602	$C=C_{ring}$stretch	Aromatic	Weak
1506	C=O	Ketone	Medium
1428	C-H	Alkane	Medium
1315	C-O	Ether	Weak
1274	CCH	Phenyl	Medium
1204	C=C-H	Alkene	Narrow
1182	CCH	Phenyl	Weak
1152	C-O-C	Ether	Medium
1024	C-H	Aromatic	Medium
	Curc-AgNPs 1:1		
3430	O-H stretch	Hydroxyl	Broad
1514	C=O	Ketone	Weak
1272	CCH	Phenyl	Broad
1130	C-O-C	Ether	Weak
1034	C-H	Aromatic	Medium
	Curc-AgNPs 1:2		
3432	O-H stretch	Hydroxyl	Broad
1512	C=O	Ketone	Weak
1268	CCH	Phenyl	Broad
1130	C-O-C	Ether	Weak
1032	C-H	Aromatic	Medium

5.3.5.2 FTIR analysis of EGCG-reduced Ag nanoparticles

FTIR analysis of EGCG and EGCG reduced Ag nanoparticles were carried out to understand how the functional groups interact as well as for providing information on the surface chemistry of Ag nanoparticles. Illustrated in Figure 5.12 is the FTIR spectra of EGCG and EGCG reduced Ag nanoparticles. In regards to the EGCG spectrum, a weak hydroxyl peak at ca. 3359 cm^{-1} is observed. This is due to the vibration of the OH stretch of phenolic hydroxyl group.[79, 80] EGCG demonstrating a sharp absorption band at ca. 1691 cm^{-1} is assigned to C=O of the ester functional group. A peak representing a C-O

bond can be found at ca. 1343 cm^{-1}. Sharp aromatic ring stretching vibrations can be observed at ca. 1615 cm^{-1}, 1527 cm^{-1} and 1447 cm^{-1}. Similarly, an aromatic alcohol C-O with a sharp band is evident at ca. 1292 cm^{-1}. Furthermore, a sharp phenol C-O peak at ca. 1217 cm^{-1} and alcohol bands at ca. 1144 cm^{-1} and 1095 cm^{-1} are present.

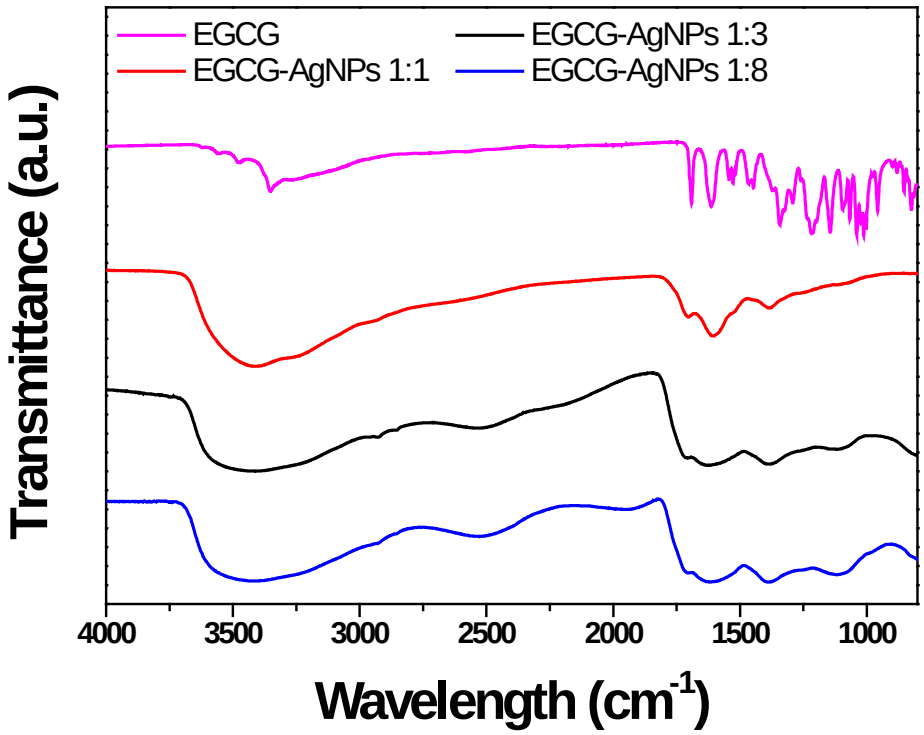

Figure 5.12- FTIR spectra of EGCG and EGCG reduced Ag nanoparticles.

Upon utilisation of EGCG in the synthesis for the formation Ag nanoparticles, numerous bands were shifted from the original EGCG spectrum. Evidence of the broadening of the hydroxyl peaks are related to the intermolecular H-bonds and O-H stretching modes in EGCG-AgNPs mole ratios of 1:1, 1:3 and 1:8 with peaks at ca. 3426 cm^{-1} and 3446 cm^{-1}.[81]

The assignment of the ester functional C=O peak was also shifted in all mole ratios with a weaker intensity. For EGCG-AgNPs 1:1 the peak shifted to ca. 1702 cm^{-1}, EGCG-AgNPs 1:3 shifted to ca. 1708 cm^{-1} and EGCG-AgNPs 1:8 shifted to ca. 1704 cm^{-1}.

Aromatic C=C band broadening and shifting is evidence in all mole ratios at ca. 1606 cm^{-1} (EGCG-AgNPs 1:1), 1630cm^{-1} (EGCG-AgNPs 1:3) and 1622 cm^{-1} (EGCG-AgNPs 1:8). Similarly, the same trend occurs for the alcohol functional group C-O in EGCG-AgNPs 1:3 and EGCG-AgNPs 1:8 with shifts at ca. 1120 cm^{-1} and ca. 1118 cm^{-1} respectively.

Since $AgSO_4$ was utilised in the synthesis, sulphate SO_4 peaks can be observed in all mole ratio spectral data post synthesis. These peaks occurred at ca. 1384 cm^{-1} (EGCG-AgNPs 1:1), 1392 cm^{-1} (EGCG-AgNPs 1:3) and 1390 cm^{-1} (EGCG-AgNPs 1:8). The structure of EGCG (Figure 5.13) and a summary of the various vibrational bands and functional groups present for EGCG and EGCG reduced Ag nanoparticles are provided in Table 5.4.

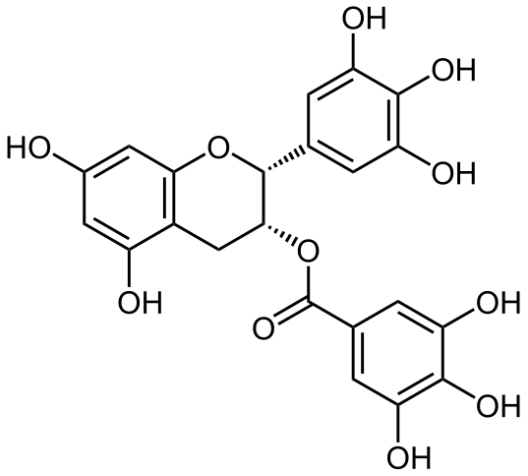

Figure 5.13- Chemical structure of EGCG.

Table 5.4- Summary of functional groups in EGCG and EGCG reduced Ag nanoparticles.

Wavenumber (cm^{-1})	Bond	Functional group	Appearance
		EGCG	
3359	O-H stretch	Hydroxyl	Weak
1691	C=O	Ester	Sharp
1615	C=C	Aromatic	Sharp
1527	C=C	Aromatic	Sharp
1447	C=C	Aromatic	Sharp
1343	C-O	Ester	Sharp
1292	C-O	Aromatic alcohol	Sharp
1217	C-O	Phenol	Sharp
1144	C-O	Alcohol	Sharp
1095	C-O	Alcohol	Sharp
		EGCG-AgNPs 1:1	
3426	O-H stretch	Hydroxyl	Broad
1702	C=O	Ester	Medium
1606	C=C	Aromatic	Strong
1384	SO_4	Sulphate	Weak
		EGCG-AgNPs 1:3	
3446	O-H stretch	Hydroxyl	Broad
1708	C=O	Ester	Medium
1630	C=C	Aromatic	Broad
1392	SO_4	Sulphate	Weak
1120	C-O	Alcohol	Weak
		EGCG-AgNPs 1:8	
3446	O-H stretch	Hydroxyl	Broad
1704	C=O	Ester	Medium
1622	C=C	Aromatic	Broad
1390	SO_4	Sulphate	Weak
1118	C-O	Alcohol	Weak

5.3.6 Antibacterial assays of functionalised Ag nanoparticles

5.3.6.1 Colony count studies for equimolar ratios of functionalised Ag nanoparticles.

Colony count method was employed to examine the antibacterial effects of functionalised Ag nanoparticles against Gram negative and Gram positive bacteria *E. coli* and *S. albus*, respectively. To determine the effects of functionalised Ag nanoparticles on bacterial growth, various concentrations of Ag^0 nanoparticles ranging from 0.1 mM to 1 mM equivalent of Ag^+ ions were applied to 10^3 CFU of bacteria as per the protocols elaborated in Chapter III and IV. Figures 5.14A and B indicate the antibacterial activity profile for Gram negative and Gram positive bacteria at equimolar ratios.

In the case of *E. coli* shown in Figure 5.14A, when all functionalised Ag nanoparticles were at equimolar ratios, there is a consistent trend of the increase of cell death across all concentrations. Among three phenolic capping agents, tyrosine reduced Ag nanoparticles exhibited the least activity across all concentrations from 0.1 mM to 1.0 mM. As the concentration of silver increases, curcumin and EGCG reduced Ag nanoparticles showed comparable activity with enhancement in antibacterial activity as a function of Ag concentration.

Similarly, in the case of *S. albus* antibacterial profile (Figure 5.14B), tyrosine reduced Ag nanoparticles again showed the lowest inhibitory effect across all concentrations. This is followed by curcumin reduced Ag nanoparticles with moderate percentage cell death across all concentrations. While curcumin reduced Ag nanoparticles showed higher activity than tyrosine reduced Ag nanoparticles, EGCG reduced Ag nanoparticles demonstrated the highest activity across all concentrations. There is a

significant increase in cell death at the higher end of the concentration range of 0.5 mM and 1.0 mM with ca. 79% and 94% respectively.

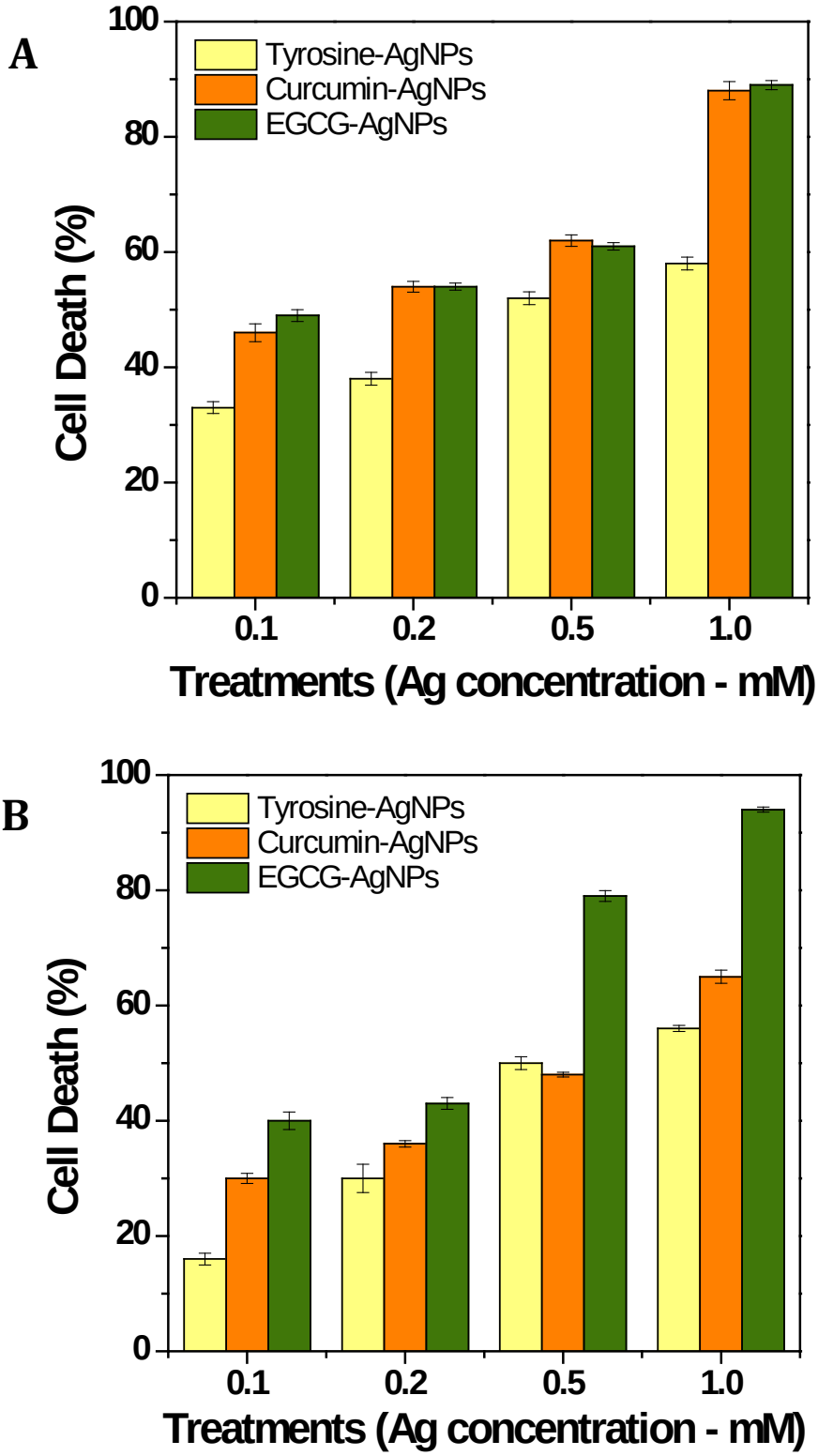

Figure 5.14- CFU expressed in percentage cell death of (A) functionalised Ag nanoparticles against Gram negative *E. coli* and (B) functionalised Ag nanoparticles against Gram positive *S. albus.*

Overall, in regards to equimolar ratios, tyrosine reduced Ag nanoparticles displayed the least activity compared to other phenolic compounds both in the case of *E. coli* and *S. albus*. However, the comparative antibacterial profiles of curcumin and EGCG reduced Ag nanoparticles were different in case of *E. coli* and *S. albus.* In case of *E. coli*, both curcumin and EGCG reduced Ag nanoparticles showed equivalent activity while in case of *S. albus,* EGCG-AgNPs showed significantly higher activity than Curc-AgNPs. The relative activity profiles of different nanoparticles are in line with the dissociation energies and ionization potentials for each phenolic compound from the literature.[70-74] In general, and particularly at lower Ag concentrations, functionalised Ag nanoparticles are shown to be relatively more effective against Gram negative bacteria *E. coli* over Gram positive *S. albus.* However, at the higher silver concentrations of 0.5 mM and 1.0 mM, EGCG reduced Ag nanoparticles produces a higher percentage cell death in the case of Gram positive *S. albus*.

5.3.6.2 Colony count studies for varied mole ratios of curcumin reduced Ag nanoparticles.

Two mole ratios of 1:1 and 1:2 (Curc:Ag) were tested against Gram negative and Gram positive bacteria. Concentrations of silver ranging from 0.1 mM to 1.0 mM were applied to 10^3 CFU of bacteria. Figures 5.15A and B illustrate the antibacterial activity of curcumin reduced Ag nanoparticles. With reference to *E. coli* as shown in Figure 5.15A, both mole ratios of curcumin reduced Ag nanoparticles exhibited a consistent trend of increasing cell death with rising silver concentration. The highest activity was achieved by curcumin reduced Ag nanoparticles comprising 1:2 mole ratio (less curcumin). At lower concentrations of silver, i.e. 0.1 mM and 0.2 mM, the average difference in

percentage cell death between the ratios of 1:1 and 1:2 are ca. 20%. The difference in cell death increases at 0.5 mM to ca. 25%. Thereafter, at the highest concentration of 1.0 mM, the variance of cell death between the two ratios is minute, ca. 5%.

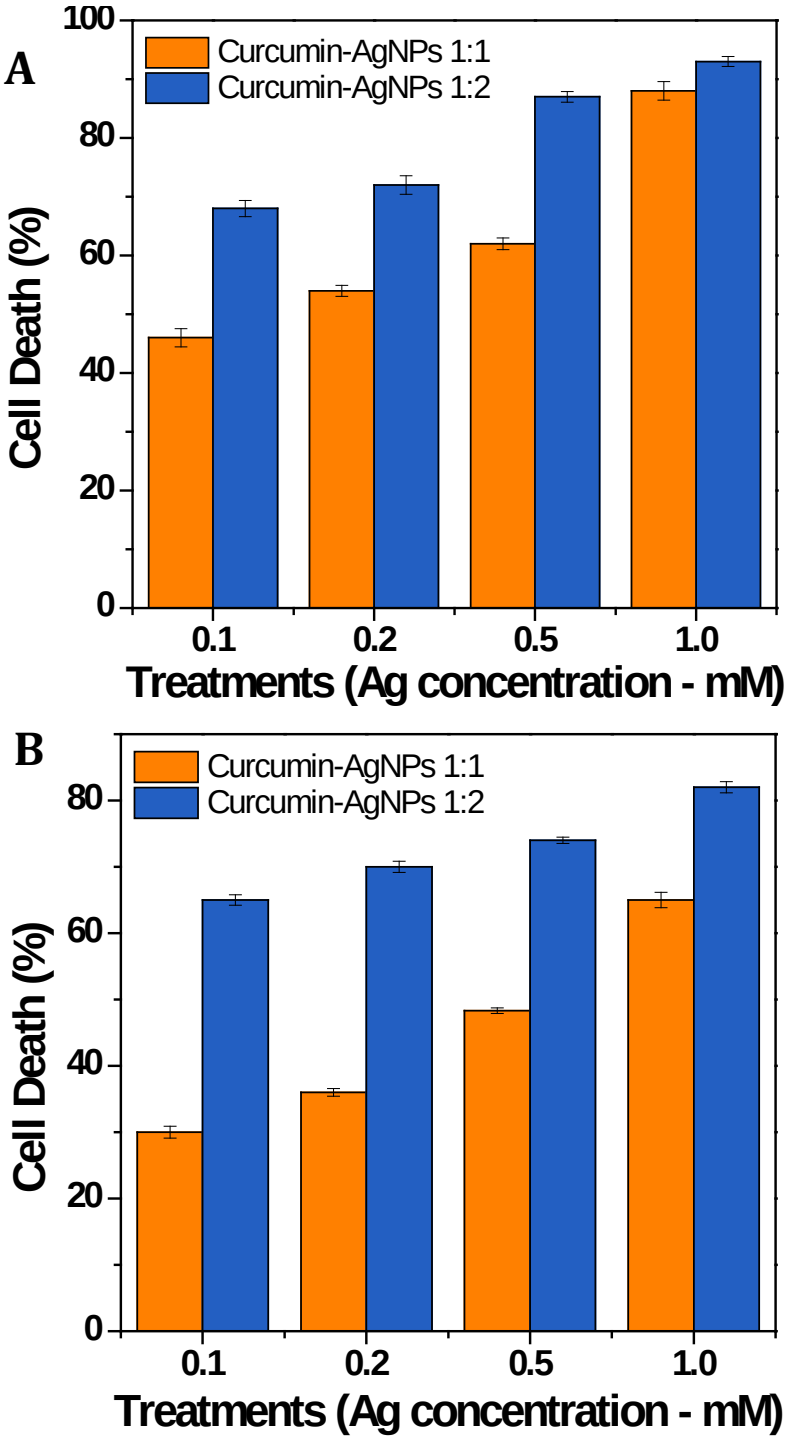

Figure 5.15- CFU expressed in percentage cell death of (A) curcumin reduced Ag nanoparticles against Gram negative *E. coli* and (B) curcumin reduced Ag nanoparticles against Gram positive *S. albus*.

Moreover, the antibacterial profile for Gram positive bacteria *S. albus* displays similar trends as *E. coli* with the increase of cell death as the silver concentration rises as shown in Figure 5.15B. Likewise, curcumin reduced Ag nanoparticles at mole ratio of 1:2 (less curcumin) demonstrated the higher inhibitory effects. The difference in percentage cell death for the Gram positive *S. albus* is greater than that observed for *E. coli*. Starting at the lowest concentration of 0.1 mM, the difference is ca. 35% followed by ca. 34% at 0.2 mM concentration. The percentage cell death for mid-range of 0.5 mM concentration was at ca. 26%, relatively similar to *E. coli*. At the highest concentration of 1.0 mM, the deviation of cell death was ca. 17% compared to merely ca. 5% in the *E. coli* study.

Interestingly, it can be observed that with less curcumin functionalised onto the surface of silver, the antibacterial activity gets enhanced. This suggests that when less curcumin is used as a capping agent, the corona layer is thinner and allows the facile nanoparticle oxidation to interact with bacteria cells.

5.3.6.3 Colony count studies for varied mole ratios of EGCG reduced Ag nanoparticles.

Three mole ratios of 1:1, 1:3 and 1:8 (EGCG:Ag) were likewise tested against Gram negative and Gram positive bacteria. Reiteratively, concentrations of silver ranging from 0.1 mM to 1.0 mM were applied to 10^3 CFU of bacteria. Figures 5.16A and B portrays the antibacterial activity of EGCG reduced Ag nanoparticles. Similarly to that of curcumin reduced Ag nanoparticles against *E. coli*, all mole ratios of EGCG reduced Ag nanoparticles displayed the same behaviour in the increase of cell death with increase in silver concentration (Figure 5.16A). As expected from curcumin study, the greatest inhibitory effects were achieved by EGCG reduced Ag nanoparticles at 1:8 mole ratio (less EGCG). At

the lowest silver concentration of 0.1 mM, equimolar EGCG reduced Ag nanoparticles exhibited a percentage cell death of ca. 49% compared to the 1:3 and 1:8 ratios which possessed an equal cell death at ca. 67%. At a silver concentration of 0.2 mM, the cell death of EGCG reduced Ag nanoparticles 1:3 remained the same at ca. 67% whereas equimolar and 1:8 mole ratios increased in percentage cell death at ca. 54% and 87% respectively. Similar increase of percentage cell death is apparent at 0.5 mM concentration, with ca. 61%, 71% and 93% for EGCG reduced Ag nanoparticles at equimolar, 1:3 and 1:8 mole ratios. At the highest silver concentration of 1.0 mM, all mole ratios of EGCG reduced Ag nanoparticles possessed comparable trends with minor percentage differences in cell death.

In the case of Gram positive *S. albus* (Figure 5.16B), equimolar EGCG reduced Ag nanoparticles once again exhibited the least inhibitory effect across all silver concentrations. It can also be noted that at the lower end of the range of 0.1 mM and 0.2 mM, the percentage cell death is only ca. 40% and 43% respectively, which is lower than that of the *E. coli* study. However, this behaviour transitioned to a higher percentage of cell death as the silver concentrations increased across all mole ratios of EGCG reduced Ag nanoparticles. This observation may suggest that at higher concentrations of silver, EGCG reduced Ag nanoparticles are significantly more active against Gram positive *S. albus* (ca. 100% cell death in the case of 1:8 mole ratio).

Once again, similar trends to curcumin reduced Ag nanoparticles antibacterial profile can be observed in this study. When the amount of EGCG is decreased to functionalise onto the surface of silver nanoparticles, higher antibacterial activity is detected. These results clearly indicate the effect of surface corona on the antibacterial activity of functionalised Ag nanoparticles. Thinner corona layer facilitate Ag nanoparticle

oxidation and interaction of Ag nanoparticles with bacterium. This interaction eventually leads to cell death due to multimode action of Ag nanoparticles.[82, 83]

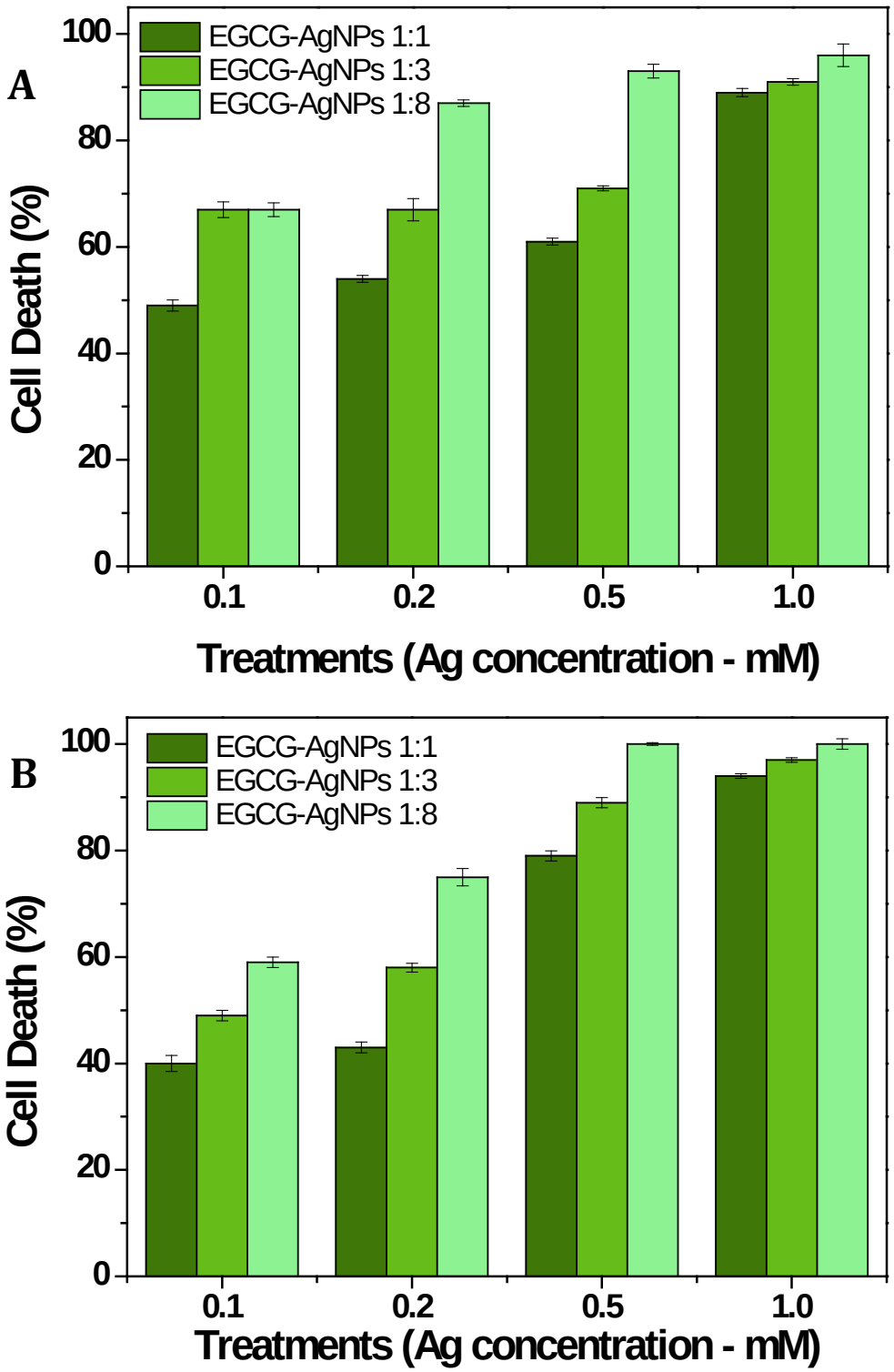

Figure 5.16- CFU expressed in percentage cell death of (A) EGCG reduced Ag nanoparticles against Gram negative *E. coli* and (B) EGCG reduced Ag nanoparticles against Gram positive *S. albus*.

5.3.7 Morphology studies of bacteria cells after the treatment of functionalised Ag nanoparticles

In relation to antibacterial activities, it is hypothesised that nanomaterials and cations mainly Ag^+ ions predominantly affect the function of membrane-bound enzymes. The inhibitory components of nanoparticles on microorganisms depict that after exposure, DNA loses its replication ability, manifestation of ribosomal subunit proteins and other cellular proteins and enzymes becomes inactive.[84-91] However, the mechanism of antibacterial action of nanomaterials is still not distinctly understood. Nevertheless, findings in the literature emphasise that microbial morphology and membrane integrity is one of the significant elements which is crucial for bacterial survival. Hence, to understand the effects of phenolic compounds in surface functionalised Ag nanoparticles on bacterial morphology, nano-scanning electron microscopy (Nano-SEM) was employed to envisage the changes in bacterial cell wall and morphology after their exposure.

SEM micrographs of *E. coli* bacteria cells before and after their treatments with functionalised Ag nanoparticles are illustrated in Figures 5.17 and 5.19. SEM images of tyrosine reduced Ag nanoparticle interaction with bacterial cells can be found in Chapter III. In observance of curcumin reduced Ag nanoparticles against *E. coli* as shown in Figure 5.17, untreated cells appear smooth and perpetual. When cells are exposed to the two different mole ratios of curcumin reduced Ag nanoparticles, cell walls of the bacteria show signs of rupture in both cases. Comparing the untreated *E. coli* cells against treated cells, the images reveal noticeable changes in cell morphology with roughening of the cell wall and the presence of curcumin reduced Ag nanoparticles scattered around the bacterial cells. Subsequently, with the exposure of curcumin reduced Ag nanoparticles, the components of *E. coli* cell wall are damaged which causes the cells to withdraw from

their original intact arrangement. This observation can confirm that curcumin reduced Ag nanoparticles (at mole ratios of 1:1 and 1:2) have considerable impact on *E. coli* bacterial cell morphology. Consequently, this reveals that in the case of Gram negative bacteria *E. coli*, curcumin reduced Ag nanoparticles demonstrates significant effects on membrane integrity.

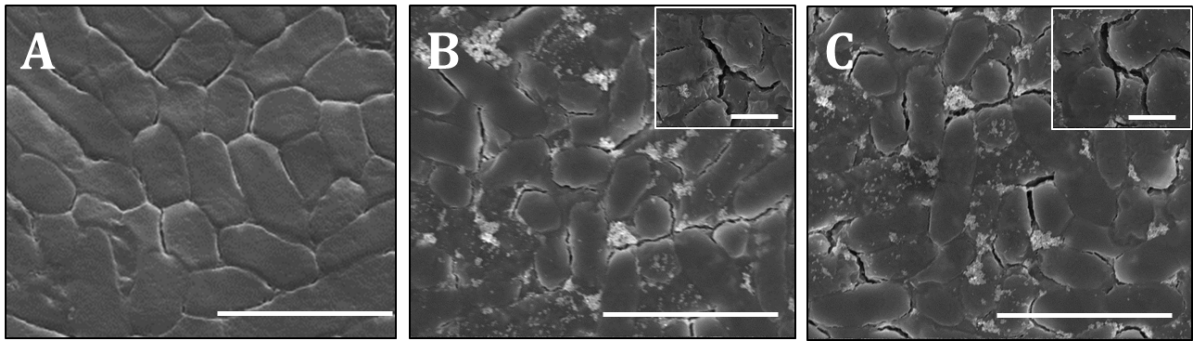

Figure 5.17- SEM micrographs of *E. coli* cells (A) untreated, and after treatment with (B) Curc- AgNPs (1:1) and (C) Curc-AgNPs (1:2) Scale bars 5 µm and insert scale bars 1 µm.

Illustrated in Figure 5.18 is the morphology of *S. albus* before and after treatment of curcumin reduced Ag nanoparticles. Untreated cells in Figure 5.18 are spherical in shape and the bacterial cluster resembles a grape-like structure. The cells possess a slightly rough surface, completely intact and undamaged in its original form. However when the cells are exposed to curcumin reduced Ag nanoparticles, there are selected fragments on the cell surface which indicates damage to the cell. The cell clusters are smoother in appearance and forms an irregular shape rather than spheres.

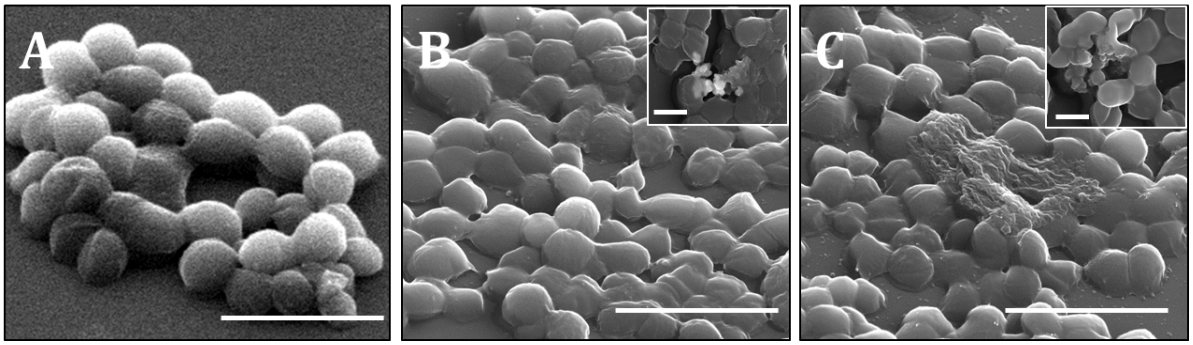

Figure 5.18- SEM micrographs of *S. albus* cells (A) untreated, and after treatment with (B) Curc-AgNPs (1:1) and (C) Curc-AgNPs (1:2) Scale bars 3 µm insert scale bars 1 µm.

Furthermore, it is evident that as the mole ratios of curcumin reduced Ag nanoparticles are increased, the greater the cell destruction is observed. Comparing the two ratios of 1:1 and 1:2, there is a significant destruction of the bacteria cell in curcumin reduced Ag nanoparticles 1:2 (Figure 5.18A). The cell wall appears to be dissolving and completely disorganised. These micrographs confirm that curcumin reduced Ag nanoparticles also exhibits cell wall integrity effects on Gram positive bacteria, though to a lesser extent.

In correlation to the antibacterial colony count studies, EGCG reduced Ag nanoparticles displayed greater impact on *E. coli* cell morphology to all ratios. It is evident from the SEM images shown in Figure 5.19 that upon treatment of EGCG reduced Ag nanoparticles, the once typically rod-shaped *E. coli* cells were ruptured and pitting is formed within the cell wall. As the mole ratios increased to 1:8, severe pitting and greater damage is observed. Breakdown of the cell wall is also evident where cells are fractured across all mole ratios. The greatest impact on the cell morphology is achieved by EGCG reduced Ag nanoparticles at 1:8 mole ratio (Figure 5.19C). By these observations, in the case of Gram negative bacteria *E. coli*, EGCG reduced Ag nanoparticles demonstrate the greatest effects of membrane integrity.

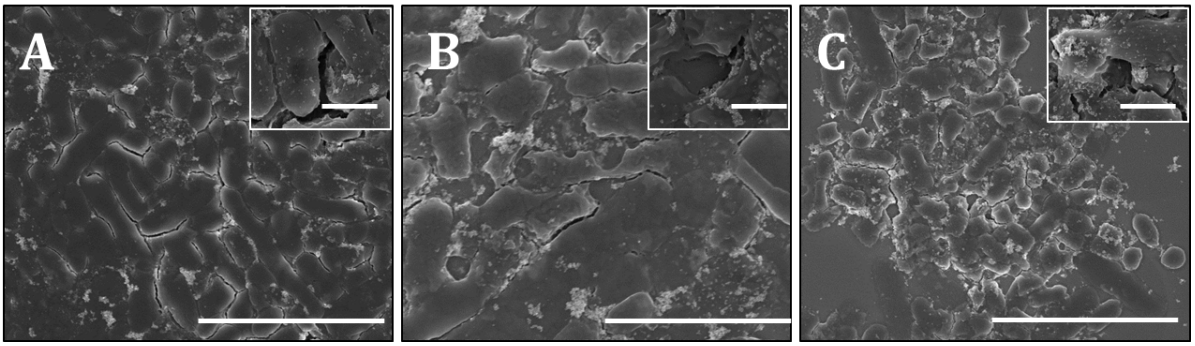

Figure 5.19- SEM micrographs of *E. coli* cells after treatment with (A) EGCG -AgNPs (1:1), (B) EGCG-AgNPs (1:3) and (C) EGCG-AgNPs (1:8) Scale bars 10 μm and insert scale bars 1 μm.

Alternatively when EGCG reduced Ag nanoparticles are exposed to Gram positive *S. albus*, morphological changes in contrast to untreated cells are observed (Figure 5.20). The SEM images displayed signs of rupture of the cell wall and slight alteration of the bacterial shape compared to the control in Figure 5.20A. Furthermore, EGCG reduced Ag nanoparticles displayed the greatest activity in the case of *S. albus* compared to all functionalised Ag nanoparticles. The treated cells appear to be exfoliating and damage to membranes is recognised by the formation of pits around the cell wall.

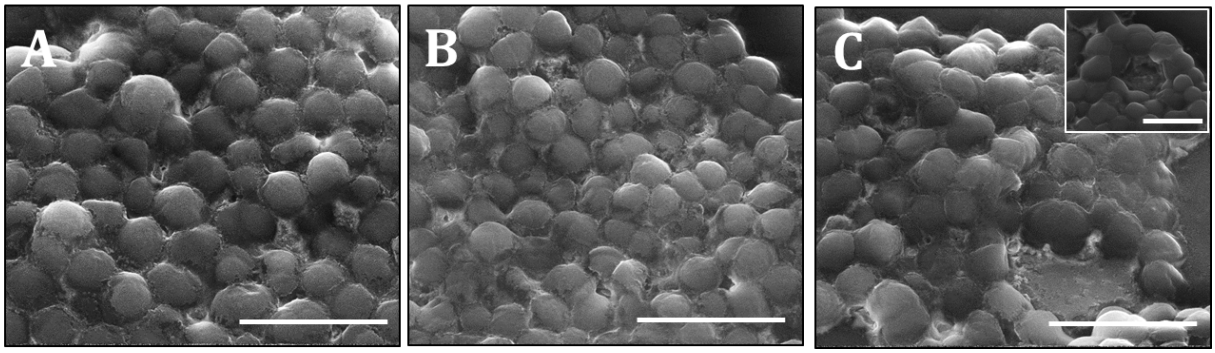

Figure 5.20- SEM micrographs of *S. albus* cells after treatment with (A) EGCG -AgNPs (1:1), (B) EGCG-AgNPs (1:3) and (C) EGCG-AgNPs (1:8) Scale bars 3 μm insert scale bar 1 μm.

Interestingly, from all the SEM observations, there are various differences between Gram positive *S. albus* and Gram negative *E. coli* bacteria. *S. albus* shows slightly less bactericidal activities in morphology changes as shown in SEM imaging. The morphological destruction of bacterial cells for *S. albus* was weaker than *E. coli*. This difference may possibly be attributed to the difference of the peptidoglycan layer of the bacterial cell between Gram positive *S. albus* and Gram negative *E. coli*; an essential function of the peptidoglycan layer is to protect against antibacterial agents. Within the Gram negative cell envelope, there exists an outer membrane, thinner peptidoglycan layer and cell membrane. Whereas a Gram positive bacteria cell envelope consists of lipoteichoic acid containing a thick peptidoglycan layer and cell membrane. The thick peptidoglycan layer of Gram positive bacteria can protect the cell during formation of pits

or reactive oxygen species (ROS) by metal nanoparticles markedly than thin peptidoglycan layer of Gram negative bacteria as larger amounts of damage are required to impact the cell wall.

5.4 Conclusions

Polyphenols are among the strongest active compounds synthesised by plants and host a unique combination of chemical, biological and physiological activities. However, their limited stability often combined with inadequate bioavailability needs to be resolved in order to make these compounds meet demands in nutrition and health. In this chapter, the results implementing various polyphenols as organic surface coronas surrounding Ag nanoparticles play a crucial role in tuning nanomaterial properties for biological applications. This study demonstrates a facile green approach to obtain various mole ratios of surface coronas involving tyrosine, curcumin and EGCG. Moreover, the antibacterial activities of these functionalised Ag nanoparticles revealed a significant role in causing damage to bacterial cells.

At equimolar ratios of all phenolic compounds, EGCG reduced Ag nanoparticles demonstrated the highest antibacterial activity in Gram positive bacteria. However in Gram negative bacteria, curcumin and EGCG reduced Ag nanoparticles were on par with one another in terms of antibacterial activity. The activity can be portrayed at the highest concentration of 1.0 mM as follows for *S. albus*: EGCG Ag nanoparticles > curcumin Ag nanoparticles > tyrosine Ag nanoparticles. As for *E. coli*: EGCG Ag nanoparticles ≥ curcumin Ag nanoparticles > tyrosine Ag nanoparticles.

Furthermore, at various mole ratios of curcumin Ag nanoparticles and EGCG Ag nanoparticles, the highest activity was achieved by EGCG reduced Ag nanoparticles in

both Gram negative and Gram positive bacteria. However, when comparing the activity between curcumin and EGCG reduced Ag nanoparticles individually in their own ratio formation, the study has shown that as the mole ratio increases with less capping of the phytochemicals, the higher the activity is demonstrated. Thus, from this study it can be concluded that a number of phenolic groups present in phytochemicals can be used to synthesise Ag nanoparticles, and also enhance antibacterial activity even at low concentrations. The greater the number of phenolic groups in the structure of capping agent, the better the performance against microbes. In this domain, these finding can accelerate the use of polyphenolic compounds in biological applications in the future as antimicrobial agents.

5.5 References

[1] Valko, M.; Rhodes, C.; Moncol, J.; Izakovic, M.; Mazur, M., Free radicals, metals and antioxidants in oxidative stress-induced cancer. *Chemico-biological interactions* **2006,** *160* (1), 1-40.

[2] Barber, D. A.; Harris, S. R., Oxygen free radicals and antioxidants: a review. *American pharmacy* **1994,** (9), 26-35.

[3] Papas, A. M., *Antioxidant status, diet, nutrition, and health*. Taylor & Francis: 1998.

[4] Baskin, S.; Salem, H., *Oxidants, antioxidants and free radicals*. Taylor & Francis: 1997.

[5] Cooper, R., *Antioxidants*. Woodland Pub Incorporated: 1997.

[6] Knight, J. A., Review: Free radicals, antioxidants, and the immune system. *Annals of Clinical & Laboratory Science* **2000,** *30* (2), 145-158.

[7] Larson, R. A., *Naturally occurring antioxidants*. Taylor & Francis: 1997.

[8] Podsędek, A., Natural antioxidants and antioxidant capacity of Brassica vegetables: A review. *LWT-Food Science and Technology* **2007,** *40* (1), 1-11.

[9] Triantaphyllou, G. B., Dimitrios Boskou, Kalliopi, Antioxidative properties of water extracts obtained from herbs of the species Lamiaceae. *International journal of food sciences and nutrition* **2001,** *52* (4), 313-317.

[10] Atoui, A. K.; Mansouri, A.; Boskou, G.; Kefalas, P., Tea and herbal infusions: their antioxidant activity and phenolic profile. *Food chemistry* **2005,** *89* (1), 27-36.

[11] Kähkönen, M. P.; Hopia, A. I.; Vuorela, H. J.; Rauha, J. P.; Pihlaja, K.; Kujala, T. S.; Heinonen, M., Antioxidant activity of plant extracts containing phenolic compounds. *Journal of agricultural and food chemistry* **1999,** *47* (10), 3954-3962.

[12] Miller, N. J.; Castelluccio, C.; Tijburg, L.; Rice-Evans, C., The antioxidant properties of theaflavins and their gallate esters—radical scavengers or metal chelators? *FEBS letters* **1996,** *392* (1), 40-44.

[13] Mandel, S.; Amit, T.; Reznichenko, L.; Weinreb, O.; Youdim, M. B., Green tea catechins as brain-permeable, natural iron chelators-antioxidants for the treatment of neurodegenerative disorders. *Molecular nutrition & food research* **2006,** *50* (2), 229-234.

[14] Dekkers, J. C.; van Doornen, L. J.; Kemper, H. C., The role of antioxidant vitamins and enzymes in the prevention of exercise-induced muscle damage. *Sports Medicine* **1996,** *21* (3), 213-238.

[15] Holiman, P. C.; Hertog, M. G.; Katan, M. B., Analysis and health effects of flavonoids. *Food Chemistry* **1996,** *57* (1), 43-46.

[16] Scalbert, A.; Manach, C.; Morand, C.; Rémésy, C.; Jiménez, L., Dietary polyphenols and the prevention of diseases. *Critical reviews in food science and nutrition* **2005,** *45* (4), 287-306.

[17] Scalbert, A.; Johnson, I. T.; Saltmarsh, M., Polyphenols: antioxidants and beyond. *The American journal of clinical nutrition* **2005,** *81* (1), 215S-217S.

[18] Zheng, W.; Wang, S. Y., Antioxidant activity and phenolic compounds in selected herbs. *Journal of Agricultural and Food chemistry* **2001,** *49* (11), 5165-5170.

[19] Bansal, V.; Bharde, A.; Ramanathan, R.; Bhargava, S. K., Inorganic materials using "unusual" microorganisms. *Advances in Colloid and Interface Science* **2012,** *179-182* (0), 150-168.

[20] Boopathi, S.; Gopinath, S.; Boopathi, T.; Balamurugan, V.; Rajeshkumar, R.; Sundararaman, M., Characterization and antimicrobial properties of silver and silver oxide nanoparticles synthesized by cell-free extract of a mangrove-associated pseudomonas aeruginosa M6 using two different thermal treatments. *Industrial & Engineering Chemistry Research* **2012,** *51* (17), 5976-5985.

[21] Bansal, V.; Rautaray, D.; Ahmad, A.; Sastry, M., Biosynthesis of zirconia nanoparticles using the fungus Fusarium oxysporum. *Journal of Materials Chemistry* **2004,** *14* (22), 3303-3305.

[22] Bansal, V.; Ramanathan, R.; Bhargava, S. K., Fungus-mediated biological approaches towards green synthesis of oxide nanomaterials. *Australian Journal of Chemistry* **2011,** *64* (3), 279-293.

[23] Shankar, S. S.; Ahmad, A.; Sastry, M., Geranium leaf assisted biosynthesis of silver nanoparticles. *Biotechnol. Prog.* **2003,** *19* (6), 1627-1631.

[24] Jha, A. K.; Prasad, K.; Prasad, K.; Kulkarni, A. R., Plant system: Nature's nanofactory. *Colloids and Surfaces B: Biointerfaces* **2009,** *73* (2), 219-223.

[25] T.C., P.; Matthew, L.; Chandrasekaran, N.; Raichur, A. M.; Mukherjee, A., *Biomimetic synthesis of nanoparticles: Science, technology and applicability*. InTech: 2010; p 534.

[26] Raveendran, P.; Fu, J.; Wallen, S. L., Completely "green" synthesis and stabilization of metal nanoparticles. *J. Am. Chem. Soc.* **2003,** *125* (46), 13940-13941.

[27] Mohanpuria, P.; Rana, N. K.; Yadav, S. K., Biosynthesis of nanoparticles: technological concepts and future applications. *Journal of Nanoparticle Research* **2008,** *10* (3), 507-517.

[28] Hatcher, H.; Planalp, R.; Cho, J.; Tortia, F. M.; Torti, S. V., Curcumin: From ancient medicine to current clinical trials. *Cellular and Molecular Life Sciences* **2008,** *65* (11), 1631-1652.

[29] Eigner, D.; Scholz, D., Ferula asa-foetida and Curcuma longa in traditional medical treatment and diet in Nepal. *Journal of ethnopharmacology* **1999,** *67* (1), 1-6.

[30] Goel, A.; Kunnumakkara, A. B.; Aggarwal, B. B., Curcumin as “Curecumin”: From kitchen to clinic. *Biochemical Pharmacology* **2008,** *75* (4), 787-809.

[31] Bhowmik, D.; Kumar, K.; Chandira, M.; Jayakar, B., Turmeric: a herbal and traditional medicine. *Archives of Applied Science Research* **2009,** *1* (2), 86-108.

[32] Downham, A.; Collins, P., Colouring our foods in the last and next millennium. *International journal of food science & technology* **2000,** *35* (1), 5-22.

[33] Tønnesen, H.; Karlsen, J., Studies on curcumin and curcuminoids. *Z Lebensm Unters Forch* **1985,** *180* (5), 402-404.

[34] De, R.; Kundu, P.; Swarnakar, S.; Ramamurthy, T.; Chowdhury, A.; Nair, G. B.; Mukhopadhyay, A. K., Antimicrobial activity of curcumin against Helicobacter pylori isolates from India and during infections in mice. *Antimicrobial agents and chemotherapy* **2009,** *53* (4), 1592-1597.

[35] Han, S.; Yang, Y., Antimicrobial activity of wool fabric treated with curcumin. *Dyes and Pigments* **2005,** *64* (2), 157-161.

[36] Basniwal, R. K.; Buttar, H. S.; Jain, V.; Jain, N., Curcumin nanoparticles: preparation, characterization, and antimicrobial study. *Journal of agricultural and food chemistry* **2011,** *59* (5), 2056-2061.

[37] Srimal, R.; Dhawan, B., Pharmacology of diferuloyl methane (curcumin), a non-steroidal anti-inflammatory agent. *Journal of pharmacy and pharmacology* **1973,** *25* (6), 447-452.

[38] Chainani-Wu, N., Safety and anti-inflammatory activity of curcumin: a component of tumeric (Curcuma longa). *The Journal of Alternative & Complementary Medicine* **2003,** *9* (1), 161-168.

[39] Aggarwal, B. B.; Surh, Y.-J.; Shishodia, S., *The molecular targets and therapeutic uses of curcumin in health and disease*. Springer: 2007; Vol. 495.

[40] Ruby, A.; Kuttan, G.; Dinesh Babu, K.; Rajasekharan, K.; Kuttan, R., Anti-tumour and antioxidant activity of natural curcuminoids. *Cancer letters* **1995,** *94* (1), 79-83.

[41] Sonkaew, P.; Sane, A.; Suppakul, P., Antioxidant activities of curcumin and ascorbyl dipalmitate nanoparticles and their activities after incorporation into cellulose-based packaging films. *Journal of agricultural and food chemistry* **2012,** *60* (21), 5388-5399.

[42] Anand, P.; Thomas, S. G.; Kunnumakkara, A. B.; Sundaram, C.; Harikumar, K. B.; Sung, B.; Tharakan, S. T.; Misra, K.; Priyadarsini, I. K.; Rajasekharan, K. N., Biological activities of curcumin and its analogues (Congeners) made by man and Mother Nature. *Biochemical pharmacology* **2008,** *76* (11), 1590-1611.

[43] Maheshwari, R. K.; Singh, A. K.; Gaddipati, J.; Srimal, R. C., Multiple biological activities of curcumin: a short review. *Life sciences* **2006,** *78* (18), 2081-2087.

[44] Wilken, R.; Veena, M. S.; Wang, M. B.; Srivatsan, E. S., Curcumin: A review of anti-cancer properties and therapeutic activity in head and neck squamous cell carcinoma. *Mol Cancer* **2011,** *10* (12), 1-19.

[45] López-Lázaro, M., Anticancer and carcinogenic properties of curcumin: considerations for its clinical development as a cancer chemopreventive and chemotherapeutic agent. *Molecular nutrition & food research* **2008,** *52* (S1), S103-S127.

[46] Aggarwal, B. B.; Kumar, A.; Bharti, A. C., Anticancer potential of curcumin: preclinical and clinical studies. *Anticancer Res* **2003,** *23* (1A), 363-398.

[47] Sharma, O. P., Antioxidant activity of curcumin and related compounds. *Biochemical Pharmacology* **1976,** *25* (15), 1811-1812.

[48] Suzuki, Y.; Miyoshi, N.; Isemura, M., Health-promoting effects of green tea. *Proceedings of the Japan Academy. Series B, Physical and biological sciences* **2011,** *88* (3), 88-101.

[49] Wolfram, S., Effects of green tea and EGCG on cardiovascular and metabolic health. *Journal of the American College of Nutrition* **2007,** *26* (4), 373S-388S.

[50] Tipoe, G. L.; Leung, T.-M.; Hung, M.-W.; Fung, M.-L., Green tea polyphenols as an anti-oxidant and anti-inflammatory agent for cardiovascular protection. *Cardiovascular & Haematological Disorders-Drug Targets (Formerly Current Drug Targets-Cardiovascular & Hematological Disorders)* **2007,** *7* (2), 135-144.

[51] Brown, M. K.; Evans, J. L.; Luo, Y., Beneficial effects of natural antioxidants EGCG and α-lipoic acid on life span and age-dependent behavioral declines in *Caenorhabditis elegans*. *Pharmacology Biochemistry and Behavior* **2006,** *85* (3), 620-628.

[52] Salah, N.; Miller, N. J.; Paganga, G.; Tijburg, L.; Bolwell, G. P.; Riceevans, C., Polyphenolic flavanols as scavengers of aqueous phase radicals and as chain-breaking antioxidants. *Archives of biochemistry and biophysics* **1995,** *322* (2), 339-346.

[53] Chen, C. W.; Ho, C. T., Antioxidant properties of polyphenols extracted from green and black teas. *Journal of food lipids* **1995,** *2* (1), 35-46.

[54] Toda, M.; Okubo, S.; Hara, Y.; Shimamura, T., Antibacterial and bactericidal activities of tea extracts and catechins against methicillin resistant *Staphylococcus aureus*. *Nihon saikingaku zasshi. Japanese journal of bacteriology* **1991,** *46* (5), 839.

[55] Hatano, T.; Tsugawa, M.; Kusuda, M.; Taniguchi, S.; Yoshida, T.; Shiota, S.; Tsuchiya, T., Enhancement of antibacterial effects of epigallocatechin gallate, using ascorbic acid. *Phytochemistry* **2008,** *69* (18), 3111-3116.

[56] Katiyar, S. K.; Elmets, C. A., Green tea polyphenolic antioxidants and skin photoprotection (Review). *International journal of oncology* **2001,** *18* (6), 1307-1313.

[57] Yang, C. S.; Lambert, J. D.; Sang, S., Antioxidative and anti-carcinogenic activities of tea polyphenols. *Archives of toxicology* **2009,** *83* (1), 11-21.

[58] Mittal, A.; Pate, M. S.; Wylie, R. C.; Tollefsbol, T. O.; Katiyar, S. K., EGCG down-regulates telomerase in human breast carcinoma MCF-7 cells, leading to suppression of cell viability and induction of apoptosis. *International journal of oncology* **2004,** *24* (3), 703-710.

[59] Saffari, Y.; Sadrzadeh, S., Green tea metabolite EGCG protects membranes against oxidative damage in vitro. *Life sciences* **2004,** *74* (12), 1513-1518.

[60] Sang, S.; Shao, X.; Bai, N.; Lo, C.-Y.; Yang, C. S.; Ho, C.-T., Tea polyphenol (−)-epigallocatechin-3-gallate: a new trapping agent of reactive dicarbonyl species. *Chemical research in toxicology* **2007,** *20* (12), 1862-1870.

[61] Singh, B. N.; Shankar, S.; Srivastava, R. K., Green tea catechin, epigallocatechin-3-gallate (EGCG): mechanisms, perspectives and clinical applications. *Biochemical pharmacology* **2011,** *82* (12), 1807-1821.

[62] Valcic, S.; Timmermann, B. N.; Alberts, D. S.; Wächter, G. A.; Krutzsch, M.; Wymer, J.; Guillén, J. M., Inhibitory effect of six green tea catechins and caffeine on the growth of four selected human tumor cell lines. *Anti-cancer drugs* **1996,** *7* (4), 461-468.

[63] Leopoldini, M.; Russo, N.; Toscano, M., The molecular basis of working mechanism of natural polyphenolic antioxidants. *Food Chemistry* **2011,** *125* (2), 288-306.

[64] Urquaiaga, I.; Leighton, F., Plant polyphenol antioxidants and oxidative stress. *Biological research* **2000,** *33* (2), 55-64.

[65] Dimitrios, B., Sources of natural phenolic antioxidants. *Trends in Food Science & Technology* **2006,** *17* (9), 505-512.

[66] Bravo, L., Polyphenols: chemistry, dietary sources, metabolism, and nutritional significance. *Nutrition reviews* **1998,** *56* (11), 317-333.

[67] Shahidi, F.; Janitha, P.; Wanasundara, P., Phenolic antioxidants. *Critical Reviews in Food Science & Nutrition* **1992,** *32* (1), 67-103.

[68] Lee, J.; Koo, N.; Min, D., Reactive oxygen species, aging, and antioxidative nutraceuticals. *Comprehensive reviews in food science and food safety* **2004,** *3* (1), 21-33.

[69] Leopoldini, M.; Marino, T.; Russo, N.; Toscano, M., Antioxidant properties of phenolic compounds: H-atom versus electron transfer mechanism. *The Journal of Physical Chemistry A* **2004,** *108* (22), 4916-4922.

[70] Moore, B. N.; Julian, R. R., Dissociation energies of X–H bonds in amino acids. *Physical Chemistry Chemical Physics* **2012,** *14* (9), 3148-3154.

[71] Vorsa, V.; Kono, T.; Willey, K. F.; Winograd, N., Femtosecond photoionization of ion beam desorbed aliphatic and aromatic amino acids: fragmentation via α-cleavage reactions. *The Journal of Physical Chemistry B* **1999,** *103* (37), 7889-7895.

[72] Murakami, Y.; Ishii, H.; Takada, N.; Tanaka, S.; MACHINO, M.; Ito, S.; Fujisawa, S., Comparative anti-inflammatory activities of curcumin and tetrahydrocurcumin based on the phenolic OH bond dissociation enthalpy, ionization potential and quantum chemical descriptor. *Anticancer research* **2008,** *28* (2A), 699-707.

[73] Takeuchi, Y.; Okuno, K.; Yoshioka, H., Characteristics of the OH radical scavenging activity of tea catechins. *Journal of radioanalytical and nuclear chemistry* **2007,** *272* (3), 455-459.

[74] Muzolf-Panek, M.; Gliszczyńska-Świgło, A.; Szymusiak, H.; Tyrakowska, B., The influence of stereochemistry on the antioxidant properties of catechin epimers. *European Food Research and Technology* **2012,** *235* (6), 1001-1009.

[75] Mulvaney, P., Surface plasmon spectroscopy of nanosized metal particles. *Langmuir* **1996,** *12* (3), 788-800.

[76] Jensen, T. R.; Malinsky, M. D.; Haynes, C. L.; Van Duyne, R. P., Nanosphere lithography: tunable localized surface plasmon resonance spectra of silver nanoparticles. *The Journal of Physical Chemistry B* **2000,** *104* (45), 10549-10556.

[77] Ejima, H.; Richardson, J. J.; Liang, K.; Best, J. P.; van Koeverden, M. P.; Such, G. K.; Cui, J.; Caruso, F., One-step assembly of coordination complexes for versatile film and particle engineering. *Science* **2013,** *341* (6142), 154-157.

[78] Kolev, T. M.; Velcheva, E. A.; Stamboliyska, B. A.; Spiteller, M., DFT and experimental studies of the structure and vibrational spectra of curcumin. *International Journal of Quantum Chemistry* **2005,** *102* (6), 1069-1079.

[79] Chen, Y. C.; Yu, S. H.; Tsai, G. J.; Tang, D. W.; Mi, F. L.; Peng, Y. P., Novel technology for the preparation of self-assembled catechin/gelatin nanoparticles and their characterization. *Journal of agricultural and food chemistry* **2010,** *58* (11), 6728-6734.

[80] Zhu, B.; Li, J.; He, Y.; Yoshie, N.; Inoue, Y., Hydrogen-bonding interaction and crystalline morphology in the binary blends of poly (ε-caprolactone) and polyphenol catechin. *Macromolecular Bioscience* **2003,** *3* (11), 684-693.

[81] Shpigelman, A.; Cohen, Y.; Livney, Y. D., Thermally-induced β-lactoglobulin–EGCG nanovehicles: Loading, stability, sensory and digestive-release study. *Food Hydrocolloids* **2012,** *29* (1), 57-67.

[82] Sharma, T. K.; Chopra, A.; Sapra, M.; Kumawat, D.; Patil, S. D.; Pathania, R.; Navani, N. K., Green synthesis and antimicrobial potential of silver nanoparticles. *International Journal of Green Nanotechnology* **2012,** *4* (1), 1-16.

[83] Daima, H. K.; Selvakannan, P.; Kandjani, A. E.; Shukla, R.; Bhargava, S. K.; Bansal, V., Synergistic influence of polyoxometalate surface corona towards enhancing the antibacterial performance of tyrosine-capped Ag nanoparticles. *Nanoscale* **2014**.

[84] Jung, W. K.; Koo, H. C.; Kim, K. W.; Shin, S.; Kim, S. H.; Park, Y. H., Antibacterial activity and mechanism of action of the silver ion in *Staphylococcus aureus* and *Escherichia coli*. *Applied and environmental microbiology* **2008,** *74* (7), 2171-2178.

[85] Sondi, I.; Salopek-Sondi, B., Silver nanoparticles as antimicrobial agent: a case study on *E-coli* as a model for Gram-negative bacteria. *J. Colloid Interface Sci.* **2004,** *275* (1), 177-182.

[86] Li, W. R.; Xie, X. B.; Shi, Q. S.; Zeng, H. Y.; Ou-Yang, Y. S.; Chen, Y. B., Antibacterial activity and mechanism of silver nanoparticles on *Escherichia coli*. *Appl. Microbiol. Biotechnol.* **2010,** *85* (4), 1115-1122.

[87] Morones, J. R.; Elechiguerra, J. L.; Camacho, A.; Holt, K.; Kouri, J. B.; Ramírez, J. T.; Yacaman, M. J., The bactericidal effect of silver nanoparticles. *Nanotechnology* **2005,** *16* (10), 2346.

[88] Pal, S.; Tak, Y. K.; Song, J. M., Does the antibacterial activity of silver nanoparticles depend on the shape of the nanoparticle? A study of the Gram-negative bacterium *Escherichia coli*. *Appl. Environ. Microbiol.* **2007,** *73* (6), 1712-1720.

[89] Feng, Q.; Wu, J.; Chen, G.; Cui, F.; Kim, T.; Kim, J., A mechanistic study of the antibacterial effect of silver ions on *Escherichia coli* and *Staphylococcus aureus*. *Journal of biomedical materials research* **2000,** *52* (4), 662-668.

[90] Schwegmann, H.; Frimmel, F. H., Nanoparticles: Interaction with microorganisms. In *Nanoparticles in the Water Cycle*, Springer: 2010; pp 165-182.

[91] Lok, C. N.; Ho, C. M.; Chen, R.; He, Q. Y.; Yu, W. Y.; Sun, H.; Tam, P. K. H.; Chiu, J. F.; Che, C. M., Silver nanoparticles: partial oxidation and antibacterial activities. *Journal of Biological Inorganic Chemistry* **2007,** *12* (4), 527-534.

Chapter VI

Mechanistic insight into antibacterial performance of silver nanomaterials

6.1 Introduction

The inhibitory effect of silver on bacterial growth have been observed in the preceding chapters where the effect of variables have been compared including; shape, synergism with antibiotics and surface corona. It has been shown that Ag nanoparticles can be synthesised via physical, chemical and biological methods. The inhibition effect of silver is perhaps the sum of distinct mechanisms of action. A number of studies have suggested that silver ions may react with thiol groups of proteins as well as with phosphorus-containing macromolecules like nucleic acid and also form a low-molecular-weight region in the centre which ultimately leads to cell death by preferably attacking the respiratory chain and cell division. Ag nanoparticles are also understood to release silver ions in the bacterial cells, which enhances their bactericidal activity.[1-3]

The antimicrobial effects of silver can also be increased by manipulation of size. Ag nanoparticles having the size range of 10 to 100 nm showed strong bactericidal potential against Gram negative and positive bacteria.[4] Ag nanoparticles of smaller than 100 nm may contain 10,000-15,000 silver atoms.[5, 6] In addition to antimicrobial activity, the

mechanisms of action and toxicity are also of paramount importance. In this chapter electrochemical, biophysical and biotechnological approaches used to elucidate the mechanism of action of silver based nanomaterials will be discussed.

Recently the oxidation potentials of polyphenols have been used to estimate their antioxidant capacity.[7] This includes the oxidation of flavonoids which are proposed to correlate with antioxidant capacity. The antioxidative activity of flavonoids are among the most effective naturally available antioxidants even in comparison to vitamin C or E. This is mainly attributed to their ability to scavenge free radicals in an environment by donation of the phenolic hydrogen atom from aromatic rings.[8] Thus, flavonoids with less positive oxidation potentials have been shown to possess higher radical scavenging.[9, 10] The reagents used in previous sections to reduce silver are susceptible to direct oxidation and thus electrochemical detection is used in this chapter to assist in mechanistic determination of their antibacterial activity. Concurrently, a measure of the oxidation potential for the various nanoparticle shapes which have been synthesised is also carried out to determine the impact oxidability has upon the antibacterial activity of these silver nanoparticles.

The traditional approach to monitor toxic chemicals in the environment is based on chemical analysis as this allows accurate and sensitive determination of the exact composition of any sample. However, when the nature of the compound is unknown, the range of analytical instrumentation necessary for a comprehensive analysis is complex and costly. As such, these procedures may fail to provide data in context of bioavailability of pollutants, effects on living systems and their synergistic interactions in mixtures. In order to address these needs, a complementary approach to base the use of living systems in a variety of environmentally oriented bioassays is required. The biological

systems used for such purposes range from a diverse range of live organisms, particularly bacteria. Their large population sizes, rapid growth rates and simplistic maintenance make them an ideal candidate for toxicity monitoring. An additional prominent component is that bacteria can be genetically modified to respond by a detectable signal to pre-determine changes in their environmental conditions.[11-15]

Genetically engineered microorganisms have played two parallel roles in the development of toxicity bioassays, which can be referred to as "lights off" and "lights on" assays.[11] The "lights off" approach is an addition to the commonly accepted microbial toxicity bioassay, bioluminescent *Vibrio fischeri*. This assay is based upon measuring the decrease in light emission by microorganisms as a function of sample concentration with a short term exposure.[16] The "lights on" approach is based on the molecular combination of a reporter system to selected promoters of different stress-responsive genes. Bacterial strains have been defined to detect the presence of either specific compounds or classes of chemicals including heavy metals,[17] dioxins and endocrine disruptors[18-20] or report on the general toxicity of the selected sample.[21, 22] With this aspect, bacterial strains have also been developed for assaying genotoxicity rather than just general toxicity. In these circumstances, the promoters serving as sensors were selected from deoxyribonucleic acid (DNA) repair operons such as the SOS system.[23-26]

In this study, a double-labelled *E. coli* cell including a single plasmid (Figure 6.1), two inducible promoters fused to different fluorescent protein genes: *recA'::*EGFP and *grpE'::*DsRed Express was employed. The *recA* promoter is part of the bacterial SOS system and its activation is considered an indication of DNA damage hazards. *grpE* is a heat shock protein, induced by a broad spectrum of chemicals as an excellent indicator of toxic cellular stress or protein damage. This combination can potentially allow an assay of

both genotoxicity and general toxicity to be carried out by the same reporter organism. This is the first study in which this dual reporter plasmid has been exploited to determine the genotoxicity and cytotoxicity of nanoparticles for bacterium.

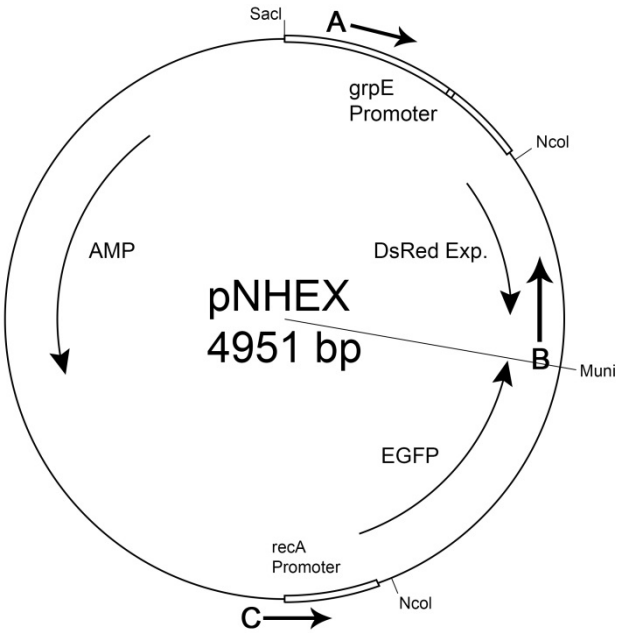

Figure 6.1- A schematic diagram of plasmid pNHEX: (A) represents restriction site that can be generated using SacI and NcoI, (B) the use of MunI and NcoI and (C) MunI and NcoI.

6.2 Experimental

6.2.1 Electrochemical methods

Cyclic voltammetry was undertaken using a conventional three-electrode setup and referenced against Ag|AgCl|KCl. The reference electrode used was composed of a silver wire in saturated solution Ag|AgCl|KCl (aqueous 3 M KCl) to make up the half-cell, separated using a porous glass frit. In order to probe the electrochemical properties of the nanoparticles a vitreous carbon working electrode (0.07070 cm^2) was loaded with each particular Ag nanoparticle by drop-casting 5 μL of 1 mM sample and allowed to dry under ambient conditions. The vitreous carbon working electrode was also used to measure the electrochemical window of the system without loading as is typical prior to electrochemical experiments. The counter electrode was 6 mm diameter graphene

(Johnson Matthey Ultra "F" purity grade). All solutions were degassed with nitrogen for 10 minutes prior to measurements taking place. To be used as a standard to measure the degree of facile Ag nanoparticle oxidation, a polycrystalline silver (0.0317 cm^2) macro electrode was also used as a working electrode.

Working electrodes were cleaned via sonicating for 10 minutes in Milli-Q water and a subsequent polish using a microcloth pad (Buehler) with 0.3 μm alumina slurry (Electron Microscopy Sciences). The surface area for each nanoparticle loading was determined by analysing the charge associated with stripping of lead which has been previously deposited using under potential deposition.[27] These methods are described by Kirowa-Eisner *et al*. using the theoretical value of 400 μC cm^{-2} for full coverage of lead on silver.[28]

6.2.2 Antibacterial applications

6.2.2.1 Bacterial membrane protein study

To study the interaction of EGCG-AgNPs and Curc-AgNPs with bacterial membrane (materials from Chapter V), crude membrane proteins were isolated from Gram negative representative strain *E. coli* (ECMP) and Gram positive *S. albus* (SAMP). These membrane preparations (100 μg) were incubated with EGCG-AgNPs and Curc-AgNPs (20 μM). The fluorescence spectra were recorded in the range of 310 to 400 nm by exciting the reaction mixture at 295 nm using a Horiba spectrofluorometer (FluoroMx-4). Furthermore, to determine the affinity of this interaction, the dissociation constant (Kd) of Ag nanoparticles with ECMP (*E. coli* membrane protein) and SAMP (*S. albus* membrane protein) were determined using the nonlinear regression equation:

$$Y = \frac{B_{max}X}{Kd + X} \quad (6.1)$$

Where Y is the fluorescence quenching, X is the concentration of nanoparticles and B_{max} is the maximum binding. In this study tyrosine reduced Ag nanoparticles were not included as there is interference with the fluorescence due to its intrinsic fluorescence property in the same region of emission.

6.2.2.2 Genotoxicity and cellular toxicity studies

To study the effect of nanoparticles at genetic (DNA) level or cellular (protein) level a dual colour bacterial reporter stain (expressed as GFP in response to DNA damage and/or DsRed (RFP) in response to cellular toxicity) harbouring a plasmid pNHEX was used. This plasmid was provided as a generous gift from Prof. S. Belkin, Hebrew University of Jerusalem. This plasmid was propagated in an *E. coli* strain RFM 443. For this study, *E. coli* strain RFM 443 (harbouring pNHEX) was cultured overnight in M9 minimal media supplemented with 1% glucose in presence of 100 µg/mL ampicillin. The overnight grown cultured bacteria were subcultured and allowed to be grown until OD_{600} was reached in order of 0.2-0.3. At this O.D. bacteria was treated with various nanoparticles, ethanol (positive control for cellular toxicity) and nalidixic acid (NAL as a positive control for genotoxicity). GFP induction in presence of nanoparticles was monitored by exciting the cells at 485 nm and emission was collected from 495-600 nm. On the other hand, RFP expression was monitored by exciting the cells at 550 nm and emission was collected from 560-750 nm using Horiba spectroflourometer.

6.3 Results and discussion

6.3.1 The oxidability for phenolic compounds and phenol-reduced nanoparticles

Illustrated in Figure 6.2A is the CV for a vitreous carbon electrode immersed in a 1 M NaOH solution (pH=14) which shows an electrochemical window of ca. 1.7 V where no Faradaic processes are occurring. The phenolic reagents which have been used to reduce silver are also probed using a vitreous carbon electrode and are shown in Figure 6.2. As can be seen in the CV for 5 mM tyrosine in 1 M NaOH (Figure 6.2B) the onset for the singular oxidation process of the phenolic compound takes place at a peak maximum of 0.511 V, slightly less positive than reported values in phosphate buffer solutions,[29, 30] which is attributed to the strong pH used in this study. Upon the reverse sweep no reduction process highlighting the irreversible oxidation of tyrosine is observed.[31] The same conditions are observed for the oxidation of tyrosine at polycrystalline platinum.[32, 33] The two processes observed in Figure 6.2C for the irreversible oxidation of curcumin (5 mM) in 0.1 M NaOH refer to the oxidation of both phenolic groups (0.224 V and 0.306 V), which are less positive than reported values at vitreous carbon and platinum electrodes for the same reasons mentioned earlier.[34, 35] The current response for 1 mM epigallocatechin gallate (EGCG) in the CV in Figure 6.2D shows an anodic current on the positive sweep consisting of three weak oxidative processes at ca. -0.182, 0.061, and 0.309 V. It is difficult to discern these peaks as the peak current decreases with pH at a vitreous carbon electrode.[36] The reverse sweep shows little cathodic current response even though EGCG has been shown to be reversible at lower pH.[36] However, as mentioned earlier the study by Novak *et al.* found a decrease in

current amplitude with increased pH.[36] The order of facile oxidation for each phytochemical is shown to follow the order EGCG < Curcumin < Tyrosine when measured in 1 M NaOH solution.

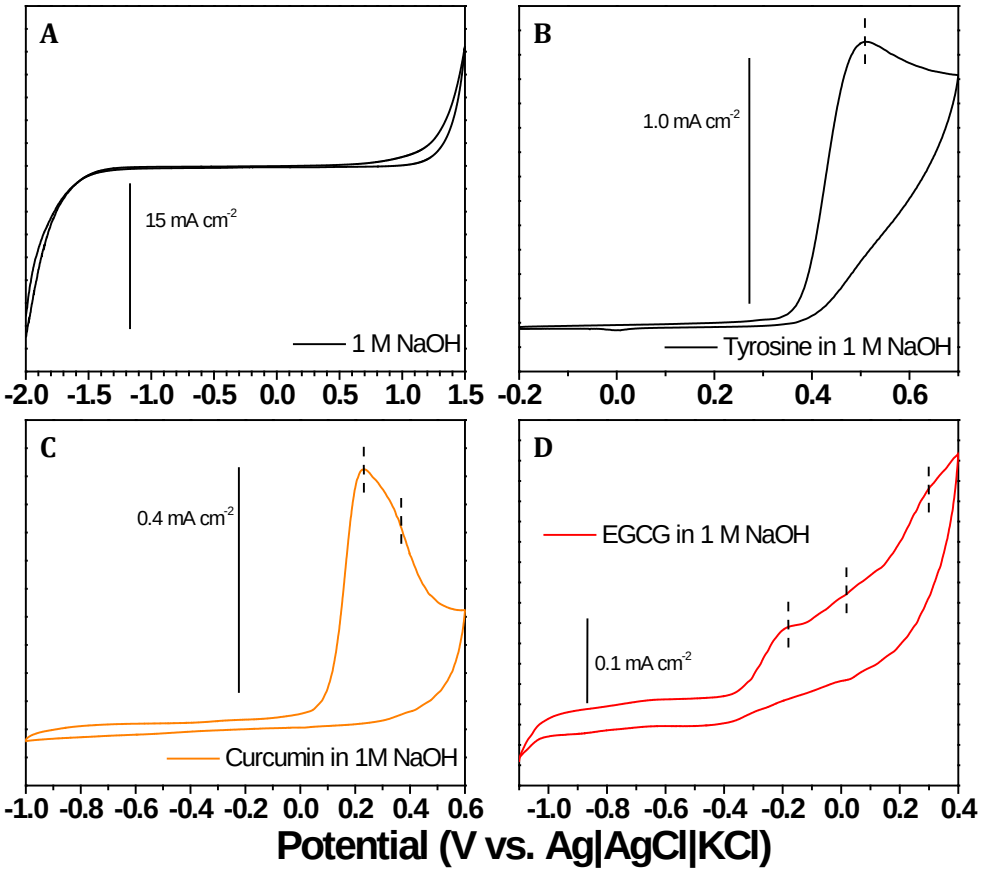

Figure 6.2-Cyclic voltammograms for neat 1 M NaOH and each phenolic compound (in 1 M NaOH) used during silver nanoparticle synthesis.

Shown in Figure 6.3 is the CVs for a polycrystalline silver electrode and each silver nanoparticle modified vitreous carbon electrode. The silver electrode is used as a standard to measure the degree of facile oxidation for each of the phenolic-reduced nanoparticles that were prepared using the various molar ratios of phenolic compounds. Depicted in Figure 6.3 is the typical CV for a silver macro electrode in alkaline medium with a main peak at ca. 0.34 V with a less positive process at 0.253 V. The more positive peak with greater current response indicates the Ag^0/Ag^+ oxidation,[37] whilst the less positive process is associated with the oxide or hydroxide transition.[38] Figure 6.3B

represents cyclic voltammetry of the silver nanoparticles synthesised using tyrosine as a reducing agent with similar behaviour to polycrystalline silver. However the onset of oxidation takes place at less positive potential with a peak of 0.335 V showing these nanoparticles are facile to oxidise compared to bulk silver metal.[37] The peak reduction potential for Tyr-AgNPs is also at more negative potentials (0.018 V) compared with the polycrystalline silver electrode (0.037 V) suggesting these oxidised nanoparticles are more stable than oxides at bulk silver metal.[37]

The onset of oxidation is again less positive for each of the other nanoparticle systems shown in Figure 6.3C and Figure 6.3D, curcumin reduced nanoparticles have peak oxidation potentials of 0.273 V, 0.288 V for ratios of 1:2 and 1:1 respectively. EGCG reduced particles have peak oxidation potentials of 0.280 V, 0.291 V, 0.293V for ratios of 1:8, 1:3, 1:1 respectively. Shown in Table 6.1, a trend can be observed for peak potentials being less positive as the amount of reducing agent used in synthesis is decreased (relative increase of silver salt). The less positive onset peak potential is indicative of the ease with which respective nanoparticles may be oxidised to release Ag^+ ions in bacterial environment. As evident in general, as the amount of a particular phytochemical coating increases (e.g. curcumin 1:2 to curcumin 1:1), it becomes more difficult to oxidise theses nanoparticles. The reduction potentials of these nanoparticles dictate the stability of the silver oxides which are formed during the positive sweep of the CV. There is a varying degree of hysteresis between samples which are also shown in Table 6.1. Thus, the particles which display most negative peak reduction potentials will exhibit the most stable oxide forms and may also be an indicator of the antibacterial activity for these platforms in longer term experiments.

Table 6.1 – Peak oxidation and peak reduction potential for Ag nanoparticle with phenolic coronas ordered lowest to highest.

Peak oxidation potential (least positive to most positive)					
Curc 1:2	**EGCG 1:8**	**Curc 1:1**	**EGCG 1:3**	**EGCG1:1**	**Tyr 1:1**
0.273 V	0.280 V	0.288 V	0.291 V	0.293 V	0.335 V
Peak reduction potential (most negative to least negative)					
Tyr 1:1	**EGCG 1:8**	**Curc 1:2**	**Curc 1:1**	**EGCG 1:3**	**EGCG1:1**
-0.017 V	-0.003 V	-0.002 V	-0.002 V	-0.002 V	0.028 V

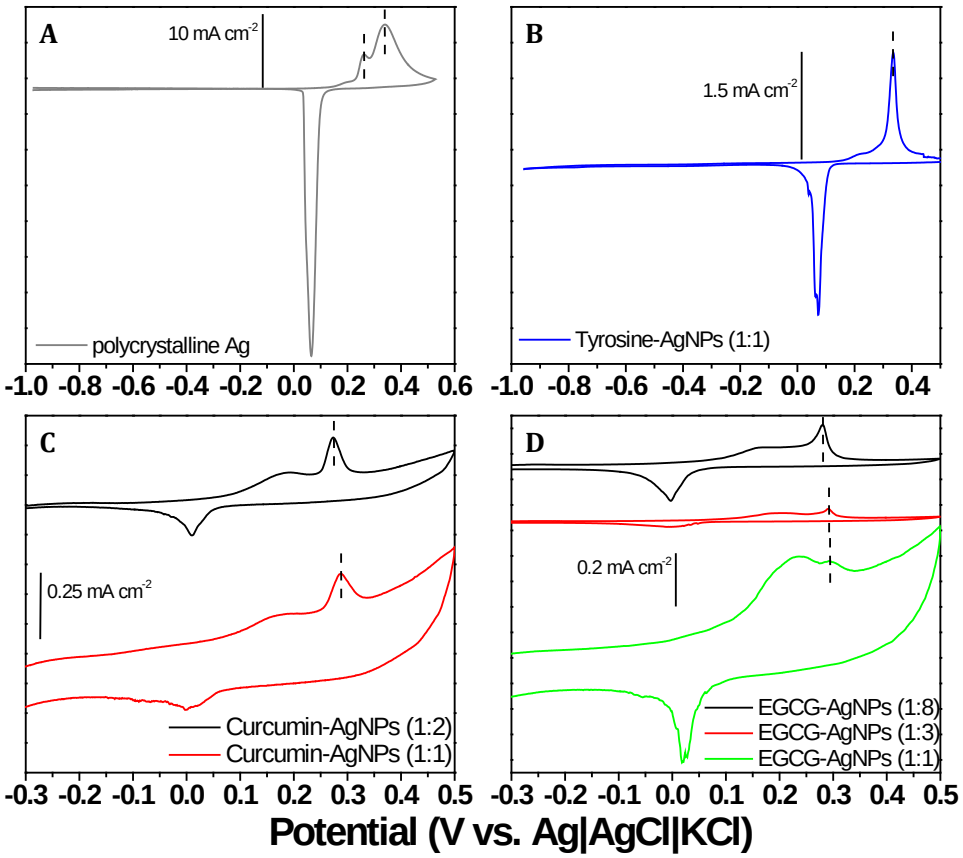

Figure 6.3 - Cyclic voltammograms for (A) polycrystalline silver and vitreous carbon electrodes modified with (B) Tyrosine-AgNPs, (C) Curcumin-AgNPs and (D) EGCG-AgNPs in 1 M NaOH.

The oxide formation process for each of the nanoparticles follows from a wide double layer charging region as seen in the case of the polycrystalline silver electrode. The capacitance in this region is largest for those nanoparticles reduced using curcumin or EGCG in a 1:1 ratio to the silver salt. There is approximately the same level of activity measured for both Curc-AgNPs suggesting that the curcumin is not impeding the oxidation of underlying silver metal even at the lower relative phytochemical

concentration (1:2 ratio). However, there is a variance in the silver activity for the EGCG-AgNPs with the largest activity being for Ag nanoparticles synthesised using the 1:1 ratio, followed by the 1:8 and 1:3 ratios. In particular for the 1:1 EGCG-AgNPs, the less positive process displays greater current density which may be complicated due to EGCG oxidation also taking place in this region.

6.3.2 The oxidability of various nanoparticle shapes

Shown in Figure 6.4 is the CVs for each different shape of silver nanoparticle loaded onto vitreous carbon electrode. The onset of oxidation is again less positive for each of the shaped nanoparticles compared to that of polycrystalline silver. The order of peak oxidation potential from least positive (facile oxidation) to most positive follows prisms, cubes then spheres. For comparison with the phytochemical reduced silver nanoparticles in Figure 6.3B, the data for Ag nanospheres pertains to Tyr-AgNPs.

Significantly, the peak reduction potentials of these nanoparticles vary with less hysteresis observed for the Ag nanocubes. The peak potentials for both oxidation and reduction are listed in Table 6.2. The most negative peak reduction potentials belongs to the silver nanoprisms which indicates that these are the most stable silver oxide of this shape dependant system.[37] No large capacitance is observed for each of the shapes in this system, unlike the Curc-AgNPs and EGCG-AgNPs prepared using 1:1 ratios.

Table 6.2-Peak oxidation and peak reduction potentials for shape-dependent Ag nanoparticles ordered lowest to highest.

Peak oxidation potential (least positive to most positive)(V)		
Ag prisms	**Ag cubes**	**Ag spheres**
0.299	0.305	0.335
Peak reduction potential (most negative to least negative)		
Ag prisms	**Ag cubes**	**Ag spheres**
-0.077	-0.017	-0.042

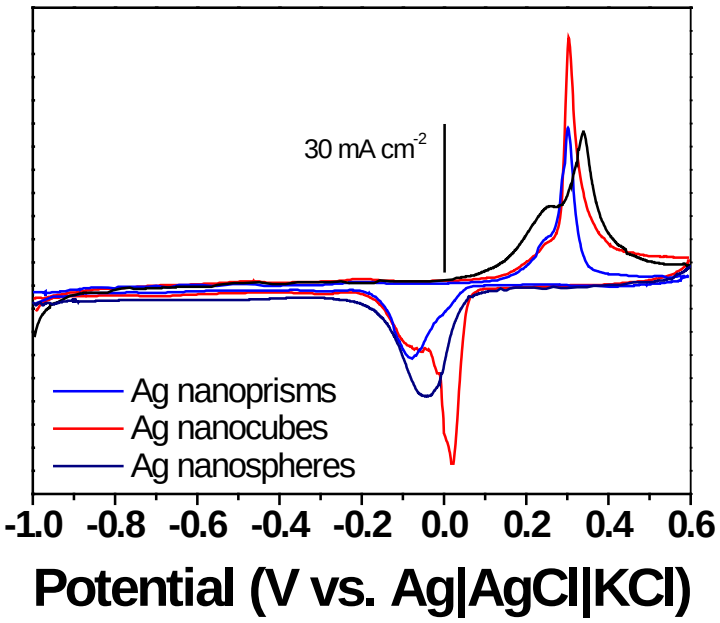

Figure 6.4- Cyclic voltammograms for Ag nanoprisms, Ag nanocubes and Ag nanospheres.

6.3.3 Comparison of oxidation potentials dependent on corona or shape with antibacterial activity.

When comparing all of the AgNPs it is clear to see that capping of the nanoparticles still facilitates silver activity (REDOX) which, when ordered according to peak oxidation potentials fits quite well with antibacterial activity results against both Gram negative and Gram positive bacteria, shown in Table 6.3. Thus the choice of phenolic compounds for silver reduction, and nanoparticle capping, can be used to tailor the effectiveness of antibacterial activity of these platforms.

Table 6.3- Comparison of antibacterial activity and oxidation potentials for each nanoparticle synthesised including the use of phenolic compounds with varying molar ratios. Antibacterial data refers to the lowest concentration loading.

Antibacterial activity of nanoparticles against *E. coli* (%)							
Curc 1:2	**EGCG 1:8**	**EGCG 1:3**	**EGCG 1:1**	**Curc 1:1**	**Ag cubes**	**Ag spheres**	**Ag prisms**
68	67	67	49	46	39	33	17
Oxidation potential for each nanoparticle (least to most positive) (V)							
Curc 1:2	**EGCG 1:8**	**Curc 1:1**	**EGCG 1:3**	**EGCG 1:1**	**Ag prisms**	**Ag cubes**	**Ag spheres**
0.273	0.280	0.288	0.291	0.293	0.299	0.305	0.335
Antibacterial activity of nanoparticles against *S. albus* (%)							
Curc 1:2	**EGCG 1:8**	**EGCG 1:3**	**EGCG 1:1**	**Curc 1:1**	**Ag cubes**	**Ag spheres**	**Ag prisms**
65	59	49	40	30	22	16	1

Values are taken from Chapter III and V, error values are omitted for concision.

From Table 6.3, it can be portrayed that Curc-AgNPs at 1:2 ratio exhibits the most effective antibacterial activity for both *E. coli* and *S. albus* at ca. 65-68% cell death across all compounds- surface corona and various shaped Ag nanoparticles. It can also be observed that there is a greater percentage cell death for Gram negative bacteria *E. coli* when treated across all silver nanomaterials. Not only does Curc-AgNPs 1:2 demonstrate the highest antibacterial activity, but also the least oxidation potential at 0.273 V.

A trend can be seen as the greater the amount of phenolic groups present in each individual phytochemical, the higher the antibacterial activity. For instance, EGCG-AgNPs 1:8 > EGCG-AgNPs 1:3> EGCG-AgNPs 1:1, and same applied for curcumin with Curc-AgNPs 1:2>Curc-AgNPs 1:1. These observations corresponds to the oxidation potentials, as the lower the potential, the facile it is to oxidise. Therefore, the greater the percentage cell death, the lower the oxidation potential which implies that these silver nanomaterials supplies the environment with silver ions easily to facilitate interaction with bacterial cells. Hence, antibacterial activity can be dictated by oxidation potentials with the contribution of surface corona. Tailoring nanoparticles to target specific bacteria through the choice of corona is very important.

Furthermore, Ag nanoparticles can undergo a shape-dependent interaction with bacterial cells irrespective of oxidation potential. Size can cause steric hindrance and although there are higher binding properties, it is less effective in antibacterial activity compared to surface functionalised Ag nanoparticles as illustrated in Table 6.3. Although surface corona studies have a close fit to oxidation potentials, however different shapes of Ag nanoparticles do not follow the same trend. Despite this, the overall potentials for each individual shape only differ at a small amount of 2–3 mV. This may be due to other variables which indicate that oxidation is not the only indicator to measure antibacterial activity.

One variable may be due to precursors used in the synthesis of various shapes of Ag nanoparticles which can play a role in the influence of antibacterial activity. In the synthesis of Ag nanospheres, tyrosine was used as a reducing and capping agent.[39] Plants possess a vast ability to synthesise aromatic substances, most of which are phenols or their oxygen-substituted derivatives.[40] Many of these are second metabolites and serves as plant defence mechanisms against predation by insects, herbivores or microorganisms. Quinones are responsible for plant pigmentation and tyrosine is usually used for the conversion.[41]

Ascorbic acid is used in the synthesis of Ag nanoprisms during the growth of the shape after seed production.[42] One study suggests that ascorbic acid alone and in combination with lactic acid inhibited the growth of *E. coli* O157:H7.[43] Their results were consistent with those reported with Tabal *et al.* where they found that ascorbic acid in concentrations ranging from 0.2-2% inhibited growth of several microorganisms in liquid broth medium.[44]

Ag nanocubes synthesised via a polyol process used polyvinylpyrrolidone (PVP) as a stabilising agent.[45] PVP is a common stabilising ingredient in the production of Ag nanoparticles.[46, 47] Not only is PVP utilised in various synthesises, it is also known as an antimicrobial agent, namely Betadine. It is a broad spectrum antiseptic for topical application in the treatment of burn and wounds.[48]

6.3.4 Interaction of nanoparticles with bacterial membrane proteins

As evident from Chapter III-V, SEM results revealed significant damage to bacterial cells. In order to elucidate the interaction of Curc-AgNPs and EGCG-AgNPs with bacterial membrane proteins, protein interaction studies were performed using fluorescence spectroscopy. Alteration in tryptophan (trp) fluorescence (for trp present in the bacterial membrane proteins) was measured as a function of protein–NPs interaction. When *E. coli* and *S. albus* membrane preparations were incubated with Curc-AgNPs and EGCG-AgNPs in HEPES buffer, a typical trend was observed. In the presence of Curc-AgNPs and EGCG-AgNPs, trp fluorescence was quenched significantly in comparison to untreated membrane preparations as shown in Figure 6.5. It is evident from the emission spectra that the trp fluorescence of ECMP was decreased significantly in presence of EGCG-AgNPs 1:1 and Curc-AgNPs 1:2. However while other nanoparticle combinations also affect fluorescent properties of membrane proteins, they do not do so as significantly as EGCG-AgNPs 1:1 and Curc-AgNPs 1:2. The two ratio combinations were chosen for further membrane protein and nanoparticles interaction studies.

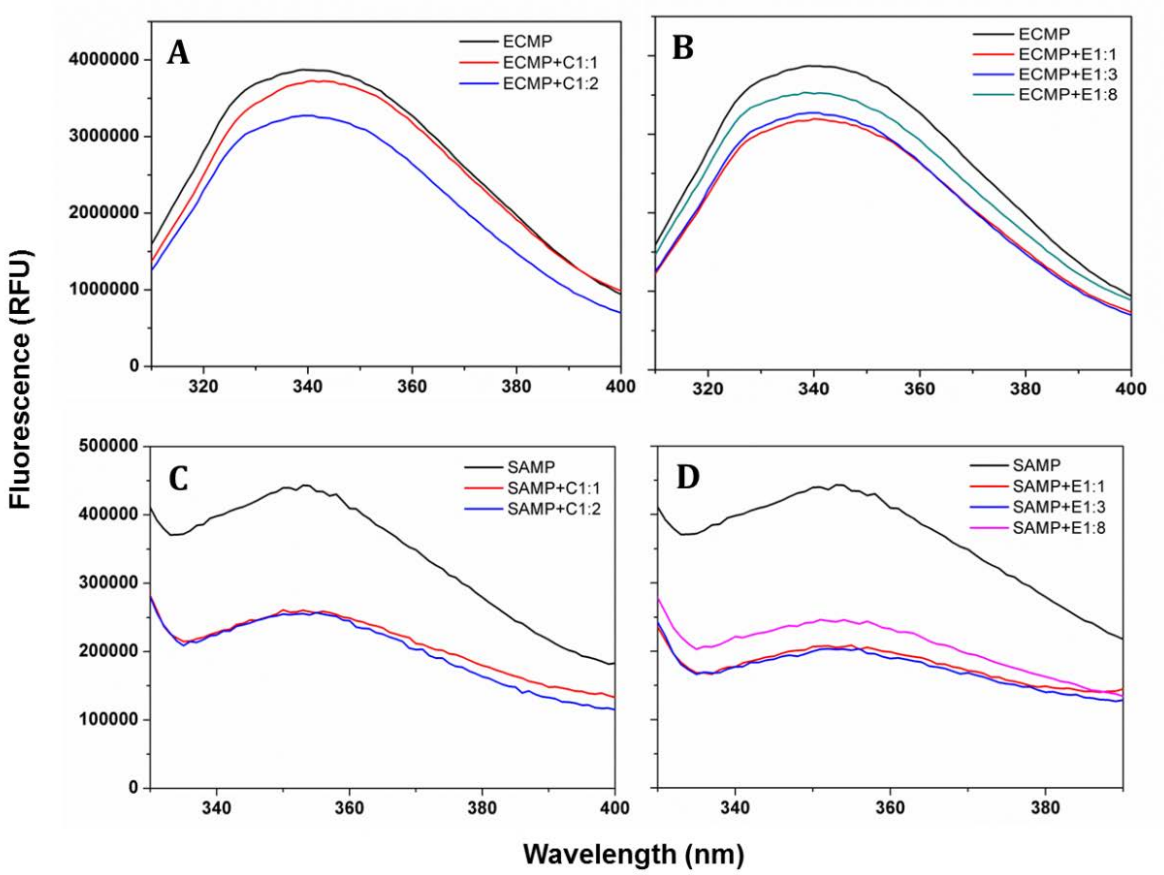

Figure 6.5- Fluorescence spectroscopy of (A) ECMP and ECMP+Curc-AgNPs, (B) ECMP and ECMP+EGCG AgNPs, (C) SAMP and SAM+Curc-AgNPs and (D) SAMP and SAMP+EGCG-AgNPs.

Figure 6.5 unequivocally demonstrates that these nanoparticles interact strongly with the ECMP as well as a similar trend occurring when these nanoparticles were incubated with SAMP. Further to determine the affinity of these interactions, a range of EGCG-AgNPs 1:1 and Cur-AgNPs 1:2 nanoparticles concentrations were incubated with ECMP and SAMP with fluorescence quenching calculated as a function of nanoparticle concentrations. With the quenching data, dissociation constant (Kd) was determined (Figure 6.6). The Kd of Curc-AgNPs (1:2) for ECMP was 11.6 µM however Kd for EGCG-AgNPs (1:1) for ECMP was 9.0 µM. This shows that EGCG has more affinity for ECMP over Curc-AgNPs which could be attributed to the strong interaction of EGCG itself over curcumin with the ECMP. Though the antibacterial potency of EGCG-AgNPs 1:1 was a bit less than other EGCG-AgNPs formulations, their experiments only demonstrate

strong membrane protein interaction. Plausible explanation to this is that EGCG is a more bulky molecule than curcumin and may interact strongly with secondary and tertiary protein structures in comparison to curcumin.[49, 50] While antibacterial activity is attributed to several mechanisms, membrane protein interaction is only one of those mechanisms. Genotoxicity (DNA damage), cytotoxicity (protein damage), production of reactive oxygen species etc. are other mechanism of bacterial cell death mediated by nanoparticles.[51-53] Curc-AgNPs demonstrated 30 fold more affinity (Kd) against SAMP (1.59 µM) in comparison to EGCG-AgNPs (50.5 µM). This evinces that curcumin possesses a slow off rate for SAMP over ECMP in terms of membrane protein binding. In general these results show that EGCG-AgNPs have high affinity for ECMP (Gram negative) over SAMP (Gram positive) while this trend is reverse in case of Curc-AgNPs. This is also evident in a study by Hamed *et al*. which shows potent activity of curcumin itself in the case of Gram positive bacteria.[54]

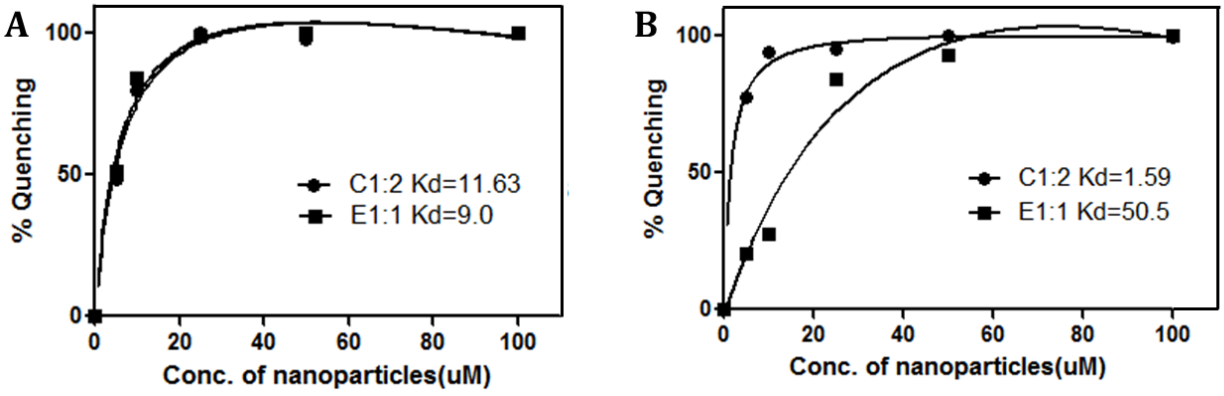

Figure 6.6- Dissociation constant (Kd) of (A) ECMP and (B) SAMP profiles.

6.3.5 Genotoxicity and cellular detection

In order to determine the nanoparticles induced genotoxicity and cytotoxicity, genetically engineered *E. coli* strain was treated with different nanoparticles preparations (each with 50 µM) for two hours and change in GFP/RFP fluorescence was followed.

Curc-AgNPs at 1:2 and EGCG-AgNPs at 1:8 ratios were used as they displayed the highest antibacterial activity. In this experiment ethanol, a known inducer of heat shock response (cellular stress or cytotoicity) and nalidixic acid an accepted inducer of SOS response were used as a positive control. As demonstrated in Figure 6.7, the presence of nanoparticles regardless of their capping material induces expression of GFP, thus this confirms the genotoxic nature (DNA damaging potential). Furthermore when bacterium is exposed to nanoparticles and the expression of RFP was monitored, induction of RFP expression in presence of Curc-AgNPs was significantly higher than ethanol. Other nanoparticles (EGCG-AgNPs and Tyr-AgNPs) also displayed induction of RFP however it was less than the Curc-AgNPs induced expression. This suggests that all nanomaterials have the same genotoxicity potential but Curc-AgNPs induces highest stress response or cytotoxicity.

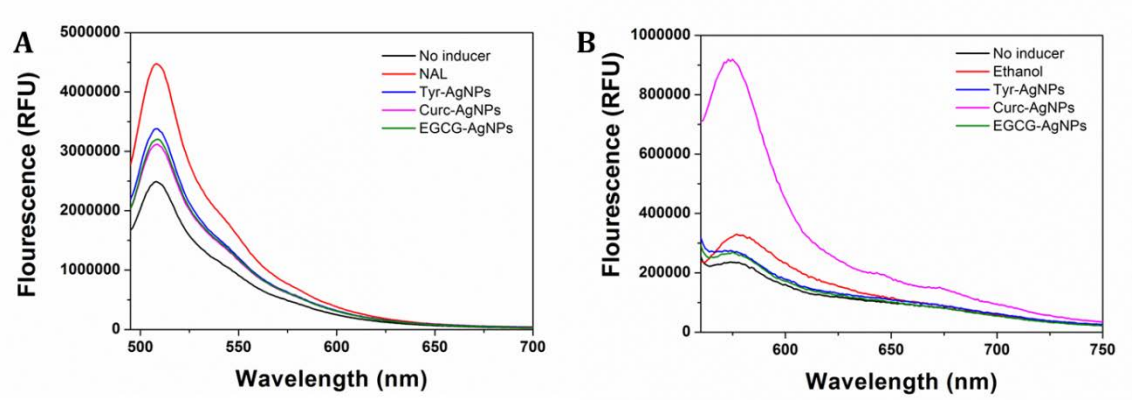

Figure 6.7- (A) GFP fluorescence profile and (B) RFP fluorescence profile.

6.4 Conclusions

The potential mechanism of antibacterial activity of the Ag nanomaterials studied in this thesis can be elucidated using some of the new techniques discussed in this chapter. From the cyclic voltammetry studies, it was found that oxidation potential can influence the antibacterial activity of various Ag nanomaterials. The lower the oxidation potential, the higher the antibacterial activity was typically observed, this may be

attributed to the facile oxidability of Ag nanomaterials to release Ag^+ into bacterial cells. Electrochemical studies correlate very well with antibacterial studies where they follow a similar trend in both functionalised Ag nanoparticles and to some extent in shape dependent Ag nanoparticles. In reference to the effect of surface corona studies, it was determined that the thinner the corona, the higher the antibacterial activity. Therefore it was found that Curc-AgNPs 1:2 exhibited the highest antibacterial activity as well as the lowest oxidation potential overall. Similar trends were demonstrated when the greater the ratio of phenolic groups present in each individual phytochemical, the higher the antibacterial activity and lower oxidation potentials, i.e. EGCG-AgNPs 1:8 > EGCG-AgNPs 1:3 > EGCG-AgNPs 1:1 and Curc-AgNPs 1:2 > Curc AgNPs 1:1.

Other variables might contribute to the influence of antibacterial activity, not just using oxidation potential as an indicator. A study on shape-dependent Ag nanoparticles revealed that oxidation potential was less relevant in assessment of antibacterial activity of these materials compared to functionalised Ag nanoparticles. Precursors used in the synthesis of the various shapes may have influenced the antibacterial activity. On the other hand, higher antibacterial activity of functionalised Ag nanoparticles is due to the phytochemicals utilised.

Bacterial membranes are considered as the first barriers that need to be overcome by antibacterial agent. However when looking at the affinity of the Ag nanomaterials with cells, it is important to study the bacterial membrane proteins present. Membrane protein interactions showed that EGCG-AgNPs displayed more affinity for ECMP compared to Curc-AgNPs. Plausibly, this can be attributed to the strong interaction of EGCG alone, being a bulky molecule. In the case of SAMP, Curc-AgNPs 1:2 with a thinner surface corona demonstrated a 30 fold increase in affinity compared to EGCG-AgNPs.

Therefore, this reveals that Curc-AgNPs possess a slow off rate for SAMP over ECMP in terms of membrane protein binding.

Since Curc-AgNPs 1:2 and EGCG-AgNPs 1:8 demonstrated the highest antibacterial activity, the genotoxicity and cellular toxicity were studied on these two systems. When bacterium is exposed to Ag nanomaterials, significant induction of RFP expression in presence of Curc-AgNPs 1:2 displayed the highest stress response. For GFP response (genotoxicity) irrespective of capping agents, Ag nanomaterials induce expressions of GFP which confirms DNA damage and SOS response. These properties are illustrated in Figure 6.8.

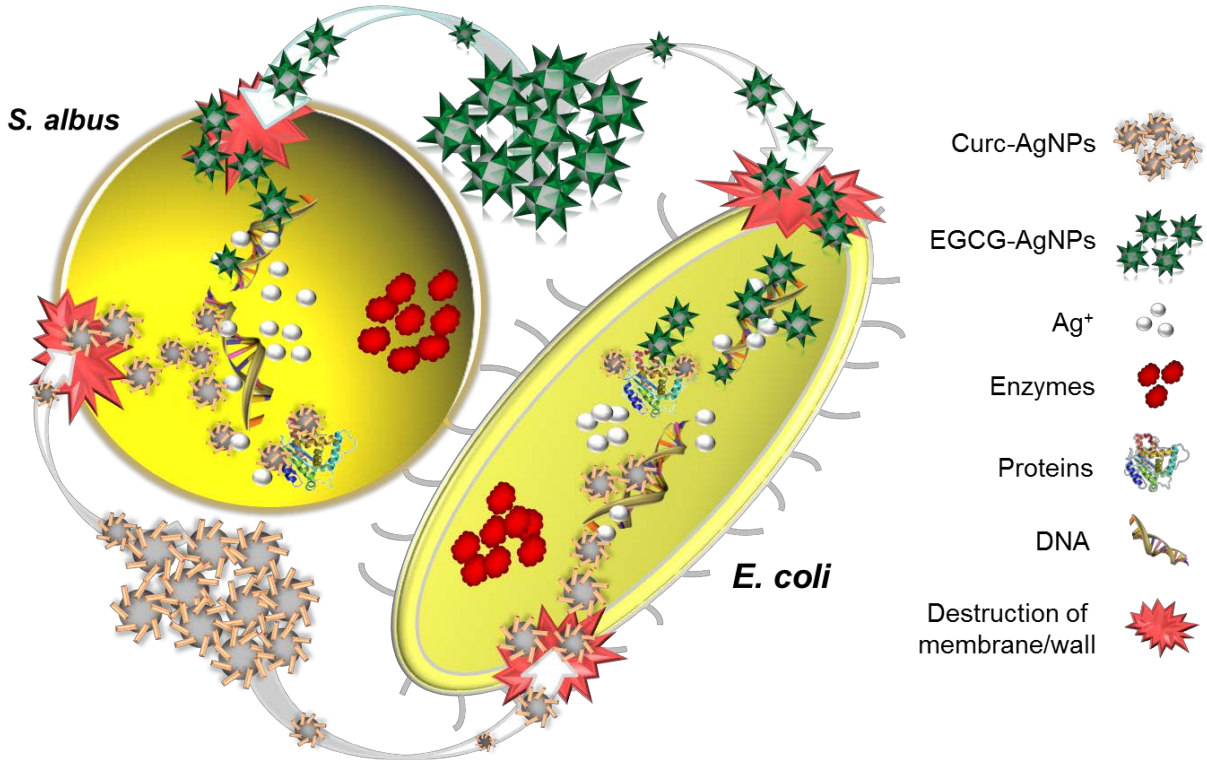

Figure 6.8- Schematic illustration of potential mechanisms of antibacterial activity of functionalised Ag nanoparticles against *E. coli* and *S. albus* based upon genotoxicity and genotoxicity data.

Therefore this thesis shows that Ag nanomaterials display different modes of action for antibacterial activity including but not limited to interaction with membranes, genotoxicity and cytotoxicity as demonstrated by GFP and RFP inductions. However, it

seems that irrespective of mode of action, a measure of oxidisation potential via cyclic voltammetry can in general be considered a reliable tool to predict the effectiveness of Ag nanomaterials antibacterial activity.

6.5 References

[1] Liau, S.; Read, D.; Pugh, W.; Furr, J.; Russell, A., Interaction of silver nitrate with readily identifiable groups: relationship to the antibacterialaction of silver ions. *Lett. Appl. Microbiol.* **1997,** *25* (4), 279-283.

[2] Feng, Q.; Wu, J.; Chen, G.; Cui, F.; Kim, T.; Kim, J., A mechanistic study of the antibacterial effect of silver ions on *Escherichia coli* and *Staphylococcus aureus*. *Journal of biomedical materials research* **2000,** *52* (4), 662-668.

[3] Choi, O.; Deng, K. K.; Kim, N.-J.; Ross Jr, L.; Surampalli, R. Y.; Hu, Z., The inhibitory effects of silver nanoparticles, silver ions, and silver chloride colloids on microbial growth. *Water research* **2008,** *42* (12), 3066-3074.

[4] Morones, J. R.; Elechiguerra, J. L.; Camacho, A.; Holt, K.; Kouri, J. B.; Ramírez, J. T.; Yacaman, M. J., The bactericidal effect of silver nanoparticles. *Nanotechnology* **2005,** *16* (10), 2346.

[5] Oberdörster, G.; Oberdörster, E.; Oberdörster, J., Nanotoxicology: an emerging discipline evolving from studies of ultrafine particles. *Environmental health perspectives* **2005**, 823-839.

[6] Warheit, D. B.; Borm, P. J.; Hennes, C.; Lademann, J., Testing strategies to establish the safety of nanomaterials: conclusions of an ECETOC workshop. *Inhalation toxicology* **2007,** *19* (8), 631-643.

[7] Janeiro, P.; Oliveira Brett, A. M., Catechin electrochemical oxidation mechanisms. *Analytica chimica acta* **2004,** *518* (1), 109-115.

[8] Rice-Evans, C. A.; Miller, N. J.; Paganga, G., Structure-antioxidant activity relationships of flavonoids and phenolic acids. *Free radical biology and medicine* **1996,** *20* (7), 933-956.

[9] Hotta, H.; Nagano, S.; Ueda, M.; Tsujino, Y.; Koyama, J.; Osakai, T., Higher radical scavenging activities of polyphenolic antioxidants can be ascribed to chemical reactions following their oxidation. *Biochimica et Biophysica Acta (BBA)-General Subjects* **2002,** *1572* (1), 123-132.

[10] Yang, B.; Kotani, A.; Arai, K.; Kusu, F., Estimation of the antioxidant activities of flavonoids from their oxidation potentials. *Analytical sciences* **2001,** *17* (5), 599-604.

[11] Belkin, S., Microbial whole-cell sensing systems of environmental pollutants. *Current Opinion in Microbiology* **2003,** *6* (3), 206-212.

[12] Cheng Vollmer, A.; Van Dyk, T. K., Stress responsive bacteria: biosensors as environmental monitors. *Advances in microbial physiology* **2004,** *49*, 131-174.

[13] Belkin, S., Genetically engineered microorganisms for pollution monitoring. In *Soil and Water Pollution Monitoring, Protection and Remediation*, Springer: 2006; pp 147-160.

[14] D'souza, S., Microbial biosensors. *Biosensors and Bioelectronics* **2001,** *16* (6), 337-353.

[15] Lei, Y.; Chen, W.; Mulchandani, A., Microbial biosensors. *Analytica Chimica Acta* **2006,** *568* (1), 200-210.

[16] Wells, P. G.; Lee, K.; Blaise, C., *Microscale testing in aquatic toxicology: advances, techniques, and practice*. CRC Press: 1997.

[17] Biran, I.; Babai, R.; Levcov, K.; Rishpon, J.; Ron, E. Z., Online and in situ monitoring of environmental pollutants: electrochemical biosensing of cadmium. *Environmental Microbiology* **2000,** *2* (3), 285-290.

[18] Min, J.; Pham, C. H.; Gu, M. B., Specific responses of bacterial cells to dioxins. *Environmental toxicology and chemistry* **2003,** *22* (2), 233-238.

[19] Matsumura, F., On the significance of the role of cellular stress response reactions in the toxic actions of dioxin. *Biochemical pharmacology* **2003,** *66* (4), 527-540.

[20] Gu, M. B.; Min, J.; Kim, E. J., Toxicity monitoring and classification of endocrine disrupting chemicals (EDCs) using recombinant bioluminescent bacteria. *Chemosphere* **2002,** *46* (2), 289-294.

[21] Van Dyk, T. K.; Majarian, W. R.; Konstantinov, K. B.; Young, R. M.; Dhurjati, P. S.; Larossa, R. A., Rapid and sensitive pollutant detection by induction of heat shock gene-bioluminescence gene fusions. *Applied and environmental microbiology* **1994,** *60* (5), 1414-1420.

[22] Bousse, L., Whole cell biosensors. *Sensors and Actuators B: Chemical* **1996,** *34* (1), 270-275.

[23] Vollmer, A. C.; Belkin, S.; Smulski, D. R.; Van Dyk, T. K.; LaRossa, R. A., Detection of DNA damage by use of *Escherichia coli* carrying recA':: lux, uvrA':: lux, or alkA':: lux reporter plasmids. *Applied and environmental microbiology* **1997,** *63* (7), 2566-2571.

[24] Köhler, S.; Belkin, S.; Schmid, R. D., Reporter gene bioassays in environmental analysis. *Fresenius' journal of analytical chemistry* **2000,** *366* (6-7), 769-779.

[25] Sagi, E.; Hever, N.; Rosen, R.; Bartolome, A. J.; Rajan Premkumar, J.; Ulber, R.; Lev, O.; Scheper, T.; Belkin, S., Fluorescence and bioluminescence reporter functions in genetically modified bacterial sensor strains. *Sensors and Actuators B: Chemical* **2003,** *90* (1), 2-8.

[26] Yagi, K., Applications of whole-cell bacterial sensors in biotechnology and environmental science. *Appl. Microbiol. Biotechnol.* **2007,** *73* (6), 1251-1258.

[27] Kirowa-Eisner, E.; Bonfil, Y.; Tzur, D.; Gileadi, E., Thermodynamics and kinetics of upd of lead on polycrystalline silver and gold. *Journal of Electroanalytical Chemistry* **2003,** *552*, 171-183.

[28] Kirowa-Eisner, E.; Tzur, D.; Gileadi, E., Underpotential dissolution of metals under conditions of partial mass-transport control. *Journal of Electroanalytical Chemistry* **2008,** *621* (2), 146-158.

[29] Jin, G.-P.; Lin, X.-Q., The electrochemical behavior and amperometric determination of tyrosine and tryptophan at a glassy carbon electrode modified with butyrylcholine. *Electrochemistry communications* **2004,** *6* (5), 454-460.

[30] Herzog, G.; Arrigan, D. W., Electrochemical strategies for the label-free detection of amino acids, peptides and proteins. *Analyst* **2007,** *132* (7), 615-632.

[31] Cheng, H.; Chen, C.; Zhang, S., Electrochemical behavior and sensitive determination of L-tyrosine with a gold nanoparticles modified glassy carbon electrode. *Analytical sciences: the international journal of the Japan Society for Analytical Chemistry* **2009,** *25* (10), 1221-1225.

[32] Zinola, C.; Rodríguez, J.; Arévalo, M.; Pastor, E., Electrochemical and FTIR spectroscopic studies of tyrosine oxidation at polycrystalline platinum surfaces in alkaline solutions. *Journal of Solid State Electrochemistry* **2008,** *12* (5), 523-528.

[33] MacDonald, S.; Roscoe, S., Electrochemical oxidation reactions of tyrosine, tryptophan and related dipeptides. *Electrochimica acta* **1997,** *42* (8), 1189-1200.

[34] Masek, A.; Chrzescijanska, E.; Zaborski, M., Characteristics of curcumin using cyclic voltammetry, UV–vis, fluorescence and thermogravimetric analysis. *Electrochimica Acta* **2013,** *107*, 441-447.

[35] Lungu, A.; Sandu, I.; Boscornea, C.; Tomas, S.; Mihailciuc, C., Electrochemical study of curcumin and bisdemethoxycurcumin on activated glassy carbon electrode. *Rev Roum Chim* **2010,** *55* (2), 109-115.

[36] Novak, I.; Šeruga, M.; Komorsky-Lovrić, Š., Electrochemical characterization of epigallocatechin gallate using square-wave voltammetry. *Electroanalysis* **2009,** *21* (9), 1019-1025.

[37] Bansal, V.; Li, V.; O'Mullane, A. P.; Bhargava, S. K., Shape dependent electrocatalytic behaviour of silver nanoparticles. *CrystEngComm* **2010,** *12* (12), 4280-4286.

[38] Ahern, A. J.; Nagle, L. C.; Burke, D. L., Electrocatalysis at polycrystalline silver in base: an example of the complexity of surface active state behaviour. *Journal of Solid State Electrochemistry* **2002,** *6* (7), 451-462.

[39] Selvakannan, P. R.; Swami, A.; Srisathiyanarayanan, D.; Shirude, P. S.; Pasricha, R.; Mandale, A. B.; Sastry, M., Synthesis of aqueous Au core−Ag shell nanoparticles using tyrosine as a pH-dependent reducing agent and assembling phase-transferred silver nanoparticles at the air−water interface. *Langmuir* **2004,** *20* (18), 7825-7836.

[40] Rios, J.; Recio, M., Medicinal plants and antimicrobial activity. *Journal of ethnopharmacology* **2005,** *100* (1), 80-84.

[41] Cowan, M. M., Plant products as antimicrobial agents. *Clinical microbiology reviews* **1999,** *12* (4), 564-582.

[42] Aherne, D.; Ledwith, D. M.; Gara, M.; Kelly, J. M., Optical properties and growth aspects of silver nanoprisms produced by a highly reproducible and rapid synthesis at room temperature. *Adv. Funct. Mater.* **2008,** *18* (14), 2005-2016.

[43] Tajkarimi, M.; Ibrahim, S. A., Antimicrobial activity of ascorbic acid alone or in combination with lactic acid on *Escherichia coli* O157: H7 in laboratory medium and carrot juice. *Food Control* **2011,** *22* (6), 801-804.

[44] Tabak, M.; Armon, R.; Rosenblat, G.; Stermer, E.; Neeman, I., Diverse effects of ascorbic acid and palmitoyl ascorbate on *Helicobacter pylori* survival and growth. *FEMS microbiology letters* **2003,** *224* (2), 247-253.

[45] Siekkinen, A. R.; McLellan, J. M.; Chen, J. Y.; Xia, Y. N., Rapid synthesis of small silver nanocubes by mediating polyol reduction with a trace amount of sodium sulfide or sodium hydrosulfide. *Chem. Phys. Lett.* **2006,** *432* (4-6), 491-496.

[46] Cho, K.-H.; Park, J.-E.; Osaka, T.; Park, S.-G., The study of antimicrobial activity and preservative effects of nanosilver ingredient. *Electrochimica Acta* **2005,** *51* (5), 956-960.

[47] Sun, Y.; Mayers, B.; Herricks, T.; Xia, Y., Polyol synthesis of uniform silver nanowires: a plausible growth mechanism and the supporting evidence. *Nano Lett.* **2003,** *3* (7), 955-960.

[48] Al-Adham, I. S.; Gilbert, P., Effect of polyvinylpyrrolidone molecular weight upon the antimicrobial activity of povidone-iodine antiseptics. *International journal of pharmaceutics* **1986,** *34* (1), 45-49.

[49] Jöbstl, E.; Howse, J. R.; Fairclough, J. P. A.; Williamson, M. P., Noncovalent cross-linking of casein by epigallocatechin gallate characterized by single molecule force microscopy. *Journal of agricultural and food chemistry* **2006,** *54* (12), 4077-4081.

[50] Yoda, Y.; Hu, Z.-Q.; Zhao, W.-H.; Shimamura, T., Different susceptibilities of *Staphylococcus* and Gram-negative rods to epigallocatechin gallate. *Journal of Infection and Chemotherapy* **2004,** *10* (1), 55-58.

[51] Sharma, T. K.; Chopra, A.; Sapra, M.; Kumawat, D.; Patil, S. D.; Pathania, R.; Navani, N. K., Green synthesis and antimicrobial potential of silver nanoparticles. *International Journal of Green Nanotechnology* **2012,** *4* (1), 1-16.

[52] Durán, N.; Marcato, P. D.; Conti, R. D.; Alves, O. L.; Costa, F.; Brocchi, M., Potential use of silver nanoparticles on pathogenic bacteria, their toxicity and possible mechanisms of action. *Journal of the Brazilian Chemical Society* **2010,** *21* (6), 949-959.

[53] Rai, M. K.; Deshmukh, S. D.; Ingle, A. P.; Gade, A. K., Silver nanoparticles: the powerful nanoweapon against multidrug-resistant bacteria. *Journal of Applied Microbiology* **2011,** *112* (5), 841-852.

[54] Hamed, O. A.; Mehdawi, N.; Taha, A. A.; Hamed, E. M.; Al-Nuri, M. A.; Hussein, A. S., Synthesis and antibacterial activity of novel curcumin derivatives containing heterocyclic moiety. *Iranian journal of pharmaceutical research: IJPR* **2013,** *12* (1), 47.

Chapter VII

Conclusions and future work

7.1 Conclusions

Bionanotechnology represent a modern and innovative approach to develop and apply new formulations based on metallic nanoparticles with antimicrobial activities. Ag nanoparticles exemplify a prominent nanomaterial with potential antibacterial applications. The studies presented in this thesis are an attempt to establish the correlation between Ag nanomaterials with their antibacterial applications. Ag nanoparticles were synthesised via various methods as well as functionalisation to enhance antibacterial activity.

Change in reactivity and properties of nanoparticles are attributed to their small size, compared with bulk materials. The smaller the size, the larger the surface-area-to volume ratio. Therefore the bactericidal activity of Ag nanoparticles is affected by the size of the nanoparticles. Dependent on the size of nanoparticles, large surface area comes in contact with the bacterial cells to provide higher percentage of interaction than bigger particles. Not only is size a factor influencing the bactericidal effects of Ag nanoparticles, but the shape of the Ag nanoparticle can play a great role. Ag nanoparticles can undergo shape-dependent antibacterial behaviour again bacterial species of both Gram negative (*E. coli*) and Gram positive (*S. albus*). Ag nanospheres, cubes and prisms were synthesised

via various chemical approaches and characterised. The comparison of different shapes was tested on representative microorganisms for their antibacterial activity. Overall, Ag nanoparticles of various shapes demonstrated antibacterial activity against all strains of bacteria used. However, among the various shapes studied, Ag nanocubes performed significantly better in terms of antibacterial activity against both Gram negative and Gram positive bacteria.

The amino acid tyrosine was utilised in the synthesis of Ag nanospheres as a capping as well as a reducing agent. These particles were the most stable as well as isotropic and were synthesised via a 1:1 ratio of silver stock to the monophenolic tyrosine amino acid which was the least complex. Hence, these particles were selected as representative Ag nanoparticles for all studies throughout the thesis. These nanoparticles were bound with various spectrums of traditional antibiotics, namely ampicillin, penicillin G and polymyxin B to enhance antibacterial activity. Furthermore, these traditional antibiotics incorporating various spectrums were employed as functional fragments to influence the antibacterial potential on the surface of Ag nanoparticles. Moreover, these Ag nanoparticle/antibiotic combinations revealed notable influence on antibacterial activity providing synergistic effects which employ a physical mode of action against bacterial cells causing cell wall cleavage and cell lysis.

Surface functionalisation of Ag nanoparticles can also influence the antibacterial effects. To study this effect, various phenolic compounds were used as organic surface coronas surrounding Ag nanoparticles which then played a crucial role in tuning nanomaterial properties for biological applications. Tyrosine, curcumin and epigallocatechin gallate (EGCG) were utilised as reducing as well as capping agents to synthesise surface functionalised Ag nanoparticles. Equimolar and various mole ratios

were employed to study the effect of relative loading of phenolic groups onto nanoparticles towards antibacterial activity. The antibacterial activities of these surface functionalised Ag nanoparticles also revealed a significant role in damage to bacterial cells.

Techniques including electrochemistry, bacterial membrane protein interaction with nanoparticles and genotoxicity as well as cellular toxicity studies could elucidate the mechanism of action of Ag based nanomaterials. Cyclic voltammetry studies that produced oxidation potential measurements provided a close fit trend with antibacterial profile of various nanomaterials. It was shown that the lower the oxidation potential, the higher the antibacterial activity detected. This may be due to the facile oxidability of Ag nanomaterials releasing Ag^{+} into bacterial membranes. Electrochemical studies were correlated with antibacterial studies where similar trends were found largely in functionalised Ag nanoparticles and to some extent in shape dependent Ag nanoparticles.

In regards to the effect of surface corona studies of various phenolic compounds, it was determined that the thinner the corona, the higher the antibacterial activity. Curcumin Ag nanoparticles 1:2 exhibited the highest antibacterial activity as well as the lowest oxidation potential across all phenolic compounds. However, when comparing with each individual group, the antibacterial activity can be determined as follows: Curc-AgNPs 1:2> Curc-AgNPs 1:1 and EGCG-AgNPs 1:8> EGCG-AgNPs 1:3> EGCG AgNPs 1:1.

It was found that further variables might contribute to the influence of antibacterial activity, not only the use of oxidation potential as an indicative technique. Although shape-dependent antibacterial activity of Ag nanoparticles were found to be

less effective compared to functionalised Ag nanoparticles, precursors used in the synthesis of different shapes of nanoparticles may have been an influence.

To understand the surface coating corona in relation to antibacterial activity, interaction of surface functionalised Ag nanoparticles to bacterial membrane protein (MP) were studied. Additionally, the effect at gene and protein level, genotoxicity and cellular toxicity experiments revealed that the affinity of Ag nanomaterial with cells is of prominent importance. Membrane protein interactions revealed that EGCG-AgNPs demonstrated more affinity for ECMP (*E. coli* membrane protein) compared to Curc-AgNPs. This might be because EGCG is a bulky molecule which alone possesses a strong interaction with bacterial membranes. However, for SAMP (*S. albus* membrane protein), Curc-AgNPs 1:2 surrounded by a thinner surface corona demonstrated a 30 fold increase in affinity compared to EGCG-AgNPs. It was therefore determined that Curc-AgNPs exhibits a slow off rate for SAMP over ECMP in relation to membrane protein binding.

Since Curc-AgNPs 1:2 and EGCG-AgNPs 1:8 demonstrated the highest antibacterial activity, the genotoxicity and cellular toxicity response were studied in detail. When bacteria were exposed to Ag nanomaterials, significant induction of RFP (red fluorescent protein) expression in presence of Curc-AgNPs 1:2 exhibited the highest stress response. For genotoxicity induction, irrespective of capping agents, Ag nanomaterials induce expressions of GFP (green fluorescent protein) which confirmed DNA damage and SOS response. Hence, Ag nanomaterials may display different modes of action for antibacterial activity which may not be limited to interaction with membranes, genotoxicity and cytotoxicity as demonstrated by GFP and RFP inductions.

Overall, various methods including electrochemical, biophysical and biotechnological approaches were employed to elucidate the mechanism of action of Ag nanostructures as demonstrated in this thesis.

7.2 Future work

Studying the influence of surface corona on biological action of different nanomaterials is an area of intensive scrutiny; therefore exploring other antioxidants to functionalise Ag nanoparticles to enhance antibacterial activity may be carried out in the future. Antioxidant properties of these compounds can be studied to assist in understanding the mode of action of these nanomaterials and their interaction with cell membranes. Although antibacterial applications of these functionalised Ag nanoparticles have been discussed in this thesis, these nanomaterials containing curcumin and EGCG, which are known for their anticancer properties, can also be utilised as potential anticancer agents. It would be interesting to investigate whether these materials show similar mode of interaction with the mammalian cells.

Since different shapes of Ag nanoparticles can play a vital role in the enhancement of antibacterial activity, other shapes of nanomaterials can also be studied against disease-causing microorganisms. Tailoring of size and shape can be further studied for their antibacterial applications. Further work to understand the interaction between different shapes of nanomaterials and microorganisms can be carried out with other antimicrobial techniques such as membrane protein interaction as well as cytotoxicity and genotoxicity studies.

The synergism of nanomaterials was tested using traditional antibiotics. This study could be further expanded to encompass a larger variety of Gram positive and

Gram negative targeting compounds, both broad and narrow spectrum. It will also be interesting to measure the synergism of antibiotics with the nanomaterials of different shapes, as well as functionalised nanospheres discussed within this thesis.

All the materials proposed in this thesis may also be studied for their antimicrobial activity against other group of microorganisms including fungi for antifungal activity. It will also be prudent to study whether these nanomaterials can be utilised in other biotechnological applications such as cytotoxicity towards mammalian cells not just microorganisms.

In summary, the work presented in this thesis clearly shows that the mode of antibacterial activity of Ag based nanomaterials is a highly complex phenomenon. This involves several steps including (i) level of interaction of nanomaterial with bacterial outer layer, (ii) uptake of nanoparticles by cell, (iii) potential oxidation of Ag nanoparticles to Ag^{+} ions and (iv) interaction of Ag^{+} ions with bacterial cellular, cytoplasmic and genetic components. This thesis shows that all these mechanistic components can be controlled by tailor-design of nanoparticles through shape control, surface control or synergism through traditional antibiotics. It is expected that these research outcomes will fuel more research in understanding the antibacterial activity of Ag based nanomaterials.